UDK 66:54(05) CODEN HMIDA 8 ISSN 0367–598 X

3

Hemijska industrija

Vol. 69

Časopis Saveza hemijskih inženjera

Chemical Industry

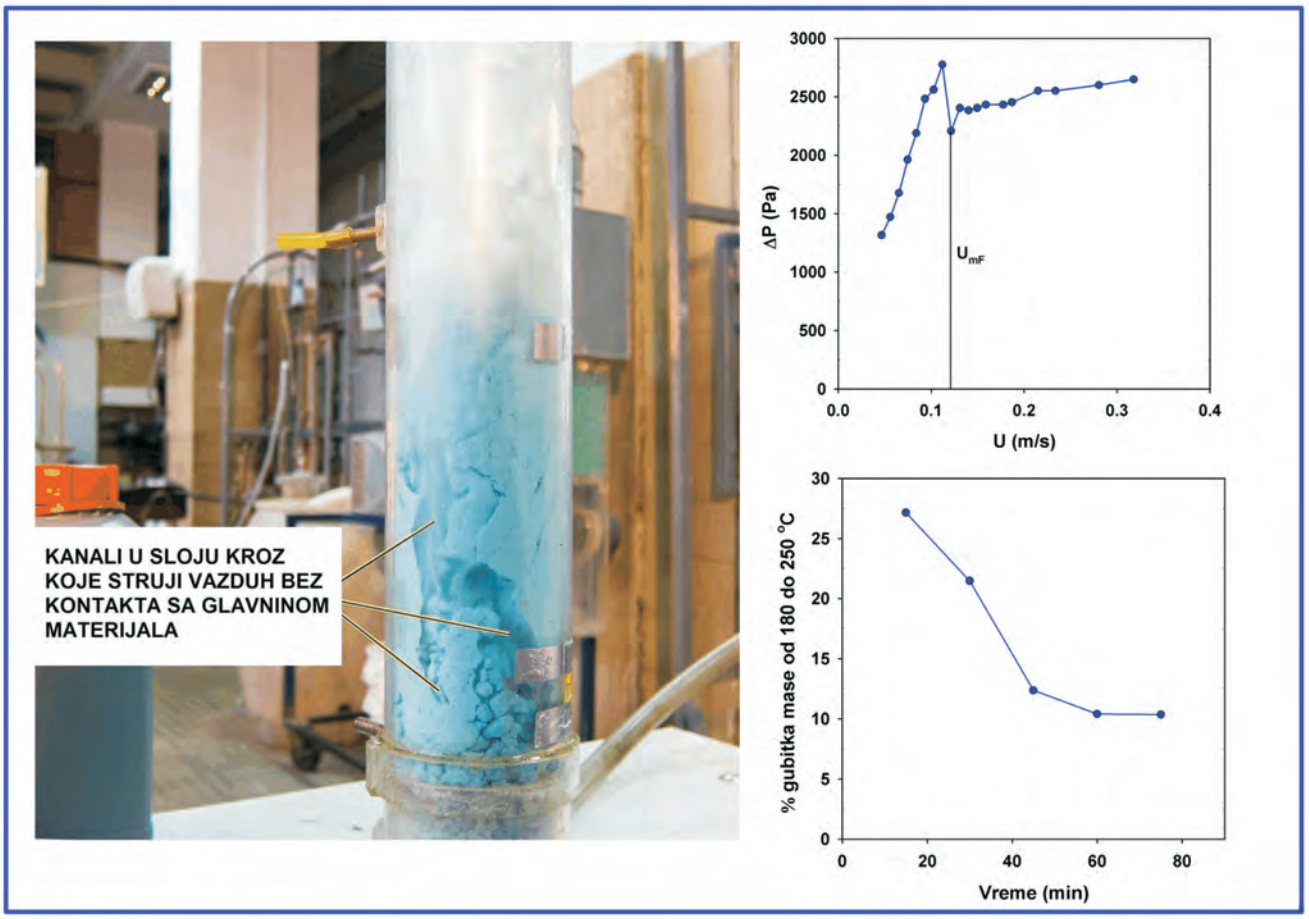

BEOGRAD, MAJ-JUN 2015. HMIDA 8, 69 (3) 219-330 (2015)

Chemical Industry
Химическая промышленность

Hemijska industrija

Časopis Saveza hemijskih inženjera Srbije
Journal of the Association of Chemical Engineers of Serbia
Журнал Союза химических инженеров Сербии

VOL. 69 **Beograd, maj–jun 2015** **Broj 3**

Redakcija
11000 Beograd, Kneza Miloša 9/I
Tel/fax: 011/3240-018
E-pošta: shi@yubc.net
www.ache.org.rs

Izlazi dvomesečno, rukopisi se ne vraćaju

Za izdavača
Tatijana Dudukoviċ

Sekretar redakcije
Slavica Desnica

Izdavanje časopisa pomaže
Republika Srbija, Ministarstvo prosvete, nauke i tehnološkog razvoja

Uplata pretplate i oglasnog prostora vrši se na tekući račun Saveza hemijskih inženjera Srbije, Beograd, broj 205-2172-71, Komercijalna banka a.d., Beograd

Kompjuterska priprema
Vladimir Panić

Štampa
Razvojno-istraživački centar grafičkog inženjerstva, Tehnološko-metalurški fakultet, Univerzitet u Beogradu, Karnegijeva 4, 11000 Beograd

Indeksiranje
Radovi koji se publikuju u časopisu *Hemijska Industrija* ideksiraju se preko *Thompson Reuters Scietific®* servisa *Science Citation Index - Expanded™* i *Journal Citation Report (JCR)*, kao i domaćeg *SCIndeks* servisa Centra za evaluaciju u obrazovanju i nauci

SADRŽAJ

SADRŽAJ Nastavak

CONTENTS

GENERALNI POKROVITELJ

Hemofarm

HEMOFARM KONCERN

VRŠAC, Beogradski put bb, tel. 013/821-345, 821-027, 821-129
BEOGRAD, Prote Mateje 70, tel. 011/344-26-63, faks: 344-17-87
E-pošta: info@hemofarm.com

IZDAVANJE ČASOPISA POMOGLA JE:

INŽENJERSKA KOMORA SRBIJE
Bulevar vojvode Mišića 37
11000 Beograd

SUIZDAVAČI

Tehnološko-metalurški fakultet
Univerziteta u Beogradu, Beograd

Prirodno-matematički fakultet Univerziteta
u Novom Sadu, Novi Sad

Hemijski fakutet
Univerziteta u Beogradu
Beograd

ITNMS
Institut za tehnologiju nuklearnih i drugih
mineralnih sirovina, Beograd

HIP PETROHEMIJA
HIP Petrohemija a.d. Pančevo

Tehnološki fakultet Univerziteta
u Novom Sadu, Novi Sad

NU Institut za hemiju,
tehnologiju i metalurgiju
Univerziteta u Beogradu,
Beograd

nevena
„Nevena Color“ d.o.o.
Leskovac

Tehnološki fakultet Univerziteta
u Nišu, Leskovac

dcp-hemigal®
DCP Hemigal, Leskovac

Procena uticaja ispuštanja otpadnih voda na kvalitet vode kanala DTD Bečej–Bogojevo

Vesna Ž. Pešić, Milena R. Bečelić-Tomin, Božo D. Dalmacija, Dejan M. Krčmar

Univerzitet u Novom Sadu, Prirodno–matematički fakultet, Departman za hemiju, biohemiju i zaštitu životne sredine, Novi Sad, Srbija

Izvod

Procena uticaja ispuštanja otpadnih voda je proces koji pomaže da se razume i oceni veličina rizika kao i verovatnoća da dođe do rizika. U radu je primenjen analitički okvir analize pritisaka i uticaja na kanal DTD Bečej–Bogojevo. Pritisak zagađenja je rezultat aktivnosti koja može direktno prouzrokovati pogoršanje statusa vodnog tela. Za procenu uticaja korišćeni su podaci o izvoru i značaju pritisaka zagađenja i podaci o stanju vodnih tela. Svi ovi koraci u procesu analize pritisaka i uticaja su doveli do istog zaključka, da je vodno telo DTD Bečej–Bogojevo pod rizikom od nepostizanja zahtevanog kvaliteta vode, iz razloga što većina vrednosti koncentracija prekoračuju propisane. Kod 33% analiziranih parametara izračunati specifični količnici rizika su veći od 1 i time se svrstavaju u kategoriju polutanata srednjeg rizika.

Ključne reči: otpadne vode, procena uticaja, DPSIR, DTD Bečej–Bogojevo, ekološki potencijal.

Dostupno na Internetu sa adrese časopisa: http://www.ache.org.rs/HI/

STRUČNI RAD

UDK 628.3:502/504(497.113Bačka)

Hem. Ind. **69** (3) 219–229 (2015)

doi: 10.2298/HEMIND140204035P

Osnovni izvori zagađivanja površinskih voda su koncentrisani izvori zagađivanja (naselja, industrija i poljoprivreda), koji ispuštaju otpadne vode preko kanalizacionog sistema ili kanala u vodoprijemnike ili ih odlažu na zemljište. Veći deo komunalnih otpadnih voda čine upotrebljene vode iz domaćinstva. Za njih je karakterističan konstantan sastav u jednom regionu u dužem periodu i njihova količina i sastav pokazuju tokom dana karakteristične varijacije, kao rezultat životnog standarda i načina življenja stanovništva. Glavna karakteristika kvaliteta komunalnih voda je sadržaj organskih i neorganskih materija. Industrijske otpadne vode potiču od proizvodnih procesa i njihova količina i sastav zavisi od niza faktora i specifična je za svaku granu industrije. Industrijske otpadne vode imaju varijabilan karakter, kako po količini tako i po kvalitetu i menjaju se po vrstama industrije. Količina industrijskih otpadnih voda može varirati u širokom opsegu, kako tokom dana tako i u dužem vremenu, što je posledica određene dinamike nastajanja otpadnih voda unutar samog proizvodnog postupka, ali i različitog intenziteta rada industrije [1].

Funkcionisanje akvatičnog sistema je kompleksno imajući u vidu različita hemijska jedinjenja prisutna u vodi i sedimentu, populaciju akvatičnih organizama, temperaturu vode, prirodu okolonog zemljišta. Najvažniji uticaji ispuštanja visokooptterećenih otpadnih voda, industrijalizacije i urbanizacije na površinske vode imaju za posledicu pad rastvorenog kiseonika, eutrofikaciju i pojavu toksičnih supstanci [2]. Supstance koje izazivaju ove efekte mogu biti organskog ili neorganskog porekla, kao što su teški metali ili organski materijali iz različitih vrsta pesticida koji se upotrebljavaju u poljoprivredi.

Da bi se imao uvid u stanje kvaliteta voda vrši se permanentna kontrola odgovarajućih parametara voda. Cilj je da se održi nivo kvaliteta voda u propisanim granicama, što se postiže primenom savremenih tehnologija proizvodnje, uvođenjem recirkulacionih i „bezvodnih“ tehnologija kao i izvođenjem sanacionih radova na izvorima zagađenja. Takvi ciljevi za održavanje kvaliteta voda promovišu se saglasno potrebama u zadatom periodu vremena za određeni ekosistem. Tako i Okvirna direktiva o vodama, kao sveobuhvatni zakonski instrument, ima za cilj uspostavljanje okvira za zaštitu svih voda koji će štititi i unaprediti status vodnih tela i sprečiti dalje pogoršanje [3].

Procena uticaja na životnu sredinu je postupak u kome se obezbeđuje odgovarajuća informaciona osnova za donošenje odluka o aktivnostima koje utiču na životnu sredinu. Tim postupkom se vrši i utvrđivanje i predlaganje mera kojima se štetni uticaji mogu sprečiti, smanjiti ili otkloniti, imajući u vidu izvodljivost i ekonomsku prihvatljivost projekta pod tim uslovima [4]. Cilj procene uticaja je utvrđivanje, opisivanje i vrednovanje neposrednih i posrednih uticaja na: život i zdravlje ljudi, floru i faunu; zemljište, vode, vazduh, klimu i pejzaž; materijalna i kulturna dobra, kao i uzajamno delovanje navedenih činilaca.

Australijska agencija za zaštitu životne sredine (EPA Victoria) je razvila smernice kako započeti procenu rizika za površinske vode, tj. „Vodič za procenu rizika

Prepiska: V.Ž. Pešić, Univerzitet u Novom Sadu, Prirodno–matematički fakultet, Departman za hemiju, biohemiju i zaštitu životne sredine, Trg Dositeja Obradovića 3, 21000 Novi Sad, Srbija.

E-pošta: vesna.pesic@dh.uns.ac.rs

Rad primljen: 4. februar, 2014

Rad prihvaćen: 15. april, 2014

ispuštanja otpadnih voda u površinske vode“ kako bi obezbedila pomoć onima koji sprovode postupak procene rizika ispuštanja otpadnih voda [5]. Ovaj vodič obezbeđuje okvirne smernice za procenu rizika i smernice za njegovu implementaciju donesenih odluka. Zasnovan je na trenutno prihvaćenim nacionalnim i internacionalnim strategijama procene rizika i omogućava da se svi potencijalni rizici mogu identifikovati i proceniti. Postoje tri glavne faze u procesu procene rizika: formulacija problema, analiza rizika i karakterizacija rizika [6]. Kroz prvu fazu se određuje cilj i opseg procene rizika kao i način upravljanja informacijama ukoliko je potrebno, a uključuje i razvoj konceptualnog modela sistema životne sredine, sistema ispuštanja otpadne vode kao i interakcija između njih. Analizom rizika se određuje verovatnoća i veličina neželjenog efekta sa specifičnim posledicama. Završna faza, karakterizacija rizika, predstavlja ocenjivanje i izveštavanje o formulaciji problema i rezultatima analize rizika kako bi se uspešno donele odluke i za svrhu upravljanja rizikom. Osnovu u procesima upravljanja vodnim ekosistemima predstavlja matematičko modelovanje i da bi se ono uspešno moglo sprovesti neophodno je dobro poznavanje uslova koji vladaju u njima, tj. obuhvata hemijske, hidrodinamičke, biološke i druge procese.

Odluka da se sprovede procena uticaja u većini slučajeva treba da potekne od industrije ili preduzeća koje je odgovorno za ispuštanje otpadne vode. Potreba procene uticaja ispuštanja otpadnih voda na površinske vode zavisi od osetljivosti vodnih tela na zagađivače i od samih pritisaka zagađivanja [7].

Kao konceptualna osnova za analizu pritisaka i uticaja, a koji uvažava složenost interakcija u životnoj sredini i pruža sredstvo za njihovo analiziranje, predstavlja analitički okvir “Vodeća sila/aktivnost relevantna za životnu sredinu, Pritisak, Stanje, Uticaj, Odgovor” (eng. “*Driver, Pressure, State, Impact, Response*”). Analiza pritisaka i uticaja je jedna od ključnih faza u izradi plana upravljanja rečnim slivom. Vodeće sile rezultuju pritiscima (emisiji polutanata) koji utiču na stanje životne sredine i koji mogu uticati na ljudsko zdravlje ili ekosisteme [8]. Odgovori (regulatori) imenuju vodeće sile da redukuju njihov direktni pritisak ili indirektni efekat na stanje životne sredine i ljudsko zdravlje (slika 1).

DPSIR analitički okvir za analizu antropogenih pritisaka, procenu uticaja i preliminarnu procenu rizika ne postizanja „dobrog statusa“ površinskih voda u planiranom vremenskom periodu se zasniva na kombinovanom korišćenju raspoloživih podataka o izvorima pritisaka, o samim pritiscima, stanju vodnih tela (u pogledu hemijskih karakteristika), propisa o zaštiti voda i životne sredine, kao i procena značajnih pritisaka i procena rizika. Kao varijanta prethodnog modela razvijen je koncept „DPCER“, tako što je stanje (S) protumačeno kao hemijski status vodnog tela (C), a uticaj (I) kao ekološki status (E). Procena verovatnoće da vodno telo neće postići dobar hemijski i ekološki status vrši se na osnovu poređenja hemijskog (C) i/ili ekološkog (E) statusa i graničnih vrednosti odabranih bioloških, hemijskih i fizičkih indikatora [9,10].

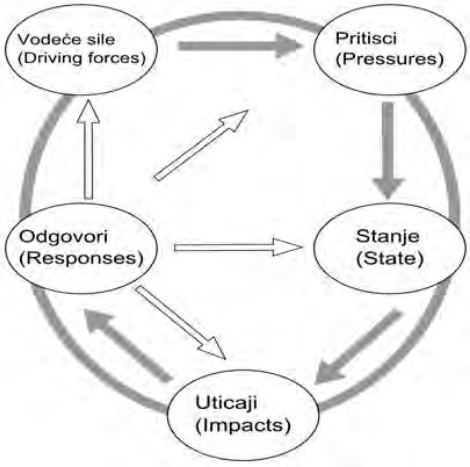

Slika 1. Ilustracija DPSIR okvira u analizi pritisaka i uticaja.
Figure 1. Illustration of DPSIR framework in the analysis of pressures and impacts.

Analiza rizika predstavlja određivanje verovatnoće i veličine dešavanja negativnih efekata sa specifičnim posledicama u vodama u određenom vremenskom periodu. Analiza rizika koristi prethodno razvijene modele i plan analize kako bi se odredio rizik. Da bi se izvršila procena rizika, neophodno je analizirati interakcije između pritisaka i vodnog tela, kako bi se utvrdilo kako te interakcije mogu uticati na ekološke uslove za postizanje dobrog kvaliteta vode [11]. Pri tome je svakako vašno uzeti u obzir veličinu pritisaka, ali i njihove kumulativne efekte, kao i osetljivost vodnih tela na pritiske [12].

Informacije koje se dobijaju tokom procene uticaja su naročito korisne donosiocima odluka i osobama koje upravljaju rizikom, jer oni moraju da ocene dobrobiti, pregledaju alternativna rešenja, uporede ili prioritizuju rizike, ocene najisplativije metode za postizanje maksimalne dobiti po okolinu ili da odrede do koje mere se uticaji po okolinu moraju smanjiti da bi se postigao željeni cilj.

Upravljanje rizikom kombinuje informacije i posledice procene uticaja sa socijalnim, pravnim, ekonomskim, političkim ili faktorima okoline u proceni opcija za upravljanje rizikom. Gde je to pogodno, može doći do dopune procesa procene uticaja sa novim podacima koji su dobijeni monitoringom i na taj način se povećava tačnost procesa procene uticaja.

U ovom radu je izvršena karakterizacija vode kanala DTD Bečej–Bogojevo i procena uticaja ispuštanja otpadnih voda.

EKSPERIMENTALNI DEO

Opis kanala DTD Bečej–Bogojevo

Kanal DTD Bečej–Bogojevo predstavlja glavni magistralni plovni put Bačke. Ulaz iz Tise nalazi se kod Bečeja na novoj bečejskoj prevodnici, a iz Dunava na prevodnici Bogojevo (slika 2). Vreme prevođenja zavisi od vodostaja Tise i Dunava, a ulazi u obe prevodnice su upravni na tok reke, što otežava manevar uplovljavanja. Pored dve sporedne, kanal ima samo jednu unutrašnju prevodnicu u Kucuri sa trajanjem prevođenja oko pola sata. Kanal povezuje 15 naseljenih mesta od kojih su kao pristaništa i pretovarna mesta značajni Bečej, Srbobran, Vrbas, Bačko Gradište i Ruski Krstur. Dug je 91,4 km.

Slika 2. Položaj kanala DTD Bečej-Bogojevo i mesta uzorkovanja.
Figure 2. The position of the channel DTD Novalja–Bogojevo and sampling.

Prema Pravilniku o utvrđivanju vodnih tela površinskih i podzemnih voda [13] kanal DTD Bečej–Bogojevo se celom svojom dužinom kategoriše kao veštačko vodno telo.

Metode uzorkovanja i analize vode

Kako bi se dobili podaci o izvorima zagađenja/pritisaka izvršeno je uzorkovanje i analiza otpadnih vode koje se ispuštaju u pomenuti kanal, ali i uzorkovanje i analiza vode kanala na više lokaliteta. Mesta uzorkovanja i analize vode kanala su odabrana tako da obuhvataju lokacije uzvodno i nizvodno od mesta ispuštanja polutanata, i na taj način se uzimaju u obzir različiti potencijalni izvori zagađenja površinske vode. Na slici 2 su označena mesta uzorkovanja vode kanala: 1 – CS Bogojevo, 2 – uzvodno od ustave Kucura, 3 – nizvodno od triangla (Vrbasa), 4 – uzvodno od uliva Krivaje (Srbobrana), 5 – nizvodno od uliva Krivaje (Srbobrana) i 6 – nizvodno od Bečeja. Uzorkovanje otpadne vode vršeno je prema smernicama za uzimanje uzoraka otpadnih voda SRPS ISO 5667-10:2007. Uzimani su dvočasovni kompozitni uzorci (sadržaj dobijen mešavinom sadržaja zahvaćenih svakih 15 min u toku 2 h). Površinske vode su uzorkovane prema standardnoj proceduri SRPS ISO 5667-4:1997. Svi uzorci su konzervisani i transportovani u laboratoriju prema smernicama za zaštitu i rukovanje uzorcima vode SRPS ISO 5667-3, gde je izvršena analiza otpadne vode na ispitivane parametre. Korišćene metode za analizu su prikazane u tabeli 1.

Tabela 1. Metode analize fizičko–hemijskih parametara
Table 1. Methods for the analysis of physical-chemical parameters

Parametar	Referenca metode	Opis metode
HPK	SRPS ISO 6060:1994	Dihromatna metoda – titrimetrijski
BPK_5	H1.002	Manometarska metoda, po uputstvu proizvođača
TOC	SRPS ISO 8245:2007	Sagorevanjem i IR
Hloridi	SRPS ISO 9297:1997	Argentometrijska titracija
Sulfati	P-V-44/A	Titrimetrijski
Amonijum	SRPS ISO H.Z1.184:1974	Spektrofotometrijski sa Nessler reagensom
Nitrati	SRPS ISO 7890-3:1994	Spektrofotometrijski sa sulfosalicilnom kiselinom
Nitriti	SRPS EN 26777:2009	Spektrofotometrijski
Ortofosfati	SRPS EN ISO 6878:2008	Spektrofotometrijski
Ukupan fosfor	SRPS EN ISO 6878:2008	Nakon digestije sa amonijum-persulfatom spektrofotometrijski
Rastvoreni kiseonik	SRPS EN 25814:2009	Elektrohemijski
pH	SRPS H.Z1.111:1987	Elektrohemijski
Elektroprovodljivost	SRPS EN 27888:1993	Konduktometrijski
Metali	EPA 7010/ EPA 7000b	Atomsko-apsorpciona spektrofotometrija

Procena uticaja je izvršena na osnovu rezultata monitoringa otpadnih voda i vode kanala u periodu 2012–2013. godina. Vrednosti fizičko-hemijskih pokazatelja prikazane u rezultatima ovog rada su srednje vrednosti na godišnjem nivou. U metodologiji procene uticaja zasnovane na riziku, kao kriterijumi su uzeti standardi za dobar hemijski kvalitet vode. Koncentracije polutanata određene na tačkama uzorkovanja su upoređene sa standardima kvaliteta i nakon toga su izračunati specifični količnik rizika za površinske vode (*SKR*) za svaku tačku/deonicu na kojoj je vršeno uzorkovanje [14]:

$$SKR = \frac{c}{SKV}$$

c –koncentracija polutanta u površinskoj vodi na mestu uzorkovanja; *SKV* – standardi kvaliteta životne sredine za polutante, uspostavljeni kako bi se procenio dobar hemijski status površinske vode.

Nakon toga izračunati su integrisani indeksi rizika (*IR*) za svaku lokaciju/deonicu na kojoj se vršilo uzorkovanje sumiranjem polutant specifičnih *SKR* vrednosti:

$$IR = \sum_{i=1}^{n} SKR_i$$

n – broj polutanata.

Na osnovu izračunatih *IR* vrednosti je izvršeno određivanje delova kanala sa najgorim kvalitetom i izračunavanje doprinosa svakog polutanta zasebno ukupnoj vrednosti indeksa rizika na svakoj lokaciji uzorkovanja. Na osnovu izračunatih SKR vrednosti izvršena je kategorizacija polutanata prema prioritetu.

REZULTATI I DISKUSIJA

Proces procene uticaja, tj. analize pritisaka i uticaja je obuhvatio identifikaciju i karakterizaciju izvora pritisaka, analizu značajnih pritisaka, procenu uticaja i procenu rizika. U tu svrhu, pored rezultata merenja u Laboratoriji za hemijska ispitivanja životne sredine, PMF, Novi Sad, korišćeni su podaci o pritiscima/zagađivačima iz aktuelnog katastra zagađivača (JVP "Vode Vojvodine").

Identifikacija i karakterizacija pritisaka zagađenja na kanalu

U kanal DTD Bečej–Bogojevo se direktno ili indirektno ispuštaju komunalne i industrijske otpadne vode iz Odžaka, Vrbasa, Srbobrana, Bačkog Gradišta i Bečeja. Pored toga, na slivu kanala DTD Bečej–Bogojevo je locirano i nekoliko manjih naselja, koji takođe spadaju u koncentrisane izvore zagađivanja, a koja nemaju izgrađenu kanalizaciju. Koncentrisani izvori zagađenja koji su odgovorni za zagađivanje kanala DTD Bečej–Bogojevo su prikazani u tabeli 2. Registrovano je ukupno 11 zagađivača koji svoje otpadne vode ispuštaju direktno ili indirektno (putem lateralnih kanala) u kanal DTD Bečej–Bogojevo. Prema šifarniku vodotokova kanal DTD Bečej–Bogojevo je podeljen na 11 deonica, od čega su na 4 deonice registrovani koncentrisani zagađivači.

Tabela 2. Identifikacija koncentrisanih izvora zagađenja na kanalu DTD Bečej–Bogojevo
Table 2. Identification of point sources of pollution in the DTD Bečej–Bogojevo

Naziv zagađivača	Delatnost	Deonica kanala DTD Bečej-Bogojevo	Prečišćavanje otpadnih voda
AD HI „Hipol" Odžaci	Hemijska industrija	Odžaci (ustava) – DTD Kosančić–Mali Stapar	Sekundarno
JKP „Usluga" Odžaci	Komunalna	Odžaci (ustava) – DTD Kosančić–Mali Stapar	Bez prečišćavanja
ITES "Lola Ribar" AD Odžaci	Proizvodnja prediva i tkanina	Odžaci (ustava) – DTD Kosančić–Mali Stapar	Primarno
JKP Standard Vrbas	Komunalna	Kucura – DTD Vrbas–Bezdan	Bez prečišćavanja
Reahem DOO Pogon za preradu alkohola, Srbobran	Prehrambena	DTD Vrbas––Bezdan – Krivaja	Primarno
JKP Graditelj Srbobran	Komunalna	DTD Vrbas––Bezdan – Krivaja	Bez prečišćavanja
JKP Vodokanal Bečej	Komunalna	Krivaja – HČ Bečej	Sekundarno
PIK Bečej, RJ Flora	Prehrambena	Krivaja – HČ Bečej	Bez prečišćavanja
DOO Fadip Bečej	Proizvodnja pogonskih mašina	Krivaja – HČ Bečej	Bez prečišćavanja
DD Remont	Popravka vozila na motorni pogon	Krivaja – HČ Bečej	Bez prečišćavanja
AD Bag-Deko Bačko Gradište	Prehrambena	Krivaja – HČ Bečej	Primarno

Na osnovu rezultata fizičko-hemijskih analiza otpadnih voda i podataka o količinama ispuštenih voda proračunate su količine zagađujućih materija (opterećenja) otpadnih voda koje se ispuštaju u kanal na dnevnom nivou (tabela 3). Najveći zagađivač na kanalu DTD Bečej–Bogojevo predstavljaju komunalne otpadne vode Vrbasa i Bečeja. Ove komunalne otpadne vode sadrže najveću količinu zagađenja, kako u pogledu sadržaja

organskih materija tako i u pogledu sadržaja nutrijenata.

Da bi se utvrdilo koja delatnost zagađivača emituje najveće opterećenje otpadnih voda, zagađivači su razvrstani po delatnostima i prikazana sumarna opterećenja otpadnih voda. Komunalne otpadne vode predstavljaju vodeću silu, tj. aktivnost relevantnu za životnu sredinu na kanalu DTD Bečej–Bogojevo, jer preko 80% ukupnog zagađenja potiče od komunalnih otpadnih voda (slika 3, 80% količine otpadnih voda, 90% organske materije (HPK, BPK) i čak 95% nutrijenata).

Deonica kanala koja je najviše opterećena komunalnim otpadnim vodama je Krivaja – HČ Bečej (od zagađivača lociranih u Bečeju) a zatim deonica Kucura – DTD Vrbas–Bezdan (od zagađivača iz Vrbasa, tabela 4). Ovde svakako treba uzeti u obzir kumulativni efekat uticaja ovih voda iz razloga što su mala rastojanja između mesta ispuštanja duž kanala.

Analiza značajnih pritisaka

Granične vrednosti za utvrđivanje značaja izvora zagađenja su zasnovane na kvantitativnom i kvalitativnom sadržaju polutanata u otpadnim vodama, a na osnovu Uredbe o graničnim vrednostima emisije zagađujućih materija u vode i rokovima za njihovo dostizanje (za komunalne otpadne vode) [15], Direktive koja se odnosi na integrisanu prevenciju i kontrolu zagađenja [16], Zakona o integrisanom sprečavanju i kontroli zagađenja [17], Evropskog registra emisije zagađenja [18] i strateškog dokumenta Nemačke državne radne grupe za vodu (LAWA) [8] (za industrijske otpadne vode), a svakako i preporukama Inter-

Tabela 3. Opterećenja otpadnih voda razvrstana prema zagađivaču
Table 3. Wastewater load divided by the polluter

Zagađivač/deonica	Količina vode m^3/dan	Suspendovane materije, kg/dan	HPK kg/dan	BPK kg/dan	Azot kg/dan	Fosfor kg/dan
AD HI „Hipol“ Odžaci	389	4,3	11,7	4,6	0,26	0,17
JKP „Usluga“ Odžaci	650	6,7	5,9	2	16	1,6
ITES „Lola Ribar“ Odžaci	25	9,5	6	2,7	0,5	0,07
Deonica Odžaci (ustava) – DTD Kosančić–Mali Stapar	1064	20,5	23,6	9,3	16,8	1,84
JKP Standard Vrbas	2500	180	1071	590	171	12
Deonica Kucura – DTD Vrbas–Bezdan	2500	180	1071	590	171	12
Reahem DOO, Srbobran	60	13,4	10,2	3,84	1	0,11
JKP Graditelj Srbobran	85	11	5,1	3,1	3,5	0,37
Deonica DTD Vrbas-Bezdan – Krivaja	145	24,4	15,3	6,94	4,5	0,48
JKP Vodokanal Bečej	1960	40	187	94	58	3,8
PIK Bečej, RJ Flora	504	14	53	24	8,4	0,41
DOO Fadip Bečej	50	0,83	1,7	0,81	1,52	0,01
DD Remont Bečej	10	0,34	0,33	0,12	0,04	0,002
AD Bag-Deko B. Gradište	248	2	59	35	0,73	0,25
Deonica Krivaja – HČ Bečej	2772	57,2	301	154	68,7	4,5
Ukupno	**6481**	**282**	**1411**	**760**	**261**	**19**

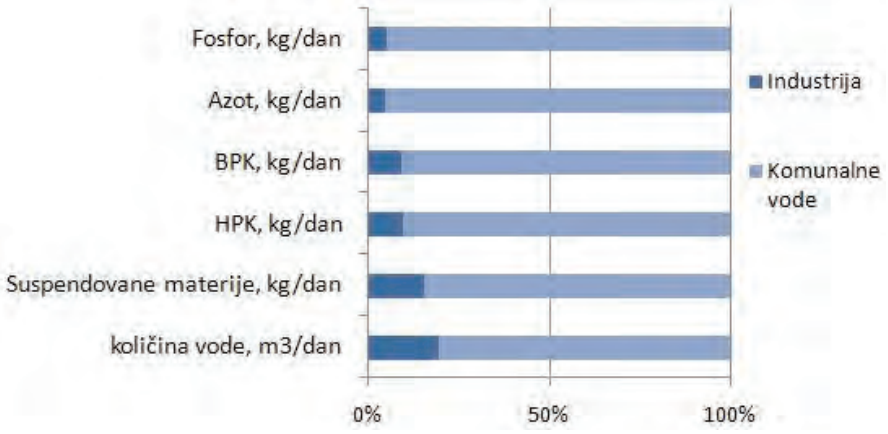

Slika 3. Prikaz opterećenja otpadnih voda prema delatnostima.
Figure 3. Showing loads of waste water by industries.

Tabela 4. Opterećenja komunalnih otpadnih voda po deonicama kanala DTD Bečej-Bogojevo
Table 4. Loads of municipal wastewater per channel sections DTD Becej-Bogojevo

Zagađivač/deonica	Količina vode m^3/dan	Suspendovane materije, kg/dan	HPK kg/dan	BPK kg/dan	Azot kg/dan	Fosfor kg/dan
Odžaci (ustava) – DTD Kosančić–Mali Stapar	650	6,7	5,9	5,9	16	1,6
Kucura – DTD Vrbas-Bezdan	2500	180	1071	590	171	12
DTD Vrbas-Bezdan – Krivaja	85	11	5,1	3,1	3,5	0,37
Krivaja – HČ Bečej	1960	40	187	94	58	3,8

nacionalne komisije za zaštitu reke Dunav (ICPDR) [19]. Za procenu značaja pritisaka kao kriterijumi koriste se granične vrednosti indikatora organskog zagađenja, nutrijenata i opasnih materija. To su vrednosti za koje se smatra da usled uticaja pritiska mogu da dovedu u pitanje ispunjenje ciljeva postizanja dobrog kvaliteta vode.

Kada su u pitanju komunalne otpadne vode, u svim analiziranim otpadnim vodama koje potiču iz četiri naseljena mesta, ustanovljeno je prekoračenje za većinu parametara (tabela 5). Sve ove otpadne vode se bez prečišćavanja ili uz nedovoljan tretman ispuštaju u kanal. Najveća odstupanja u pogledu kvaliteta komunalnih otpadnih voda su kod voda koje potiču iz Vrbasa. Pored toga, komunalne otpadne vode Srbobrana i Bečeja prekoračuju pomenute kriterijume po većini parametara. Na osnovu dobijenih rezultata može se reći da sve komunalne otpadne vode predstavljaju značajan pritisak na recipijent u koji se ulivaju.

Prema kriterijumima za industrijske otpadne vode, nijedno industrijsko postrojenje ne predstavlja značajan pritisak na recipijent, pošto su emitovana opterećenja manja od kriterijuma (tabela 6). Međutim, pritisci iz pojedinih izvora ne deluju nezavisno već imaju kumulativno dejstvo na konkretno vodno telo i tada se pritisci integrišu. Ali i kada bi se ove vrednosti integrisale, ne bi bilo prekoračenja kriterijuma.

Pored toga, koncentracije pokazatelja kvaliteta su upoređivane sa Uredbom o graničnim vrednostima emisije [15], da bi se utvrdilo u kojoj meri postoji ispunjenost propisanih vrednosti (tabela 7). Otpadne vode pomenutih zagađivača se ispuštaju nedovoljno prečišćene, nijedan zagađivač nema tercijaran tretman a samo dva od jedanaest zagađivača imaju sekundaran tretman. Ustanovljeno je da postoje prekoračenja propisanih zahtevanih vrednosti u 53% slučajeva.

Procena uticaja na osnovu monitoringa recipijenta

Izmerene vrednosti parametara zagađujućih materija u kanalu DTD Bečej–Bogojevo su upoređivane sa vrednostima koje propisuje Pravilnik o parametrima ekološkog i hemijskog statusa površinskih voda i para-

Tabela 5. Kriterijumi značaja pritiska za komunalne vode
Table 5. Criteria of relevant pressure for water utilities

Parametar	JKP Odžaci	JKP Vrbas	JKP Srbobran	JKP Bečej	Značajan izvor ako je:
BPK, mgO_2/l	0	230	36	47	> 25 mgO_2/l
HPK, mgO_2/l	9	417	60	94	> 125 mgO_2/l
Ukupan azot, mgN/l	25	67	41	29	> 10 mgN/l
Ukupan fosfor, mgP/l	2,5	4,5	4,4	2	> 1 mgP/l
Suspendovane materije, mg/l	10	70	127	20	> 35 mg/l

Tabela 6. Kriterijumi značaja pritiska za industrijske otpadne vode
Table 6. Criteria relevant pressure for industrial wastewater

Parametar	Hipol Odžaci	ITES Odžaci	Reahem Srbobran	Flora Bečej	Fadip Bečej	Remont Bečej	Bag-deko B. Gradište	Značajan izvor ako je:
HPK, t/dan	0,0004	0,09	0,04	0,002	0,001	0,001	0,007	> 2 t/dan
Arsen, kg/god	–	–	–	–	–	–	–	> 5 kg/god
Kadmijum, kg/god	–	–	–	–	–	–	–	> 5 kg/god
Hrom, kg/god	–	–	–	–	–	–	–	> 50 kg/god
Bakar, kg/god	–	–	–	–	0,002	–	–	> 50 kg/god
Nikl, kg/god	–	–	–	–	0,001	–	–	> 20 kg/god
Olovo, kg/god	–	–	–	–	0,002	–	–	> 20 kg/god
Cink, kg/god	–	–	–	–	0,067	–	–	> 100 kg/god
Živa, kg/god	–	–	–	–	–	–	–	> 1 kg/god

Tabela 7. Poređenje izmerenih koncentracija zagađujućih materija u otpadnim vodama sa propisanim vrednostima (X – prekoračeni kriterijumi, ✓ – zadovoljeni kriterijumi)
Table 7. Comparison of measured concentrations of pollutants in wastewater with prescribed values (X – exceeded criteria, ✓ – met criteria)

Zagađivač	HPK, mgO_2/l	BPK, mgO_2/l	Azot, mgN/l	Fosfor, mgP/l	Suspendovane materije, mg/l
AD HI „Hipol“ Odžaci	✓	✓	✓	✓	✓
JKP „Usluga“ Odžaci	✓	✓	X	X	✓
ITES „Lola Riba“ Odžaci	X	X	X	X	X
JKP Standard Vrbas	X	X	X	X	X
Reahem DOO, Srbobran	X	X	X	✓	X
JKP Graditelj Srbobran	✓	X	X	X	X
JKP Vodokanal Bečej	✓	X	X	✓	✓
PIK Bečej, RJ Flora	✓	X	X	✓	✓
DOO Fadip Bečej	✓	✓	X	✓	✓
DD Remont Bečej	✓	✓	✓	✓	X
AD Bag-Deko Bač.Gradište	X	X	✓	X	✓

metrima hemijskog i kvantitativnog statusa podzemnih voda [20], Uredba o graničnim vrednostima zagađujućih materija u površinskim i podzemnim vodama i sedimentu i rokovima za njihovo dostizanje [21] i Uredba o graničnim vrednostima prioritetnih i prioritetnih hazardnih supstanci koje zagađuju površinske vode i rokovima za njihovo dostizanje [22] i prikazane su u tabeli 8. Kanal DTD Bečej – Bogojevo je veštačko vodno telo za koje se utvrđuje ekološki potencijal, ali se kanal DTD Bečej–Bogojevo uliva u Tisu, kod koje treba biti postignut dobar status, te su iz tog razloga merene vrednosti upoređivane sa vrednostima koje propisuju pomenuta tri pravilnika/uredbe.

Najuzvodnija lokacija (deonica) CS Bogojevo je zadovoljavajućeg kvaliteta vode. Ovaj kvalitet vode odgovara kvalitetu Dunava i nije ugrožen s obzirom da na datoj deonici nema registrovanih koncentrisanih zagađivača. Na ostalim ispitivanim lokacijama uzorkovanja i merenja postoje prekoračenja bar jednog pokazatelja kvaliteta u odnosu na vrednosti koje su propisane za dobar potencijal/status voda. To znači da je kvalitet vode kanala DTD Bečej–Bogojevo takav da ne odgovara II klasi, tj. dobrom potencijalu/statusu voda. Najviše pokazatelja kvaliteta koji odstupaju od zahtevanog su na lokacijama nizvodno od triangla i nizvodno od Bečeja, tj. na deonicama DTD Vrbas-Bezdan – Krivaja i Krivaja – HČ Bečej. Triangl je mesto uliva kanala DTD Vrbas-Bezdan u DTD Bečej-Bogojevo. Kvalitet kanala DTD Vrbas-Bezdan je veoma loš, jer je ovaj kanal recipijent velike količine nedovoljno prečišćenih otpadnih voda Vrbasa, Kule, Crvenke [23,24]. Stoga i on sam predstavlja značajan pritisak na ispitivani kanal. Na osnovu rezultata merenja pokazatelja kvaliteta vode kanala DTD Bečej–Bogojevo, njen nezadovoljavajući kvalitet na pomenutim deonicama posledica je ispuštanja visoko opterećenih otpadnih voda Vrbasa i Bečeja (pre svega komunalnih otpadnih voda).

Specifični količnik rizika

Na osnovu izmerenih koncentracija izračunat je specifični količnik rizika za površinske vode (SKR) na svakoj deonici kao i indeks rizika (IR) i prikazani u tabeli 9.

Kriterijumi za specifični količnik rizika propisuju da polutanti koji prelaze maksimalne dozvoljene koncentracije, date u domaćoj zakonskoj regulativi [20–22], manje od deset puta se svrstavaju u kategoriju polutanata srednjeg prioriteta a ukoliko prelaze više od deset puta svrstavaju se u kategoriju polutanata visokog prioriteta. Na osnovu dobijenih rezultata i izračunatih specifičnih količnika rizika, dolazi se do zaključka da se većina analiziranih parametara mogu svrstati u kategoriju srednjeg rizika. Ni jedan od analiziranih polutanata nije prevazišao MDK više od deset puta ni na jednoj od lokacija na kojima je vršeno uzorkovanje. Na svakoj lokaciji postoji manji ili veći broj polutanata srednjeg rizika, osim na najuzvodnijoj lokaciji (CS Bogojevo). Od svih izračunatih specifičnih količnika rizika, 33% su veći od 1 i time se svrstavaju u kategoriju polutanata srednjeg rizika.

Na slici 4 je grafički prikazan odnos izračunatih indeksa rizika prema lokacijama uzorkovanja na kanalu. Najveći indeks rizika je za delove kanala nizvodno od triangla i nizvodno od Bečeja, tj. deonice kanala DTD Vrbas-Bezdan – Krivaja i Krivaja – HČ Bečej. S obzirom na to da veći indeks rizika znači i lošiji kvalitet vode, ovi delovi kanala su i najlošijeg kvaliteta. Iz dobijenih rezultata se vidi da nijedan od parametara sa liste prioritetnih supstanci nema specifični količnik rizika veći od 1. Međutim, u ovom slučaju drugi parametri imaju više vrednosti specifičnih količnika rizika i iz tog razloga je potrebno uzeti u obzir i duge parametre, iako nisu prioritetne supstance. Parametri koji intenzivno doprinose visokom indeksu rizika su HPK, BPK, ukupan organski ugljenik, amonijum jon, fosfor i ortofosfati. Ovi pokazatelji su svakako bitni jer izazivaju niz direktnih nega-

Tabela 8. Vrednosti parametara zagađujućih materija upoređene sa propisanim vrednostima
Table 8. The values of the parameters of pollutants compared with the standard values

Parametar	Deonica kanala						MDK za II klasu (dobar potencijal)
	Dunav – prevodnica Bogojevo	DTD N.Sad-Savino Selo – Kucura	DTD Vrbas-Bezdan - Krivaja		Krivaja – HČ Bečej		
	Lokacija uzorkovanja						
	CS Bogojevo	Uzvodno od ustave Kucura	Nizvodno od triangla (uzvodno od Srbobrana)	Uzvodno od uliva Krivaje	Nizvodno od uliva Krivaje	Nizvodno od Bečeja	
pH	8,30	8,2	7,7	7,9	7,9	8,71	6,5-8,5[a]
Rastvoreni kiseonik, mgO_2/l	10,3	7,2	4	3,5	7,3	6,30	>5,0[a]
BPK_5, mgO_2/l	<4	9	16,7	12,3	7	8	6,0[a]
TOC, mg/l	1,1	3,4	4,1	4,2	4,6	7,1	7,0[a]
Hloridi, mg/l	14	18	20	18,7	21	60	50[a]
Amonijum, mgN/l	0,02	0,2	0,6	0,6	0,5	0,40	0,2[a]
Nitrati, mgN/l	0,71	0,2	0,1	0,2	0,05	0,57	3,0[a]
Ortofosfati, mgP/l	0,01	0,2	0,9	0,2	0,3	0,37	0,2[a]
Ukupan fosfor, mgP/l	0,12	0,2	1,1	0,3	0,3	0,44	0,3[a]
HPK, mgO_2/l	<16	22	40	36	21	37	15[b]
Nitriti, mgN/l	0,01	0,02	0,03	0,03	0,04	0,09	0,03[b]
Ukupan azot, mgN/l	1,2	1,9	0,2	1,4	0,9	1,22	2[b]
Gvožđe, mg/l	<0,07	0,5	0,4	0,2	0,2	0,14	0,5[b]
Mangan, mg/l	0,02	0,1	0,1	0,1	0,2	0,1	0,1[b]
Cink, mg/l	0,02	0,1	0,1	0,04	0,03	0,02	1[b]
Hrom, µg/l	<0,44	4,8	100	5,6	0,9	< 0,44	50[b]
Bakar, µg/l	2,1	8	5,5	4,8	15,4	0,5	40[b]
Arsen, µg/l	3,1	5,7	5,3	4,6	5,2	3,9	10[b]
Nikal, µg/l	1,1	13	6,7	2,1	7,7	<1,09	20[c]
Kadmijum, µg/l	<0,15	0,3	0,5	0,3	0,2	<0,15	0,6[c]
Olovo, µg/l	<2,92	4,2	2,9	2,9	2,9	<2,92	7,2[c]

[a]Pravilnik o parametrima ekološkog i hemijskog statusa površinskih voda [20]; [b]Uredba o graničnim vrednostima za površinske vode [21]; [c]Uredba o graničnim vrednostima prioritetnih i prioritetnih hazardnih supstanci [22]

Tabela 9. Specifični količnik rizika za površinske vode (SKR)
Table 9. The specific ratio of risk to surface water (SKR)

Parametar	Dunav – Prevodnica Bogojevo	DTD N.Sad-Savino Selo – Kucura	DTD Vrbas-Bezdan – Krivaja		Krivaja – HČ Bečej	
	CS Bogojevo	Uzvodno od ustave Kucura	Nizvodno od triangla (uzvodno od Srbobrana)	Uzvodno od uliva Krivaje	Nizvodno od uliva Krivaje (Turija kod mosta)	Nizvodno od Bečeja
Rastvoreni kiseonik, mgO_2/l	0,49	0,69	1,25	1,43	0,68	0,79
BPK_5, mgO_2/l	0	1,50	2,78	2,05	1,17	1,33
TOC, mg/l	0,16	0,49	0,59	0,60	0,66	1,01
Hloridi, mg/l	0,28	0,36	0,40	0,37	0,42	1,20
Amonijum, mgN/l	0,10	1,00	3,00	3,00	2,50	2,00
Nitrati, mgN/l	0,24	0,07	0,03	0,07	0,02	0,19
Ortofosfati, mgP/l	0,05	1,00	4,50	1,00	1,50	1,85
Ukupan fosfor, mgP/l	0,40	0,67	3,67	1,00	1,00	1,47
HPK, mgO_2/l	0	1,47	2,67	2,40	1,40	2,47
Nitriti, mgN/l	0,33	0,67	1,00	1,00	1,33	3,00

Tabela 9. Nastavak
Table 9. Continued

Parametar	Dunav – Prevodnica Bogojevo	DTD N.Sad-Savino Selo – Kucura	DTD Vrbas-Bezdan – Krivaja		Krivaja – HČ Bečej	
	CS Bogojevo	Uzvodno od ustave Kucura	Nizvodno od triangla (uzvodno od Srbobrana)	Uzvodno od uliva Krivaje	Nizvodno od uliva Krivaje (Turija kod mosta)	Nizvodno od Bečeja
Ukupan azot, mgN/l	0,60	0,95	0,10	0,70	0,45	0,61
Gvožđe, mg/l	0	1,00	0,80	0,40	0,40	0,28
Mangan, mg/l	0,20	1,00	1,00	1,00	2,00	1,00
Cink, mg/l	0,02	0,10	0,10	0,04	0,03	0,02
Hrom, µg/l	0	0,10	2,00	0,11	0,02	0,00
Bakar, µg/l	0,05	0,20	0,14	0,12	0,39	0,01
Arsen, µg/l	0,31	0,57	0,53	0,46	0,52	0,39
Nikal, µg/l	0,06	0,65	0,34	0,11	0,39	0
Kadmijum, µg/l	0	0,50	0,83	0,50	0,33	0
Olovo, µg/l	0	0,58	0,40	0,40	0,40	0
IR	3,28	13,6	26,1	16,8	15,6	17,6

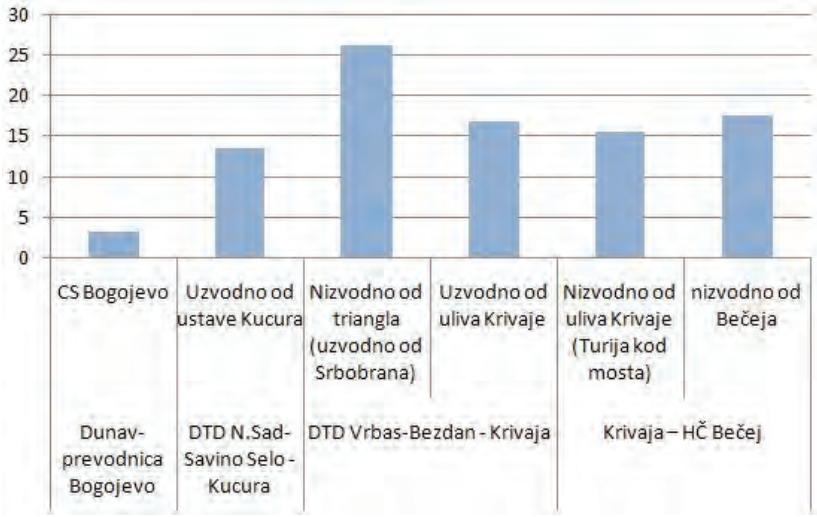

Slika 4. Indeks rizika za analizirane polutante prema lokaciji na kojoj su uzorkovani.
Figure 4. The risk index for analyzing pollutants according to the location where they have been sampled.

tivnih efekata u recipijentu (smanjenje koncentracije rastvorenog kiseonika, eutrofikaciju).

Procena rizika na osnovu rezultata monitoringa ukazuje da je vodno telo DTD Bečej–Bogojevo pod rizikom od nepostizanja dobrog kvaliteta (ekološkog potencijala), iz razloga što većina izmerenih vrednosti koncentracija prekoračuju propisane granične vrednosti.

ZAKLJUČAK

Cilj rada je bio da se utvrdi uticaj ispuštanja otpadnih voda na kanal DTD Bečej–Bogojevo. Procena uticaja je izvršena na osnovu podataka o otpadnim vodama zagađivača koji ispuštaju vode u kanal DTD Bečej–-Bogojevo direktno ili indirektno i podataka o monitoringu vode kanala.

Najveći broj zagađivača je lociran u velikim gradovima koji su pored kanala DTD Bečej–Bogojevo (Odžaci, Vrbas, Srbobran i Bečej). Putem otpadnih voda se u kanal DTD Bečej–Bogojevo dnevno ispusti 1,4 t HPK, 0,8 t BPK, 260 kg azota, 19 kg fosfora i 282 kg suspendovanih materija. Prema podacima o opterećenju otpadnih voda može se videti da su najveći zagađivači Vrbas i Bečej. Ovo zagađenje je vrlo koncentrisano, tj. potiče sa svega par kilometara udaljenosti duž kanala, što je naročito pogoršano zbog toga što je protok vode u kanalu veoma mali, tako da pojedini koncentrisani zagađivači imaju kumulativno dejstvo na recipijent. Veliki broj otpadnih voda se ispušta nedovoljno prečišćen i koncentracije zagađujućih materija ne zadovoljavaju propisane granične vrednosti emisije.

Rezultati fizičko–hemijskih analiza vode kanala DTD Bečej–Bogojevo pokazuju da je kvalitet vode kanala DTD Bečej–Bogojevo nezadovoljavajući. Prema domaćoj zakonskoj regulativi postoji prekoračenje maksimalno dozvoljenih vrednosti za II klasu vodotoka (dobar potencijal/status voda) za većinu parametara na svim lokacijama uzorkovanja (rastvoreni kiseonik, sadržaj organskih materija izražen kao BPK i nutrijenti). Najugroženije lokacije/deonice su nizvodno od Vrbasa i nizvodno od Bečeja, dok je najbolji kvalitet vode kanala na najuzvodnijoj od ispitivanih lokacija (kod CS Bogojevo).

Na osnovu dobijenih rezultata i izračunatih specifičnih količnika rizika, dolazi se do zaključka da su kod 33% analiziranih parametara izračunati specifični količnici rizika veći od 1 i time se svrstavaju u kategoriju polutanata srednjeg rizika. Ono što se još zapaža je da na svakoj lokaciji postoji manji ili veći broj polutanata srednjeg rizika, osim na najuzvodnijoj lokaciji, gde i nema registrovanih zagađivača. Najveći indeks rizika je za delove kanala nizvodno od Vrbasa i Bečeja. S obzirom na to da veliki indeks rizika znači i loš kvalitet vode, ovaj deo kanala je i najugroženiji što se tiče kvaliteta vode.

Procena rizika na osnovu rezultata monitoringa ukazuje da je vodno telo DTD Bečej–Bogojevo verovatno pod rizikom od nepostizanja zahtevanog kvaliteta vode, iz razloga što većina vrednosti prekoračuju granične vrednosti. Na ovo su ukazali i podaci o pritiscima, značajnim pritiscima iz koncentrisanih izvora i rezultati monitoringa vode kanala. S obzirom da se oko kanala nalazi pretežno poljoprivredno zemljište, pretpostavlja se da značajan doprinos ovim koncentrisanim izvorima imaju i difuzni izvori zagađivanja.

Zahvalnica

Istraživanja su finansirana od strane Ministarstva prosvete, nauke i tehnološkog razvoja (Projekat TR37004).

LITERATURA

[1] B. Dalmacija, J. Agbaba, Zagađujuće materije u vodenom ekosistemu i remedijacioni procesi. Univerzitet u Novom Sadu, Prirodno-matematički fakultet, Novi Sad, 2008.

[2] D.L. Shun, Streams and Rivers, in: Handbook of Environmental Engineering Calculations, C.C.Lee, D.L.Shun, Eds., 2nd ed., McGeaw-Hill, New York, 2007.

[3] Council Directive 2000/60/EC of 23 October 2000 establishing a framework for Community action in the field of water policy OJ L 327/1, 22.12.2000.

[4] US EPA: National Research Needs Conference Proceedings: Risk-based Decision-making for Onsite Wastewater Treatment, EPRI, Palo Alto, CA. Environmental Protection Agency and National Decentralised Water Resources Capacity Development Project: 1001446, 2001.

[5] EPA Victoria: Guideline for environmental management – Risk-based assessment of ecosystem protection in ambient waters. EPA publication 961, Australia, 2004.

[6] USEPA: Guidelines for Ecological Risk Assesment. Federal Register 63: 26846-26924, 14 May, 1998.

[7] EPA Victoria: Guidelines for risk assessment of wastewater discharges to waterways. EPA publication 1287, Australia, 2009, pp. 1–16.

[8] WFD CIS Policy Summary to Guidance Document No. 3 - Analysis of Pressures and Impacts, Luxembourg: Office for Official Publications of the European Communities, 2003.

[9] S. Rekolainen, J. Kamari, M. Hiltunen, T.M. Saloranta, A conceptual framework for identifying the need and role of models in the implementation of the Water Framework Directive, Int. J. River Basin Manage. **4** (2003) 347––352.

[10] B. Stojanović, M. Milovanović, D. Vulić, Primena „DPCER" koncepta za analizu pritisaka i uticaja na vodna tela, Zbornik radova Konferencije „VODA 2008", Srpsko društvo za zaštitu voda, Mataruška banja, 3–6. jun 2008, str. 1-4.

[11] Guidance on pressures and impacts methodology, Guidance document no.GW4, Environmental Protection Agency (EPA), Ireland, 2003.

[12] UK TAG Work Plan Task 7.a – General Principles for the Pressures and Impacts Analysis, London, 2003.

[13] Pravilnik o utvrđivanju vodnih tela površinskih i podzemnih voda, Sl. glasnik RS, 96/2010.

[14] FOKS Report, Risk-based approach to assessment of water pollution sources. Institute for Ecology of Industrial Areas, Katowice, Central Europe and European Union, 2011, pp. 12–27.

[15] Uredba o graničnim vrednostima emisije zagađujućih materija u vode i rokovima za njihovo dostizanje, Sl. glasnik RS, 67/2011.

[16] Council Directive 96/61/EC of 24 September 1996 concerning integrated pollution prevention and control.

[17] Zakon o integrisanom sprečavanju i kontroli zagađenja, Sl. glasnik RS, 135/04.

[18] Guidance document for implementation of an European pollutant emission register according to article 15 of Council Directive 96/61/EC concerning integrated pollution prevention and control (IPPC),EPER, 2000.

[19] Danube river basin roof report, ICPDR, 2005.

[20] Pravilnik o parametrima ekološkog i hemijskog statusa površinskih voda i parametrima hemijskog i kvantitativnog statusa podzemnih voda, Sl. glasnik RS, 74/2011.

[21] Uredba o graničnim vrednostima zagađujućih materija u površinskim i podzemnim vodama i sedimentu i rookvima za njihovo dostizanje, Sl. glasnik RS, 50/2012.

[22] Uredba o graničnim vrednostima prioritetnih i prioritetnih hazardnih supstance koje zagađuju površinske vode i rokovima za njihovo dostizanje, Sl. glasnik RS, 35/2011.

[23] Studija: Analiza otpadnih voda zagađivača na vodnom području JVP „Vode Vojvodine" u cilju proširenja i ažuriranja baze podataka i identifikacije vodećih sila i značajnih pritisaka na odabranim vodotocima, Nosilac pro-

jekta: B. Dalmacija, Prirodno–matematički fakultet, Novi Sad, 2013.

[24] Projekat: Monitoring kvaliteta površinskih voda u AP Vojvodini u 2013. godini, Nosilac projekta: B. Dalmacija,Prirodno–matematički fakultet, Novi Sad.

SUMMARY

IMPACT ASSESSMENT OF WASTEWATER DISCHARGE ON WATER QUALITY OF DTD CANAL BEČEJ–BOGOJEVO

Vesna Ž. Pešić, Milena R. Bečelić-Tomin, Božo D. Dalmacija, Dejan M. Krčmar

University of Novi Sad, Department for chemistry, biochemistry and environmental protection, Trg Dositeja Obradovića 3, 21000 Novi Sad, Serbia

(Professional paper)

Pressure and impact analysis requires information on the main drivers and changes in conditions. In order to analyze such pressures and impacts, each river basin requires: an analysis of its characteristics, a review of the impact of human activity on the status of the surface water and an economic analysis of water use. Pressure and impact analysis plays a central role in the planning of river basin management. The quality of the stream at any point depends on several major factors: lithology of the basin, weather conditions, climate and human impacts. Most of the polluters are located in the big cities next to the DTD Bečej–Bogojevo canal (Odžaci,Vrbas, Srbobran and Bečej). Per year, 2900000 m^3 of wastewater was discharged into the Bečej-Bogojevo section of the DTD canal: 1,4 t COD, 0,8 t BOD, 260 kg of nitrogen, 19 kg of phosphorus and 282 kg of suspended solids. Of the total volume of wastewater, 20% comes from industry and 80% from municipal wastewater. Most of the wastewaters from the studied polluters is discharged untreated or insufficiently treated (only primary treatment). This poor quality wastewater threatens the receipients into which its is discharged. Comparison of the wastewater quality results to the Decree on emission limits and deadlines for their achievement, shows that many polluters exceed the limits for all parameters (COD, BOD, nitrogen, phosphorus and suspended solids). On the basis of the physicochemical analysis of the water from the DTD Bečej–Bogojevo canal it can be concluded that the water quality is unsatisfactory. According to the national legislation, the water quality exceeds the values for good potential streams for most parameters at all sampling locatio dissolved oxygen, organic matter and nutrients). Thus, we can conclude that the water in the studied section of the DTD Bečej–Bogojevo canal does not meet the criteria for „good ecological potential“. The most vulnerable locations are downstream of the Vrbas and downstream of the Bečej, while the best quality canal water is at the furthest upstream location (CS Bogojevo). Risk assessment, based on monitoring results, indicates that the water of the studied section of the DTD Bečej–Bogojevo canal is probably at risk of failing to meet the objectives of the Water Framework Directive, as 33% of the analyzed parameters to calculate specific risk ratios were greater than 1, and thus falls into the category of medium risk pollutants. In order to achieve the quality (to achieve good status and good potential), there must be a response from industrial producers, which consists primarily of comprehensively understanding the problems and implementing measures to minimize the impact of these problems.

Keywords: Wastewater • Impact assesment • DPSIR • DTD Bečej–Bogojevo • Ecological potential

Leachability and physical stability of solidified and stabilized pyrite cinder sludge from dye effluent treatment

Djurdja V. Kerkez[1], Milena R. Becelic-Tomin, Milena B. Dalmacija, Dragana D. Tomasevic, Srdjan D. Roncevic, Gordana V. Pucar, Bozo D. Dalmacija

University of Novi Sad, Faculty of Sciences, Department of Chemistry, Biochemistry and Environmental Protection, Novi Sad, Serbia

Abstract

The aim of this paper is to explore the possibilities of using solidification/stabilization (S/S) treatment for toxic sludge generated in dye effluent treatment, when pyrite cinder is used as catalytic iron source in the modified heterogeneous Fenton process. S/S treatment was performed by using different clay materials (kaolin, bentonite and native clay from the territory of Vojvodina) and fly ash in order to immobilize toxic metals and arsenic presented in sludge. For the evaluation of the extraction potential of toxic metals and the effectiveness of the S/S treatment applied, four single-step leaching tests were performed. Leaching test results indicated that all applied S/S treatments were effective in immobilizing toxic metals and arsenic presented in sludge. X-Ray diffraction analysis confirmed the formation of pozzolanic products, and compressive strength measurement proved the treatment efficacy. It can be concluded that the S/S technique has significant potential for solving the problem of hazardous industrial waste and its safe disposal.

Keywords: industrial waste, pyrite cinder, metal leaching, solidification/stabilization.

Available online at the Journal website: http://www.ache.org.rs/HI/

SCIENTIFIC PAPER

UDC 628.4.038:666.327(497.113):54

Hem. Ind. **69** (3) 231–239 (2015)

doi: 10.2298/HEMIND140304036K

Hazardous industrial wastes are an inevitable source of environmental pollution. Leachates from these wastes could contaminate potable water sources and affect human health. Poor waste management systems have been identified as one of the most important environmental problems in Serbia. One of the potential hazardous waste problem in Serbia is pyrite cinder generated in sulfuric acid production. About 500,000 t of pyrite cinders have been disposed in landfills in several locations in Serbia without any form of protection (www.ekoplan.gov.rs). The increasingly large dumps not only take up plenty of land, but most importantly, pose a serious threat to the environment. A high content of iron oxide of this type of waste, in the form of hematite and magnetite, is the basis for the research regarding the possibility of its use as a source of catalytic iron in the modified heterogeneous Fenton process in wastewater treatment, especially in dye effluent treatment [1–3]. If a waste material is the source of iron and a catalytic support in a heterogeneous Fenton process, on the one hand it can reduce the cost of the application of these processes, and on the other hand to enable the use of waste for the purpose of waste water treatment. After the utilization of this waste material in a heterogeneous Fenton process, generated sludge is mainly composed of the used pyrite cinder. As pyrite cinder also contains traces of toxic/hazardous heavy metals such as Cu, Zn, Pb, and As [4–7], generated sludge may be toxic and cannot be disposed directly without previous treatment. Stabilization and solidification (S/S) are characterized as the best available techniques for the treatment of hazardous and other waste types [8], and have been extensively used as the final treatment steps prior to the disposal of industrial wastes. Typically, the stabilization processes also involve some form of the physical solidification [9]. During S/S applications, the toxic constituents which are present in the waste are physically and chemically fixed [10]. In this way their mobility is significantly reduced, so their threat to the environment is minimized, and compliance with existing regulatory standards is ensured. By finding suitable S/S methods for a particular hazardous waste, we can achieve not only successful disposal of hazardous waste, but after proper modification, we can also provide a possibility for its next utilization in the building industry [9]. Clays and fly ash have widespread usage as low-cost binders. The pozzolanic nature of fly ash means it can be used in a variety of construction applications [11]. In Serbia, fly ash from power plants has the largest share in total waste produced (69%), but is put to very limited use. Quantifying the environmental impact of S/S materials in real environmental scenarios is crucial for selecting proper disposal and reuse alternatives and for certification of immobilization technologies. The performance of S/S treated wastes is gen-

Correspondence: Dj.V. Kerkez, Department of Chemistry, Biochemistry and Environmental Protection, Faculty of Sciences, University of Novi Sad, Trg Dositeja Obradovica 3, 21000 Novi Sad, Serbia.
E-mail: djurdja.kerkez@dh.uns.ac.rs
Paper received: 4 March, 2014
Paper accepted: 11 April, 2014

erally measured in terms of leaching tests [12]. Batch leaching tests with a single extraction are the preferred choice for regulatory assessment due to their simplicity, improved reproducibility, and shorter time requirements. Serbian legislative also uses the Toxicity Characteristic Leaching Procedure — TCLP and DIN 3841-4 S4 complementary procedure for the evaluation of waste characteristics. Additionally, the Synthetic Precipitation Leaching Procedure — SPLP and Waste Extraction Test — WET leaching tests are also widely applied leaching tests for examining S/S efficacy, as they are also tests which mimic conditions in the field, contributing to a better risk assessment of the applied treatment [13]. The main objectives of this study can be summarized as follows: 1) assessing the characteristics of generated sludge from dye effluent treatment and evaluating its environmental risk (metal distribution according to sequential extraction and sample digestion), metal leaching according to TCLP and DIN 3841-4 S4 procedure); 2) S/S treatment of generated sludge with the addition of clays and fly ash; 3) defining metal distribution and evaluation of their environmental risk in selected S/S mixtures according to MWSE; 4) evaluation of the effectiveness of S/S treatment by assessing the leaching potential and environmental impact based on the different leaching procedures (TCLP, DIN 3841-4 S4, SPLP and WET procedure); (5) investigation of S/S matrices binding mechanisms by X-ray diffraction (XRD) and their potential usage by determining compressive strength.

MATERIALS AND METHODS

Used sludge was obtained after heterogeneous Fenton treatment of dye effluent, where pyrite cinder was used as catalytic iron source. For this treatment used pyrite cinder was obtained from IHP "Prahovo" A.D., Serbia. Class C coal fly ash was provided by the Kolubara (Serbia) thermal power plant. It is rich in calcium (> 20% CaO) with self-cementing properties, and therefore does not require addition of activator. Kaolin and bentonite are commercially purchased clays and native clay was sampled near brick works at site Potisje, Kanjiza near Krivaja river basin.

Initial sludge characterization and sample preparation

Raw sludge sample and selected S/S mixtures were characterized by performing sequential extraction as described in [14]. Milestone, Stare E microwave was used for digestion in order to determine pseudo total metal and As contact. Also initial TCLP and DIN 3841-4 S4 procedures were performed on raw sludge sample.

All materials were dried at 105 °C to constant mass and then mixed in established proportions, in order to create stable and durable S/S matrices. Samples were designated by capital letter (S: sludge, B: bentonite, K: kaolin, G: native clay and F: fly ash) followed by a number, indicating the percent weight of the given attribute. The content of each material was expressed as a percentage of the total solids weight. For the leaching tests, 6 types of samples (containing 5% of appropriate clay and 20 and 30% of fly ash) were prepared according to ASTM D1557-00 [15], with a detailed description of the sample preparation provided in [8]. After 28 days, the monolithic samples were crushed and then subjected to the leaching experiments and further characterization.

Leaching procedures

The Toxicity Characteristic Leaching Procedure – TCLP was performed according to the USEPA protocol [16]. The samples were extracted at a liquid to solid (L/S) ratio of 20:1 in capped polypropylene bottles on a rotary tumbler at 30 rpm for 18 h. The German standard leaching test – DIN 3841-4 S4 according to [17], uses a grained sample with particle size smaller than 10 mm. Leaching is performed with deionised water at a 10:1 L/S ratio, and a 24-h testing period. Waste Extraction Test – WET [18] uses a citrate acid solution pH buffered with sodium hydroxide, a 10:1 L/S ratio, and a 48-h testing period. The WET extraction solution is prepared with a combination of 0.2 M citric acid solution and 4.0 N NaOH to pH 5.0±0.1. One liter of this solution is added to a 100-g sample and rotated for 48 h. The Synthetic Precipitation Leaching Procedure SPLP test is performed according to [19]. The extraction fluid is made of two inorganic acids (nitric and sulphuric acid) to simulate acidic rainwater (pH 4.2). In a similar fashion as the TCLP, a 100-g sample of waste material is placed in a 2-L extraction vessel and mixed with the extraction fluid. The mixture is rotated for 18± 2 h at 30 rpm. All tests were applied to every sample in triplicate. Mean values were used and the *RSD*s (n = 3) were below 5%.

Characterization on S/S mixtures

X-ray diffraction (XRD) was performed on the selected prepared monolithic matrices at 28 days of age, before the leaching tests. The monolithic matrices were crushed and dried, ground to powder and then subjected to XRD analysis (Philips PW1710 automated X-ray powder diffractometer was used).

Compressive strength was determined by using a penetrometer which measures the penetration resistance of undisturbed samples in kPa. The results are interpreted according to [11,20].

RESULTS AND DISCUSSION

The results obtained by performing sequential extraction on raw sludge sample as well as on selected S/S mixtures, are summarized in Fig. 1. On the y-axis the

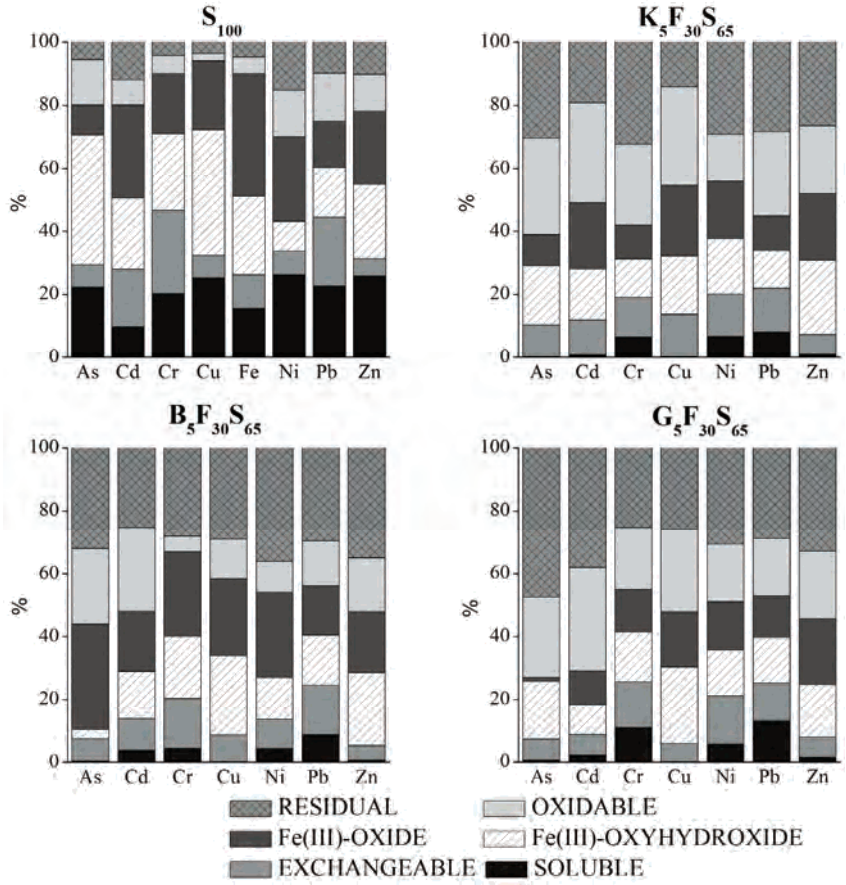

Figure 1. Metal distribution in raw sludge sample and selected S/S mixtures.

percentages of extracted metals were presented in relation to the pseudo total metal content. The following reduction of metal mobility can be observed in raw sludge sample: Cr >Pb> Ni > Cu > Zn > As > Cd > Fe. Percent of extracted, more mobile metals, in soluble and exchangeable fraction ranges from 47% for Zn to 28% for Pb and 26% for Fe in relation to total metal concentration.

In the raw sludge sample, as can be seen in Figure 1, all metals except iron and cadmium show a high risk to the environment, while iron, cadmium and arsenic show a moderate risk in terms of their content in soluble and exchangeable fraction [21,22]. Metals in these fractions are the most mobile and the most easily biologically accessible in the environment [2324]. The presence of metals in these phases increases the possibility of contamination of groundwater and surface water near the disposal site of such waste [25]. By comparing the results of the sequential extraction procedure of raw sludge sample and obtained S/S mixtures, a reduction of all metals and arsenic in soluble and exchangeable phase can be observed. There is almost no As, Zn and Cu present in soluble phase. All S/S mixtures represent moderate or low risk to the environment. Characterization results of raw sludge by using the TCLP and DIN 3841-4 S4 extraction test, normalized by national legislation in order to determine the nature of waste [26], are shown in Tables 1 and 2. Arsenic, copper, lead and zinc are leached in concentrations greater than allowed by the TCLP procedure, characterizing this waste as toxic, posing a risk to human health and the environment. Also arsenic, cadmium, copper, lead and zinc exceeded DIN 3841-4 S4 regulatory levels based on which raw sludge can be considered as hazardous waste.

The results of TCLP test on treated samples were presented in Table 1. This test is specifically designed to mimic the acidic conditions of the sanitary landfill, as well as to identify wastes that have the potential to contaminate groundwater. The leached concentrations of metals and arsenic from all mixtures are far below the limit values according to the Regulation on categories, testing and classification of waste [26]. Therefore, it can be concluded that these materials do not possess toxic properties and can be considered safe and non-hazardous for disposal.

The results of DIN 3841-4 S4 test on treated samples were presented in Table 2. The majority of leached concentrations were lower than those obtained by the TCLP test, since this test uses deionized

Table 1. Leached metal and arsenic concentrations and limit values for metals according to TCLP procedure, 10^{-2} mg L^{-1}

Sample	Component						
	As	Cd	Cr	Cu	Ni	Pb	Zn
S100	516	42.1	216	9830	629	1380	27800
K5F20S75	15.6	3.30	6.80	1672	14.5	3.50	163
K5F30S65	11.8	1.20	5.50	991	9.20	0.200	145
B5F20S75	12.3	1.70	6.90	928	10.1	3.20	127
B5F30S65	1.02	1.60	2.90	798	4.60	0.20	104
G5F20S75	10.4	2.90	6.30	685	11.3	2.80	114
G5F30S65	8.60	2.20	3.60	684	6.20	2.30	112
Limit values	500	100	500	2500	2000	500	25000

Table 2. Leached metal and arsenic concentrations according to DIN 3841-4 S4 test (10^{-2} mg kg^{-1}); A– maximum allowed concentration of accepting waste as inert L/S = 10 (L/kg); B* – maximum allowed concentration of accepting waste as non-hazardous L/S = 10 L/kg [22]; *Z2 upper recommended value of usage[24]*

Sample	Component						
	As	Cd	Cr	Cu	Ni	Pb	Zn
S100	2610	543	83.2	18900	258	12200	32600
K5F20S75	75.1	17.7	5.40	26.3	7.70	73.7	71.8
K5F30S65	40.3	10.9	1.90	8.60	1.60	8.80	70.9
B5F20S75	96.2	5.50	1.50	7.40	3.40	12.2	66.1
B5F30S65	60.3	5.30	0.300	7.10	0.500	5.80	59.0
G5F20S75	124	9.00	1.40	7.80	12.2	27.7	81.1
G5F30S65	123	4.50	1.10	4.10	1.30	20.6	77.8
A*	50	4	50	200	40	50	400
B*	200–2500	100–500	1000–7000	5000–10000	1000–4000	1000–5000	5000–20000
LAGA Z2*	50	5	100	200	100	100	400

water as a leaching agent. These results were interpreted by using the national regulations for the testing and classification of waste [25], as well as by comparing it with the values prescribed by the European Union [27]. Only As and Cd were leached in significant concentrations, but even from the aspect of these metals all specimens represent non-hazardous waste. Also lead was leached above the limit value for inert waste only in the mixture containing 5% of kaolin and 20% of fly ash. From the aspect of LAGA criteria stipulated by German National Working Group on Waste [28], all specimens meet the set values from the aspect of Cr, Cu, Ni, Pb and Zn and can be further used.

Leached metal concentrations by WET test is generally demonstrated that there is a problem with the leaching of arsenic and copper in all S/S mixtures (Table 3), especially if there is a lower share of appropriate immobilization agents. Leached metal concentrations are higher than those obtained by TCLP test [29,30]. The test is conducted at L/S ratio of 1:10 whereas the ratio of the TCLP test is twice as higher.

Table 3. Leached metal and arsenic concentrations according to WET test, 10^{-2} mg L^{-1}; limit values for metals according to CCR regulative [14]

Sample	Component						
	As	Cd	Cr	Cu	Ni	Pb	Zn
K5F20S75	1027	9.30	74.5	5677	68.7	8.90	452
K5F30S65	900	8.70	58.7	4073	66.9	3.50	379
B5F20S75	882	8.20	72.1	4210	62.3	5.80	382
B5F30S65	637	8.10	45.1	2897	53.8	4.80	238
G5F20S75	977	9.00	65.1	3408	61.7	12.5	449
G5F30S65	721	8.60	49.7	3211	53.1	11.2	376
Limit values	500	100	500	2500	2000	500	25000

Also, citrate ion, as a multidentate ligand, used in WET test has the capacity to build a stable chelate with metals, which results in increased metal leaching [31]. Cd, Cr, Ni, Pb and Zn did not show a greater tendency for leaching, so from the aspect of these metals, the mixtures are considered to be adequately stabilized and solidified material. Arsenic is generally leached from S/S mixtures containing fly ash and clay which is consistent with similar studies [13]. Cu also leached above the permissible limits, but with the increase of fly ash share there was an obvious reduction of leaching.

The results of the applied SPLP test on S/S mixture of sludge with chosen clays and fly ash are presented in Table 4. SPLP test reproduces the conditions of acid rain and is used to estimate the mobility of metals when the waste is disposed of in an inappropriate manner. It showed that in almost all S/S mixtures there is no increased metal leaching. With the increase of the mass fraction of immobilization agents in the mixtures, leaching of toxic metals and arsenic is reduced. Generally leach concentrations of metals according to SPLP test were lower than those obtained by TCLP test. This difference in leaching may be due to the different complexation abilities of acid used. TCLP test uses acetic acid, which binds metals strongly, causing them to leach in greater extent [30]. SPLP is also commonly used test for risk assessment of contaminated soil and waste onto surface and groundwater, as well as for the risk assessment process for useful use of solid waste. In this paper, the leach metal concentrations were compared with the emission limit values of waste water from surface waste disposal prescribed by the Regulation on limit values of pollutants in water and deadlines for achieving them [32].

The X-ray analysis indicated the formation of pozzolanic products after a period of 28 days (Fig. 2). Calcium silicate hydrate (CSH) and the calcium silicate hydroxide (CHS) were identified in all samples. Hematite, magnetite, pyrite and quartz, which are identified in all the S/S mixtures, originate from treated sludge. In general, formation of pozzolanic components, and the presence of calcite and gypsum, further confirms that these matrices have good potential to be used as construction materials [20,33].

The measurement results of compressive strength of tested S/S mixtures are shown in Figure3. According to the EPA [34], S/S materials with hardness greater than 0.35MPa shall be considered to have sufficient compressive strength. This minimum value is proposed in order to create a stable foundation for the disposal of these materials in landfills. In the UK, acceptable strength after 28 days is 0.7MPa, but the value of 0.35 is acceptable depending on the test sample [35].

Studies have shown that the values of compressive strength for majority of stabilized and solidified wastes samples ranged from 0.06 to 19.9 MPa [36]. Compressive strength depends on the quality of pore structure and cementitious materials. This depends primarily on the type and quantity of the constituents which constitutes the pore structure (hydratation products) and pozzolanic reactions which take place in the S/S mixtures [37]. Overall, an increasing proportion of fly ash in the S/S mixtures proved to be negative in terms of compressive strength, but all obtained mixtures of clay and fly ash still can be used as a base for roads and bulk materials as they all exhibit compressive strength requirement of 0.35 MPa.

CONCLUSIONS

The assessment of the sludge, generated in dye effluent treatment, based on the sequential extraction, as well as the initial TCLP and DIN 3841-4 S4 testing, showed that this waste can be considered as hazardous due to high metal and As content. The S/S treatment applied, using tree different clays and fly ash, appeared to be effective in the remediation of sludge from dye effluent treatment when using pyrite cinder as catalytic iron source. Sequential extraction indicated that after the treatment there was a significant change in metal and As distribution. Namely, after the S/S treatment, metal content in soluble and exchangeable phase decreased and consequently the environmental risk was

Table 4. Leached metal and arsenic concentrations according to SPLP test, 10^{-2} mg L^{-1}; emission limit values for waste water from surface waste disposal [28]

Sample	Component						
	As	Cd	Cr	Cu	Ni	Pb	Zn
K5F20S75	9.10	2.10	0.500	3.20	1.10	2.70	42.2
K5F30S65	5.50	0.500	0.100	1.80	0.400	2.00	25.7
B5F20S75	3.70	2.00	0.400	15.5	1.10	2.50	75.5
B5F30S65	1.80	0.900	0.100	2.50	0.900	1.30	56.1
G5F20S75	11.9	1.50	2.50	2.80	1.90	6.80	314
G5F30S65	7.80	1.40	0.100	2.70	0.200	1.20	116
Limit values	10	10	50	50	100	50	200

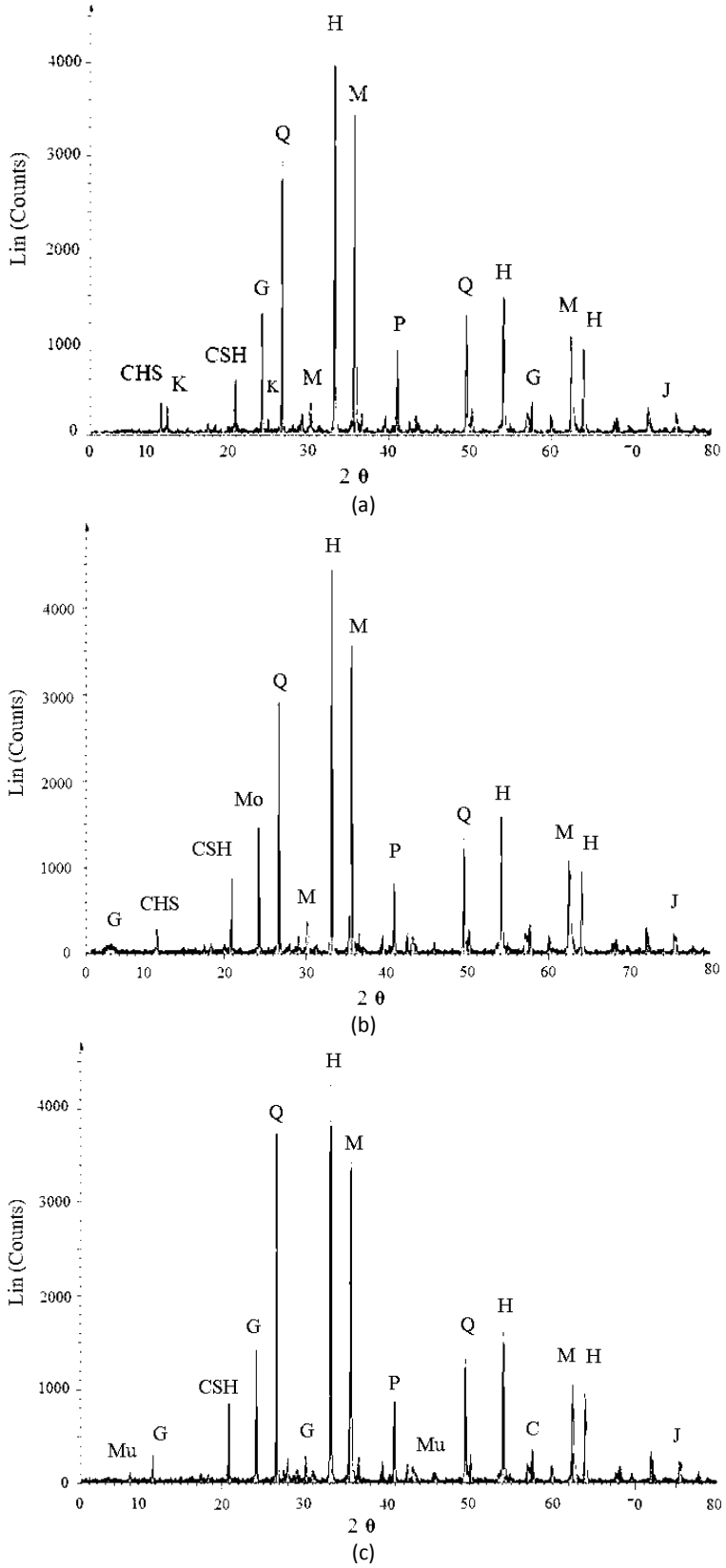

Figure 2. X-Ray diffraction analysis (XRD) applied on S/S mixtures with: a) 5% kaolinite and 30% of fly ash, b) 5% bentonite and 30% of fly ash and c) 5% native clay and 30% of fly ash; the identified chemical species are following: H – hematite, M – magnetite, P – pyrite, Q – quartz, C – calcite, G – gypsum, CSH – calcium silicate hydrate, CHS – calcium hydroxide silicate, J – jarosite, Mo – montmorilonite, K-kaolinite and Mu-muscovite.

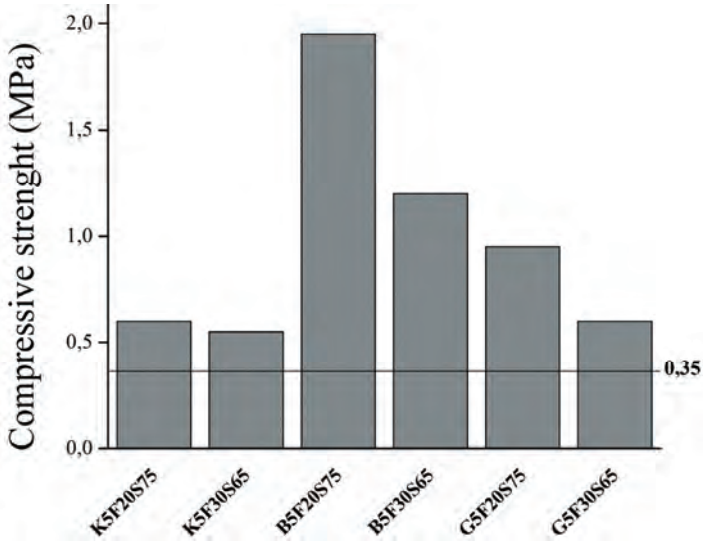

Figure 3. Compressive strength (MPa) of obtained S/S mixtures after 28 days.

reduced. The single-step leaching tests TCLP, DIN 3841-4 S4, WET and SPLP were applied to evaluate the extraction potential of metals and As in S/S matrices. The results showed that in all S/S samples very limited leaching occurred, and leached metal and As concentrations are in majority of cases below the proposed regulatory limits. XRD analyses confirmed the formation of pozzolonic compounds in all S/S samples. From the aspect of compressive strength analysis, produced S/S materials are viable for safe disposal and can also be considered as acceptable for "controlled utilization". This may justify the application of such already-expensive remediation procedures, especially when it comes to treating materials containing a mixture of pollutants. In addition, this kind of waste treatment is advantageous from an economic point of view, because in this way hazardous industrial wastes are immobilized and stabilized using low-cost binders. An additional advantage of using fly ash as an immobilizing agent in the S/S treatment of this kind of sludge is the simultaneous disposal of two waste types. These results represent a promising technology in the field of green remediation.

Acknowledgement

This work has been produced with the financial assistance of the Ministry of Education, Science and Technological Development of the Republic of Serbia (Projects No. III43005 and TR37004).

REFERENCES

[1] H. Che, S. Bae, W. Lee, Degradation of trichloroethylene by Fenton reaction in pyrite suspension, J. Hazard Mater. **185** (2011) 1355–13561.

[2] M. Bečelić-Tomin, B. Dalmacija, D. Tomašević, J. Molnar, Lj. Rajić, Primena piritne izgoretine u mikrotalasnom Fenton procesu obezbojavanja rastvora sintetske boje, Hem. Ind. **67** (2013) 399–409.

[3] M. Becelic-Tomin, B. Dalmacija, Lj. Rajic, D. Tomasevic, Dj. Kerkez, M. Watson, M.Prica, Degradation of Anthraquinone Dye Reactive Blue 4 in Pyrite Ash Catalyzed Fenton Reaction, Sci. World J., 2014 (http://dx.doi.org/10.1155/2014/234654).

[4] A.M. Álvarez-Valero, R. Sáez, R. Pérez-López, J. Delgadoa, J.M. Nieto, Evaluation of heavy metal bio-availability from Almagrera pyrite-rich tailings dam (Iberian Pyrite Belt, SW Spain) based on a sequential extraction procedure, J. Geochem. Explor. **102** (2006) 87–94.

[5] J.Viñals, M.J. Balart, A. Roca, Inertization of pyrite cinders and co-inertization with electric arc furnace flue dusts by pyroconsolidation at solid state, Waste Manage. **22** (2002) 773–782.

[6] N. Tugrul, E.M. Derun, M. Piskin, Utilization of pyrite ash wastes by pelletizationprocess, Powder Technol. **176** (2007) 72–76.

[7] N. Tugrul, E.M. Derun, M. Piskin, Effects of calcium hydroxide and calcium chloride addition to bentonite in iron ore pelletization, Waste Manage. Res. **24** (2006) 446––455.

[8] M. Dalmacija, B. Dalmacija, D. Krčmar, M. Prica, Lj. Rajić, S. Rončević, O. Gavrilović, Solidifikacija/stabilizacija sedimenta vodotoka Krivaja zagađenog metalima, Hem. Ind. **66** (2012) 469–478.

[9] A. Gailius, B. Vacenovska, R. Drochytka, Hazardous Wastes Recycling by Solidification/Stabilization Method, Medziagotyra. **16** (2010) 165–169.

[10] S. Ucaroglu, I. Talinli, Recovery and safer disposal of phosphate coating sludge by solidification/stabilization. Recovery and safer disposal of phosphate coating sludge by solidification/stabilization, J Environ Manage. **105** (2012) 131–137.

[11] R. del Valle-Zermeño, J. Formosa, J.M. Chimenos, M. Martínez, A.I. Fernández, Aggregate material formulated with MSWI bottom ash and APC fly ash for use as

secondary building material, Waste Manage. **33** (2013) 621–627.

[12] C. Jing, X. Meng, G.P. Korfiatis, Lead leachability in stabilized/solidified soil samples evaluated with different leaching tests, J Hazard Mater. **114** (2004) 101–110.

[13] M. Dalmacija, M. Prica, B. Dalmacija, S. Roncevic, M. Klasnja, Quantifying the environmental impact of As and Cr in stabilized/solidified materials, Sci. Total Environ. **412**–**413** (2011) 366–374.

[14] M. Sima, B. Dold, L. Frei, M. Senila, D. Balteanu, J. Zobrist, Sulfide oxidation and acid mine drainage formation within two active tailings impoundments in the Golden Quadrangle of the Apuseni Mountains, Romania, J. Hazard. Mater. **189** (2011) 624–639.

[15] ASTM D1557-00, Standard test method for laboratory compaction characteristics of soil using modified effort American Society for Testing Materials. Annual Book of ASTM standards: ASTM D1557-91, vol. 4.08, Philadelphia, P: ASTM.

[16] USEPA, Toxicity characteristic leaching procedure, method 1311, 2002 (www. EPA.gov/SW-846/1311.pdf).

[17] DIN 38414-4, Teil 4: Schlamm und Sedimente, Gruppe S., Bestimmung der EluierbarkeitmitWasser S4, Beuth-Verlag, Berlin, 1984.

[18] CCR. California code of regulations.Title 22, Ch. 11, article 5, Appendix II, 1998.

[19] USEPA.Synthetic precipitation leaching procedure, method 1312, 2002a (www. EPA.gov/SW-846/1312.pdf), 2002.

[20] H. Patel, S. Pandey, Evaluation of physical stability and leachability of Portland Pozzolona Cement (PPC) solidified chemical sludge generated from textile wastewater treatment plants, J. Hazard. Mater. **207**–**208** (2012) 56–64.

[21] C. K. Jain, Metal fractionation study on bed sediments of River Yamuna, India, Water Res. **38** (2004) 569–578.

[22] Y. Zhou, X.A. Ning, X. Liao, M. Lin, J. Liu, J. Wang, Characterization and environmental risk assessment of heavy metals found in fly ashes from waste filter bags obtained froma Chinese steel plant, Ecotox Environ Safe. **95** (2013) 130–136.

[23] K.V. Singh, P.K. Singh, D. Mohan, Status of heavy metals in water and bed sediments of river Gomti- a tributary of the Ganga river, India, Environ Monit Assess. **105** (2005) 43-67.

[24] H.M. Zakir, N. Shikazono, K. Otomo, Geochemical distribution of trace metals and assessment of anthropogenic pollution in sediments of Old Nakagawa River, Tokyo, Japan, Am. J. Environ. Sci. **4** (2008) 661–672.

[25] M. Rawat, A. Ramanathan, V. Subramanian, Quantification and distribution of heavy metals from small-scale industrial areas of Kanpur city, India, J. Hazard. Mater. **172** (2009) 1145–1149.

[26] Official Gazzete, Ministry of Energy, Development and the Environment, Regulation on categories, testing and classification of waste. The Official Gazette 56/2010 (2010).

[27] Official Journal of the European Communities, L11, Council Decision 2003/33/EC of 19 December 2002 establishing criteria and procedures for the acceptance of waste at landfills pursuant to Article 16 of and Annex II to Directive 1999/31/EC, 2003.

[28] LAGA. Cooperation of the German federal authorities on waste, Anforderungenan die stofflicheVerwertung von mineralischenReststoffen/Abfällen; 5th September 1995, Berlin, Erich Schmidt Verlag, 1996.

[29] T. Townsend, B. Dubey, T. Tolaymat, H. Solo-Gabriele, Preservative leaching from weathered CCA-treated wood, J. Environ. Manage. **75** (2005) 105–113.

[30] T. Townsend, T. Tolaymat, H. Solo-Gabriele, B. Dubey, K. Stook, L. Wadanambi, Leaching of CCA-treated wood: implications for waste disposal, J. Hazard. Mater. **114** (2004) 75–91.

[31] W. Stumm, J. Morgan, Aquatic chemistry: chemical equilibria and rates in natural waters, Ch. 6, third ed., Wiley, New York, 1996.

[32] Official Gazette of RS, 67, 13-41. (2011) and 48 (2012). Regulation on limit values of pollutants in water and deadlines for their achievement. Ministry of Energy, Development and Environmental Protection of the Republic of Serbia.

[33] M. Erdem, A. Özverdi, Environmental risk assessment and stabilization/solidification of zinc extraction residue: II. Stabilization/solidification, Hydrometallurgy **105** (2011) 270–276.

[34] Guide to disposal of chemically stabilized and solidified wastes, U.S. EPA SW872 (1982).

[35] C.D. Hills, S.J.T. Pollard, Influence of interferences effect on the mechanical, microstructural and fixation characteristics of cementsolidified hazardous waste forms, J. Hazard. Mater. **52** (1997) 171–191.

[36] R. Malviya, R. Chaudhary, Factors affecting hazardous waste solidification/stabilization: a review, J. Hazard. Mater. **137** (2006) 267–276.

[37] V. Zivica, Hardening and properties of cement-based materials incorporating heavy metals oxides, B. Mater. Sci. **20** (1997) 677–683.

IZVOD

IZLUŽIVANJE I FIZIČKA STABILNOST SOLIDIFIKOVANOG I STABILIZOVANOG MULJA PIRITNE IZGORETINE KOJI POTIČE IZ TRETMANA EFLUENATA KOJI SADRŽE BOJE

Djurdja V. Kerkez, Milena R. Bečelić-Tomin, Milena B. Dalmacija, Dragana D. Tomaševic, Srdjan D. Rončević, Gordana V. Pucar, Božo D. Dalmacija

Univerzitet u Novom Sadu, Prirodno–matematički fakultet, Departman za hemiju, biohemiju i zaštitu životne sredine, Novi Sad, Srbija

(Naučni rad)

Ovaj rad se bavi istraživanjem mogućnosti korišćenja solidifikacije/stabilizacije (S/S) u tretmanu toksičnog mulja nastalog u tretmanu obojenih efluenata, kada je piritna izgoretina korišćena kao izvor katalitičkog gvožđa u modofokovanom heterogenom Fenton procesu. S/S tretman je izveden uz korišćenje različitih glina (kaolin, bentonit, lokalna glina sa teritorije Vojvodine) i letećeg pepela u cilju imobilizacije toksičnih metala i arsena prisutnih u mulju. Za procenu potencijala ekstrakcije toksičnih metala i arsena, kao i za efektivnost primenjenog S/S tretmana, izvedena su četiri testa izluživanja u jednom koraku. Svaki test koristi različito sredstvo za izluživanje kako bi se oponašali realni uslovi u životnoj sredini. Generalno, sekvencijalna ekstrakcija S/S smeša pokazala je smanjenje sadržaja metala i arsena u rastvornoj i izmenjivoj fazi u poređenju sa uzorkom sirovog mulja. Rezultati testova izluživanja ukazuju da je primenjeni S/S tretman bio efikasan u imobilizaciji toksičnih metala i arsena prisutnih u mulju. Takođe, X-ray difrakciona analiza potvrdila je formiranje pozolaničkih proizvoda, a merenja pritisne čvrstoće potvrdila su efikasnost tretmana. Stoga može se zaključiti da S/S tehnika ima značajan potencijal pri rešavanju problema opasnog industrijskog otpada i njegovog bezbednog odlaganja.

Ključne reči: Industrijski otpad • Piritna izgoretina • Izluživanje metala • Solidifikacija/stabilizacija

Evaluation of water, sucrose and minerals effective diffusivities during osmotic treatment of pork in sugar beet molasses

Milica R. Nićetin[1], Lato L. Pezo[2], Biljana Lj. Lončar[1], Vladimir S. Filipović[1], Danijela Z. Šuput[1], Snežana Zlatanović[2], Biljana P. Dojčinović[3]

[1]*University of Novi Sad, Faculty of Technology, 21000 Novi Sad, Serbia*
[2]*University of Belgrade, Institute of General and Physical Chemistry, 11000 Beograd, Serbia*
[3]*University of Belgrade, Institute of Chemistry, Technology and Metallurgy, 11000 Belgrade, Serbia*

Abstract

Effective diffusivities of water, sucrose and minerals in osmotic treatment of pork cubes (M. *triceps brachii*) were calculated using Response Surface Methodology (RSM), with respect to temperature (20, 35 and 50 °C) and concentration of sugar beet molasses, (60, 70 and 80 mass%). The numerical solution of Fick's law for unsteady-state mass transfer in a perfect cube configuration was used to calculate the effective diffusivities of water, sucrose and minerals (Na, K, Ca and Mg). Zugarramurdi and Lupin's model was used to predict the equilibrium condition, which has shown to be appropriate for water loss and solute uptake during osmotic treatment. Effective diffusivity of water was found to be in the range of 6.95×10^{-10}–8.03×10^{-10} m^2 s^{-1}, the sucrose effective diffusivity was between 6.39×10^{-10} and 8.25×10^{-10} m^2 s^{-1}, while diffusivities for minerals (m^2 s^{-1}) were in the range: 6.34×10^{-10}–8.82×10^{-10} for Na, 6.27×10^{-10}–7.43×10^{-10} for K, 6.44×10^{-10}–8.94×10^{-10} for Ca and 3.47×10^{-10}–5.66×10^{-10} for Mg.

Keywords: pork, sugar beet molasses, osmotic treatment, diffusion, mass transfer.

Available online at the Journal website: http://www.ache.org.rs/HI/

SCIENTIFIC PAPER

UDC 637.5'64:544:664.151.2

Hem. Ind. **69** (3) 241–251 (2015)

doi: 10.2298/HEMIND131003037N

Physicochemical, sensory and technological properties of fresh meat are related with water content. Water is held in myofibrils, functional organelles of meat, but also it may exist in the intracellular space between myofibrils and sarcoplasm. The water content in meat depends on many factors, including the tissue itself and how the product is handled (time, temperature, treatments) [1–3].

Various meat preservation techniques usually include the introduction of high salt content, but nowadays consumers demand lower content of salt incurporated in the final product [4]. The interest of consumers in processed products with lower salt content is due to changes in the sensory preferences, but the main reason is the public concern as regards the high intake of sodium in the diet, which is known to increase the threat of cardiovascular damage [5]. The decrease of sodium content by partial substitution of sodium chloride with some other salts (like potassium chloride) is one of the most commonly used methods [6–8]. Nevertheless, there is little knowledge regarding the influence of the salts formulation on the kinetics and its influence on the salting step [6], as in the post-salting stage [9–12]. Recently, the mineral uptakes in pork brined with NaCl and K-lactate for obtaining low sodium meat products have been studied [13].

One of the preservation techniques for producing food with low water content and improved nutritional, sensorial and functional properties is osmotic treatment (OT). Osmotic treatment of foods presents some advantages compared with common drying techniques, such as minimizing heat damage to the color and flavor, inhibiting enzymatic browning and reducing energy costs. The use of OT as a complementary treatment in food processing, particularly prior to drying and freezing operations, reduces energy requirements of these processes. The technique aims to dehydrate food products by immersing them in hypertonic solution.The diffusion of water is accompanied by the simultaneous counter-diffusion of solute(s) from the osmotic solution into the meat tissue. Since the membrane responsible for osmotic transport is not perfectly selective, other solutes can also be leached into the osmotic solution [2,14]. Osmotic treatment of meat with salt solutions leads to complex phenomena, due to the dynamics of the actin–myosin–salt interactions which modify continuously the relative importance of mass transfer mechanisms.

The use of NaCl solutions during osmotic treatment provokes an increase of the muscles water holding capacity [3]. This is due to existing Cl^- bonds with actin and myosin filaments, which increase negative charges, amplifying the repelling forces among the filaments, leading to muscle swelling. The direction of liquid flow

Correspondence: M.R. Nićetin, University of Novi Sad, Faculty of Technology, Bulevar Cara Lazara 1, 21000 Novi Sad, Serbia.
E-mail: milican85@live.com
Paper received: 3 October, 2013
Paper accepted: 12 March, 2014

in the intercellular spaces cannot be predicted only from the solution osmotic pressure because capillary forces play a major role on liquid flow. Osmotic treatment of raw meat with salt solutions leads to salt and water transfers, in the same directions or in countercurrent, depending on the osmotic solution concentration.

Different approaches have been proposed to explain the rates of mass transfer during osmotic treatment. The first is based on the tissue cellular structure, and the water transport is modeled according to the thermodynamics of irreversible processes [3,15]. Alternatively, the analytical solutions of Fick's second law of diffusion in non-stationary solids of different geometries can be used, allowing estimation of effective diffusion coefficients for water and solutes [16–24]. Rastogi *et al*. [14] reported Fickian unsteady-state diffusion as the most appropriate mechanism for the estimation of diffusion coefficients during osmo-concentration. However, the major drawback in the application of this law is the long experimental time required to attain equilibrium water loss.

Much work has been done in developing models to predict the mass-transfer kinetics of osmotic treatment, and some empirical and semi-empirical models have been proposed, [22–24]. These models correlate processing variables with water loss or solid gain without taking into account the underlying phenomena, and include multivariable regressions, response surface analysis, models derived from mass balances and others. Although mechanistic models give a description of the mass-transfer mechanism, the diffusion approach has a number of assumptions which are difficult to fulfill [1,25], and the effective diffusivity becomes an adjustable kinetic parameter that strongly depends on the experimental conditions and the physical properties of the meat [26]. Also, a cellular physiology approach depends on the knowledge of a large number of biophysical properties, such as membrane permeability and material properties, elastic modulus, void fraction and tortuosity, which are not always available [2,15,25]. On the other hand, even though the empirical and semi-empirical models that have been proposed in the literature give a reasonable fit to experimental data, their use is limited because they are only capable of representing data in conditions similar to those on which such models were developed, and they cannot take into account the process complexity [26, 27]. Andrade *et al.* [28] determined the effective diffusivity of sucrose and water during osmotic treatment of jenipapo based on analytical solution of Fick's second law. Schmidt *et al*. [26], studied the osmotic treatment kinetics of chicken breast cuts over a range of salt concentrations.

The use of a ternary system (water/sugar/salt) in the osmotic treatment of fruits has been studied by some researchers [29], and results have shown that higher rates of water loss are achieved when salt is added, even with solutions with low concentrations of solutes [30]. Most of the works published using the ternary solution provide only diffusion of solids, through determination of total solids by a gravimetric method, without analyzing separately the diffusion of the two solutes used in the solution, [29–31]. According to Bohuon *et al*. [32], the use of ternary solutions presents some advantages in the osmotic treatment process, without excessive over-sweetness or over-salting the product and without reaching the limits of saturation.

No studies relating to the osmotic treatment of pork cubes using sugar beet molasses were found in the current literature. Sugar beet molasses is an excellent medium for osmotic treatment, primarily due to the high dry matter (more than 80%) and specific nutrient content. According to Sauvant *et al*. [33] and Grbeša [34] the concentrations of cations in sugar beet molasses are as follows: 3920 mg K/100 g, 680–1300 mg Na/100 g, 100 mg Ca/100 g, 50–320 mg Mg/100 g and 11.7 mg Fe/100 g. The specific chemical composition (approximately 51% sucrose, 1% raffinose, 0,25% glucose and fructose, 5% proteins, 6% betaine, 1,5% nucleosides, purine and pyramidine bases, organic acids and bases) and high content of solids (around 80%) provide high osmotic pressure in the solution, so molasses appear to be an excellent osmotic medium [35,36].

The current study intends to investigate the effects of sugar beet molasses concentration and immersion duration on the effective diffusivities of water and solutes during the osmotic treatment of pork. Sugar beet molasses as hypertonic solution is presented in this article because of high dry matter content and the enrichment of the food material in minerals and vitamins, which penetrate from molasses to the meat tissue. This investigation is also focused on finding the appropriate mathematical model for water loss, solid gain, sugars and minerals content, during OT of pork in sugar beet molasses. Simple regression models were proposed for calculation of the effective diffusivities of water, sucrose and minerals (Na, K, Ca and Mg) as function of the independent variables. The presented Na, K, Ca and Mg diffusivities during osmotic treatment of pork are presented for the first time, with no data to be compared in the literature.

MATERIALS AND METHODS

Osmotic treatment

Pork (*M. triceps brachii*, 24 h *post mortem*) was purchased just before use. Initial moisture content of

the fresh meat was 72.83%. Before the osmotic treatment, fresh meat was cut into cubes, dimension of nearly 1×1×1 cm^3. Sugar beet molasses solution, with initial dry matter content of 85.04%, was obtained from the sugar factory Pećinci, Serbia. Distilled water was used for dilution of solutions. Sugar beet molasses, was diluted to concentration of 60, 70 and 80 mass%. The sample to solution mass ratio was 1:5. The process was performed in laboratory jars at processing temperature of 20, 35 and 50 °C, with agitation on every 15 min under atmospheric pressure. The jars were kept in water bath, in order to retain samples at constant temperature. The osmotic treatment process was performed in a period of 0–5 h. Samples were withdrawn from the osmotic solution at determined intervals of time (1, 3 and 5 h), drained and dried with filter paper to remove adhering solution.

Analytical determinations

Dry matter content of the fresh and treated samples was determined by drying the material at 105 °C for 24 h in a heat chamber until constant weight was achieved (Instrumentaria Sutjeska, Croatia). All weight measurements were carried out in accordance to AOAC method [37]. Soluble solids content of the molasses solutions was measured using Abbe refractometer, (Carl Zeis Jenna, Germany) at 20 °C.

Mineral content of the raw pork and osmotic treated pork in the solution of sugar beet molasses was investigated. The combination of thermal treatment at 350 °C, and wet acidic treatment at 160 °C, was used for preparation of the samples. The dry samples were processed for minerals determination by wet digestion, where approx. 5 g each were weighed exactly to four decimal places, and transferred to vessels into which 4.5 ml 65% HNO_3 and 10.5 ml 35% HCl were added. The treatments were repeated to obtain the white sediments that were dissolved in 0.07 M HNO_3.

The content of minerals present in the corresponding solutions was determined by inductively coupled plasma optic emission spectrometry (ICP-OES). ICP-OES measurement was performed using Thermo Scientific ICAP 6500 Duo ICP (Thermo Fisher Scientific, Cambridge, United Kingdom) spectrometer equipped with RACID86 Charge Injector Device (CID) detector, standard glass concentric nebulizer, quartz torch, and alumina injector. Multi-elemental plasma standard solution (Multi-Element Plasma Standard Solution 4, Specpure®, 1000 μg/ml) certified by Alfa Aesar GmbH & Co KG, Germany, was used to prepare calibration solutions for ICP-OES measurement. Measurements were performed on emission-lines NaI (818.326 nm), KI (766.490 nm), CaI (431.865 nm) and MgI (285.213 nm). Value of radio frequency power of generator (RF) was 950 W, and radial plasma view was used. Samples were analyzed in triplicate.

Sucrose and invert sugar content have been determined according to Luff-Schoorl method, based on Cu^{2+} reduction. By using this method, values of the total invert sugar (%) and natural invert sugar (%) content, could be determined. Based on this result, sucrose content (%) in the fresh and dehydrated pork could be calculated. All experiments were repeated three times.

Kinetic model

The developed model, based on Fick's unsteady-state law of diffusion, determines the amount of water leaving the meat cube and the solutes diffusing into the meat as a function of time. According to Crank (1975), [38], Fick's second law solution for diffusion, for perfect cubes, assuming the diffusion to be perpendicular to the surface of the cube, is given by Eq. (1):

$$X_r = \frac{x_t - x_0}{x_{eq} - x_0} = \frac{8}{\pi^2} \sum_{i=0}^{\infty} \exp\left(-i^2 \pi^2 D_{eff} \frac{t}{L^2} \right) \quad (1)$$

where X_r denotes the dimensionless values of water loss, sucrose uptake or minerals uptake; x_t, x_0 and x_{eq} are the moisture or the solute contents of a sample at treatment time t, at the outset and at equilibrium, respectively; D_{eff} (m^2 s^{-1}) is the effective diffusivity, L (m) is the half thickness of the sample and t (s) is the immersion time.

For long drying periods, Eq. (1) can be simplified to the first term of the series, and moisture ratio can be expressed in the logarithmic form:

$$\ln X_r = \ln \frac{8}{\pi^2} - \left(\pi^2 \frac{D_{eff} t}{L^2} \right) \quad (2)$$

$$D_{eff} = D_0 \exp\left(-\frac{E_a}{TR} \right) \quad (3)$$

where the effect of temperature on effective diffusivity is expressed using Arrehnius type relationship. E_a is the activation energy of moisture diffusion (kJ mol^{-1}), D_0 is the diffusivity value for infinite moisture content, and R represent universal gas constant (kJ mol^{-1}). T is absolute process temperature (K).

Values of the effective diffusion coefficient (D_{eff}) were obtained by non-linear regression analysis from Eq. (1), taking into account the first two terms of the series, as shown in Eq. (2) [39].

The following assumptions were used in the development of the model: samples of pork cubes are perfect cubes (dimension 1×1×1 cm^3); initial water and solute concentrations in the pork cubes are uniform; the process is isothermal; simultaneous counter-current flows; the diffusion of water from the pork cubes and the diffusion of sugar and salt into the pork cubes are only considered; other mass transfers do not occur;

shrinkage is neglected; external resistance to mass transfer is negligible.

The following mathematical model, with an exponential approach to the equilibrium value of moisture and solutes contents, was proposed by Zugarramurdi and Lupin [40]:

$$\frac{\mathrm{d}X_i(t)}{\mathrm{d}t} = k_i\left(X_i^*(t) - X_i(t)\right) \quad (4)$$

$$X_i(t) = \frac{m_i(t)}{m - \sum_{j=1, j\neq i}^{n} m_j}, \; X_i^*(t) = \frac{m_i^*(t)}{m - \sum_{j=1, j\neq i}^{n} m_j} \quad (5)$$

where i represents the index of moisture, or mineral content, m_i is mass of i-th component at time t, m_i^* is mass of i-th component at equilibrium, m is total mass, k_i is specific rate constant for variation of i-th component.

Equilibrium (4) can be integrated with the following initial condition (t = 0):

$$X_i(0) = X_i^0 \quad (6)$$

The solution is:

$$X_i(t) = X_i^* + e^{-k_i t}\left(X_i^0 - X_i^*\right) \quad (7)$$

The assumption was made that the Zugarramurdi and Lupines' model Eq. (7) would predict the moisture and solutes content in the kinetics of pork cubes, including equilibrium solute content during the process.

Experimental design and data analysis

The experimental data were used for effective diffusivities calculation using Eq. (2). Effective diffusivities of moisture content, minerals (Na, K, Ca and Mg) and sucrose content were calculated considering the diffusive model expressed in Eq. (2), and the estimation of "equilibrium" conditions (x_{eq}), for certain temperature and sugar beet molasses concentration, using Zugarramurdi and Lupines' model, Eq. (7). After calculation of effective diffusivities values for certain temperature and sugar beet molasses concentration, 3^2 full factorial experimental design (3 level-2 parameter) with 9 runs (1 block) was accepted for moisture, minerals and sucrose effective diffusivities presentation (Table 2). It was used to design tests for osmotic treatment of pork cubes considering two factors: sugar beet molasses solution concentrated 60, 70 and 80 mass%, and temperature (20, 35 and 50 °C). The considered dependent variables were the effective diffusivity of water (D_w), the effective diffusivity of sucrose (D_{suc}) and effective diffusivity of minerals (D_{Na}, D_K, D_{Ca} and D_{Mg}).

The following second order polynomial (SOP) model was fitted to the data. Six models of the following form were developed to relate four responses (Y) and three process variables (X):

$$Y_k = \beta_{k0} + \sum_{i=1}^{2}\beta_{ki}X_i + \sum_{i=1}^{2}\beta_{kii}X_i^2 + \beta_{k12}X_1X_2, \; k = 1\text{–}6 \quad (8)$$

where: β_{kn} are constant regression coefficients; Y, either $D_w(Y_1)$, $D_{suc}(Y_2)$, $D_{Na}(Y_3)$, $D_K(Y_4)$, $D_{Ca}(Y_5)$ or $D_{Mg}(Y_6)$; X_1 osmotic temperature; X_2 solution concentration.

Descriptive statistical analyses for calculating the means and the standard error of the mean were performed using MicroSoft Excel 2007 software. All obtained results were expressed as the mean ± standard deviation (*SD*). Regression analysis and analysis of variance (ANOVA) tests for lack of fit, determination of the regression coefficients and generation of contour plots were performed, using StatSoft Statistica 10 software (Statsoft Inc., Tulsa, OK, USA) [41].

The response variables Y were calculated by multiple regressions, and response surface equations were calculated using a definitive model which considered only the influence of significant factors ($p < 0.05$). The response surfaces were drawn by plotting Y as a function of two factor variables, molasses concentration and immersion temperature.

RESULTS AND DISCUSSION

Obtained results are presented in Table 1.

Water loss and solute uptake

At the beginning of osmotic process there is an initially high rate of water loss and a quick incurporation of solutes, followed by a slower rate of water loss and solute uptake in the later stages of the process, Table 1. During osmotic treatment of pork cubes, the moisture content (x_w; g water per g of dry solids), sucrose content (x_{suc}; g per g of sample) and mineral content (x_{Na}, x_{Ca}, x_K, x_{Mg}, mg per g of sample) were experimentally determined in samples at different immersion times for all of the experiments. Moisture and solute contents at equilibrium conditions were determined using Zugarramurdi and Lupines' model, Eq. (7), and are given in Table 2. Zugarramurdi and Lupines' equation proved to be suitable for modeling water removal, sucrose and minerals uptake, as the determination coefficients were above 0.98 for all treatments (Table 2).

Effective diffusivities of water, sucrose and minerals

The effective diffusivities at any given set of conditions were calculated using non-linear regression analysis from Eq. (2). It is generally assumed that diffusion occurs at a constant rate under the influence of a uniform moisture gradient. However, this does not appear to be true in biological materials, especially

Table 1. Changes in water loss and solute uptake during osmotic treatment of pork cubes

Immersion time, h	Temp. °C	Solution concentration, %	Water loss %	Solid gain, mg/g				
				Na	K	Ca	Mg	Sucrose
1	20	80	0.22	174.01	502.71	45.28	19.23	4.80
3	20	80	0.40	284.68	822.41	74.08	31.46	7.85
5	20	80	0.47	348.19	1005.88	90.61	38.48	9.60
1	20	60	0.24	227.11	656.09	59.10	25.10	6.26
3	20	60	0.38	321.43	928.57	83.65	35.53	8.86
5	20	60	0.42	368.59	1064.81	95.92	40.74	10.16
1	20	70	0.23	172.43	498.14	44.87	19.06	4.75
3	20	70	0.39	274.93	794.23	71.55	30.39	7.58
5	20	70	0.45	330.26	954.08	85.94	36.50	9.11
1	35	80	0.29	247.34	714.55	64.37	27.34	6.82
3	35	80	0.46	350.01	1011.13	91.08	38.69	9.65
5	35	80	0.52	405.51	1171.49	105.53	44.82	11.18
1	35	60	0.28	247.67	715.48	64.45	27.37	6.83
3	35	60	0.41	333.98	964.84	86.91	36.91	9.21
5	35	60	0.44	373.14	1077.96	97.10	41.24	10.29
1	35	70	0.29	219.38	633.75	57.09	24.25	6.05
3	35	70	0.44	313.87	906.73	81.68	34.69	8.65
5	35	70	0.48	361.20	1043.46	94.00	39.92	9.96
1	50	80	0.38	352.84	1019.32	91.82	39.00	9.73
3	50	80	0.54	447.51	1292.80	116.46	49.46	12.34
5	50	80	0.59	495.01	1430.03	128.82	54.71	13.65
1	50	60	0.34	300.39	867.81	78.17	33.20	8.28
3	50	60	0.47	378.71	1094.05	98.55	41.86	10.44
5	50	60	0.49	409.86	1184.05	106.66	45.30	11.30
1	50	70	0.36	298.49	862.31	77.68	32.99	8.23
3	50	70	0.51	384.98	1112.16	100.18	42.55	10.62
5	50	70	0.54	424.31	1225.78	110.42	46.90	11.70

Table 2. Parameters of Zugarramurdi and Lupin's model fitted to experimental data

Temp., °C	Solution conc., %	*WL*		X_{Na}		X_K		X_{Ca}		X_{Mg}		$X_{Sucrose}$	
		x_∞^{WL}	r^2	x_∞^{Na}	r^2	x_∞^{K}	r^2	x_∞^{Ca}	r^2	x_∞^{Mg}	r^2	$x_\infty^{Suc.}$	r^2
20	80	0.65	0.998	479.03	0.998	1490.72	0.997	121.27	0.993	37.80	0.915	12.93	0.991
20	60	0.59	0.997	369.61	0.997	1067.75	0.995	96.18	0.993	40.85	0.940	10.19	0.996
20	70	0.51	0.994	413.60	0.999	1239.10	0.998	108.65	0.995	35.00	0.993	11.38	0.994
35	80	0.67	0.996	465.03	0.993	1348.58	0.998	124.10	0.994	43.21	0.953	12.93	0.991
35	60	0.58	0.992	386.08	0.999	1096.43	0.995	105.77	0.996	41.73	0.993	10.87	0.994
35	70	0.54	0.999	386.46	0.997	1116.45	0.994	100.57	0.991	42.71	0.908	10.66	0.998
50	80	0.68	0.997	524.29	0.994	1514.61	0.999	136.44	0.996	66.99	0.989	14.46	0.995
50	60	0.62	0.998	406.63	0.997	1174.71	0.996	111.46	0.993	180.11	0.998	11.33	0.993
50	70	0.54	0.999	401.91	0.996	1161.06	0.995	104.59	0.991	44.42	0.994	11.08	0.999

after the initial stages of the process, as the physical structure of the material begins to change as the osmotic treatment continues. A non-uniform moisture gradient is developed over the course of osmotic treatment and the effective diffusivity changes with geometrical position of specific point inside the material, and time duration of treatment [14]. In meat, $D_{w,}$ generally, shows a decreasing trend over time because of the shrinkage phenomenon [42]. Thus, it is assumed that in meat materials D_w does not show a pseudo linear correlation with time, as was also reported by Rastogi *et al*. [14].

Values of effective diffusivity of water, sucrose and minerals at different temperatures and concentrations

Table 3. Average effective diffusivities of water, sucrose and minerals ($10^{10}/m^2 \cdot s^{-1}$) during osmotic treatment of pork

Temp., °C	Solution conc., %.	D_w	D_{Na}	D_K	D_{Ca}	D_{Mg}	$D_{Suc.}$
20	80	6.92	5.08	4.89	5.35	2.72	5.22
20	60	7.15	5.21	5.08	5.52	2.89	5.38
20	70	7.39	5.50	5.28	5.64	3.29	5.54
35	80	7.28	5.47	5.24	5.54	3.27	5.44
35	60	7.46	5.52	5.43	5.78	3.55	5.65
35	70	7.64	5.73	5.64	5.96	4.07	5.86
50	80	7.80	6.14	5.83	5.83	4.74	5.80
50	60	7.93	6.11	6.03	6.14	5.14	6.06
50	70	8.06	6.24	6.25	6.39	5.77	6.32

of the osmotic solution are presented in Table 3. These results are in agreement with fundamental theories which state that mass diffusivity strongly depends on the temperature, pressure, and on the components involved. Many investigations require the effective diffusivity to be determined at a range of precise temperatures. Frequently, the relationship between effective diffusivity and temperature follows a first order rate process described by an Arrhenius relationship, Eq. (2).

Several authors have made important model studies on the diffusion coefficients of sodium chloride and other solutes in meat [13,23,24,43]. The diffusion coefficient is suggested to be affected by changes in Na concentration, swelling and degree of treatment [23].

Table 4 presents the analysis of perturbation caused by temperature and concentration.

The regression coefficients for the six diffusive models, obtained by the fitting of experimental data to Eqs. (1) and (2), using Eq. (3), are presented in Table 4. These models were obtained considering only the influence of significant factors ($p < 0.05$), thus some insignificant interaction parameters are absent in the regression equations.

The determination coefficients (r^2) for D_w, D_{Suc}, D_{Na} . D_K, D_{Ca} and D_{Mg}. models were 0.993, 0.998, 0.999, 0.992, 0.999 and 0.998, respectively. The average error between the predicted values and experimental values (calculated by Eq. (2)) were below 10%. According to Andrade *et al*. [28], values of average error below 10% indicate an adequate fit for practical purposes. To verify the significance of the models, analysis of variance (ANOVA) was conducted and the results indicate that all models were significant with minor lack of fit, suggesting they adequately represent the relationship between responses and factors.

For D_w calculation, only interactions between temperature and concentration, and quadratic term of concentration were not significant at $p < 0.05$ level. These two independent variables positively affect D_w. The linear effect of temperature mostly influenced D_w calculation, followed by the linear effect of molasses concentration. Similarly, it was verified in the literature that D_w is dependent on the temperature, the osmotic solution concentration (using different sugars – sucrose, glucose, fructose, maltodextrin and sorbitol), and on the combination of both parameters for the osmotic treatment [25,27]. These researchers modeled D_w calculation, using non-linear regression and found an equation much alike to the equation determined in this study (Table 4).

Figure 1 presents response surfaces for D_w, valid for temperatures ranging from 20 to 50 °C, sugar beet concentrations between 60 and 80%. Figure 1 shows that the influence of temperature on D_w is stronger than the influence of molasses concentrations. It is also possible to observe the quadratic effect of these variables and the effect of the interaction between temperature and concentration on D_w calculation. Higher values of D_w were obtained at temperatures between 45 and 50 °C, and molasses concentrations from 75 to 80%. Experiment 9 was performed in these operating conditions, and it showed the highest values for the effective diffusivity of water (Table 3).

In this study, obtained results for effective diffusivity of water are in the range of 6.92×10^{-10}–8.06×10^{-10} $m^2 \cdot s^{-1}$. The effective diffusivities of water in shark filets during brining, found by Mujaffar & Sankat [18], were between 0.17×10^{-9} and 0.24×10^{-9} $m^2 \cdot s^{-1}$, at temperatures between 20–50 °C, in NaCl solution. The differences between the results of this study and the results found in the literature could be explained by the use of different types of materials. Another reason for this difference is the use of a sugar beet molasses solution during dehydration process. The presence of the different nutrients in the osmotic solution affects the mechanism involved in the simultaneous flows of water removal and solute penetration and, consequently, affects the diffusivity values.

Table 4 and Fig. 1 show that the influence of temperature on $D_{Suc.}$ is stronger than the influence of molasses concentrations. Higher values of $D_{Suc.}$ were obtained at higher temperatures and higher molasses concentrations. The effective diffusivity of sucrose in

*Table 4. Analysis of perturbation of response variables (D_w. D_{Na} . D_K. D_{Ca}. D_{Mg}. $D_{Suc.}$) × 10^{10} ($m^2 \cdot s^{-1}$) caused by changes in osmotic temperature and solution concentration; * – significant at p < 0.05 level, 95% confidence limit*

D	Source	Effect	*t*(3)	*p*	–95% Conf. lim.	+95% Conf. lim.	Reg. coeff.
D_w	Mean/Interc.*	2.995±0.014	207.702	<0.01	2.949	3.040	2.995±0.014
	Temp. lin.*	0.307±0.016	19.410	<0.01	0.256	0.357	0.153±0.008
	Temp. quad.	0.012±0.027	0.424	0.70	–0.075	0.099	0.006±0.014
	Conc. lin.*	0.137±0.016	8.666	<0.01	0.087	0.187	0.068±0.008
	Conc. quad.	0.006±0.027	0.236	0.83	–0.081	0.094	–
	Temp. x Conc.	–0.037±0.019	–1.907	0.15	–0.098	0.025	–
D_{Na}	Mean/Interc.*	2.214±0.010	228.994	<0.01	2.184	2.245	2.214±0.010
	Temp. lin.*	0.355±0.011	33.479	<0.01	0.321	0.388	0.177±0.005
	Temp. quad.*	0.109±0.018	5.955	0.01	0.051	0.168	0.055±0.009
	Conc. lin.*	0.114±0.011	10.794	<0.01	0.081	0.148	0.057±0.005
	Conc. quad.*	0.047±0.018	2.584	0.08	–0.011	0.106	0.024±0.009
	Temp. x Conc.*	–0.031±0.013	–2.374	0.09	–0.072	0.010	–0.015±0.006
D_K	Mean/Interc.*	2.157±0.004	534.840	<0.01	2.144	2.170	2.157±0.004
	Temp. lin.*	0.385±0.004	87.251	<0.01	0.371	0.400	0.193±0.002
	Temp. quad.*	0.106±0.008	13.796	<0.01	0.081	0.130	0.053±0.004
	Conc. lin.*	0.154±0.004	34.770	<0.01	0.140	0.168	0.077±0.002
	Conc. quad.*	0.019±0.008	2.457	0.09	–0.006	0.043	0.009±0.004
	Temp. x Conc.	0.002±0.005	0.365	0.74	–0.015	0.019	–
D_{Ca}	Mean/Interc.*	2.302±0.014	167.602	<0.01	2.258	2.346	2.302±0.014
	Temp. lin.*	0.249±0.015	16.544	<0.01	0.201	0.297	0.124±0.008
	Temp. quad.	0.033±0.026	1.259	0.30	–0.050	0.116	–
	Conc. lin.*	0.162±0.015	10.791	<0.01	0.114	0.210	0.081±0.008
	Conc. quad.*	–0.026±0.006	–5.207	0.05	–0.038	0.080	–0.013±0.003
	Temp. x Conc.	0.039±0.018	2.125	0.12	–0.019	0.098	–
D_{Mg}	Mean/Interc.*	1.420±0.005	274.093	<0.01	1.403	1.436	1.420±0.005
	Temp. lin.*	0.905±0.006	159.562	<0.01	0.887	0.923	0.453±0.003
	Temp. quad.*	0.380±0.010	38.700	<0.01	0.349	0.412	0.190±0.005
	Conc. lin.*	0.322±0.006	56.777	<0.01	0.304	0.340	0.161±0.003
	Conc. quad.*	0.098±0.010	9.969	<0.01	0.067	0.129	0.049±0.005
	Temp. x Conc.*	0.079±0.007	11.336	<0.01	0.057	0.101	0.039±0.003
$D_{Suc.}$	Mean/Interc.*	2.269±0.008	280.026	<0.01	2.243	2.295	2.269±0.008
	Temp. lin.*	0.272±0.009	30.671	<0.01	0.244	0.300	0.136±0.004
	Temp. quad.	0.010±0.015	0.673	0.55	–0.039	0.059	0.005±0.008
	Conc. lin.*	0.157±0.009	17.718	<0.01	0.129	0.186	0.079±0.004
	Conc. quad.	–0.001±0.015	–0.051	0.96	–0.050	0.048	–
	Temp. x Conc.*	0.031±0.011	2.841	0.07	–0.004	0.065	0.015±0.005

pork cubes was found to be in the range of 5.22×10^{-10}– -6.32×10^{-10} $m^2 \cdot s^{-1}$.

The effective diffusivity of Na in pork cubes, obtained in this study, was estimated and values between 5.08×10^{-10}–6.24×10^{-10} $m^2 \cdot s^{-1}$ were found (Table 3), and it was compared with other studies. Schmidt *et al.* [26] investigated osmotic treatment in chicken breast cuts, at 5 °C, under stirring conditions, in NaCl solutions, between 0 and 20%. Obtained effective diffusivities of Na were between 2.5×10^{-10} and 2.8×10^{-10} $m^2 \cdot s^{-1}$. Gravier *et al*. [24] used NaCl solutions between 30 and 200g/L for osmotic treatment of pork, and the obtained effective diffusivities ranged between 0.6×10^{-10} and 5.0×10^{-10} $m^2 \cdot s^{-1}$. Figure 1 and Table 4 show that the influence of temperature on $D_{Na.}$ is stronger than the influence of molasses concentrations. Higher values of $D_{Na.}$ were obtained using higher temperatures and higher molasses concentrations.

The results shown in Fig.1 and Table 4 indicate that the influence of temperature is stronger than the impact of molasses concentration for D_K, D_{Ca} and D_{Mg} calculation. Higher effective diffusion values were obtained at higher temperatures and higher molasses concentrations. The effective diffusivities for K, Ca and

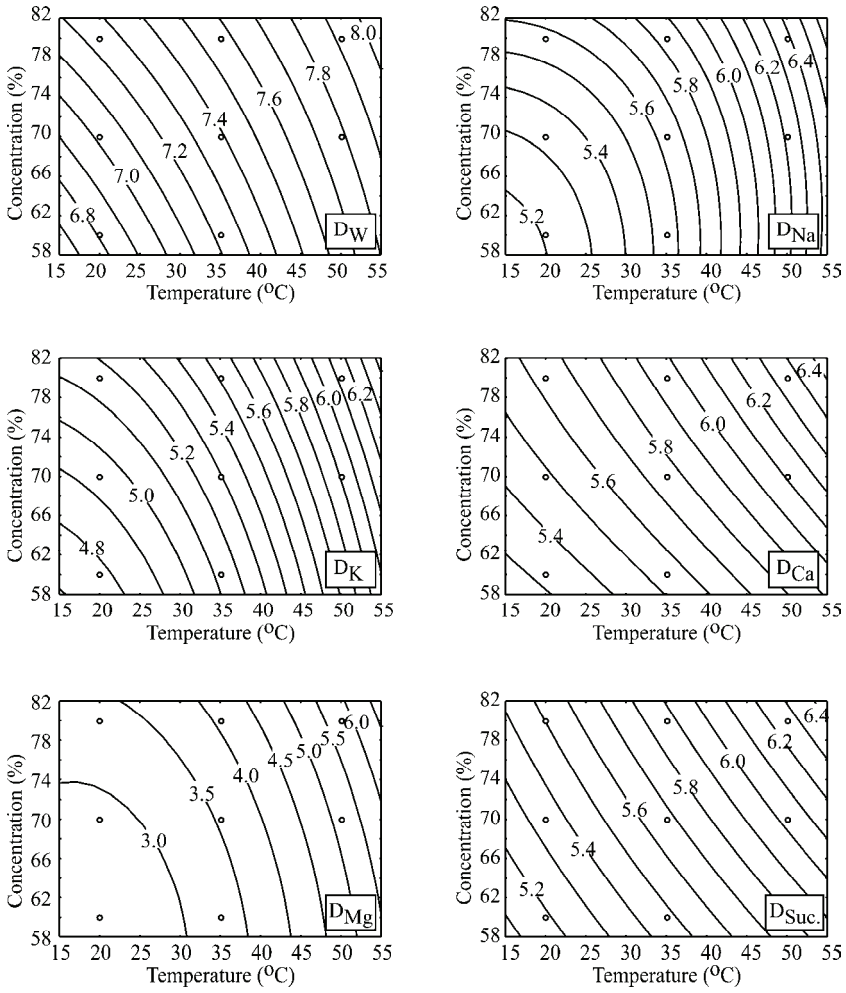

Figure 1. Response surface for effective diffusivity of water, Na, K, Ca Mg and sucrose as a function of temperature and molasses concentrations ($\times10^{-10}$ $m^2 \cdot s^{-1}$).

Mg in meat cubes were estimated, and values between 4.89×10^{-10} and 6.25×10^{-10}, 5.35×10^{-10} and 6.39×10^{-10} and 2.72×10^{-10} and5.77×10^{-10} $m^2 \cdot s^{-1}$ were obtained. Due to the lack of data in the literature, presented results could not be compared.

The differences between the results of this study and the results found in the literature can be explained by the use of different cultivars of pork cubes, and also with different degrees of maturation. Another reason for these differences is the use of sugar beet molasses solution. The presence of the different minerals in the osmotic solution affects the mechanism involved in the simultaneous flows of water removal and solute penetration, and, consequently, affects the diffusivities values.

CONCLUSIONS

During dehydration experiments of pork in sugar beet molasses solution, performed at different immersion times (1, 3 and 5 h), sugar beet molasses concentrations (60, 70 and 80%) and temperatures (20, 35 and 50 °C), equilibrium moisture content decreased with the temperature rise, while equilibrium content of observed minerals increased with the temperature enhancement. Zugarramurdi and Lupin's model was used for equilibrium values evaluation, and coefficients of determination showed good fitting capabilities.

Fick's unsteady-state diffusion equation has shown to be suitable for determining the mass effective diffusivity of water and solutes in pork cubes. The temperature and osmotic solution composition showed significant effects on all the responses studied. Increases in temperature, and/or molasses concentration led to higher effective diffusivity of water. Effective diffusivities of sucrose were higher at higher temperatures and molasses concentrations. For the above conditions of osmotic treatment, the effective diffusivity of water was found to be in the range of 6.92×10^{-10} and 8.06×10^{-10} $m^2 \cdot s^{-1}$. The sucrose effective diffusivity was between 6.39×10^{-10} and 8.25×10^{-10} m^2 s^{-1}, while diffusivities (m^2 s^{-1}) for minerals were in the range 6.34×10^{-10}–8.82×10^{-10} for Na, 6.27×10^{-10}–7.43×10^{-10} for K, 6.44×10^{-10}–8.94×10^{-10} for Ca and 3.47×10^{-10}–

-5.66×10^{-10} for Mg. Second order polynomial models fitted the effective diffusion data well.

Acknowledgements

This work was supported by the Ministry of Education, Science and Technological Development of the Republic of Serbia, Grant: TR 31055, for 2011–2014 project period.

REFERENCES

[1] J.M. Barat, M. Aliño, A. Fuentes, R. Grau, J.B. Romero, Measurement of swelling pressure in pork meat brining, J. Food Eng. **93** (2009) 108–113.

[2] A. Collignan, P. Bohuon, F. Deumier, I. Poligné, Osmotic treatment of fish and meat products, J. Food Eng. **49** (2001) 153–162.

[3] F.C.Schmidt, B.A.M. Carciofi, J.B. Laurindo, Salting operational diagrams for chicken breast cuts: hydration–dehydration. J. Food Eng. **91** (2008) 36–44.

[4] E. Desmond, Reducing salt: a challenge for the meat industry, Meat Sci. **74** (2006) 188–196.

[5] WHO/FAO (World Health Organization/Food and Agriculture Organisation) Diet, nutrition and the prevention of chronic diseases. WHO Technical Report Series 916. Geneva, World Health Organization, 2003.

[6] M. Aliño, R. Grau, F. Toldrá, E. Blesa, M.J. Pagán, J.M. Barat, Influence of sodium replacement on physicochemical properties of dry-cured loin, Meat Sci. **83** (2009) 423–430.

[7] M. Aliño, R. Grau, F. Toldrá, M.J. Pagán, J.M. Barat, Physicochemical changes in dry cured hams salted with potassium, calcium and magnesium chloride as a partial replacement for sodium chloride, Meat Sci. **86** (2010) 331–336.

[8] M. Armenteros, M.C. Aristoy, J.M. Barat, F. Toldrá, Biochemical changes in dry-cured loins salted with partial replacements of NaCl by KCl, Food Chem. **117** (2009) 627–633.

[9] M. Aliño, R. Grau, A. Fernández-Sánchez, A. Arnold, J.M. Barat, Influence of brine concentration on swelling pressure of pork meat throughout salting, Meat Sci. **86** (2010) 600–606.

[10] M. Armenteros, M.C. Aristoy, J.M. Barat, F. Toldrá, Biochemical and sensory properties of dry-cured loins as affected by partial replacement of sodium by potassium, calcium and magnesium J. Agr. Food Chem. **57** (2009) 9699–9705.

[11] E. Blesa, M. Aliño, J.M. Barat, R. Grau, F. Toldrá, M.J. Pagán, Microbiology and physico-chemical changes of dry-cured ham during the post-salting stage as affected by partial replacement of NaCl by other salts, Meat Sci. **78** (2008) 135–142.

[12] J. Gelabert, P. Gou, L. Guerrero, J. Arnau, Effect of sodium chloride replacement on some characteristics of fermented sausages, Meat Sci. **65** (2003) 833–839.

[13] A. Costa-Corredor, I. Muñoz, J. Arnau, P. Gou, Ion uptakes and diffusivities in pork meat brine-salted with NaCl and K-lactate, LWT – Food Sci. Technol. **43** (2010) 1226–1233.

[14] N.K. Rastogi & K.S.M.S. Raghavarao, K. Niranjan, D. Knorr, Recent developments in osmotic dehydration: methods to enhance mass transfer. Trends Food Sci. Tech. **13** (2002) 48–59.

[15] E. Spiazzi, R. Mascheroni, Mass transfer model for osmotic dehydration of fruits and vegetables. I. Development of the simulation model. J. Food Eng. **34** (1997) 387–410.

[16] A. Chiralt, P. Fito, J.M. Barat, A. Andrés, González-Martínez, C., I. Escriche, M.M. Camacho, Use of vacuum impregnation in food salting process. J. Food Eng. **49** (2001) 141–151.

[17] V.R.N. Telis, P.F. Romanelli, A.L.Gabas, J.T. Romero, Salting kinetics and salt diffusivities in farmed caiman muscle. Pesqui. Agropecu. Bras. **38** (2003) 529–535.

[18] S. Mujaffar, C. Sankat, The mathematical modeling of the osmotic dehydration of shark fillets at different brine temperatures, Int. J. Food Sci. Tech. **40** (2005) 1–12.

[19] G. Volpato, E.M.Z. Michielin, S.R.S. Ferreira, J.C.C. Petrus, Kinetics of the diffusion of sodium chloride in chicken breast (Pectoralis major) during curing, J. Food Eng. **79** (2007) 779–785.

[20] H. N. Lazarides, V. Gekas, Mavroudis, N. Apparent mass diffusivities in fruit and vegetable tissues undergoing osmotic processing. J. Food Eng. **31** (1997) 315–324.

[21] B. Singh, A. Kumar, A. K. Gupta, Study of mass transfer kinetics and effective diffusivity during osmotic dehydration of carrot cubes, J. Food Eng. **79** (2007) 471–480.

[22] A.S. Pajonk, R. Saurel, J. Andrieu, Experimental study and modeling of effective NaCl diffusion coefficients values during Emmental cheese brining., J. Food Eng. **60** (2003) 307–313.

[23] C. Vestergaard, J. Risum, J. Adler-Nissen, Na-MRI quantification of sodium and water mobility in pork during brine curing, Meat Sci. **69** (2005) 663–672.

[24] N. Graiver, A. Pinotti, A. Califano, N. Zaritzky, Diffusion of sodium chloride in pork tissue, J. Food Eng. **77** (2006) 910–918.

[25] F. Kaymak-Ertekin, M. Sultanoglu, Modelling of mass transfer during osmotic dehydration of apples, J. Food Eng. **46** (2000) 243–250.

[26] F.C. Schmidt, B.A.M. Carciofi, J.B. Laurindo, Application of diffusive and empirical models to hydration, dehydration, and salt gain during osmotic treatment of chicken breast cuts, J. Food Eng. **91** (2009) 553–559.

[27] A. Ispir, I.T. Togrul, Osmotic dehydration of apricot: kinetics and the effect of process parameters. Chem. Eng. Res. Des. **87** (2009) 166–180.

[28] S.A.C. Andrade, B.B.Neto, A.C. Nóbrega, P.M. Azoubel, N.B. Guerra, Evaluation of water and sucrose diffusion coefficients during osmotic dehydration of jenipapo (Genipa americana L.), J. Food Eng. **78** (2007) 551–555.

[29] A.M. Sereno, R. Moreira, E. Martinez, Mass transfer coefficients during osmotic dehydration of apple single and combined aqueous solution of sugar and salts. J.Food Eng. **47** (2001) 43–49.

[30] S. Rodrigues, F.A.N. Fernandes, Dehydration of melons in a ternary system followed by air-drying, J. Food Eng. **80** (2007) 678–687.

[31] G. Sacchetti, A. Gianotti, M. Dalla Rosa, Sucrose-salt combined effects on mass transfer kinetics and product acceptability. Study on apple osmotic treatments, J. Food Eng. **49** (2001) 163–173.

[32] P. Bohuon, A. Collignan, G. M. Rios, A.L. Raoult-Wack, Soaking process in ternary liquids: experimental study of mass transport under natural and forced convection, J. Food Eng. **37** (1998) 451–469.

[33] D. Sauvant, J.-M. Perez, G. Tran, Tables de composition et de valeur nutritive des matières premières destinées aux animaux d'élevage: Porcs, volailles, bovins, ovins, caprins, lapins, chevaux, poissons, 2ème édition revue et corrigée. INRA Editions, Versailles, France. 2004.

[34] D. Grbeša, Assessment methods and tables of chemical composition and nutritional value of food (in Croatian), Zagreb: Faculty of Agriculture, University of Zagreb, Croatian Society of Agronomists, 2004, pp. 134–137.

[35] N.M. Mišljenović, G.B. Koprivica, L.L. Pezo, LJ.B. Lević, B.LJ. Ćurčić, V. S. Filipović, M. R. Nićetin, Optimization of the osmotic dehydration of carrot cubes in sugar beet molasses, Therm. Sci. **16** (2012) 43–52.

[36] L.L. Pezo, B.Lj. Ćurčić, V.S. Filipović, M.R. Nićetin, G.B. Koprivica, N.M. Mišljenović, Lj. B. Lević, Artificial neural network model of pork meat cubes osmotic dehydration, Hem. Ind. **67** (2013) 465–475.

[37] AOAC Official methods of analysis, Association of Official Analytical Chemists, Moisture Content in Plants, Washington, DC, 930.04, 1990.

[38] J. Crank, The mathematics of diffusion, 2nd ed., Clarendon, Oxford, 1975.

[39] N.K. Rastogi, K.S.M.S. Raghavarao, Water and solute diffusion coefficients of carrot as a function of temperature and concentration during osmotic dehydration, J. Food Eng. **34** (1997) 429–440.

[40] A. Zugarramurdi, H.M. Lupin, A model to explain observed behavior on fish salting. J. Food Sci. **45** (1980) 1305–1311.

[41] Statistica (Data Analysis Software System). 2010. v.10., StatSoft, Inc., Tulsa, OK (www.statsoft.com).

[42] J.M. Barat, S. Rodríguez-Barona, A. Andrés, P. Fito, Influence of increasing brine concentration in the cod salting process, J. Food Sci. **65** (2002) 1922–1925.

[43] C.L. Hansen, F. Van Der Berg, S. Ringgaard, H. Stødkilde-Jørgensen, A.H. Karlsson, Diffusion of NaCl in meat studied by 1H and 23Na magnetic resonance imaging, Meat Sci. **80** (2008) 851–856.

IZVOD

PRIVIDNI KOEFICIJENTI DIFUZIJE VODE, SAHAROZE I MINERALA PRI OSMOTSKOM TRETMANU SVINJSKOG MESA U MELASI ŠEĆERNE REPE

Milica R. Nićetin[1], Lato L. Pezo[2], Biljana Lj. Lončar[1], Vladimir S. Filipović[1], Danijela Z. Šuput[1], Snežana Zlatanović[2], Biljana P. Dojčinović[3]

[1]*Univerzitet u Novom Sadu, Tehnološki fakultet, 21000 Novi Sad, Srbija*
[2]*Univerzitet u Beogradu, Institut za opštu i fizičku hemiju, 11000 Beograd, Srbija*
[3]*Univerzitet u Beogradu, Institut za hemiju, tehnologiju i metalurgiju, 11000 Beograd, Srbija*

(Naučni rad)

Metoda odzivne površine (Response Surface Methodology - RSM) je korišćena pri matematičkom modelovanju i izračunavanju vrednosti prividne (efektivne) difuzije vode, saharoze i minerala tokom osmotskog tretmana kockica svinjskog mesa (*M. triceps brachii*), na temperaturi 20, 35 i 50 °C i pri koncentracijama osmotskog rastvora (melasa šećerne repe) od 60, 70 i 80 mas.%. Numeričko rešavanje Fikovog (Fick) zakona o prenosu mase, pri nestacionarnim uslovima, za idealnu kocku je korišćeno za izračunavanje efektivnog koeficijenta difuzije vode, saharoze i minerala (Na, K, Ca and Mg). Sadržaj vlage i minerala je izmeren u tri ponavljanja. Korišćen je model Cuguramurdija (Zugarramurdi) i Lupina (Lupin) za predviđanje ravnotežnih uslova i ispostavilo se da je taj model pogodan za izračunavanje gubitka vlage i priraštaja suve materije tokom procesa osmotskog tretmana. Metoda odzivnih površina, koje se široko koristi za modelovanje i kontrolu procesa u prehrambenoj industriji, a u ovom radu je korišćena za predviđanje efektivnog koeficijenta difuzije vode, saharoze i minerala, pri određenoj temperaturi imerzije i koncentraciji melase šećerne repe. Matematički modeli koji su dobijeni na osnovu eksperimentalnih podataka obrađuju kompleksne nelinearne relacije sa interakcijama između procesnih promenljivih. Dobijene vrednosti efektivne difuzivnosti ($m^2\ s^{-1}$) za vodu bili su u rasponu od $6{,}95\times10^{-10}$ do $8{,}03\times10^{-10}$, za efektivnu difuzivnost saharoze bili su između $6{,}39\times10^{-10}$ i $8{,}25\times10^{-10}$, dok su difuzivnosti za minerale bile u opsezima: $6{,}34\times10^{-10}$–$8{,}82\times10^{-10}$ (Na), $6{,}27\times10^{-10}$–$7{,}43\times10^{-10}$ (K), $6{,}44\times10^{-10}$–$8{,}94\times10^{-10}$ (Ca) i $3{,}47\times10^{-10}$–$5{,}66\times10^{-10}$ (Mg). Korišćenjem razvijenih matematičkih modela dobijene su vrednosti efektivnih koeficijenata difuzije, sa tačnošću izraženom preko koeficijenata determinacije (r^2) za D_w, D_{Suc}, D_{Na} . D_K, D_{Ca} i D_{Mg}, i to: 0,993; 0,998; 0,999; 0,992; 0,999 i 0,998, redom. Širok opseg procesnih promenljivih veličina razmatranih u formiranju ovih modela, kao i njihova laka implementacija u tabelarnim proračunima, čini ove modele veoma praktičnim za projektovanje i kontrolu procesa.

Ključne reči: Svinjsko meso • Melasa šećerne repe • Osmotski tretman • Difuzija • Prenos mase

Sorption of cadmium ions from saline waters onto Fe(III)-zeolite

Aysha Ali Ahribesh[1], Slavica Lazarević[1], Branislav Potkonjak[2], Andjelika Bjelajac[3], Djordje Janaćković[1], Rada Petrović[1]

[1]*Faculty of Technology and Metallurgy, University of Belgrade, Belgrade, Serbia*
[2]*Institute of Chemistry, Technology and Metallurgy, University of Belgrade, Belgrade, Serbia*
[3]*Innovation center of the Faculty of Technology and Metallurgy, University of Belgrade, Belgrade, Serbia*

Abstract

The sorption of Cd^{2+} from natural seawater, artificial seawater, distilled water and NaCl solution of the same ionic strength as the seawater onto zeolite modified by iron(III) oxide (Fe(III)-zeolite) was investigated. The sorption was found to be time, concentration and pH dependent. The sorption capacity at the initial pH 7 decreased in the following order: distilled water > NaCl solution > artificial seawater > natural seawater. The isotherm study showed that Langmuir isotherm model could be adequately applied for the sorption in distilled water, indicating the homogeneous monolayer coverage at Fe(III)-zeolite surface, while the Freundlich isotherm model showed a better fit than the Langmuir model of the sorption data in saline waters, indicating multilayer heterogeneous coverage at the sorbent surface. The values of Freundlich parameter *n* suggested that the sorption was a favorable process and bonds between Cd^{2+} and Fe(III)-zeolite surface were stronger in NaCl solution than in natural and artificial seawater. Kinetics analysis showed that the mechanism of Cd^{2+} sorption from natural seawater differed from the sorption mechanism out of distilled water, NaCl solution and artificial seawater. The intra-particle diffusion kinetic model indicated that both boundary layer diffusion and intra-particle diffusion influenced the rate of sorption.

Keywords: sorption, cadmium ions, Fe(III)-zeolite, seawater, modeling.

Available online at the Journal website: http://www.ache.org.rs/HI/

SCIENTIFIC PAPER

UDC 66.081:546.48:551.464

Hem. Ind. **69** (3) 253–260 (2015)

doi: 10.2298/HEMIND140122038A

Cadmium is one of the most toxic heavy metals. It tends to accumulate in the body and it has varying degrees of toxicity. Cadmium causes serious diseases such as renal damage, anemia, hypertension, cancer, and kidney failure [1,2]. According to the World Health Organization (WHO) the maximum concentration of cadmium in drinking water should be 0.003 mg/L [3].

The common sources of cadmium in natural waters are soil and air pollution due to the several industrial applications such as cadmium plating and production of Cd-Ni batteries, copper alloys, paints, plastics, phosphates, ferilizers, and pigments [3,4].

There are various technologies for the removal of cadmium and other heavy metals from water systems: chemical precipitation, ion exchange, sorption, membrane processing, electrochemical treatment, etc. [5,6]. Among these procedures, the sorption is considered as one of the most attractive and powerful technique for heavy metals removal from solutions at low concentrations. By proper selection of the sorbent, the sorption can be a simple, environmental friendly and low cost operation of high efficiency [7,8]. A variety of sorbents, including clay minerals, zeolites, agricultural waste biomass, biopolymers, metal oxides, different industrial by-products, microorganisms, and activated carbon have been used for cadmium removal [8].

Zeolites have been extensively used as sorbents for heavy metals because they have great affinity for divalent metal ions [9]. The sorption capacity and selectivity of zeolite to heavy metal ions can be further improved by various modifications. It was shown that zeolites modified by oxides or hydroxides of trivalent iron had significantly higher affinity for Zn^{2+}, Cu^{2+}, Mn^{2+}, Pb^{2+} and Cd^{2+}, compared to the unmodified zeolite [10–14]. Iron(III) could be present in zeolite in different forms [15]: a) in framework positions (isomorphously substituted), b) in cationic positions in the zeolite channels, c) as binuclear or oligonuclear iron complexes in the extra-framework positions, d) as iron oxide FeO_x nanoparticles and e) as large iron oxide particles (Fe_2O_3) located on the surface of the zeolite crystals. Much higher capacity of the iron(III)-modified zeolite for Pb^{2+}, Cd^{2+} and Zn^{2+} in comparison to parent zeolite was explained [14] by: higher specific sorption resulting from the new functional groups on the surface; ion exchange due to the presence of easily exchangeable ions; the hydroxide precipitation caused by the higher point of zero charge.

The purpose of this work was to investigate the sorption of cadmium ions from natural seawater and various aqueous solutions on zeolite, modified by

Correspondence: R. Petrović, Faculty of Technology and Metallurgy, University of Belgrade, Karnegijeva 4, Belgrade, Serbia.
E-mail: radaab@tmf.bg.ac.rs
Paper received: 22 January, 2014
Paper accepted: 16 April, 2014

iron(III) oxide. Cadmium ion solutions of different concentrations in natural and artificial seawater were used for the experiments. For comparison, the sorption of cadmium from solutions prepared with distilled water was studied, as well as using NaCl solution of the same ionic strength as the seawater. The influence of the initial pH (pH_i) on the sorption from different water systems was evaluated. The sorption capacities of the sorbent at pH_i 7 were determined based on sorption isotherms, and experimental results were analyzed using theoretical models of sorption isotherms. The results of sorption kinetics of cadmium from different water systems were processed using the kinetic models.

EXPERIMENTAL

Materials

Sorbent

Zeolite modified by iron(III) oxide (Fe(III)-zeolite) was synthesized according to previously published method [10–14]. A natural zeolite from the Slanci locality, Serbia, was used as a starting material. The natural zeolite contained clinoptilolite, as a dominant phase, with lower contents of quartz and feldspar. The modified zeolite was prepared by adding, under stirring, of 180 cm^3 of 5 M KOH solution to a suspension of 20.0 g of the natural zeolite and 100 cm^3 of a freshly prepared 1 M $FeCl_3$ solution. The suspension was diluted by distilled water up to 2 dm^3 and held in a closed polyethylene flask at 70 °C for 60 h. Then, the reaction vessel was removed from the oven, and the red precipitate was centrifuged and washed until the negative reaction of Cl^- ions occurred and it was finally dried.

XRD analysis showed lower crystallinity of Fe(III)-zeolite in comparison to the parent zeolite. In addition, it was shown that Fe(III)-zeolite contained amorphous iron(III) oxides. The modification caused the specific surface area increasing from 18 to 175 m^2/g and the point of zero charge increasing from 7.5±0.1 to 9.3±0.1 [14].

Water samples

The four types of water were used:

1. Distilled water.

2. Natural seawater obtained of the coast of Greece and passed through 2 μm filter. The pH value of natural seawater was about 8. The analysis of seawater was done by a Metrohm ion chromatography instrument, 861 Advanced Compact IC MSM II. The concentrations of the main ions in the natural seawater are presented in Table 1.

3. Artificial seawater, prepared by dissolving 28.6 g NaCl, 0.65 g KCl, 5.26 g $MgCl_2.6H_2O$, 4.77 g $MgSO_4 \cdot 7H_2O$, 1.16 g $CaSO_4$ and 0.05 g NaBr in 1 dm^3 of distilled water in order to obtain the composition similar to the composition of the natural seawater.

4. NaCl solution, prepared by dissolving 40.2 g NaCl in 1 dm^3 of distilled water in order to obtain the solution of the same ionic strength as the seawater.

Table 1. Composition of the natural seawater used in the experiments

Ion	mg/dm^3	mmol/dm^3
Cl^-	19990	564.13
Na^+	11244	488.9
K^+	342	8.74
Mg^{2+}	1099	45.22
Ca^{2+}	343	8.56
SO_4^{2-}	2679	27.91
Br^-	49.4	0.62

Sorbate solution preparation

The stock solutions of cadmium, containing 100 mg Cd^{2+}/dm^3, were prepared by dissolving 0.1372 g of $Cd(NO_3)_2 \cdot 4H_2O$ in 500 cm^3 of each type of water. The solutions of different cadmium concentration ranging from 5 to 75 mg/dm^3, were prepared from stock solutions, by dilution.

The pH of the solutions for the sorption experiments was adjusted by 0.1 M KOH or 0.1 M HNO_3 solution.

Sorption experiments

The sorption experiments were performed by batch technique at room temperature (25±1 °C). The general method used for this study is described as follows: 20 cm^3 of different cadmium solutions were placed in 50 cm^3 reagent bottle, the pH value was adjusted and then the constant amount of Fe(III)-zeolite (0.02 g) was added to each bottle, followed by shaking for a given period of time.

The effect of initial pH value (pH_i) on Cd^{2+} sorption onto Fe(III)-zeolite was investigated with Cd^{2+} solution of 50 mg/dm^3 concentration, by varying pH_i from 4.0 to 8.0. The suspensions were shaken for 24 h.

The sorption isotherms for Cd^{2+} sorption out of different types of water onto Fe(III)-zeolite at pH_i 7.0±0.1 were determined by establishing the equilibration of Cd^{2+} solution of different concentration and Fe(III)-zeolite for 24 h.

The kinetics analysis of the sorption was done by using Cd^{2+} solutions of 100 mg/dm^3, at pH_i 7.0±0.1.

After all the experiments, the sorbent was separated from the solution using filter paper. The final solution pH (pH_f) was measured using a pH meter (InoLab WTW series pH 720). The initial concentrations of Cd^{2+}, as well as the concentrations after the sorption, were

determined using the atomic absorption spectrometer (AAS) (Perkin Elmer 730).

The equilibrium sorption capacity, q_e, was calculated using the equation:

$$q_e = \frac{c_i - c_e}{m} V \text{ (mg Cd}^{2+}\text{/g Fe(III)-zeolite)} \quad (1)$$

while the quantity of Cd^{2+} sorbed after the period of time t (q_t) was calculated according to equation:

$$q_t = \frac{c_i - c_t}{m} V \text{ (mg Cd}^{2+}\text{/g Fe(III)-zeolite)} \quad (2)$$

where V is the volume of the solution; c_i is the initial Cd^{2+} concentration, c_e is the equilibrium (residual) Cd^{2+} concentration; m is the weight of sorbent and c_t is the concentration of Cd^{2+} after period of time t.

Models of isotherms

The Langimur [16] and Freundlich [17] isotherms were applied to the experimental data to study the sorption capacity and to describe the solid–liquid sorption process:

$$\text{Langmuir model: } q_e = \frac{q_m k_L c_e}{1 + k_L c_e} \quad (3)$$

$$\text{Freundlich model: } q_e = k_F c_e^{1/n} \quad (4)$$

where q_e is the amount of solute sorbed per unit mass of the sorbent at equilibrium (mg/g); c_e is the equilibrium concentration of the solute in the bulk solution (mg/dm^3); q_m is the maximum sorption capacity (monolayer capacity, mg/g); k_L is the Langmuir constant related to the free energy of sorption (dm^3/ mg); k_F is a constant which is an indicator of the sorption capacity ((mg/g)(mg/dm^3)^n); and n is an sorption intensity parameter.

Sorption kinetics

The pseudo-first order equation [18] and the pseudo-second order equation [19,20] were applied to sorption kinetic data to describe the mechanism of sorption:

Pseudo-first order equation:

$$\log(q_e - q_t) = \log q_e - \frac{k_1 t}{2.303} \quad (5)$$

Pseudo-second order equation:

$$\frac{t}{q_t} = \frac{1}{k_2 q_e^2} + \frac{t}{q_e} \quad (6)$$

where q_e and q_t are sorption capacity at equilibrium and at time t, respectively (mg/g); k_1 is the rate constant of pseudo first order model (1/min); and k_2 is the rate constant of the pseudo second order model (g/(mg·min)).

In order to assess the nature of the diffusion process in Cd^{2+} sorption onto Fe(III)-zeolite, the intra-particle diffusion model, proposed by Weber and Morris [21] was used:

$$q_t = k_{td} t^{0.5} + C \quad (7)$$

where k_{td} (mg/(g·min$^{0.5}$)) is the intra-particle diffusion rate constant, and C (mg/g) is a constant that gives information about thickness of the boundary layer. This model considered the intra-particle diffusion as the rate controlling step when the value of C is close to zero.

RESULTS AND DISCUSSION

Effect of the initial pH

The influence of initial pH value on the sorption capacity of Fe(III)-zeolite for Cd^{2+} in different types of water is presented in Fig 1. The final pH values are indicated in this figure.

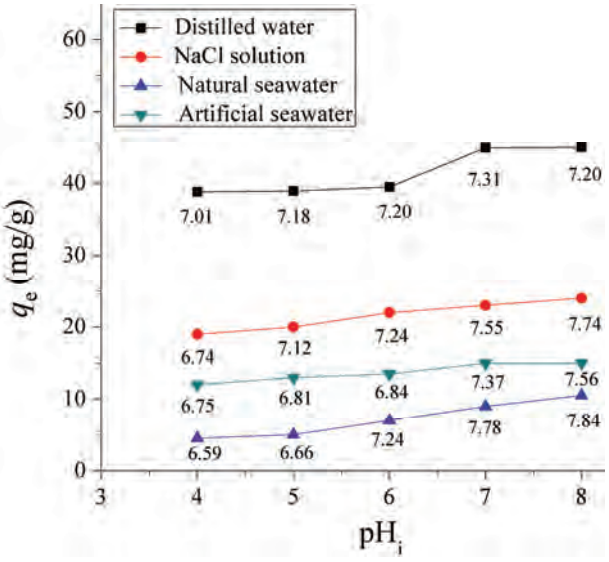

Figure 1. The comparison of the effect of the initial pH on the sorption capacity of Fe(III)-zeolite for Cd^{2+} from different types of water (the numbers in the figure indicate the final pH values). Concentration of Cd(II) solution was 50 mg/dm^3.

According to Fig. 1, the cadmium sorption efficiency on Fe(III)-zeolite increased when the initial pH was increased. This appeared because Fe(III)-zeolite was highly selective to H_3O^+ when the concentration of these ions was high. The values of pH_f, for $pH_i \leq 7$, indicate that H_3O^+ associates with the functional groups on the Fe(III)-zeolite surface. As pH_i was lower, the negative charge of the surface became lower and the positive charge higher, which decreased the sorption of positively charged cadmium ions. At pH_i 8, pH_f values

were lower than the initial ones, which indicates releasing of H_3O^+ into the solution because of the surface functional groups dissociation. Thus, the Cd^{2+}sorption at pH_i 8 was higher than at lower pH_i. These results show that pH values at which the surface charge was changed from positive to negative and vice versa were lower than pH_{PZC} of Fe(III)-zeolite [14], which indicates that the specific sorption is included in the process of Cd^{2+} sorption, as it was shown in previous investigation for the solutions in distilled water [14].

It should be noted that there was no indication of $Cd(OH)_2$ precipitation during adsorption at higher pH values. For the Cd^{2+} concentration of 50 mg/dm^3, the saturation for $Cd(OH)_2$ precipitation is at pH ≈8.5 (according to the value of the solubility product constant of $Cd(OH)_2$). However, in order to start precipitation (nucleation of solid phase from liquid phase), super saturation is necessary [22], which means that $Cd(OH)_2$ precipitation starts at pH higher than 8.5. If there are some dispersed particles in solution (like the sorbent in Cd^{2+} solution), a super saturation for nucleation is less than in solution without dispersed particle, but still pH value for the beginning of precipitation is higher than pH value for saturation. According to that, it can be said with certainty that there was no $Cd(OH)_2$ precipitation during the experiments.

It can be seen from Fig. 1 that the order of sorption capacity of Fe(III)-zeolite for Cd^{2+}, at all pHs is: distilled water > NaCl solution > artificial seawater > natural seawater. Obviously, the ions from saline waters decrease sorption capacity of Fe(III)-zeolite for Cd^{2+}, because those ions compete with Cd^{2+} for the sorption sites at the surface of the sorbent. The higher-valence ions have more competitive effect than monovalence ions [23], which explains the lower sorption capacity of the sorbent in artificial and natural seawaters than in NaCl solution: besides Na^+, both seawaters contain higher-valence ions, such as Ca^{2+} and Mg^{2+}. The lowest sorption capacity of the Fe(III)-zeolite in natural seawater can be explained by the presence of some other ions (carbonate and bicarbonate) and organic matter that are not present in artificial seawater.

Further investigations, the determination of sorption isotherms and kinetic analysis, were done at the initial pH 7.

Effect of the initial cadmium ions concentration – sorption isotherms

Figure 2 shows the sorption isotherms for Cd^{2+} on Fe(III)-zeolite from different types of water. The equilibrium concentration and the uptake of Cd^{2+} increase as the initial Cd^{2+} concentration increases. This appeared since at lower initial concentration the ratio of the initial number of metal ions to the number of available surface sites of sorbent is low. With the increase in the initial Cd^{2+} concentration, more Cd^{2+} were left in the solution due to the saturation of the binding sites.

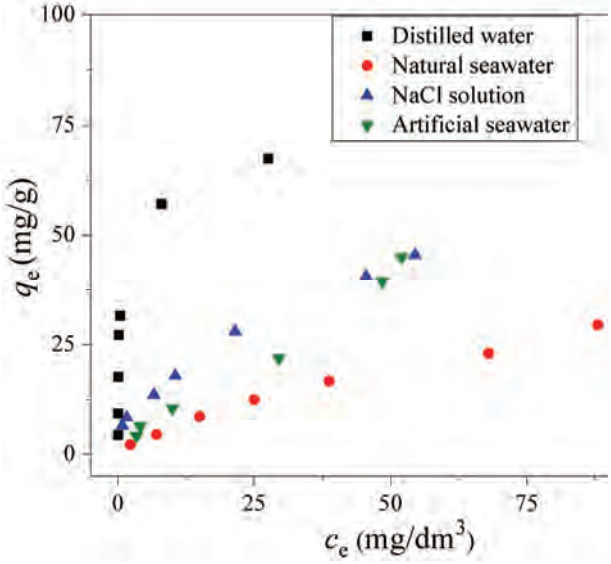

Figure 2. The comparison of sorption isotherms for Cd^{2+} on Fe(III)-zeolite from different types of water at initial pH 7.

The final pHs of the solutions in distilled water were between 8.98 (for c_i = 5 mg/dm^3) and 7.02 (for c_i = 100 mg/dm^3), which indicates that the specific sorption increased with c_i increase. In the case of NaCl solutions, pH_f was between 8.70 and 7.43. Lower pH_f for c_i = 5 mg/dm^3 than for solution in distilled water can be explained by the specific sorption of Na^+ on the sorbent surface. Na^+ are generally indifferent ions, which mean that they can not be specifically sorbed, but that is possible when the concentration is very high. Higher pH_f in NaCl solution for c_i = 100 mg/dm^3 than in the same solution in distilled water indicates lower specific sorption. Thus, the specific sorption is less pronounced in NaCl solution than in distilled water. The effect of ions in artificial seawater on the specific sorption is even more pronounced, because the pH_f changed from 7.89 to 7.48. Higher valence ions in artificial seawater can be specifically sorbed more than Na^+, so pH_f for c_i = = 5 mg/dm^3 was much lower than in NaCl solution and distilled water. The final pHs in natural seawater were approximately 7.8 for all concentration, due to the buffering effect as a result of the presence of bicarbonates.

By comparing the sorption isotherms (Fig. 2) it is obvious that the order of sorption capacity of Fe(III)--zeolite for Cd^{2+}, at initial pH 7 is: distilled water > NaCl solution > artificial seawater > natural seawater. This order is the same as in the investigation of the effect of the initial pH value on Cd^{2+} sorption.

Isotherms modeling

The sorption equilibrium data were analyzed by linear form of the Langmuir and Freundlich models.

The Langmuir isotherm model assumes monolayer sorption, where the energy of sorption for each sorbate species is the same and independent of surface coverage. The sorption occurs only on localized sites and involves no interactions between sorbed species [16,24–28].

The Freundlich isotherm model describes sorption on heterogeneous surfaces where sorption sites have different energies of sorption. This empirical model can be applied to multilayer sorption, which can include chemisorption (if active sites are strong enough) followed by physisorption [17,24–28].

The corresponding Langmuir and Freundlich parameters for Cd^{2+} sorption onto Fe(III)-zeolite from different types of water are given in Table 2. The correlation coefficient values indicate the superiority of Langmuir over Freundlich model for the sorption from distilled water, while Freundlich model is better for modeling of the sorption from saline waters. According to this, it can be concluded that ions from saline waters influence not only sorption capacity, but also cause change of sorption mechanism. The sorbent surface was homogeneous during the sorption from distilled water and the sorption took place until monolayer was formed, while in the case of the sorption from saline waters, sorbent surface was heterogeneous and more than one layer of Cd^{2+} were formed.

The feasibility of Cd^{2+} sorption from distilled water in the investigated concentration range can be expressed in terms of a dimensionless constant R_L (Eq. (8)), called the constant separation factor or equilibrium parameter [24,25,27]:

$$R_L = \frac{1}{1 + k_L c_i} \quad (8)$$

where k_L is the Langmuir constant (dm^3/mg), and c_i is the initial concentration (mg/dm^3). According to the value of R_L it is possible to assess irreversibility of the sorption process: as the value of R_L closer to zero, the process is more irreversible. When the value of k_L is infinitely large, which means that the bond between a sorbent and a sorbate is infinitely strong, the sorption process is irreversible ($R_L = 0$). The dependence of R_L on c_i in the investigated range of Cd^{2+} concentration in distilled water is presented in Fig. 3. It can be seen that R_L for the Cd^{2+} sorption from distilled water has very low values, which indicate favorable sorption and high degree of irreversibility.

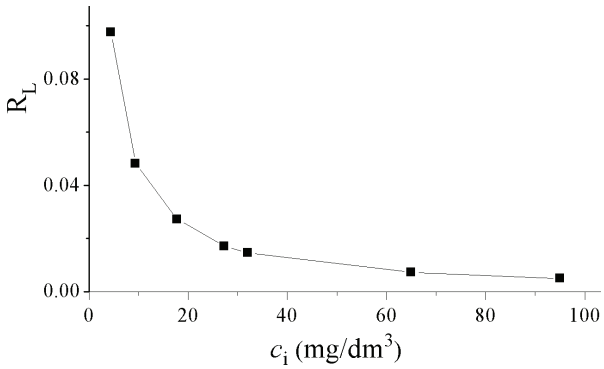

Figure 3. The dependence of R_L on the initail Cd^{2+} concentration.

In the case of the sorption from saline water, the Freundlich constant k_F had the lowest value for the seawater, slightly larger for the artificial seawater and the largest for the NaCl solution, meaning that the sorption capacity of Fe(III)-zeolite decreased in the following order: NaCl solution > artificial seawater > > natural seawater. These results are in accordance with the conclusions made from studying the influence of pH_i value on sorption capacity and according to sorption isotherms obtained for different types of water.

The Freundlich parameter n is a sorption intensity parameter, where the strength of sorption bonds is higher when n is higher. In that way, the value of n is an indication of the favorability of adsorption. Values of n > 1 represent favorable nature of adsorption [24–28]. According to the values of n for Cd^{2+} sorption from saline water (Table 2) it can be concluded that the sorption was a favorable process and that bonds between Cd^{2+} and Fe-zeolite surface were stronger in NaCl solution than in natural and artificial seawater. Obviously, the presence of higher-valence ions in seawaters, such as Ca^{2+} and Mg^{2+} influenced the strength of bonds between Cd^{2+} and the surface sites on the adsorbent.

Table 2. The Langmuir and Freundlich parameters and the correlation coefficients for Cd^{2+} sorption onto Fe(III)-zeolite from different types of water

Type of water	Langmuir parameters			Freundlich parameters		
	q_m / mg g^{-1}	k_L / dm^3mg^{-1}	R^2	k_F / ((mg/g) $(mg/dm^3)^n$)	$1/n$	R^2
Distilled water	68.027	2.10	0.997	4.328	0.335	0.767
Natural seawater	43.478	0.017	0.864	1.090	0.702	0.993
NaCl solution	53.763	0.071	0.912	2.268	0.466	0.984
Artificial seawater	9.091	0.122	0.127	1.305	0.744	0.919

Effect of contact time

The effect of contact time on Cd^{2+} sorption onto Fe(III)-zeolite from different types of water is presented in Fig 4. As it was expected, the extent of Cd^{2+} removal increased with the contact time. The Cd^{2+} uptake was rapid at the beginning, then was slow in the case of the sorption from distilled water, NaCl solution, and artificial seawater, while the sorption from seawater was slow at the beginning, and then increased. Such difference in time-dependence of sorption from seawater and other types of water can be explained by the presence of some organic compounds in natural seawater which can influence the rate of sorption.

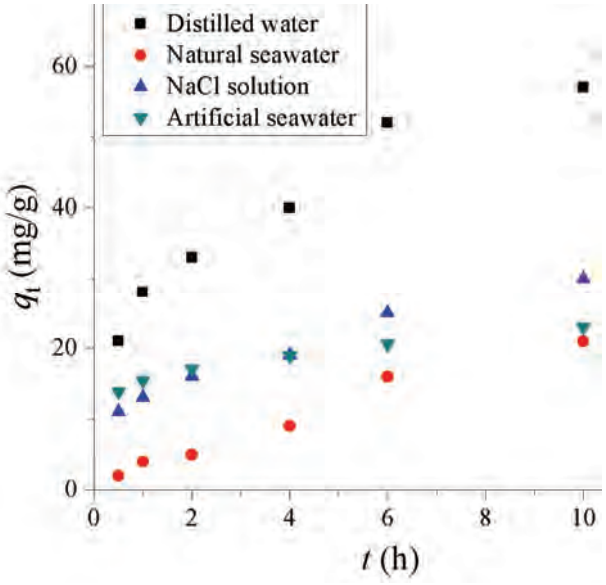

Figure 4. The effect of contact time on the Cd^{2+} sorption onto Fe(III)-zeolite from different types of water. Concentration of Cd^{2+} solution was 100 mg/dm^3.

Kinetics models

The sorption kinetics data were analyzed by three, most widely used kinetics models, *i.e.*, the pseudo-first order, pseudo-second order, and intra-particle diffusion models. The kinetic constants and correlation coefficients of these models are given in Table 3.

The pseudo-first order model is based on the assumption that the sorption rate is proportional to the number of free sites, while in the case of the pseudo-second-order kinetic model, the rate of sorption is proportional to the square of the number of unoccupied sites. According to the values of correlation coefficients (Table 3), it can be seen that pseudo-first order model can be applied for all the types of water, but for distilled water a slightly higher correlation coefficient was obtained for the pseudo second order model. In addition, pseudo-second-order model fits well the kinetics data of the Cd^{2+} adsorption from NaCl solution and artificial seawater, while in the case of natural seawater the correlation coefficient is very low. In that way, kinetics analysis showed that the mechanism of Cd(II) sorption from natural seawater differs from the sorption mechanism out of distilled water, NaCl solution and artificial seawater.

Sorption of any metal ion from aqueous phase onto porous materials proceeds by a multi-step process, and the rate of the sorption is controlled by either the film diffusion (external mass transfer) or the intra-particle diffusion rate or both [24,25,29–32]. In order to identify the diffusion mechanism, the intra-particle diffusion model (Eq. (7)) was applied and dependences q_t versus $t^{0.5}$ for all types of water are presented in Fig. 5. All the dependences consisted of two linear portions, indicating that the two stages occurred during sorption. The first portion is attributed to the boundary layer diffusion and the second one to the region where the intra-particle diffusion is involved in the sorption process [24,25,29–32]. Figure 5 shows differences between natural seawater and other types of water: the first linear part is longer for natural seawater than for other types of water, which means that boundary layer diffusion was included in sorption from seawater more than from other types of water. It can be supposed that some components from natural seawater, for example organic components, sorb at the surface of the sorbent, block some active sites at the outer surface of the sorbent and increase boundary layer.

The values of intra-particle diffusion rate constant, k_{td}, calculated from the second linear part of the dependence q_t versus $t^{0.5}$ (Fig. 5) are presented in Table 3. The highest value of k_{td} was obtained for distilled water, probably because there are no other dissolved substances that could slow down the Cd^{2+} diffusion in the pores.

Table 3. The kinetic parameters and correlation coefficients for the Cd^{2+} sorption onto Fe(III)-zeolite from different types of water

Type of water	Pseudo-first order constants		Pseudo-second order constants			Intra-particle diffusion model constants	
	$k_1\times10^3$ / min^{-1}	R^2	q_e / mg g^{-1}	k_2 / g mg^{-1}·min^{-1}	R^2	k_{td} / g mg^{-1} min$^{-0.5}$	R^2
Distilled water	4.61	0.90	64.27	$1.67\cdot10^{-4}$	0.98	1.82	0.96
Seawater	3.90	0.96	47.62	$2.59\cdot10^{-5}$	0.52	1.29	0.90
NaCl solution	3.68	0.93	33.33	$2.67\cdot10^{-4}$	0.95	1.01	0.98
Artificial seawater	3.23	0.99	23.92	$1.01\cdot10^{-3}$	0.99	0.50	0.99

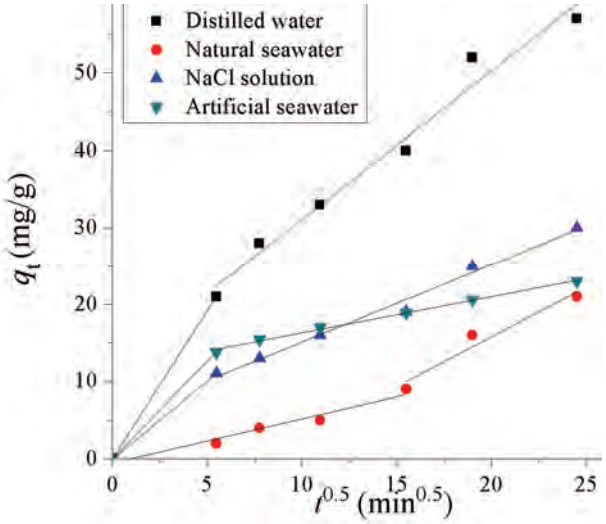

Figure 5. Weber–Morris intraparticle diffusion model plot for the Cd^{2+} sorption onto Fe(III)-zeolite from different types of water.

CONCLUSIONS

The sorption potential of zeolite modified by iron(III) oxide to cadmium ions from different types of water was evaluated. It was shown that the sorbent capacity and sorption mechanisms are highly influenced by the presence of competitive ions in water. The sorbent capacity at initial pH 7 decreased in the following order: distilled water > NaCl solution > artificial seawater > natural seawater. The Freundlich isotherm model provides the best fit to the sorption equilibrium data obtained from saline waters, which indicates heterogeneity of the sorbent surface and the multilayer adsorption. The sorption was a favorable process and bonds between cadmium ions and Fe(III)--zeolite surface were stronger in NaCl solution than in natural and artificial seawater. In the case of sorption from distilled water, the sorption equilibrium data were best fitted by the Langmuir model, indicating homogeneous and monolayer sorption. Kinetics analysis showed that both boundary layer diffusion and intra-particle diffusion influenced the rate of the sorption from all types of water. In the case of the sorption from natural seawater, the intraparticle diffusion was significant at longer contact times than in the case of other types of water.

Acknowledgements

The authors would like to acknowledge the financial support of the Ministry of Education, Science and Technological Development of the Republic of Serbia, Project No. III 45019.

REFERENCES

[1] K. S. Low, C. K. Lee, S. C. Liew, Sorption of cadmium and lead from aqueous solutions by spent Grain, Process Biochem. **36** (2000) 59–64.

[2] J. Hizal, R. Apak, Modeling of cadmium(II) adsorption on kaolinite-based clays in the absence and presence of humic acid, Appl. Clay Sci. **32** (2006) 232–244.

[3] H.K. Boparai, M. Joseph, D.M. O'Carroll, Kinetics and thermodynamics of cadmium ion removal by adsorption onto nano zerovalent iron particles, J. Hazard. Mater. **186** (2011) 458–465.

[4] E. Gutiérrez-Segura, M. Solache-Ríos, A. Colín-Cruz, C. Fall, Adsorption of cadmium by Na and Fe modified zeolitic tuffs and carbonaceous material from pyrolyzed sewage sludge, J. Environ. Manage. **97** (2012) 6–13.

[5] M. Ahmad, A.R.A. Usman, S.S. Lee, S. Kim, J. Joo, J.E. Yang, Y.S Ok, Eggshell and coral wastes as low cost sorbents for the removal of Pb^{2+}, Cd^{2+} and Cu^{2+} from aqueous solutions, J. Ind. Eng. Chem. **8** (2012) 198–204.

[6] R. Schmuhl, HM. Krieg, K. Keizer, Adsorption of Cu(II) and Cr(VI) ions by chitosan: Kinetics and equilibrium studies, Water SA **27** (2001) 1–7.

[7] G. Crini, Recent developments in polysaccharide-based materials used as adsorbents in wastewater treatment, Prog. Polym. Sci. **30** (2005) 38–70.

[8] F. Fu, Q. Wang, Removal of heavy metal ions from wastewaters: A review, J. Environ. Manage. **92** (2011) 407–418.

[9] S. Wang, Y. Peng, Natural zeolites as effective adsorbents in water and wastewater treatment, Chem. Eng. J. **156** (2010) 11–24.

[10] A. Dimirkou, Uptake of Zn^{2+} by a fully iron-exchanged clinoptilolite, Case study of heavily contaminated drinking water samples. Water Res. **41** (2007) 2763–2773.

[11] M. Doula, Synthesis of a clinoptilolite–Fe system with high Cu sorption capacity, Chemosphere **67** (2007) 731––740.

[12] M.K. Doula, A. Dimirkou, Use of an iron-overexchanged clinoptilolite for the removal of Cu^{2+} from heavily contaminated drinking water samples, J. Hazard. Mater. **151** (2008) 738–745.

[13] M.K. Doula, Simultaneous removal of Cu, Mn and Zn from drinking water with the use of clinoptilolite and its Fe-modified form, Water Res. **43** (2009) 3659–3672.

[14] M.T. Mihajlović, S.S. Lazarević, I.M. Janković-Častvan, B. M. Jokić, Đ.T. Janaćković, R.D. Petrović, A comparative study of the removal of lead, cadmium and zinc ions from aqueous solutions by and Fe(III)-modified zeolite, Chem. Ind. Chem. Eng. Q. **21** (2015) 295−303.

[15] P.J. Ramírez, G. Mul, F. Kapteijn, J.A. Moulijn, A.R. Overweg, J.A. Doménech, A. Ribera, I.W.C.E. Arends, Physicochemical characterization of isomorphously substituted FeZSM-5 during activation, J. Catal. **207** (2002) 113–126.

[16] I. Langmuir, The adsorption of gases on plane surfaces of glass, mica and platinum, J. Am. Chem. Soc. **40** (1918) 1361–1403.

[17] H. Freundlich, Concerning adsorption in solutions. Zeitschrift für Physikalische Chemie. **57** (1906) 385–470.

[18] S. Lagergren, Zur theorie der sogenannten adsorption gelöester stoffe, Kungliga Svenska Vetenskapsakademiens Handlingar. **24** (1898) 1–39.

[19] Y.S. Ho, G. McKay, Sorption of dye from aqueous solution by peat, Chem. Eng. J. **70** (1998) 115–124.

[20] G. McKay, Y.S. Ho, Pseudo-second order model for sorption processes, Process Biochem. **34** (1999) 451–465.

[21] W.J. Weber, J.C. Morris, Kinetics of adsorption on carbon from solution, J. Sanit. Eng. Div. Am. Soc. Civil Eng. **89** (1963) 31–60.

[22] M.N. Rahaman, Ceramic Processing and Sintering, Second Edition, Marcel Dekker Inc., New York, 2003.

[23] J.C. Crittenden, R.R. Trussell, D.W. Hand, K.J. Howe, G. Tchobanoglous, Water Treatment: Principles and Design, John Wiley & Sons. Inc., Hoboken, NJ, 2005.

[24] C. Luo, Z. Tian, B. Yang, L. Zhang, S. Yan, Manganese dioxide/iron oxide/acid oxidized multi-walled carbon nanotube magnetic nanocomposite for enhanced hexavalent chromium removal, Chem. Eng. J. **234** (2013) 256–265.

[25] E.S. Dragan, D.F.A. Loghin, Enhanced sorption of methylene blue from aqueous solutions by semi-IPN composite cryogels with anionically modified potato starch entrapped in PAAm matrix, Chem. Eng. J. **234** (2013) 211–222.

[26] X. Wang, R. Sun, C. Wang, pH dependence and thermodynamics of Hg(II) adsorption ontochitosan-poly-(vinyl alcohol) hydrogel adsorbent, Colloids Surfaces, A **441** (2014) 51–58.

[27] M. Naushad, Surfactant assisted nano-composite cation exchanger: Development, characterization and applications for the removal of toxic Pb^{2+} from aqueous medium, Chem. Eng. J. **235** (2014) 100–108.

[28] O.S. Ayanda, O.S. Fatoki, F.A. Adekola, B.J. Ximba, Removal of tributyltin from shipyard process wastewater by fly ash, activated carbon and fly ash/activated carbon composite: adsorption models and kinetics, J. Chem. Technol. Biotechnol. **88** (2013) 2201–2208.

[29] M.V. Dinu, E.S. Dragan, Evaluation of Cu^{2+}, Co^{2+} and Ni^{2+} ions removal from aqueous solution using a novel chitosan/clinoptilolite composite: Kinetics and isotherms, Chem. Eng J. **160** (2010) 157–163.

[30] A.K. Bhattacharya, T.K. Naiya, S.N. Mandal, S.K. Das, Adsorption, kinetics and equilibrium studies on removal of Cr (VI) from aqueous solutions using different low-cost adsorbents, Chem. Eng J. **137** (2008) 529–541.

[31] M. Nasiri Sarvi, T.B. Bee, C.K. Gooi, B.W. Woonton, M.L. Gee, A.J. O'Connor, Development of functionalized mesoporous silica for adsorption and separation of dairy proteins, Chem. Eng J. **235** (2014) 244–251.

[32] M.C.S. Faria, R.S. Rosemberg, C.A. Bomfeti, D.S. Monteiro, F. Barbosa, L.C.A. Oliveira, M. Rodriguez, M.C. Pereira, J.L. Rodrigues, Arsenic removal from contaminated water by ultrafine d-FeOOH adsorbents, Chem. Eng J. **237** (2014) 47–54.

IZVOD

SORPCIJA JONA KADMIJUMA IZ SLANIH VODA NA Fe(III)-ZEOLITU

Aysha Ali Ahribesh[1], Slavica Lazarević[1], Branislav Potkonjak[2], Andjelika Bjelajac[3], Djordje Janaćković[1], Rada Petrović[1]

[1]*Tehnološko–metalurški fakultet, Univerzitet u Beogradu, Karnegijeva 4, Beograd, Srbija*
[2]*Institut za hemiju, tehnologiju i metalurgiju, Univerzitet u Beogradu, Njegoševa 12, Beograd, Srbija*
[3]*Inovacioni centar Tehnološko-metalurškog fakulteta, Univerzitet u Beogradu, Beograd, Srbija*

(Naučni rad)

U ovom radu je ispitivana sorpcija Cd^{2+} iz prirodne morske vode, laboratorijski pripremljene morske vode, destilovane vode i rastvora NaCl, iste jonske jačine kao morska voda, na zeolitu modifikovanom gvožđe(III)-oksidom. Pokazano je da sorpcija zavisi od vremena, početne koncentracije Cd^{2+} i pH vrednosti. Sorpcioni kapacitet Fe(III)-zeolita za Cd^{2+} pri početnoj pH 7 opada u sledećem nizu: destilovana voda > NaCl rastvor > laboratorijski pripremljena morska voda > prirodna morska voda. Modelovanje rezultata ispitivanja sorpcije u ravnotežnim uslovima je pokazalo da se adsorpcija iz destilovane vode može opisati Langmirovim modelom, što ukazuje na homogenu sorpciju i formiranje monosloja na površini Fe(III)-zeolita. Rezultati sorpcije iz slanih voda se bolje opisuju Frojndlihovim nego Langmirovim modelom, što ukazuje na višeslojnu sorpciju na heterogenoj površini sorbenta. Vrednosti Frojndlihovog parametra *n* pokazuju da je sorpcija Cd^{2+} na Fe(III)-zeolitu favorizovan proces i da su veze između Cd^{2+} i površine Fe(III)-zeolita jače u NaCl rastvoru nego u prirodnoj i laboratorijski pripremljenoj morskoj vodi. Kinetička analiza sorpcije je pokazala da se mehanizam sorpcije iz prirodne morske vode razlikuje od mehanizma sorpcije iz ostalih ispitivanih tipova vode. Kinetički model unutarčestične difuzije je pokazao da i difuzija kroz granični sloj i unutarčestična difuzija određuju brzinu sorpcije. Difuzija kroz granični sloj je u većoj meri zastupljena kod sorpcije iz morske vode nego u slučaju sorpcije iz drugih ispitivanih tipova vode.

Ključne reči: Sorpcija • Kadmijum jon • Fe(III)-zeolit • Morska voda • Modelovanje

Energy integration of nitric acid production using Pinch methodology

Gorica R. Ivaniš[1], Marija Lazarević[2], Ivona R. Radović[1], Mirjana Lj. Kijevčanin[1]

[1]*University of Belgrade, Faculty of Technology and Metallurgy, Belgrade, Serbia*
[2]*Galenika Fitofarmacija, Belgrade, Serbia*

Abstract

Pinch methodology was applied to the heat exchangers network (HEN) synthesis of nitric acid production. The integration is analyzed in two ways, and the results are presented as two different solutions: *i*) the first solution is based on the original heat transfer equipment arrangement and *ii*) in order to eliminate the shortages of the first solution the second HEN was obtained using process simulation with optimized process parameters. Optimized HEN, with new arrangement of heat exchangers, gave good results in energy and process optimization.

Keywords: Pinch methodology, energy integration, minimum temperature difference, nitric acid production, total costs.

Available online at the Journal website: http://www.ache.org.rs/HI/

PROFESSIONAL PAPER

UDC 661.56:66.011

Hem. Ind. **69** (3) 261–268 (2015)

doi: 10.2298/HEMIND140204039I

Synthesis of heat exchanger networks allows significant reduction in energy requirements [1–6], and it is one of the main research areas in energy optimization in the past decades. Consequently the high number of methods for process and energy optimization and integration were developed. One of the most efficient methods for energy optimization is Pinch methodology, based on heat exchangers network (HEN) optimization, and leading to industrial processes optimization and efficient energy utilization of industrial systems.

Pinch methodology is very suitable for a detailed energy analysis of the process, but also for comparison of different alternative networks solutions [7–15].

The aim of this work is to analyze the nitric acid production and to present the optimal solution for the energy integration of the investigated process. Nitric acid is very important product of the chemical industry. It is a process with high energy consumption, and with units based on high energy demands, such as the heat exchangers, heaters and refrigerators. Heat exchangers network along with available utilities represent the part of the industrial systems where process costs can be significantly reduced by optimizing process parameters. In this paper comparison of the two HENs was performed: one, based on parameters proposed in the literature [1] and other, the optimized solution based on adjusted process data.

Heat integration methods

In late 70s B. Linnhoff and T. Umeda [15] and their coworkers found a "bottleneck of heat exchange" or Pinch point, when they were analyzing the heat transfer in the process. Since then, the Pinch methodology was introduced in process analysis. This method represents an extremely useful tool for analysis and process and energy synthesis. Pinch methodology is a sequential graphical HENs method based on the first law of thermodynamics and some constrains originated from the second law of thermodynamics [3].

In industrial processes, the heat is transferred between process of hot and cold streams or between process of streams and utilities (fluids used for additional heating or cooling, such as steam, cooling water, etc.). In order to save energy, there is a tendency to design an industrial process where maximum heat amount is being transferred between process streams, so the needs for external heating and cooling are minimized. This is accomplished by optimizing the existing HEN, which is the main goal of Pinch methodology. In addition to energy savings, better thermal process integration reduces a number of process units (heat exchangers or others) and leads to additional financial savings.

Pinch method also could be presented with hot and cold streams composite curves or grand composite curves [1–15], constructed on the process streams and their thermo-physical parameters. At the Pinch point composite curves are closest to each other and temperature between them is minimum temperature difference (ΔT_{min}). Pinch point divides process into two parts. The area above the Pinch can be considered as heat sink, which means it only receives the heat from external heat source ($Q_{h,min}$), while area below the Pinch presents process heat source and requires external heat sink ($Q_{c,min}$) [16].

Data required for the energy networks analysis are: source and target temperatures of process streams, heat transfer flow rate or enthalpy changes of process

Correspondence: M.Lj. Kijevčanin, University of Belgrade, Faculty of Technology and Metallurgy, Karnegijeva 4, Belgrade, Serbia.
E-mail: mirjana@tmf.bg.ac.rs
Paper received: 4 February, 2014
Paper accepted: 24 April, 2014

streams. Inlet (source) temperatures are those temperatures at which a fluid is available in the process.

Heating and cooling demands of each stream is determined based on the heat capacity flow rate *CP* (kW/°C), defined as:

$$CP = mc_p \quad (1)$$

and for the hot and cold streams' matches in the area above the Pinch heat capacity flow rate of process streams shall follow the rule:

$$CP_h \leq CP_c \quad (2)$$

while in the area below the Pinch the opposite rule applies:

$$CP_h \geq CP_c \quad (3)$$

Also, in the cases where there are no matches between streams that follow the *CP* rules, the appropriate rule could be fulfilled by splitting hot stream in two or more branches above Pinch, or cold stream below Pinch point.

In this paper, HINT software [17] was used for the HEN design of nitric acid production in Petrochemical Industry-Kutina, located in Croatia [1,2] with simplified process flow diagram presented in Figure 1 [1]. This process includes 17 heat exchangers, 2 turbines (steam or gas driven), 2 compressors, 3 filters, 2 separators and 3 reactors. Boilers are used for the high pressure steam production. For the additional heating and cooling requirement, for 16 process streams, the medium pressure steam (12.2 bar), low pressure steam (4.4 bar), cooling water and boiler feed water are available.

The liquid ammonia flows into the evaporator where it evaporates by the indirect steam heating (in heat exchangers E103, E112 and E113), as shown in Figure 1. For the drops or impurities removal the ammonia vapour passes through a filter (F102), and finally vapour stream is at 8.1 bar. On the other hand, air is compressed (C101) to the same pressure, heated to a temperature of 200–300 °C, and purified in the filter (F101) before mixing with ammonia. Gaseous mixture containing about 10% of ammonia is prepared before the reaction that takes place in the reactor (R101).

The product of the catalytic oxidation of ammonia is hot gaseous mixture containing NO, steam and non-reacted components of air, nitrogen and oxygen. Yield achieved at 8.1 bar is 95%, while at atmospheric pressure it reaches 97–98%. The resulting gaseous mix-

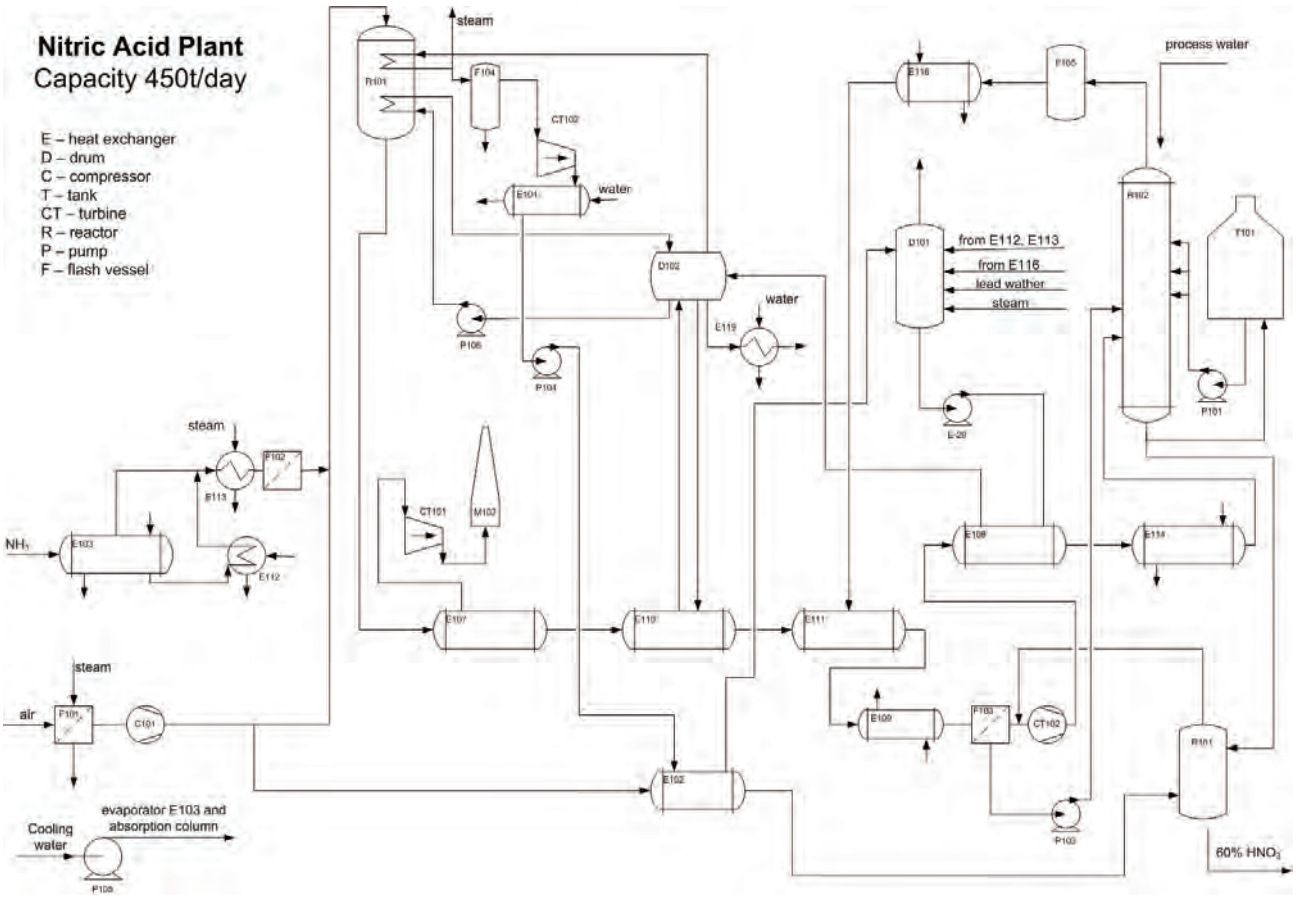

Figure 1. Process flow diagram of nitric acid synthesis plant.

ture is cooled in heat exchangers (E107, E110 and E111) and the released energy is used for steam production. Obtained steam is used for ammonia and air preheating. Cooling the mixture to a moderate temperature allows regeneration of the catalyst.

After catalyst regeneration gas blend is rapidly cooled further in the condenser (E109) to the temperature of 50 °C. Absorption of nitrogen oxides in the water leads to the formation of diluted nitric acid whose concentration is 2–30% and it is introduced to the top of the absorption tower (R102). The cooled gaseous mixture, containing NO, NO_2, N_2O_4 and a non-reacted part of N_2 and O_2 from air, is inlet in the lower part of the absorber. In the absorber the remaining NO is oxidized to NO_2 and N_2O_4 with the simultaneous absorption of NO_2 in water, and this stream is also inlet into the absorber. An additional quantity of air is necessary in order to complete the oxidation of NO. If the absorption is performed at atmospheric pressure, concentration of produced nitric acid is about 45–50%, while at raised pressures the acid concentration could be up to 70% [18–20].

Table 1 presents all data [2] of the above described process used for the further energy integration.

RESULTS AND DISCUSSION

The first step in our analysis was synthesis of the HEN based on the original data proposed by Matijašević and Otmačić [1].

Originally proposed ΔT_{min} = 38 °C was used for energy cascade and for the matches between all considered process streams, and based on that minimum heating and cooling demands are determined:

- minimum heating demand: $Q_{h,min}$ = 0.48 kW. Since obtained value is very small, it could be considered as a consequence of slightly incorrect flow measurements and it was neglected in further analysis,
- minimum cooling demand: $Q_{c,min}$ = 25114.7 kW and
- Pinch temperature is 277 °C ($T_{P,}$h = 296 °C and $T_{P,c}$ -= 258 °C).

Diagrams of grand composite curve for this process are shown in Figure 2.

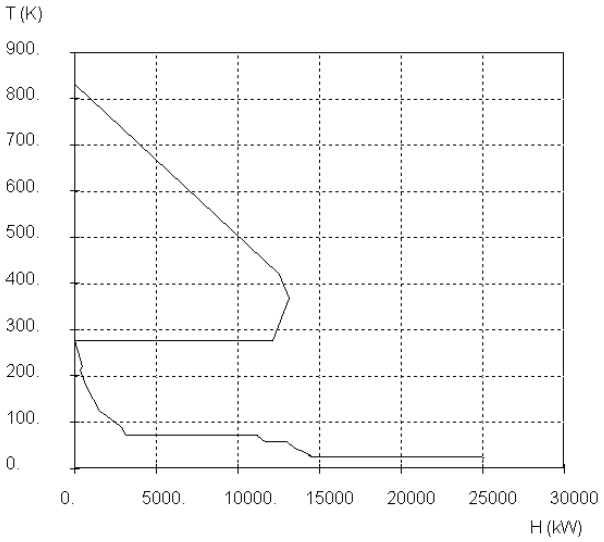

Figure 2. Grand composite curve.

Next step in heat integration is HEN synthesis, and according to the original scheme – process contains 17 units used for heat transfer (9 heat exchangers and 8 coolers). As mentioned above, process does not require

Table 1. Process streams data [2]

Stream	Description	Type	T_s / °C	T_t / °C	ΔH / kW	CP / kW °C^{-1}
1	$NH_{3,l}$	Cold	8.5	8.5	133.5	-
2	$NH_{3,g}$	Cold	8.5	100.0	366.0	4.0
3	LP NO*x*	Hot	850.0	90.0	-23104.0	30.4
4	H_2O_g	Hot	90.0	90.0	-8033.1	-
5	$NO_{x\ mix\ l,g}$	Hot	90.0	38.0	-1809.6	34.8
6	HP NO_x	Hot	232.0	76.0	-4695.6	30.1
7	$H_2O_{\ steam}$	Hot	76.0	76.0	-1296.5	-
8	$NO_{x\ mix\ l,g}$	Hot	76.0	46.0	-876.0	29.2
9	Top gases	Cold	25.0	350.0	7475.0	23.0
10	Secondary air	Hot	194.0	120.0	-355.2	4.8
11	HP steam	Cold	258.0	400.0	2584.4	18.2
12	Steam condensate	Hot	44.0	44.0	-10467.5	-
13	HP steam	Cold	258.0	258.0	12150.2	-
14	Turbine condensate	Cold	50.0	70.0	360.0	18.0
15	Boiler feedwater	Cold	105.0	200.0	2631.5	27.7
16	Cooling water	Hot	255.0	50.0	-164.0	0.8

additional heating so in a grid diagram there are no heaters, as it is shown in Figure 3.

Since all data were extracting from process flowmeters, due to some inconsistency, and in order to obtain more realistic network, some corrections were made [1]:

- Heat capacity flow rate (mass flow rate) of stream 11, *CP*, is adjusted from 18.2 to 18.14 kW/°C. As a consequence, enthalpy of this stream is reduced from 2584.4 to 2575.88 kW. Accordingly, the minimum heating demands (0.48 kW) were neglected.

- Heat capacity flow rate of stream 10 is corrected from 4.8 to4.865 kW/°C, and in this way enthalpies of streams 10 and 14 are equalled and these streams are efficiently linked through exchanger number 6 with capacity of 360 kW. An important note is that exchanger 7, which connects streams 6 and 15, has temperature difference between hot and cold stream smaller than ΔT_{min} = 38 °C. Minimum temperature difference for exchanger 7 is 32 °C [2].

The summary of the obtained results is presented in Table 2.

Based on the analysis of the given HEN it can be concluded that exchanger 5 (connecting streams 3 and 9) transfers heat through Pinch point.

In order to have comprehensive insight in heat transfer optimization, capital costs and heating and cooling demands were also simultaneously analyzed. The total costs of HEN can be calculated based on capital and energy costs.

Energy costs could be calculated as:

$$\text{Total energy costs} = \Sigma Q_u C_u \quad (4)$$

In the considered case, the hot utility requirement is 5359.48 kW and this roughly corresponds to the amount of heat that is transmitted through “pinch”. Cooling water demand (cold utility) is 25115.7 kW.

Utility costs are [21]:

- steam costs: 296.64 $/(kW year);
- cooling water costs: 221.76 $/(kW year).

Using all the above mentioned parameters total energy costs could be calculated as:

- heating costs; 359.48 kW×296.64 $/(kW year) = = 1 589 836.15 $/year;
- cooling costs: 25115.7 kW×221.76 $/(kW year) = = 5 569 657.63 $/year;
- total energy costs: 1 589 836.15 + 5 569 657.63 = = 7 159 493.78 $/year.

Value of capital costs depends on economic factors such as interest on loan, payback time, investment factors, etc. Total capital costs are calculated using equations:

$$C(\$) = [N_{min}\{a + b(A_{min}/N_{min})^c\}]_{AP} + [N_{min}\{a + b(A_{min}/N_{min})^c\}]_{BP} \quad (5)$$

or

$$C(\$)_{RT} = a + bA^c \quad (6)$$

It should be noted that if ΔT_{min} increases heat that is transferred within the system decreases and therefore lower heat transfer area is required, and leads to the

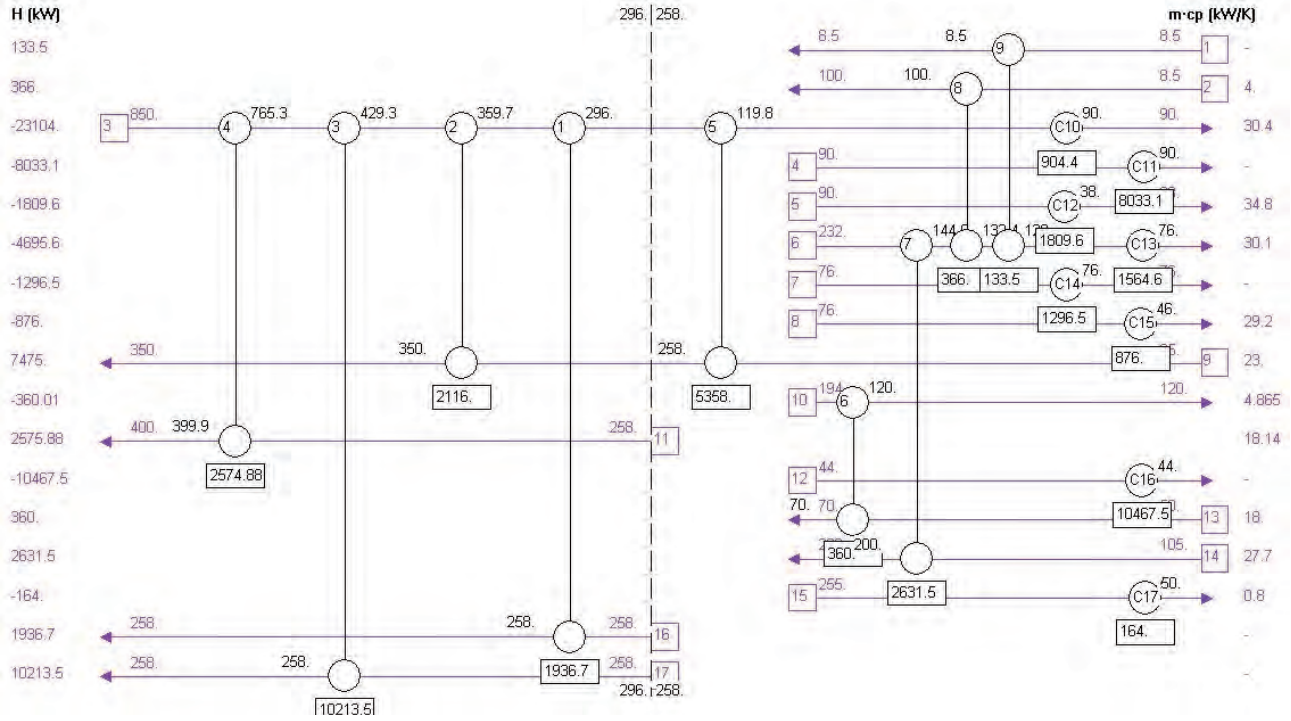

Figure 3. HEN based on original data of nitric acid production process [2].

Table 2. Parameters of heat exchangers and coolers used for cost calculations in the first solution [1]

HE	Transfered heat, kW	Hot stream (h)	$T_{h,s}$ / °C	$T_{h,t}$ / °C	Cold stream (c)	$T_{c,s}$ / °C	$T_{c,t}$ / °C	Required heat transfer area, m^2	Costs, $
1	1936.7	3	359.7	296.0	16	258.0	258.0	29.93	12630
2	2116.0	3	429.313	359.7	9	258.0	350.0	23.50	12070
3	10213.5	3	765.283	429.3	17	258.0	258.0	33.00	12900
4	2574.9	3	850.0	765. 3	11	258.0	399.9	5.39	10470
5	5358.0	3	296.0	119.8	9	25.0	258.0	86.22	17590
6	360.0	10	194.0	120.0	13	50.0	70.0	3.81	10340
7	2631.5	6	232.0	144.6	14	105.0	200.0	73.81	16500
8	366.0	6	144.6	132.4	2	8.5	100.0	4.72	10420
9	133.5	6	132.4	128.0	1	8.5	8.5	1.10	10100
10	904.4	3	119.8	90.0	Utility	-	-	10.77	10950
11	8033.1	4	90.0	90.0	Utility.	-	-	114.76	20100
12	1809.6	5	90.0	38.0	Utility.	-	-	47.26	14160
13	1564.6	6	128.0	76.0	Utility	-	-	19.76	11740
14	1296.5	7	76.0	76.0	Utility	-	-	23.15	12040
15	876.0	8	76.0	46.0	Utility	-	-	22.40	11970
16	10467.5	12	44.0	44.0	Utility	-	-	436.15	48380
17	164.0	15	255.0	50.0	Utility	-	-	1.65	10140

decreasing of the capital costs (if $c < 1$). On the other hand, if ΔT_{min} increases the requirement for the additional heat transfer utilities increases (energy costs increase and there is higher external energy demand). When these two types of costs with the opposite trends are summed the total costs could be obtained. Illustrative curve of total cost is presented in Figure 4.

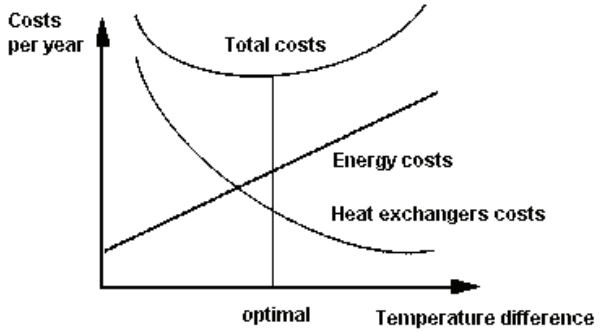

Figure 4. Total costs vs. $\Delta T_{min.}$

Capital costs were calculated using Eq. (6), with the values of constants a = 10000, b = 88 and c = 1 [22] for the heat transfer area from 10 to 1000 m^2.

Finally, total costs of the HEN are calculated by summing total capital costs and total energy costs. Total costs are 252,500 + 7,159,493.78 = 7,411,993.78 $/year.

Further analysis of the process is performed due to the problem in ΔT_{min} noticed in the first solution, and consequently the second solution will be proposed.

Since optimal value of ΔT_{min}=38 °C also is adopted in this case, overall heating and cooling demands remained the same. Therefore, the same corrections of heat capacity flow rates of streams 10 and 11 were performed in this case as in the previous solution. Since our goal was to maintain ΔT_{min} at the optimal values, some rearrangements of the stream connections were performed, as it is shown in Figure 5. For the area above the Pinch, stream connections are similar to the one from the previous solution, except that stream 13 is not divided. For the area bellow the Pinch for the optimal HEN, the heat exchanger number 4 was considered, but with adjusted ΔT_{min} to the optimal value of 38 °C.

In this way, comparing to the first solution given in the text above, the heat transfer through the Pinch is avoided.

The summary of the obtained results is presented in Table 3.

According to the obtained results the total heating demands are 0 and total cooling demands are 27,688.3 KW.

Using data found for the second solution, the next results were obtained:

- heating demands are equal to 0;
- cooling costs is: 27,688.3 kW×221.76 $/(kW year) = 6,140,157.41 $/year;
- Total energy cost is equal to the cooling costs.

Total annual capital costs are 251,220 $/year. Finally, summing total capital and total energy costs total annual costs are 251,220 + 6,140,157.41 = 6,391,377.41 $/year.

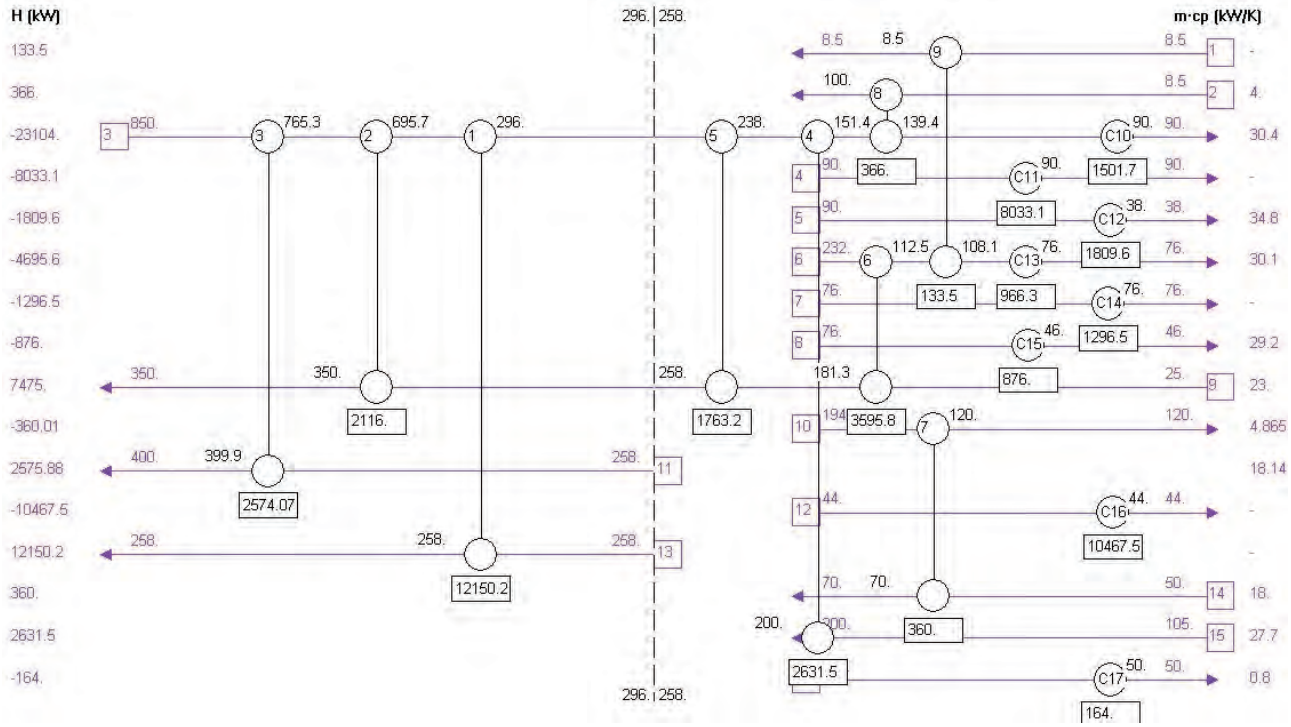

Figure 5. Optimized HEN of nitric acid production process.

Table 3. Parameters of heat exchangers and coolers used for cost calculations in optimized solution

HE	Transfered heat, kW	Hot stream (h)	$T_{h,s}$ / °C	$T_{h,t}$ / °C	Cold stream (c)	$T_{c,s}$ / °C	$T_{c,t}$ / °C	Required heat transfer area, m^2	Costs, $
1	12150.2	3	695.7	296.0	13	258.0	258.0	74.29	16540
2	2116.	3	765. 3	695.7	9	258.0	350.0	4.96	10440
3	2574.1	3	850.0	765.3	11	258.0	399.9	5.38	10470
4	2631.5	3	238.0	151.4	15	105.0	200.0	62.54	15500
5	1763.2	3	296.0	238.0	9	181.3	258.0	37.75	13320
6	3595.8	6	232.0	112.5	9	25.0	181.3	53.33	14690
7	360.0	10	194.0	120.0	14	50.	70.0	3.81	10340
8	366.0	3	151.4	139.4	2	8.5	100.0	4.30	10380
9	133.5	6	112.5	108.1	1	8.5	8.5	1.31	10120
10	1501.7	3	139.4	90.0	Utility	-	-	16.23	11430
11	8033.1	4	90.0	90.0	Utility.	-	-	114.76	20100
12	1809.6	5	90.0	38.0	Utility	-	-	47.26	14160
13	966.3	6	108.1	76.0	Utility	-	-	13.64	11200
14	1296.5	7	76.0	76.0	Utility	-	-	23.15	12040
15	876.0	8	76.0	46.0	Utility	-	-	22.40	11970
16	10467.5	12	44.0	44.0	Utility	-	-	436.15	48380
17	164.0	16	255.0	50.0	Utility	-	-	1.65	10140

CONCLUSION

Aim of this work was to show utilization of the Pinch methodology and heat exchangers network synthesis on the reduction of the process heating and cooling demands. The HEN is applied to the nitric acid production in the plant Petrochemical Industry-Kutina, located in Croatia.

Results of two different HENs are presented: the first one presents established HEN, but with some deviations from the Pinch rules [1], while the second strictly follows all rules of Pinch methodology. In both cases the total number of equipment used for heat

transfer is the same (totally 17) and in the both HENs additional process heating is not required.

In the first solution the minimum temperature difference between hot and cold streams in all process matches is not defined as optimal heat transfer through the Pinch point, so inorder to avoid those shortcomings a different arrangement of heat exchangers is made in the second solution.

According to the obtained results, designing the HEN with new heat exchanger arrangement leads to improved results, and annual saving of about 14 %. This proves that using the Pinch methodology and better process and energy integration could lead to the significant energy and financial savings for each industrial plant.

Nomenclature

CP – heat capacity flowrate
$Q_{,\mathrm{h\,min}}$ – minimum heating demands
$Q_{\mathrm{c\,,min}}$ – minimum cooling demands
Q_{u} – utility demands
C_{u} – costs of utilities
C – capital costs
N_{min} – minimum number of units
A_{min} – minimum required heat transfer area
A – heat transfer area
a, b, c – heat exchangers cost parameters
T - temperature
HE – heat exchanger

Subscripts

t – target conditions
s – source conditions
c – cold stream
h – hot stream.

Acknowledgement

The authors gratefully acknowledge the financial support received from the Research Fund of Ministry of Education, Science and Technological Development, Serbia, and the Faculty of Technology and Metallurgy, University of Belgrade (Project no. 172063).

REFERENCES

[1] Lj. Matijašević, H. Otmačić, Energy recovery by pinch tehnology, Appl. Therm. Eng. **22** (2002) 477–484.

[2] Lj. Matijašević, Toplinska analiza procesa - I. Sinteza mreže izmjenjivača topline pinch postupkom, Hem. Ind. **55** (2006) 403–412.

[3] L. Sun, X. Luo, Synthesis of multipass heat exchanger networks based on pinch technology, Comput. Chem. Eng. **35** (2011) 1257–1264.

[4] R. Smith, State of the Art in Process Integration, Appl. Therm. Eng. **20** (2000) 1337–1345.

[5] F.X.X. Zhu, L. Vaideeswaran, Integration in Analysis and Optimization of Energy. Systems, Appl. Therm. Eng. **20** (2000) 1381–1392.

[6] K.C. Furman, N.V. Sahinidis, A critical review and annotated bibliography for heat exchanger network synthesis in the 20th century, Ind. Eng. Chem. Res. **41** (2002) 2335-2370.

[7] M. Kijevčanin, B. Đorđević, O. Ocić, M. Crnomarković, M. Marić, S. Šerbanović, Energy and economy savings in the process of methanol synthesis using pinch technology, J. Serb. Chem. Soc. **69** (2004) 827–837.

[8] R. Domenichini, M. Gallio, A. Lazzaretto, Combined production of hydrogen and power from heavy oil gasification: Pinch analysis, thermodynamic and economic evaluations, Energy **35** (2010) 2184–2193.

[9] F. Friedler, Process integration, modelling and optimisation for energy saving and pollution reduction, Appl. Therm. Eng. **30** (2010) 2270–2280.

[10] S. Fujimoto, T. Yanagida, M. Nakaiwa, H. Tatsumi, T. Minowa, Pinch analysis for bioethanol production process from lignocellulosic biomass, Appl. Therm. Eng. **31** (2011) 3332–3336.

[11] M. H. Panjeshahi, E. G. Langeroudi, N. Tahouni, Retrofit ammonia plant for improving energy efficiency, Energy **33** (2008) 46–64.

[12] X. Feng, J. Pu, J. Yang, K.H. Chu, Energy recovery in petrochemical complexes through heat integration retrofit analysis, Appl. Energy **88** (2011) 1965–1982.

[13] C. Bengtsson, R. Nordman, T. Bemtsson, Utilization of excess heat in the pulp and paper industry – a case study of technical and economic opportunities, Appl. Therm. Eng. **22** (2002) 1069–1081.

[14] M. De Monte, E. Padoano, D. Pozzetto, Waste heat recovery in a coffee roasting plant, Appl. Therm. Eng. **23** (2003) 1033–1044.

[15] P. Rašković, S. Stoiljković, Pinch design method in the case of a limited number of process streams, Energy **34** (2009) 593–612.

[16] http://www.rossiters.org/associates/images/pinch-curve.jpg (accessed 30.12.2013).

[17] A. Martin, F. A. Mato, Hint: An educational software for heat exchanger network design with the pinch method, Education for Chem. Eng. **3** (2008) e6–e14.

[18] Available and Emerging Technologies for Reducing Greenhouse Gas Emissions from the Nitric Acid Production Industry, U.S. Environmental Protection Agency Research, Triangle Park,NC, 27711, 2010, p3–p7.

[19] http://www.epa.gov/ttnchie1/ap42/ch08/final/c08s08.pdf (accessed 10.12.2013).

[20] http://www.fertilizerseurope.com/fileadmin/user_upload/publications/tecnical_publications/guidence_techn_documentation/EFMABATNIT.pdf (accessed 10.12.2013).

[21] S.-G. Yoon, J. Lee, S. Park, Heat integration analysis for an industrial ethylbenzene plant using pinch analysis, Appl. Therm. Eng. **27** (2007) 886–893.

[22] G. Towler, R. Sinnott, Chemical Engineering Design, Principles, Practice and Economics of Plant and Process Design, Elsevier, London, 2008.

IZVOD

ENERGETSKA INTEGRACIJA PROIZVODNJE AZOTNE KISELINE PRIMENOM *PINCH* METODOLOGIJE

Gorica R. Ivaniš[1], Marija Lazarević[2], Ivona R. Radović[1], Mirjana Lj. Kijevčanin[1]

[1]*Univerzitet u Beogradu, Tehnološko-metalurški fakultet, Beograd, Srbija*
[2]*Galenika Fitofarmacija, Beograd, Srbija*

(Stručni rad)

U ovom radu je pokazano kako se primenom *Pinch* metodologije omogućava smanjenje ukupnih zahteva za dodatnim grejanjem i hlađenjem unutar procesa. Primenom *Pinch* metodologije analizirana je mreža razmenjivača toplote u postrojenju za proizvodnju azotne kiseline u Petrohemijskoj industriji-Kutina u Hrvatskoj. Razmenjivači toplote, grejači i hladnjaci, zajedno sa procesnim strujama koje se greju i hlade, čine mrežu razmenjivača toplote. Pored procesnih struja i razmenjivača toplote koji služe za razmenu toplote između procesnih struja, u razmatranje se uključuju i pomoćni medijumi za grejanje i hlađenje. Ova analiza može dovesti do znatnih energetskih i ekonomskih ušteda unutar postrojenja. U ovom radu sinteza mreže razmjenjivača toplote u postojenju za proizvodnju azotne kiseline je izvršena korišćenjem programskog paketa HINT. U radu su prikazana dva rešenja energetske integracije: *i*) rešenje bazirano na originalnim podacima i pristupu datom u literaturi [11] i *ii*) rešenje zasnovano na procesnim parametrima nešto izmenjenim u cilju poboljšanja integracije. U oba rešenja broj instalisanih uređaja za razmenu toplote je 17. Predložena optimalna vrednost minimalne razlike temperatura toplih i hladnih struja od 38 °C je zadržana u drugom rešenju, dok je u prvom, kako je to detaljno prikazano u rezulatima, u pojedinim delovima mreže ova vredbost izmenjena. Zadržavanjem optimalne minimalne razlike temperatura unutar procesa, kao i drugačijim rasporedom aparata, izbegnuto je i prenošenje toplote kroz *Pinch* u drugom rešenju. U oba slučaja se ne zahteva dodatno grejanje procesnih struja, tako da se ne koriste pomoćni fluidi za grejanje. Dobijeni rezultati pokazuju da su ukupni troškovi rada postrojenja na godišnjem nivou smanjeni za oko 14% što je jasan dokaz da se primenom *Pinch* metodologije i boljom energetskom integracijom procesa mogu postići značajne finansijske uštede u industrijskim postrojenjima.

Ključne reči: *Pinch* metodologija • Energetska integracija • Minimalna razlika temperatura • Proizvodnja azotne kiseline • Ukupni troškovi

A new experimental method to prevent paraffin–wax formation on the crude oil wells: A field case study in Libya

Elnori E. Elhaddad[1], Alireza Bahadori[2], Manar El-Sayed Abdel-Raouf[3], Salaheldin Elkatatny[4]

[1]*University of Belgrade, Faculty of Mining and Geology, Department of Petroleum Engineering, Belgrade, Serbia*
[2]*Southern Cross University, School of Environment, Science and Engineering, Lismore, NSW Australia*
[3]*Egyptian Petroleum Research Institute, Egypt*
[4]*Cairo University, Faculty of Engineering, petroleum Department, Giza, Egypt*

Abstract

Wax formation and deposition is one of the most common problems in oil producing wells. This problem occurs as a result of the reduction of the produced fluid temperature below the wax appearance temperature (range between 46 and 50 °C) and the pour point temperature (range between 42 and 44 °C). In this study, two new methods for preventing wax formation were implemented on three oil wells in Libya, where the surface temperature is, normally, 29 °C. In the first method, the gas was injected at a pressure of 83.3 bar and a temperature of 65 °C (greater than the pour point temperature) during the gas-lift operation. In the second method, wax inhibitors (trichloroethylene–xylene (TEX), ethylene copolymers and Comb polymers) were injected down the casings together with the gas. Field observations confirmed that by applying these techniques, the production string was kept clean and no wax was formed. The obtained results show that the wax formation could be prevented by both methods.

Keywords: pour point temperature, wax appearance temperature, chemical inhibitors, gas-lift.

Available online at the Journal website: http://www.ache.org.rs/HI/

PROFESSIONAL PAPER

UDC 622.323/.324:622.24(612):66

Hem. Ind. **69** (3) 269–274 (2015)

doi: 10.2298/HEMIND130717040E

Paraffin and/or waxes are alkanes, long-chain compounds which separate out from the crude oil when their temperature drops below 46 and 50 °C, forming wax deposition. Without an effective control, the wax deposition could increase substantially with time, causing low productivity and blockage in the tubing string [1,2]. At temperatures lower than the wax appearance temperature (WAT), crystals of wax will form either in the bulk fluid or on cold surfaces where they will build up, consequently, fouling the surface [3––5]. The wax appearance temperature (WAT) or cloud point is the temperature at which wax starts to emerge from the solution as the crude oil is cooled at the atmospheric pressure. Pour point refers to the temperature at which the petroleum fluids stop flowing when the vessel is inverted for up to five seconds [6,7].

Gas-lift wells require low gas-lift rates, which result in low pressure in the casing and this often causes cold flow of the produced fluid [8,9]. Sometimes, the cold flow leads to wax formation and deposition in the production strings, and the financial consequences could be enormous [3,10].

Correspondence: E. Elhaddad, Faculty of Mining and Geology, Petroleum Engineering Department, University of Belgrade, Belgrade, Serbia.
E-mail: norimab2014@ gmail.com
Paper received: 17 July, 2013
Paper accepted: 25 April, 2014

Typically, for modest crude producers, injection of a small quantity of gas lowers the pressure and, consequently, lowers the temperature of the injected gas to the temperatures which may be lower than the bottom hole temperature [6,9]. In addition, it also makes the temperature of the lifted crude to drop lower than the pour point temperature on the surface. As a result, the tubing ends-up is blocked, and this significantly reduces the flow of the produced crude to the surface [11,12].

Problem statement

Production wells are designed to lift the crude oil using low pressure in the casing side which results in cold flow of the extracted fluid. The recommended injection pressure of the gas ranges from 77.22 to 82.74 bar. Nonetheless, an oil production well of lower capacity requires a small volume of gas to lift their fluid, and in this case, a gas chock is installed in order to control the volume of the gas injected into the gas-lift well. When gas flow is choked, the pressure drops and as a result, the temperature of the gas flowing down the casing also drops. Reduction in the temperature at the surface of the casing results in the cooling of the gas at the casing. This reduction of the gas temperature becomes larger for deeper wells. Cooled gas reduces the temperature of the lifted oil, sometimes below the pour point temperature at the surface. This condition worsens during winter in countries experi-

encing extreme weather conditions and it may limit the flow of oil or entirely plug the tubing.

METHODS

In this research, two types of field experiments were conducted on three oil wells in Libya: wells A–C. Experiment No.1 involved testing the effectiveness of injecting gas at pressures higher than the ranges leading to the pour point temperature and WAT to prevent wax formation. The optimum pressure for the gas injection was calculated using a mathematical technique. In the experiment No.2 chemical inhibitors were injected down the casings of wells A–C together with the gas. The temperature of the lifted crude oil cooled down below the WAT and pour point temperature. Trichloroethylene-xylene (TEX) was injected into well A; ethylene copolymers were injected into well B and comb polymers were injected into well C.

Experiment No. 1

This experiment involved testing the effectiveness of injecting gas at pressures higher than the ranges leading to the pour point temperature and the wax appearance temperature (WAT), to prevent wax formation. This technique was applied in three oil wells in Libya, wells A–C, which are low oil production wells. They are also low pressure/low temperature wells (LPLT), and, therefore, the gas-lift technique is extensively used to produce oil [9]. The gas was injected into the three wells at a temperature of 65 °C which is above both the WAT and pour point to prevent deposition of wax in the production strings. Observation was carried out every day for 14 days.

Table 1 illustrates a percentage of wax deposition in the production strings of the three oil wells prior to using the new technique. Also, Table 1 shows the production per day, bubble point pressure, previously used pressure, and maximum possible production per day of oil wells A–C.

Experiment No. 2

This experiment involved testing the effectiveness of injecting chemical inhibitors down the casing together with the gas to keep the tubing clean. Without the use of chemical inhibitors, wax starts to deposit in the production string once the temperature at the casing surface drops below the WAT (Figure 1) and a further drop in the temperature leads to an increase of wax deposits, making the tubing very unclean, and this significantly disrupts the flow of crude oil to the surface [11,12].

In this experiment, chemical inhibitors were injected down the casings of wells A–C together with

Table 1.Percentage of wax deposition in the production strings of the wells before using the new method

Well	Pressure bar	Bubble point pressure, bar	Temperature of the surface casing, °C	WAT, °C	Pour point °C	Production m^3/day	Maximum possible production from well, m^3/day	Wax deposition in production strings, %
A	60.673	234.421	33	46	42	71.55	302.1	95
B	62.052	234.421	35	48	43	79.49	286.2	80
C	65.500	234.421	37	50	44	87.45	270.3	57
Average	62.742	234.421	–	–	–	79.49	286.2	–

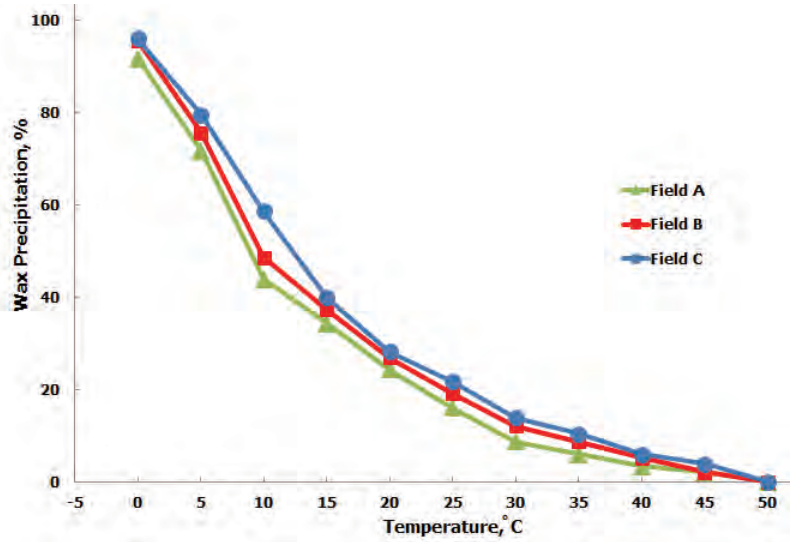

Figure 1.Percentage of wax deposition with temperature of casing before the injection of chemical inhibitors.

the gas. Trichloroethylene-xylene (TEX) was injected into well A; ethylene copolymers were injected into well B and comb polymers were injected into well C. The temperature of the crude oil was then reduced below the WAT, and pour point temperature to determine whether the chemical inhibitors reduced the temperature at which wax crystals begin to form. Sampling of the crude oil was then carried out every day for 14 days at the wellhead for each of the three oil wells.

Determination of optimal pressure for injection

Vogel's equation was used to calculate the optimum injection pressure [13]:

$$\frac{q_x}{q_{x(\max)}} = \left[1 - 0.20\left(\frac{p_{wf}}{pr}\right) - 0.80\left(\frac{p_{wf}}{pr}\right)^2\right] \quad (1)$$

where x = O (oil, in case of oil), L (liquid, in case of liquid production, oil + water), q_x = measured stabilized productivity surface flow rate, $q_{x(max)}$ = maximum production rate at the maximum drawdown, P_{wf} = 0, P_{wf} = measured stabilized flowing pressure in the wellbore and *pr* = average reservoir pressure.

This equation is applicable to any reservoir in which gas saturation increases as pressure decreases. Also, it could be applied to wells with a water cut, since the increasing gas saturation will concomitantly reduce the permeability to water. This approach has been used successfully for wells with water cuts up to 97% [13]. The equation provides the optimum pressure which is required to produce oil without wax formation, as well as the optimum pressure that maximizes the well potential in terms of production of barrels per day. The calculation of optimum injection pressure was, according to the Eq. (1), and it was found to be in the ranges (from 83.0 to 86.3 bar). It is worth noticing that, this equation has previously been used for the same calculation by Caicedo [14].

According to the results obtained from this calculation, gas under pressure of 68.95, 79.29 and 83.3 bar were injected into the tubing's of wells A–C respectively to create pressure in the wellbore and lift the crude oil to the surface.

RESULTS AND DISCUSSION

Effect of injected gas pressure

The results obtained from experiment No.1 showed that a significant wax deposition was observed in the production string for well A. The main reason for that result is the low injected gas pressure of 68.94 bar, which led to a drop in the injected gas temperature down the casing. Consequently, the temperature at the surface of the casing was lowered, cooling down the temperature of the lifted crude to 39 °C which is below the pour point temperature, causing wax to form within the production string.

For well B, a relatively small amount of wax deposition was observed in the production string. Even though the gas was injected into the tubing with comparatively high pressure of 79.29 bar, this pressure was not high enough to prevent the formation of wax crystals in the production string. The temperature of the casing dropped to the point at which the injected gas temperature was 42 °C (below the WAT and pour point temperature), which resulted in wax deposition, but the wax deposition was not as much as observed in a well A. As For well C, no wax deposition was observed in the production string.

The previous findings indicate that the injected gas pressure of (83.29 bar) was sufficiently high to provide the appropriate temperature of the gas injected down the casing. As a result, the temperature of the produced crude oil on the casing surface was around 55 °C, which was higher than the pour point temperature and WAT, so no wax deposition was formed in the production string.

Table 2 illustrates a percentage of wax precipitation in the production strings for the three wells after using this new method with optimal pressure for wax formation prevention. From these results, it can be concluded that using gas pressures as high as (83.3 bar) in the gas-lift technique, is effective in lifting the oil from the wellbore to the surface without the formation of wax in the production strings.

Effect of chemical inhibitors

Figure 1 represents a percentage of wax deposition with temperatures of casing before the injection of chemical inhibitors. It is clear from Figure 1 that wax starts to deposit in the production strings once the temperature at the casing surface drops below 50 °C,

Table 2.Percentage of wax precipitation after using the new method with optimal pressure

Oil well	Pressure/temperature bar/°C	Pour point, °C	WAT, °C	Temperature of the surface casing, °C	Wax deposition in production string, %
A	68.95/65	42	46	39	10
B	79.3/65	43	48	42	5
C	83.3/65	44	50	55	Less than 2

the WAT, and a further drop in temperature leads to severe increase of wax deposits.

The results obtained from experiment No.2 are illustrated in Figure 2 and Table 3. Figure 2 represents a reduction of wax deposition percentage with temperatures of casing after the injection of chemical inhibitors. The results indicate that, the temperatures at which wax began to deposit in the tubing were reduced significantly after the injection of chemical inhibitors down the tubing together with the gas. It can be also seen from Figure 2 that no wax was formed after injecting the chemical inhibitors for the three oil wells even at the temperature of 30 °C, as compared to 50 °C in the case without injecting the chemical inhibitors.

Table 3 shows a percentage of wax precipitation at 0°C before and after the usage of chemical inhibitors at a temperature of zero degrees Celsius (0 °C). Table 3 shows that the percentage of wax precipitation was reduced to half its value after the usage of chemical inhibitors at a temperature of 0 °C.

Although three different types of chemical inhibitors were used in these experiments, they were effective in reducing the amount of wax deposition in the tubing with the reduction in the temperature of the crude oil. These results may be explained as follows: The chemical inhibitor TEX is made up of structures with sections, interact with the forming wax crystals and prevent its growth, keeping the tubing clean [15––17]. Ethylene copolymers and Comb polymer's chemical inhibitors are imperative in preventing gelling and/or wax deposition in pipelines. This is primarily because they alter the wax crystals in order to prevent them from agglomerating and depositing, and thus keeping the tubing clean [18–20]. Moreover, all TEX, ethylene copolymers and Comb polymers are wax crystal modifiers which attack the nucleating agents of the wax deposits, breaking it down and preventing paraffin crystals from agglomerating [21]. This has also been explained to result from their ability to keep the nucleating agents within the solution [22,23].

The results obtained from the experiment No.2 show that injecting chemical inhibitors down the casing together with the gas offer potential solutions to the problem of wax deposition in oil wells employing the gas-lift technique.

CONCLUSION

Based on the results obtained, it can be concluded that wax deposition in oil producing wells can be prevented during the gas-lift operations by two methods. The first method is injecting the gas at a

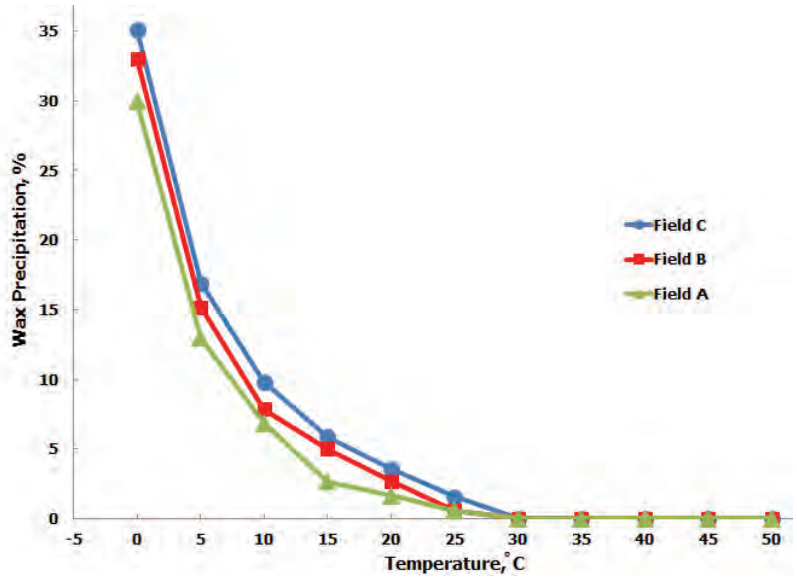

Figure 2.Reduction of wax deposition percentage with temperature of casing after the injection of chemical inhibitors.

Table 3.Percentage of wax precipitation at 0 °C before and after the injection of chemical inhibitors

Oil well	Pour point, °C	WAT, °C	Wax deposition in the production strings			
			Before		After	
			Temperature, °C	Wax deposition, %	Temperature, °C	Wax deposition, %
A	42	46	0	94	0°	30
B	43	48	0	96	0°	33
C	44	50	0	98	0°	35

pressure of (86.3 bar) which results in a surface casing temperature above the wax appearance temperature and the pour point temperature (52 °C). The second method is injecting chemical inhibitors with the gas down the casing. In this method TEX, ethylene copolymers and comb polymers have been used and have proved effective in reducing the wax formation temperature, thus enabling injecting the gas at lower pressures. The method selection should be based on economic estimations.

REFERENCES

[1] http://ar.scribd.com/doc/249802218/Halliburton (10 December, 2014).

[2] A. Kadir, I. Ismail, P. Sengodan, Managing Paraffin Wax Deposition in Oil Deposition. Springer, Birmingham, 2006, pp. 34–41.

[3] R. Dalirsefat, F. Feyzi, A Thermodynamic Model for Wax Deposition Phenomena, Fuel **86** (2007) 1402–1408.

[4] N.J. Hyne, Nontechnical Guide to Petroleum Geology, Exploration, Drilling, and Production, 2nd ed., Pennwell Books, Coventry, 2012, pp. 420–426.

[5] Y. Bai, and Q. Bai, Wax and Asphaltenes. Subsea Engineering Handbook, Elsevier, Amsterdam, 2012, pp. 483––504.

[6] S. Khresno, Gas Lift and Wax Problem. Oxford University Press, Oxford, 2010, p. 14.

[7] J. Coutinho, J. Daridon, Low-Pressure Modeling of Wax Formation in Crude Oils, Energy and Fuels **15** (2001) 1454–1460.

[8] K. Baker, Understanding Paraffin and Asphaltene Problems in Oil and Gas Wells, Oxford University Press, Oxford, 2003.

[9] C. Narvaez, A. Ferrer, S. Corpoven, Prevention of Paraffin Well Plugging by Plunger-Lift Use, Production Operations Symposium, Oklahoma City, OK, 2009.

[10] Z. Jeirani, A. Lashanizadegan, S. Ayatollahi, J. Javanmardi, The Possibility of Wax Formation in Gas Fields: A Case Study, J. Nat. Gas Chem. **16** (2007) 293–300.

[11] E.K. Kelechukwu, A. Hikmat, S. Ahmmed, Prediction of Wax Deposition Problems of Hydrocarbon Production System, J. Pet. Sci. Eng. **108** (2013) 128–136.

[12] M.E. Newberry, K.M. Barker, Formation Damage Prevention Through the Control of Paraffin and Asphaltene Deposition, Society of Petroleum Engineers, 1985.

[13] J.V. Vogel, Inflow Performance Relationships for Solution-Gas Drive Wells, JPT **20** (1986) 83–92.

[14] S. Caicedo, Estimating IPR Curves in Intermittent Gas Lift Wells from Standard Production Tests, Society of Petroleum Engineers, 2001.

[15] A. Aiyejina, D.Chakrabarti, A. Pilgrim, M. Sastry, Wax Formation in Oil Pipelines: A Critical Review, Int. J. Multiphase Flow **37** (2011) 671–694.

[16] A. Sulaimon, G. K. Falade, W. DeLandro, A Proactive Approach for Predicting and Preventing Wax Deposition in Production Tubing Strings: A Niger Delta Experience, Acad. J. **1** (2010) 26–36.

[17] J. Becker. Crude Oil Waxes, Emulsions, and Asphaltenes, PennWell Corporation, Liverpool, 2007, pp. 164–167.

[18] N. Thanh, M. Hsieh, and R.P. Philp. Waxes and Asphaltenes in Crude Oils, Org. Geochem. **30** (1999) 119–132.

[19] C.J. Oseghale, E.J. Akpabio, O. Edebor, Mitigating Potential Risk of Paraffin Wax Deposition on Oil Pipelines in Niger Delta. J. Eng. Appl. Sci. **7** (2012) 348–352.

[20] R. Venkatesan, J.L. Creek, Wax Deposition during Production Operations: SOTA, Offshore Technology Conference, 2007.

[21] C. Del. Paraffin Deposition in Oil Production Society of Petroleum Engineers, 2001.

[22] W. Chen, Z. Zhao, Thermodynamic Modeling of Wax Precipitation in Crude Oils. Chin. J. Chem. Eng. **14** (2006) 685–689.

[23] V.A. Adewusi, Prediction of wax deposition potential of Hydrocarbon Systems from Viscosity-Pressure Correlations, Fuel **67** (1997) 1079–1083.

IZVOD

NOVA EKSPERIMENTALNA METODA ZA SPREČAVANJE FORMIRANJA PARAFINSKIH NASLAGA–VOSKA NA NAFTNIM BUŠOTINAMA: STUDIJA NA NAFTNIM POLJIMA U LIBIJI

Elnori E. Elhaddad[1], Alireza Bahadori[2], Manar El-Sayed Abdel-Raouf[3], Salaheldin Elkatatny[4]

1Univerzitet u Beogradu, Rudarsko–geološki fakultet, Katedra za eksploataciju nafte i tehniku dubinskog bušenja, Beograd, Srbjia
[2]Southern Cross University, School of Environment, Science and Engineering, Lismore, NSW Australia
[3]Egyptian Petroleum Research Institute, Egypt
[4]Cairo University, Faculty of Engineering, petroleum Department, Giza, Egypt

(Stručni rad)

Formiranje i taloženje parafinskih naslaga je jedan od najčešćih problema na naftnim bušotinama. Ovaj problem se javlja usled opadanja temperature nafte ispod temperature formiranja voska (između 46 i 50 °C) i temperature tečenja (između 42 i 44 °C). U ovom istraživanju dve nove metode za sprečavanje formiranja naslaga parafina su primenjene na tri izvorišta nafte u Libiji, gde su normalne temperature okoline 29 °C. U prvoj metodi se gas prilikom ispumpavanja nafte ubacivao pod pritiskom od 83.3 bar i temperaturom od 65 °C (veća od temperature tečenja). Druga metoda se sastojala u ubrizgavanju sredstava za rastvaranje parafina (trihloroetilenksilena (TEX), etilen kopolimera i comb polimera) u bušotinu zajedno sa gasom. Istraživanje je pokazalo da je primenom ovih tehnika bušotina bila čista i bez naslaga parafina. Ovi rezultati pokazuju da se formiranja naslaga parafina može sprečiti ovim metodama.

Ključne reči: Temperatura tečenja • Temperatura formiranja voska • Hemijski inhibitori • Gas lift

Proračun i optimizacija procesa proizvodnje bakar(II)-sulfat-monohidrata iz bakar(II)-sulfat-pentahidrata u sušnicama sa fluidizovanim slojem

Tatjana Kaluđerović Radoičić, Ivona Radović, Marija Ivanović, Nevenka Rajić, Željko Grbavčić

Univerzitet u Beogradu, Tehnološko–metalurški fakultet, Beograd, Srbija

Izvod

U ovom radu analiziran je proces dobijanja bakar(II)-sulfat-monohidrata iz bakar(II)-sulfat--pentahidrata, poznatijeg kao „plavi kamen“, u sušnicama sa fluidizovanim slojem. Bakar(II)-sulfat-pentahidrat je kristalohidrat u čijoj su kristalnoj strukturi četiri molekula vode vezana za bakar(II)-jon dok je peti molekul vode slobodan, tj, vodoničnim vezama povezan za sulfat-anjon. Optimalna temperatura zagrevanja kao i dužina zagrevanja za uklanjanje četiri molekula vode iz molekula pentahidrata utvrđeni su na osnovu termogravimetrijske (TGA) analize. Za analizu su upotrebljene čestice različite granualcije: srednjeg prečnika 0,17 mm i 0,5 mm. U poluindustrijskom postrojenju određene su krive fluidizacije i krive sušenja analiziranih uzoraka. Nakon laboratorijskih i poluindustrijskih eksperimenata izvršeno je materijalno i energetsko bilansiranje realnog postrojenja sa kapacitetom proizvodnje od 300 t mesečno. Proračuni neophodne količine agensa za sušenje i dimenzija postrojenja izvršeni su korišćenjem programskih paketa SuperPro Designer 5.1 i Simprosys 3.0. Takođe, analizirana je i mogućnost recirkulacije agensa za sušenje.

Ključne reči: sušenje u fluidizovanom sloju, bakar(II)-sulfat-pentahidrat, bakar(II)-sulfat-monohidrat, TGA analiza.

Dostupno na Internetu sa adrese časopisa: http://www.ache.org.rs/HI/

STRUČNI RAD

UDK 66.047:661.856:54

Hem. Ind. **69** (3) 275–286 (2015)

doi: 10.2298/HEMIND140211043K

Bakar(II)-sulfat-pentahidrat ($CuSO_4 \cdot 5H_2O$) predstavlja jednu od najznačajnijih soli bakra koja je bila poznata još starim Egipćanima. U XIX veku otkriveno je da ima fungicidno dejstvo što je podstaklo njenu industrijsku proizvodnju. Koristi se takođe kao algicid, herbicid, za uništavanje korova, a najviše u smeši sa krečom u vinogradarstvu. U prirodi se nalazi kao izrazito plavo jedinjenje, so koja je u obliku kristalohidrata, poznata kao „plavi kamen“. Osim kao pentahidrat, bakar(II)-sulfat se javlja još u nekoliko oblika u zavisnosti od stepena hidratacije od kojih se najčešće upotrebljavaju bakar(II)-sulfat-monohidrat i anhidrovani bakar(II)-sulfat. Bakar(II)-sulfat se široko primenjuje u poljoprivredi, kao agens za sušenje, u proizvodnji tekstila, kože, industriji boja, itd.

U kristalnoj rešetki bakar(II)-sulfat-pentahidrata, četiri molekula vode nalaze se u koordinacionoj sferi Cu(II)-jona, dok je peti molekul slobodan (slika 1). Peti molekul vode povezan je vodoničnim vezama sa sulfat--jonom. Četiri molekula vode vezana su za Cu(II) koordinacionim vezama. Posmatrano u prostoru, četiri molekula vode raspoređena su tako da se atomi kiseonika iz molekula vode nalaze na temenima kvadrata u čijem centru je smešten Cu(II). Dužine sve četiri veze su jednake i iznose 0,19–0,20 nm [1–4].

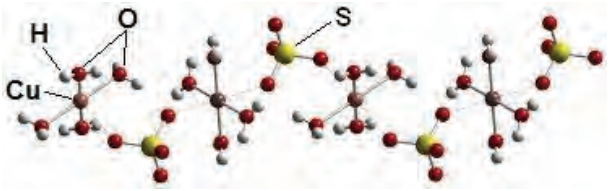

Slika 1. Šematski prikaz kristalne strukture bakar(II)-sulfat--pentahidrata. ”O” označava atome kiseonika, ”S” atome sumpora, ”H” atome vodonika i ”Cu” atome bakra.
Figure 1. Schematic representation of the crystal structure of copper (II) sulfate pentahydrate. "O" is oxygen atom, "S" is sulfur atom, "H" is hydrogen atom, and "Cu" is copper atom.

Pažljivim zagrevanjem kristalohidrata dolazi do postepene dehidratacije. Na oko 70 °C proizvod zagrevanja $CuSO_4 \cdot 5H_2O$ je trihidrat, $CuSO_4 \cdot 3H_2O$. U ovom kristalohidratu, atomi kiseonika iz tri molekula vode i atom kiseonika iz sulfat-jona obrazuju deformisan kvadrat u kome su veze Cu(II) i atoma kiseonika iz molekula vode nešto kraće (0,196 nm). Daljim zagrevanjem, moguće je izvršiti potpunu dehidrataciju i dobiti anhidrovanu so, $CuSO_4$, kod koje je Cu(II) vezan za atome kiseonika iz sulfat-jona [1–4].

Proces uklanjanja vlage iz vlažnog materijala – sušenje, je veoma rasprostranjen industrijski proces kojim se dobijaju proizvodi željenih karakteristika. Uklanjanje vlage se može vršiti mehaničkim, hemijskim, termičkim ili drugim postupcima u zavisnosti od kapaciteta proizvodnje, vrste vlažnog materijala kao i od prirode vezane vlage [5,6]. Uređaj u kome se obavlja proces uklanjanja vlage naziva se sušnica i ona je deo postrojenja za sušenje. Najrasprostranjeniji su termički postupci ukla-

Prepiska: T. Kaluđerović Radoičić, Univerzitet u Beogradu, Tehnološko–metalurški fakultet, Karnegijeva 4, Beograd, Srbija.
E-pošta: tanjak@tmf.bg.ac.rs
Rad primljen: 11. februar, 2014
Rad prihvaćen: 25. mart, 2014

njanja vlage, medju kojima prednjači konvektivni postupak kod koga se sušenje vlažnog materijala obavlja posredstvom zagrejanog gasovitog agensa. U industrijskoj upotrebi je veliki broj konvektivnih sušnica vrlo različitih konstruktivnih karakteristika (rotacione, pneumatske, sprej sušnice, sušnice sa pokretnom trakom, tunelske, gravitacione i dr.), a među najrasprostranjenijim su sušnice sa fluidizovanim slojem.

Sušnice sa fluidizovanim slojem se intenzivno koriste za sušenje praškastog i zrnastog materijala, kao i za pastasti i tečni materijal koji se posebnim postupkom nanose na inertnu česticu (nosač). Fluidizovanje vlažnog materijala se ostavaruje strujanjem agensa za sušenje uz pomoć distributera gasovite faze. Primenjuje se u različitim industrijskim procesima i to za sušenje hemikalija, hrane, biomaterijala, ugljovodonika, u proizvodnji pića, lekova, keramike, pesticida, boja i pigmenata, polimera i dr. Prednosti ovog načina sušenja su u dobrom mešanju čestica, velikoj brzini prenosa mase i toplote i lakom transportu materijala. Za sušenje praškastih čestica veličine od 50–200 μm, fluidizovane sušnice su u prednosti u odnosu na ostale tipove [5].

Fluidizovani sloj se formira prolaskom gasa sa dna kolone kroz sloj čvrstih čestica koje se u njoj nalaze. U cilju ravnomerne raspodele gasa u sloju, na dno kolone se ugrađuje distributor. Ukoliko je brzina gasa mala, sloj će ostati nepokretan tj. čestice ostaju u pakovanom sloju. Pad pritiska kroz pakovani sloj raste sa povećanjem brzine gasa, do trenutka kada se dostigne minimalna brzina fluidizacije. U tom trenutku je pritisak po jedinici mase sloja jednak težini sloja i dolazi do fluidizacije. Ova tačka se naziva tačkom minimalne fluidizacije, a brzina gasa je minimalna brzina fluidizacije, U_{mf} [7]. Proces sušenja se obično izvodi pri površinskoj brzini gasa koja je nekoliko puta (2–4) veća od minimalne brzine fluidizacije [5,7].

Na proces sušenja u fluidizovanom sloju utiče veliki broj parametara, a jedan od najbitnijih je veličina čestica. Geldart [8] je izvršio klasifikaciju materijala prema načinu ponašaja prilikom fluidizacije. Materijale je podelio u četiri grupe označene kao A, B, C i D. Na slici 2 prikazana je Geldartova klasifikacija materijala. Sa ovog dijagrama moguće je na osnovu prečnika čestice i razlike gustina čestica i fluida odrediti grupu u koju čestice spadaju. Karakteristike grupa čestica po Geldartu [8] su sledeće:

Grupa A. U ovu grupu spadaju materijali koji se mogu aerisati, tj. produvavanjem gasa kroz sloj ovakvog materijala doći će do razdvajanja čestica. Ovakvo ponašanje je karakteristično za male i relativno lake čestice čija je gustina, $\rho_p < 1400$ kg m^{-3}. Ove čestice lako fluidizuju. Pri većim brzinama gasa sloj je okarakterisan malim mehurima.

Grupa B. U ovu grupu spadaju svi materijali slični pesku. Najčešće su to čestice veličine od 40 do 500 μm, čija je gustina 1400 do 4000 kg m^{-3}. Ove čestice lako fluidizuju, ali u sloju dolazi do intenzivnog stvaranja mehura, čija se veličina povećava po visini sloja.

Grupa C. Kohezivni ili vrlo fini praškovi. U ovom slučaju fluidizacija je praktično nemoguća jer su međučestične privlačne sile velike. U ovom slučaju gas formira kanale u sloju, kroz koje prolazi praktično bez kontakta sa česticama.

Grupa D. U ovu grupu spadaju krupne i/ili teške čestice ($d_p > 500$ μm, $\rho_p > 1400$ kg m^{-3}), koje se takođe ne mogu fluidizovati. Ovde je brzina rasta mehura veoma velika i praktično trenutno se formiraju klipovi gasa u materijalu. Materijali iz ove grupe se mogu fontanovati [8].

U ovom radu izvršen je proračun industrijskog postrojenja za proizvodnju 500 kg/h bakar(II)-sulfat-monohidrata polazeći od bakar(II)-sulfat-pentahidrata. Radi

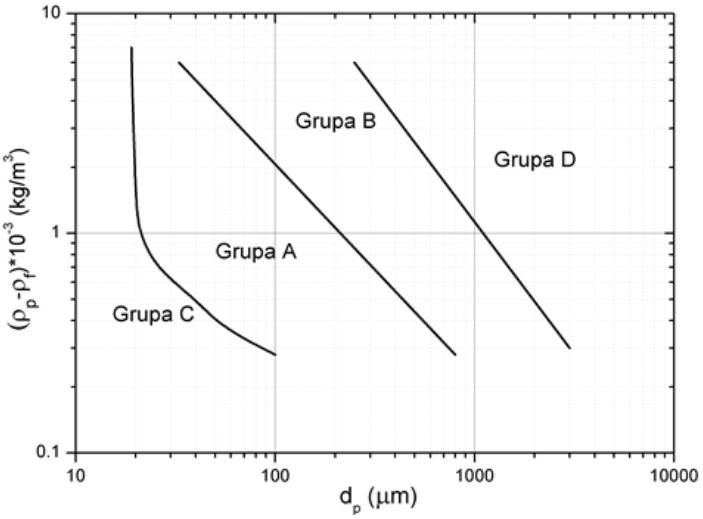

Slika 2. Dijagram $(\rho_p-\rho_f) = f(d_p)$, prema Geldartu [8].
Figure 2. The diagram $(\rho_p-\rho_f) = f(d_p)$ according to Geldart [8].

dobijanja podataka potrebnih za odabir i proračun sušnice, prethodno su izvršena laboratorijska ispitivanja polazne sirovine ($CuSO_4 \cdot 5H_2O$), kao i osušenog proizvoda ($CuSO_4 \cdot H_2O$). Takođe, konstruisan je laboratorijski sistem u kome su ispitane fluidizacione karakteristike materijala i određena kriva sušenja. U radu je izvršen odabir i proračun industrijskog postrojenja za sušenje, kao i materijalno i energetsko bilansiranje procesa.

MATERIJAL I METODE

U ovom radu je kao polazna sirovina korišćen bakar(II)-sulfat-pentahidrat proizvođača kompanije "NEKK Europe" Ltd., Velika Britanija. Analizirana su dva uzorka $CuSO_4 \cdot 5H_2O$ različitih granulometrijskih karakteristika, koji će u daljem tekstu biti označeni kao uzorak 1 i uzorak 2. Osnovne karakteristike materijala date su u tabeli 1. U cilju dobijanja podataka potrebnih za projektovanje postrojenja za proizvodnju $CuSO_4 \cdot H_2O$, izvršene su granulometrijska i termogravimetrijska (TGA) analiza polazne sirovine, kao i ispitivanja fluidizacionih karakteristika materijala i kinetike sušenja u laboratorijskom postrojenju.

Granulometrijska analiza izvršena je korišćenjem metode standardnih sita, odnosno prosejavanjem materijala. Uređaj za prosejavanje sastojao se od rama na koji su učvršćena sita po rastućoj veličini okaca. Ram je zajedno sa sitima pričvršćen za elektromotor koji proizvodi oscilatorne udare koji se zatim prenose na čitav sistem. Prosejavanje materijala je vršeno tokom 15 min, jer duže vreme prosejavanja može da dovede do abrazije. Kao rezultat prosejavanja dobijeni su maseni udeli pojedinih frakcija čestica, na osnovu čega je moguće izvršiti granulometrijsku analizu. Kao reprezentativan prečnik za svaku frakciju uzima se aritmetička sredina dimenzije okaca gornjeg i donjeg sita.

Termogravimetrijska (TGA) analiza – dehidratacija bakar(II)-sulfat-pentahidrata je urađena korišćenjem simultanog TG-DSC-DTG termičkog analizatora SDT Q600, TA Instruments. Uzorci mase 6–10 mg zagrevani su u otvorenim lončićima izrađenim od aluminijum-oksida (proizvođač TA Instruments) zapremine 90 µl. Tokom zagrevanja, protok vazduha iznosio je 100 cm^3/min, a brzina zagrevanja 10 °C/min. Za analizu su upotrebljene dve granulacije kristalohidrata i zagrevanje je obavljeno u dva različita režima: kontinualno do 500 °C i izotermski na temperaturama 160, 170 i 180 °C u trajanju 30–90 min.

Sušenje u fluidizovanom sloju

U cilju ispitivanja fluidizacionih karakteristika materijala (minimalne brzine fluidizacije i pada pritiska u fluidizovanom sloju) izvršena su hidrodinamička ispitivanja u laboratorijskoj fluidizacionoj koloni kružnog poprečnog preseka, prečnika D=60 mm. Šematski prikaz aparature dat je na slici 3. Aparatura se sastoji od kolone sa česticama kroz koju se propušta vazduh prethodno zagrejan električnim grejačem (c). Protok vazduha se meri rotametrom (b). Ostali elementi sistema prikazani su na slici 3.

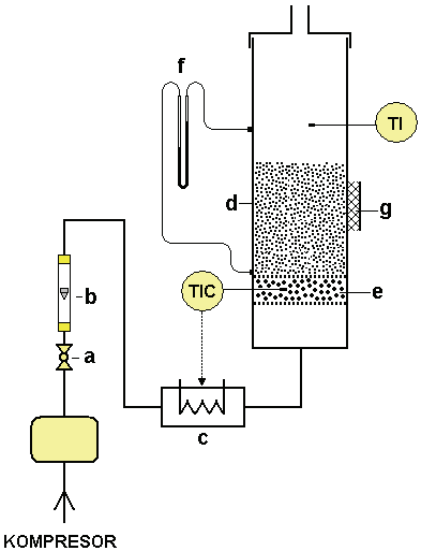

Slika 3. Šematski prikaz laboratorijske kolone za sušenje u fluidizovnom sloju; a) ventil, b) rotametar, c) električni grejač, d) kolona, e) distributor, f) manometar I g) termička izolacija.
Figure 3. Schematic representation of the laboratory drying fluidized bed column; a) valve, b) rotameter, c) electric heater, d) column, e) distributor, f) gauge and g) thermal insulation.

Materijalno i energetsko bilansiranje sušnice

Proračun industrijskog postrojenja za proizvodnju $CuSO_4 \cdot H_2O$ izvršen je korišćenjem programskih paketa Simprosys 3.0 [9] i SuperPro Designer 5.1 [10].

Tabela 1. Osnovne karakteristike materijala
Table 1. Basic properties of the materials

Naziv	$CuSO_4 \cdot 5H_2O$[a]	$CuSO_4 \cdot H_2O$[a]
CAS[b] registarski broj	7758-99-8	10257-54-2
Molekulska masa, $gmol^{-1}$	249,68	177,62
Gustina, kg m^{-3}	2284	3200
Nasipna gustina, kg m^{-3}	1205[c]	1190[c]
Rastvorljivost u vodi, g L^{-1} (20 °C)	320	–

[a]Karakteristike po specifikaciji proizvođača (NEKK Europe, Ltd.), osim nasipne gustine; [b]Chemical Abstracts Service; [c]eksperimentalna vrednost

Simprosys 3.0 [9] je programski paket dizajniran za proračun masenog i energetskog bilansa procesa sušenja, isparavanja ili kombinacije ova dva procesa. Simprosys 3.0 ima mogućnost bilansiranja 20 jedinica (sušnice za čvrste i tečne materijale, ciklon, filter za vazduh, filter vreća, elektrostatički filter, ventilator, kompresor, mokri skruber, skruber kondenzator, pumpa, grejač, hladnjak, kompresor, razmenjivač toplote, mešač i dr.) čijim se povezivanjem može bilansirati čitavo postrojenje. Simprosys daje mogućnost simulacije procesa sa recirkulacijom toka sušenog materijala ili vazduha. Na osnovu postavljenih zahteva jednostavno se dobijaju maseni i energetski bilans kao i potrebni parametri sušenja (potreban protok vazduha za sušenje, kapacitet i snaga ventilatora, energija razmenjena u grejaču i dr.). U okviru rezultata bilansa dobijaju se vrednosti toplotne efikasnosti i specifične toplotne potrošnje sušnice. Menjanjem ulaznih i izlaznih parametara optimizuju se uslovi rada pojedinačnih uređaja i čitavog postrojenja.

SuperPro Designer 5.1 [10] je programski paket koji služi za materijalno i energetsko bilansiranje kao i za dimenzionisanje postrojenja, u ovom slučaju sušnica. Ovaj programski paket za razliku od Simprosys softvera daje mogućnost proračuna konstruktivnih karakteristika sušnica za: sušnice sa pokretnom trakom, sprej sušnice, rotacione sušnice, dobošaste sušnice, sušnice sa fluidizovanim slojem i sublimacione sušnice.

REZULTATI I DISKUSIJA

Granulometrijska analiza materijala

Rezultati granulometrijske analize dve vrste uzoraka polazne sirovine $CuSO_4 \cdot 5H_2O$ (uzorci 1 i 2), kao i osušenog proizvoda $CuSO_4 \cdot H_2O$ dobijenog od ovih uzoraka prikazani su na slici 4. Uzorak 1 sušen je u fluidizovanom sloju, dok je uzorak 2 sušen u pakovanom sloju. Sa slike 4 se može videti da se tokom procesa sušenja praktično ne menja granulometrijski sastav ni kod jednog od uzoraka, budući da osušeni proizvod ($CuSO_4 \cdot H_2O$) ima neznatno niži granulometrijski sastav u odnosu na početni materijal ($CuSO_4 \cdot 5H_2O$). Na osnovu granulometrijske analize utvrđeno je da je srednji prečnik čestica iz uzorka 1 $d_{p,sr1}$ = 0,5 mm, dok je srednji prečnik čestica uzorka 2 $d_{p,sr2}$ = 0,17 mm.

TGA analiza

Mehanizam dehidratacije bakar(II)-sulfat-pentahidrata predmet je brojnih studija u proteklih osamdesetak godina [1–4]. Rezultati ukazuju da ovaj materijal ima neka jedinstvena termička svojstva. Na primer, brzina dehidratacije $CuSO_4 \cdot 5H_2O$ tokom zagrevanja zavisi od eksperimentalnih uslova. Kristali $CuSO_4 \cdot 5H_2O$ ispoljavaju i tzv. Smith–Topley efekat po kome proces dehidratacije zavisi od napona vodene pare [1–4].

Proces dehidratacije bakar(II)-sulfat-pentahidrata do monohidrata može se prikazati sledećom hemijskom jednačinom:

$$CuSO_4 \cdot 5H_2O \rightarrow CuSO_4 \cdot H_2O + 4H_2O \quad (1)$$

Tokom dehidratacije pod vakuumom, monohidrat nastaje već na 70 °C, dok se zagrevanjem na vazduhu na 70 °C dobija trihidrat. Energija aktivacije za proces dehidratacije u vakuumu značajno je manja (oko 50 115 kJ mol^{-1}) u odnosu na dehidrataciju u vazduhu (115 kJ mol^{-1}). Proces dehidratacije takođe zavisi od veličine čestica $CuSO_4 \cdot 5H_2O$ kao i od brzine zagrevanja.

Na slici 5 prikazani su rezultati TGA analize uzorka 1 ($d_{p,sr1}$ = 0,5 mm), dok su na slici 6 prikazani rezultati analize uzorka 2 ($d_{p,sr2}$ =0,17 mm).

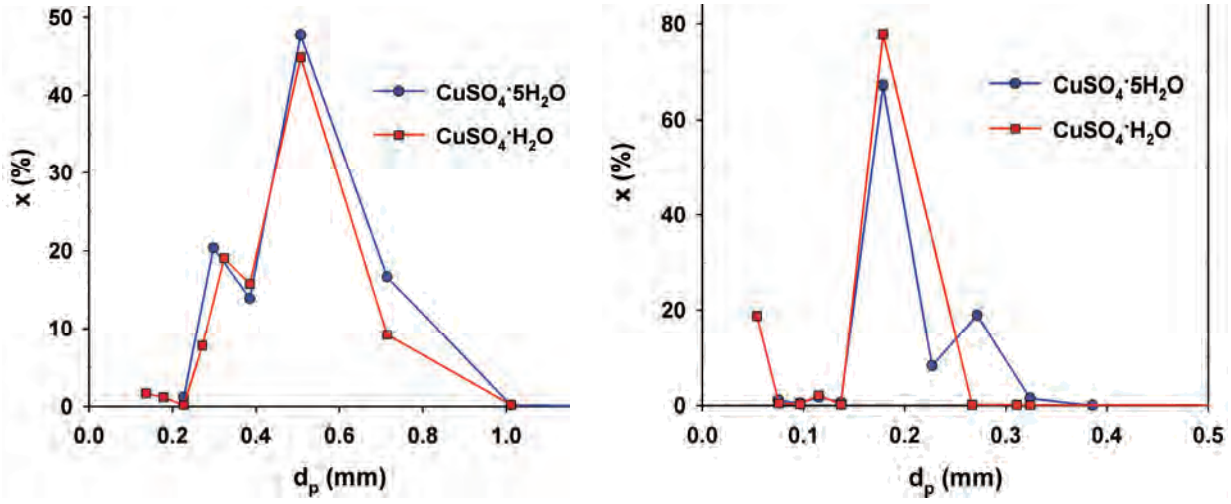

(a) (b)

Slika 4. Granulometrijska analiza uzoraka. a) Uzorak 1 pre i posle sušenja, b) uzorak 2 pre i posle sušenja.
Figure 4. Granulometric analysis of the samples. a) Sample 1 before and after drying, b) sample 2 before and after drying.

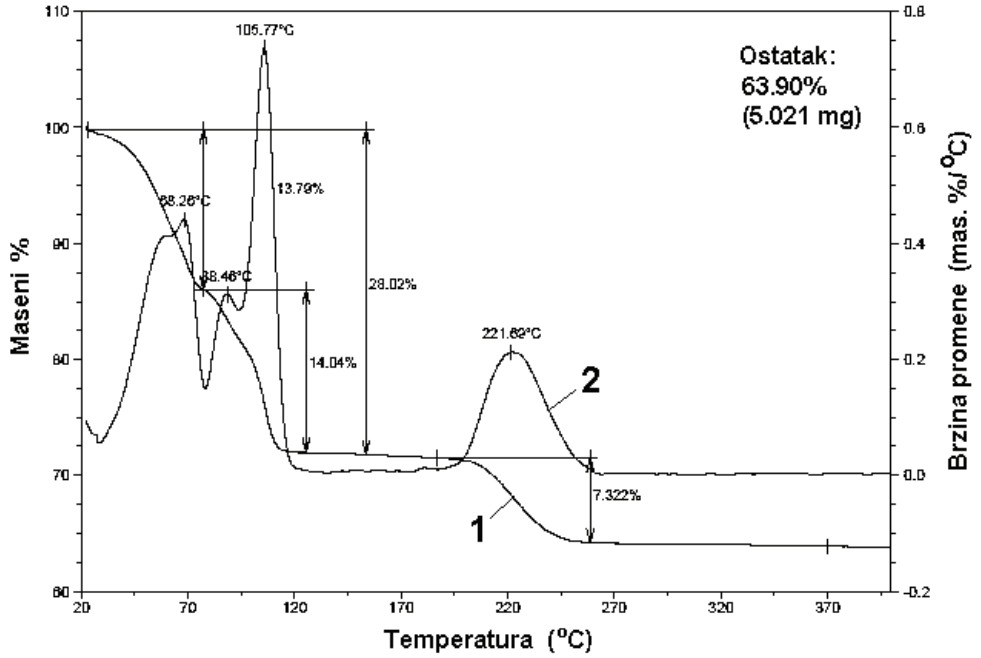

Slika 5. Rezultati TGA analize uzorka 1. 1 – TG-kriva - promena mase sa temperature; 2 – DTG-kriva-brzina promene mase.
Figure 5. TGA analysis of sample 1. 1 – TG-curve – mass change mass vs. temperature; 2 – DTG-curve-rate of mass change.

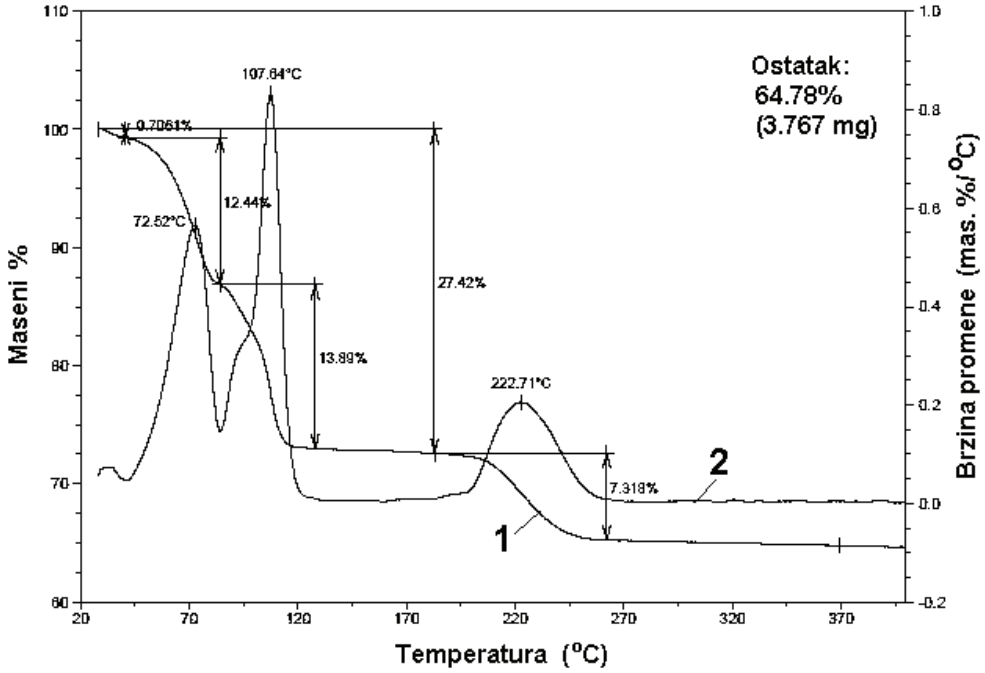

Slika 6. Rezultati TGA analize uzorka 2. 1 – TG-kriva – promena mase sa temperaturom; 2 – DTG-kriva – brzina promene mase.
Figure 6. TGA analysis of the sample 2. 1 – TG-curve – mass change vs. temperature; 2 – DTG-curve – rate of mass change.

Tri DTG-maksimuma na slici 5 ukazuju da se proces dehidratacije u temperaturnom intervalu 20–300 °C odvija u tri koraka. Prvi maksimum se nalazi na 68,3 °C, drugi na 105,8 °C i treći na 221,7 °C. Svaki od ovih maksimuma prati određen gubitak mase koji se može očitati sa TG-krive.

Kristalohidrat $CuSO_4 \cdot 5H_2O$ ima molarnu masu 249,5 g/mol. Prvom koraku (na 68,3 °C) odgovara gubitak mase od oko 14 mas.%. Iz ovog podatka može se izračunati molarna masa segmenta koji napušta rešetku kristalohidrata:

$$0{,}14 \times 249{,}5 = 35{,}9 \approx 36 \quad (2)$$

Pošto dva molekula vode imaju relativnu molekulsku masu 36, može se zaključiti da se u ovom koraku odigrava sledeća hemijska reakcija:

$$CuSO_4 \cdot 5H_2O + \text{toplota} \rightarrow CuSO_4 \cdot 3H_2O + 2H_2O \quad (3)$$

Gubitak mase u drugom koraku (105,8 °C) takođe iznosi oko 14 mas.% što odgovara reakciji:

$$CuSO_4 \cdot 3H_2O + \text{toplota} \rightarrow CuSO_4 \cdot H_2O + 2H_2O \quad (4)$$

Kako se sa dijagrama može zapaziti, nastali monohidrat termički je stabilan u temperaturnom opsegu od 120–195 °C. Naime, u ovom temperaturnom opsegu ne dolazi do promene mase uzorka. Peti molekul vode napušta kristalohidrat u trećem koraku, na 221,7 °C što odgovara gubitku mase od 7,3 mas.%. Zaostali proizvod je anhidrovana so, $CuSO_4$ (teorijska vrednost za procentni sadržaj jednog molekula H_2O u molekulu $CuSO_4 \cdot 5H_2O$ iznosi 7,03 mas.%). Sa slike 6 takođe se može zaključiti da se dehidratacija monohidrata odigrava u širem temperaturnom intervalu (195–250 °C).

Rezultati prikazani na slici 6 u skladu su sa literaturnim navodima koji ukazuju da veličina zrna utiče na mehanizam dehidratacije [11]. Prvi i drugi korak se u slučaju uzorka 2, u kome je granulacija manja, odigravaju na nešto višoj temperaturi (72,5 i 107,6 °C, redom) u odnosu na uzorak 1 (krupnija granulacija), dok se temperatura odigravanja trećeg koraka značajnije ne menja (222,7 °C). Ono što je od značaja za ovaj rad je da temperaturni opseg u kome je monohidrat termički stabilan ostaje praktično nepromenjen (120–195 °C).

Da bi se ispitala kinetika dehidratacije, oba uzorka zagrevana su izotermski na tri temperature od kojih se 180 °C pokazalo da predstavlja optimalnu temperaturu za izvođenje procesa dobijanja monohidrata iz pentahidrata. Na slici 7 prikazane su zavisnosti promene mase uzoraka sa vremenom pri izotermskom zagrevanju uzoraka na 180 °C.

Sa dijagrama na slici 7a zapaža se da uzorak 1 zagrevanjem tokom 35 min na 180 °C gubi 28,9 mas.% što u potpunosti odgovara gubitku mase (28,1 mas.%) tokom reakcije prikazane sledećom hemijskom jednačinom:

$$CuSO_4 \cdot 5H_2O + \text{toplota} \rightarrow CuSO_4 \cdot H_2O + 4H_2O \quad (5)$$

Reakcija prelaska pentahidrata u monohirat za uzorak sitnije granulacije (slika 7b) traje 50 min, tj. neophodno je obezbediti duže vreme zagrevanja nego u slučaju uzorka koji je krupnije granulacije što još jednom potvrđuje da brzina dehidratacije zavisi od veličine zrna.

Sušenje bakar(II)-sulfat-pentahidrata u fluidizovanom sloju

Ispitivanja fluidizacionih osobina materijala, kao i kinetike sušenja izvršena su u laboratorijskoj fluidizacionoj koloni kružnog poprečnog preseka, prečnika D = = 60 mm.

Prema Geldartovoj klasifikaciji materijala [8] oba uzorka spadaju u grupu B materijala sličnih pesku, koji dobro fluidizuju ($d_{p,sr1}$ = 0,5 mm, $d_{p,sr2}$ = 0,17 mm, $\rho_p - \rho \approx \rho_p$ = 2284 kg m^{-3}). Međutim, na osnovu ispitivanja u laboratorijskoj fluidizacionoj koloni zaključeno je da samo uzorak 1 ($d_{p,sr1}$ = 0,5 mm) pokazuje dobre fluidizacione karakteristike tipične za agregativno fluidizovane slojeve grupe B po Geldart-ovoj klasifikaciji. Uzorak 2 ($d_{p,sr2}$ = 0,17 mm), iako se prema svojim osobinama (prečniku i gustini čestica) nalazi u grupi B po Geldartu, gotovo ne fluidizuje usled stvaranja kanala kroz koje protiče veći deo gasa u sloju (slika 8), bez kontakta sa masom materijala, što je tipično za sitne kohezivne materijale grupe C po Geldartu. Ovakvi materijali mogu se fluidizovati na taj način što se u sloj postavljaju različiti mehanički elementi (mešalica ili vibrirajuće rešetke).

S obzirom na činjenicu da uzorak 2 ne fluidizuje, kriva fluidizacije data je samo za uzorak 1. Na slici 9

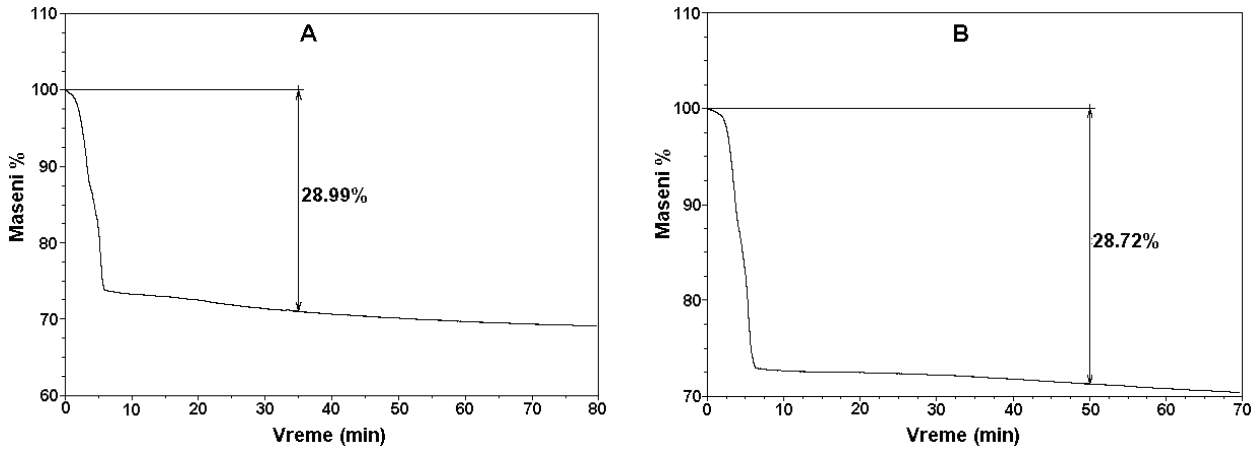

Slika 7. Rezultat TGA analize – promena mase uzorka sa vremenom tokom izotermskog zagrevanja na 180 °C, a) uzorak 1 i b) uzorak 2.
Figure 7. Results of the TGA analysis – sample mass change vs. time during isothermal heating at 180 °C, a) sample 1 and b) sample 2.

prikazana je kriva fluidizacije ovog uzorka dobijena u laboratorijskoj fluidizacionoj koloni prečnika D = 60 mm. Sa slike 9 se može videti da je kriva fluidizacije za materijal iz uzorka 1 klasičnog oblika. Minimalna brzina fluidizacije ovog materijala očitana sa grafika iznosi U_{mf} = 0,121 m s^{-1}.

Slika 8. Fluidizacija čestica srednjeg prečnika 0,17 mm.
Figure 8. Fluidization of particles of mean diameter 0.17 mm.

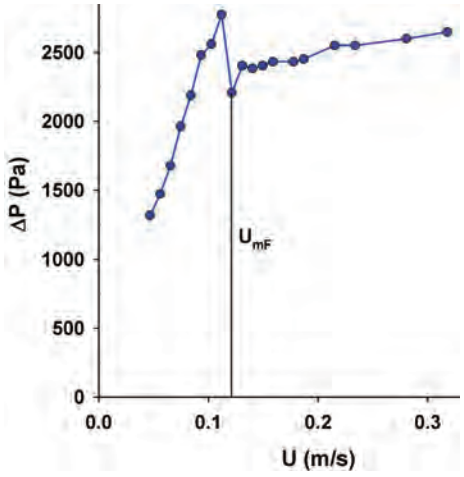

Slika 9. Kriva fluidizacije uzorka 1 (srednjeg prečnika 0,5 mm).
Figure 9. Fluidization curve of sample 1 (mean diameter 0.5 mm).

S obzirom na činjenicu da je TGA analizom utvrđena optimalna ulazna temperatura grejnog fluida – vazduha od 180 °C, kriva sušenja je određena pri ovoj ulaznoj temperaturi vazduha. Izlazna temperatura vazduha iznosila je 120 °C, a brzina vazduha 0,5 m s^{-1}. Pri ovim uslovima, praćena je dinamika procesa sušenja (slika 10) na osnovu čega je zaključeno da vreme kontakta u sloju treba da iznosi minimalno 60 min. Na slici 10 prikazan je gubitak mase materijala sušenog u fluidizovanom sloju tokom različitih vremenskih intervala (15, 30, 45, 60 i 75 min), zagrevanjem na temperaturu od 250 °C, odnosno na temperaturu pri kojoj dolazi do gubitka i poslednjeg molekula vode iz kristalne rešetke na osnovu TGA analize. Teorijski gubitak mase do koga dolazi usled gubitka jednog molekula H_2O iz $CuSO_4 \cdot H_2O$ tokom ovog zagrevanja iznosi 10,14%. Dostizanje ove vrednosti pokazuje da je materijal sušen u fluidizovanom sloju pri pomenutim temperaturnim uslovima zaista monohidrat, $CuSO_4 \cdot H_2O$. Kao što se sa slike 10 može videti, ova vrednost je dostignuta posle 60 min sušenja, na osnovu čega je zaključeno da minimalno vreme boravka u sušnici treba da iznosi 60 min.

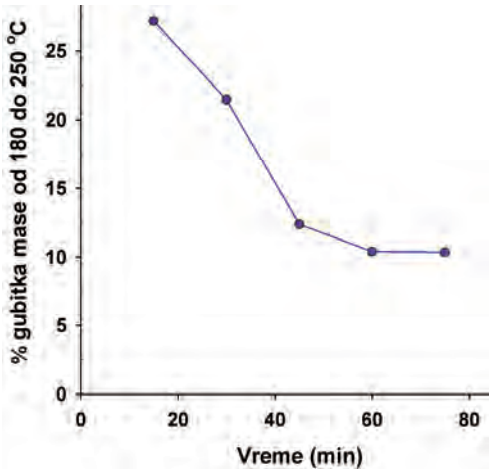

Slika 10. Kriva sušenja za čestice uzorka 1, srednjeg prečnika 0,5 mm.
Figure 10. Drying curve of the sample 1, with mean diameter 0.5 mm.

Rezultati proračuna

Nakon završenih laboratorijskih ispitivanja kojima je utvrđeno da čestice srednjeg prečnika 0,17 mm ne fluidizuju, dalji proračuni su nastavljeni za čestice sa krupnijom granulacijom srednjeg prečnika 0,5 mm i za kolonu kružnog poprečnog preseka.

Dimenzije sušnice izračunavaju se postavljanjem energetskog bilansa procesa uz pretpostavku da se toplota koja se dovede u sušnicu zagrejanim vazduhom predaje vlažnom materijalu i utroši na zagrevanje suve materije i vlage, kao i na uparavanje jednog dela vlage:

$$\left(1-F_{gub}\right)\rho_g U_g c_{pg} \Delta T_g A_c = \\ = \left(\dot{m}_{sm} c_{psm} + \Delta\dot{m}_w c_{pw}\right)\Delta T_{vm} + \Delta\dot{m}_w r_w \quad (6)$$

gde je F_{gub} faktor gubitka toplote u okolinu, za koju je usvojena iskustvena vrednost 0,05. ρ_g, U_g i c_{pg} su gustina gasa, površinska brzina gasa i specifični toplotni kapacitet gasa, redom. ΔT_g je razlika temparature gasa na ulazu u kolonu T_u i temperature sušenja T_s; A_c je površina poprečnog preseka kolone, $\dot{m}_{sm}$ je maseni protok osušenog materijala. c_{psm} i c_{pw} su specifični toplotni kapaciteti suvog materijala odnosno vlage. ΔT_{vm} je razlika temperature sušenja i temperature vlažnog materijala na ulazu u sušnicu koja je u ovom proračunu iznosila 10 °C, $\Delta\dot{m}_w$ je količina isparene vlage u

jedinici vremena a r_w je latentna toplota isparavanja vode.

Minimalna brzina fluidizacije jedna je od najvažnijih karakteristika procesa fluidizacije. Izračunava se iz Ergunove jednačine [7]:

$$150\frac{(1-\varepsilon_{mf})^2}{\varepsilon_{mf}^3}\frac{\mu_g}{d_p^2}U_{mf}+1{,}75\frac{1-\varepsilon_{mf}}{\varepsilon_{mf}}\frac{\rho_g}{d_p}U_{mf}^2 = \\ =(1-\varepsilon_{mf})g(\rho_p-\rho_g) \quad (7)$$

gde je ε_{mf} poroznost sloja u stanju minimalne fluidizacije, ρ_g i μ_g su gustina i viskoznost gasa, U_{mf} je minimalna brzina fluidizacije, dok su d_p i ρ_p prečnik i gustina čestica, redom. Druga karakteristična brzina u fluidizacionim sistemima je brzina taloženja usamljene čestice, U_t, koja se se naziva i brzinom odnošenja. Za sitne čestice možemo pretpostaviti laminarni režim taloženja čestica, te se brzina odnošenja (taloženja) može odrediti iz izraza [7]:

$$U_t=\sqrt{\frac{3{,}1d_pg(\rho_p-\rho_g)}{\rho_g}} \quad (8)$$

U ovom radu za fluidizacioni broj U_g/U_{mf}, usvojena je vrednost 4, što znači da je za brzinu gasa usvojena četiri puta veća vrednost od minimalne brzine fluidizacije.

Nominalno vreme boravka vlažnog materijala u sušnici izračunava se prema jednačini:

$$\tau=\frac{m_s}{\dot{m}_{vm}} \quad (9)$$

gde je m_s statička masa sloja a $\dot{m}_{vm}$ maseni protok vlažnog materijala, tj. bakar(II)-sulfat-pentahidrata. Za proizvodni kapacitet od 500 kg h^{-1} bakar(II)-sulfat-monohidrata, maseni protok bakar(II)-sulfat-pentahidrata iznosi 702,5 kg h^{-1}. Na osnovu prethodno definisanih jednačina proračunata je neophodna količina agensa za sušenje (vazduha), utrošak toplote za zagrevanje agensa za sušenje sa ambijetalne temperature na 180 °C, kao i dimenzije kolone za proizvodnju 500 kg h^{-1} bakar(II)-sulfat-monohidrata. Takođe, proračunate su i vrednosti specifične potrošnje vazduha i toplote neophodne za uklanjanje 1 kg vode.

Parametri neophodni za proračun kao i rezultati proračuna su prikazani u tabeli 2.

Izračunata vrednost minimalne brzine fluidizacije (0,214 m s^{-1}) je nešto veća od minimalne brzine fluidizacije dobijene iz eksperimentalnih ispitivanja (slika 9). Do ove razlike dolazi usled toga što je u proračunu minimalne brzine fluidizacije korišćena srednja vrednost prečnika čestica uzorka 2 od 0,5 mm. Granulometrijskom analizom je pokazano da uzorak 2 sadrži i sitnije čestice, kao što se može videti sa slike 4. Ove sitnije čestice počinju da fluidizuju pri brzinama nižim od 0,214 m s^{-1}, što se vidi iz eksperimentalne krive fluidizacije.

Za zadati proizvodni kapacitet neophodno je utrošiti 10309,1 kg h^{-1} ambijentalnog vazduha za koji je za zagrevanje vazduha sa 10 na 180 °C potrebno utrošiti 494,1 kW toplote. Na osnovu jednačine (6) proračunata je neophodna površina poprečnog preseka kolone od 3,78 m^2, čime se za kolonu kružnog poprečnog preseka dobija prečnik kolone od 2,19 m. Za odnos visina/prečnik kolone uzeta je vrednost 3. Usvaja se statička visina sloja od 0,2 m, na osnovu čega se proračunava zapremina nasipnog sloja, odnosno statička masa sloja. Iz jednačine (9) proračunato je nominalno vreme boravka od 1,42 h što je dovoljno vreme da se obavi proces sušenja.

Proračun iz Super Pro Designer programskog paketa

U programskom paketu Super Pro Designer moguće je izvršiti materijalno bilansiranje sušnice sa fluidizovanim slojem. Na slici 11 prikazan je izgled prozora iz programskog softvera Super Pro Designer 5.1.

Za potrebe proračuna neophodno je zadati sledeće parametre: ulaznu i izlaznu temeraturu materijala, ulaznu temperaturu agensa za sušenje, protok materijala na ulasku u sušnicu i brzinu isparavanja vlage po jedinici zapremine, za koju je iz literature preuzeta iskustvena vredost od 40 kgH_2O/(h m^3) [5]. Ostali parametri imaju vrednosti date u tabeli 2. Kao izlazne podatke softver proračunava maseni protok agensa za sušenje, maseni protok osušenog materijala kao i dimenzije kolone (prečnik i visinu). U tabeli 3 su prikazani rezultati dobijeni bilansiranjem sušnice u fluidizovanom sloju u softverskom paketu Super Pro designer. Prilikom proračuna dimenzije kolone usvojen je odnos visine i prečnika vrednosti 3, što je bila vrednost preporučena u softveru.

Ovaj softver takođe pruža mogućnost ekonomske evaluacije uređaja na bazi zadatih cena materijala i opreme postrojenja. Ako se ove cene preuzmu iz samog softvera procenjena vrednost proračunate sušnice u fluidizovanom sloju iznosi 67393 $.

Poređenjem rezultata dobijenih u Super Pro Designer programskom softveru i rezultata prikazanih u tabeli 2, zapaža se da se vrednosti neophodnog masenog protoka vazduha za sušenje dobijene na bazi prethodno definisanih jednačina i primenjenog softvera jako malo razlikuju. Značajnije razlike se dobijaju u dimenzijama sušnice. Imajući u vidu da je prečnik kolone iz Super Pro Designer značajno manji, a vrednosti masenog protoka vazduha vrlo slične, to znači da će brzina vazduha u ovakvoj koloni biti značajno veća (oko 2,8 m s^{-1}). Treba napomenuti da se kao ulazni podatak za proračun u Super Pro Designer unosi vrednost prečnika čestica, ali nije moguće uneti raspodelu veličina čestica polidisperzne smeše. Zato su i rezultati proračuna iz ovog programskog paketa direktno primenljivi

Tabela 2. Termofizički parametri čestica i vazduha [12,13] i rezultati proračuna za čestice $d_{p,sr}$ = 0,5mm
Table 2. Thermophysical parameters of particles and air [12,13] and the results of calculations for the particles of $d_{p,av}$ = 0.5 mm

Parametar	Vrednost	Jedinica
Usvojeni procesni parametri		
Ulazna temperatura vazduha T_u	180	°C
Temperatura sušenja T_s	120	°C
Fluidizacioni broj U_g/U_{mf}	4	–
Karakteristike čestica $CuSO_4 \cdot 5H_2O$		
Gustina čestica ρ_p	2284	kg m^{-3}
Statička poroznost sloja ε_0	0,42	–
Nasipna gustina čestica ρ_{pbulk}	1325	kg m^{-3}
Specifični toplotni kapacitet suve materije c_{psm}	0,8	kJ (kg °C)$^{-1}$
Karakteristike tečne faze		
Specifični toplotni kapacitet vode c_{pw}	4,189	kJ (kg °C)$^{-1}$
Latentna toplota isparavanja vode r_w	2268	kJ (kg °C)$^{-1}$
Karakteristike fluidizovanog sloja		
Poroznost u stanju minimalne fluidizacije ε_{mf}	0,43	–
Gustina vazduha na temperaturi sušenja ρ_g	0,8858	kg m^{-3}
Viskoznost vazduha na temperaturi sušenja μ_g	$2{,}241 \cdot 10^{-5}$	Pa s
Specifični toplotni kapacitet suvog vazduha c_{pg}	1,015	kJ (kg °C)$^{-1}$
Minimalna brzina fluidizacije na temperaturi sušenja U_{mf}	0,214	m s^{-1}
Površinska brzina vazduha na temperaturi sušenja U_g	0,86	m s^{-1}
Brzina taloženja *Ut*	6,20	m s^{-1}
Dimenzije kolone za fluidizaciju		
Faktor gubitka toplote u okolinu, F_g	0,05	–
Potrebna površina kolone A_c	3,78	m^2
Prečnik kolone D_c	2,19	m
Visina kolone *H*	6,58	m
Usvojena visina sloja H_{us}	0,20	m
Zapremina nasipnog sloja V_n	0,76	m^3
Statička masa sloja m_s	1001,2	kg
Nominalno vreme boravka τ	1,42	h
Utrošak vazduha i toplote		
Maseni protok vazduha $\dot{m}_g$	2,86	kg s^{-1}
Maseni protok vazduha po času	10309,1	kg s^{-1}
Utrošak toplote *Q*	494,1	kW
Specifična potrošnja toplote *q*	8787	kJ (kg H_2O)$^{-1}$
Specifična potrošnja vazduha *L*	50,92	kJ (kg H_2O)$^{-1}$

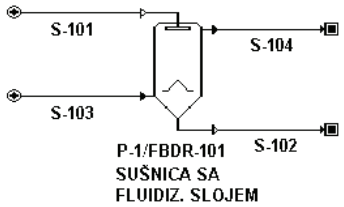

Slika 11. Sušnica sa fluidizovanim slojem u Super Pro Designer, gde su S-101 i S-102 ulazna i izlazna struja materijala, S-103 i S-104 ulazna i izlazna struja vazduha za sušenje.
Figure 11. Fluidized bed dryer from Super Pro Designer, where S-101 and S-102 denote input and output streams of drying material, S-103 and S-104 denote input and output streams of drying air.

Tabela 3. Maseni protok vazduha i proračunate dimenzije kolone za sušenje bakar(II)-sulfat-pentahidrata u programskom paketu Super Pro Designer
Table 3. Air mass flow and size of the drying column for copper (II) sulfate pentahydrate calculated by Super Pro Designer

Parametar	Vrednost	Jedinica
Maseni protok svežeg vazduha	10116,0	kg h^{-1}
Maseni protok osušenog proizvoda	500,18	kg h^{-1}
Prečnik kolone	1,29	m
Visina kolone	3,87	m

na monodisperzne materijale, dok je za njihovu primenu na polidisperzne smeše potrebno prilagoditi brzine vazduha za sušenje, da ne bi došlo do odnošenja velikog broja sitnijih čestica iz sloja.

Proračun iz Simprosys programskog paketa

U programskom paketu Simprosys 3.0 je moguće izvršiti materijalno i energetsko bilansiranje čitavog postrojenja za sušenje. Na slici 12 je šematski prikazano postrojenje za sušenje bakar(II)-sulfat-pentahidrata koji pored sušnice i grejača uključuje i uređaje za pripremu agensa za sušenje kao i za njegovo prečišćavanje od zaostalih čestica pre njegovog ispuštanja u atmosferu. Na istoj šemi je prikazana i mogućnost mešanja dela vazduha iskorišćenog za sušenje sa ambijentalnim vazduhom u cilju povećanja energetske efikasnosti procesa. Nedostatak ovog programskog paketa je što ne uzima u obzir konstruktivne karakteristike sušnice, kao ni kinetiku procesa sušenja, što ograničava njegovu primenu samo na materijalno i energetsko bilansiranje procesa.

Ambijentalni vazduh (gas 1) ulazi u ventilator nakon koga se meša sa delom struje iskorišćenog vazduha (gas 10). Tako nastala smeša vlažnog vazduha (gas 3) ulazi u grejač u kome se zagreva na 180 °C čime je spreman za sušenje. Nakon sušnice, iskorišćeni vazduh (gas 5) prolazi kroz ciklon i filter za vazduh u kojima se prečišćava od čestica koje su odnete strujom vazduha. Nakon filtra za vazduh, deo iskorišćenog vazduha odlazi u atmosferu (gas 8), a deo se recirkuliše i meša sa strujom svežeg vaduha.

Poznato je da procesi sušenja spadaju u termički veoma zahtevne procese. U cilju povećanja energetske efikasnosti procesa sušenja često se vazduh koji izlazi iz sušnice ponovo vraća u proces kada to njegovi procesni parametri (temperatura i sadržaj vlage) dozvoljavaju. S obzirom da u ovom slučaju vazduh iz sušnice izlazi na 120 °C a da ambijentalni vazduh ulazi na 10 °C, njihovim mešanjem u odgovarajućem odnosu potreba za toplotom razmenjenom u grejaču će se smanjiti. U tabeli 4 dat je uporedni prikaz potrebne količine ambijentalnog vazduha i utroška toplote na grejaču za slučaj da se u postrojenju obavlja: *i*) proces bez recirkulacije vazduha, *ii*) proces u kome se 30% iskorišćenog vazduha vraća u proces i *iii*) proces u kome se 70% iskorišćenog vazduha vraća u proces i pre grejača meša sa svežim vazduhom.

Tabela 4. Rezultati materijalnog i energetskog bilansiranja procesa sušenja bakar(II)-sulfat-pentahidrata u programskom paketu Simprosys
Table 4. Material and energy balancing of the drying process of copper (II) sulfate pentahydrate in the software package Simprosys

Parametar	Vrednost	Jedinica
Proces bez recirkulacije vazduha		
Maseni protok svežeg vazduha	12426,4	kg h^{-1}
Utrošak toplote	591,5	kW
Proces sa recirkulacijom 30% vazduha		
Maseni protok svežeg vazduha	8490,1	kg h^{-1}
Utrošak toplote	453,2	kW
Proces sa recirkulacijom 70% vazduha		
Maseni protok svežeg vazduha	3479,2	kg h^{-1}
Utrošak toplote	384,0	kW

Na osnovu rezultata iz Tabele 4 zapaža se da se toplota najmanje troši pri procesu recirkulacije vazduha od 70% i da je tada potreban najmanji protok vazduha na ulazu u postrojenje. Najveća potrošnja toplote se javlja u slučaju bez recirkulacije, tako da ukoliko želimo da smanjimo taj utrošak, najbolje je konstruisati postrojenje sa recirkulacijom.

Poređenjem rezultata koje daje Symprosis sa prethodno analiziranim pristupima zapaža se da je za proces bez recirkulacije vazduha u Symprosis-u proračunata oko 20% veća količina agensa za sušenje (12426,4 kg h^{-1}) nego što je to bio slučaj kod računskog proračuna (10309,1 kg h^{-1}) i Super Pro Designera (10116,0). Kao posledica zahtevane veće količine vazduha i iznos toplote je veći za oko 20%. Imajući u vidu da primenjeni programski paketi ne daju metodologiju proračuna ne može se pouzdano utvrditi uzrok odstupanja u rezultatima.

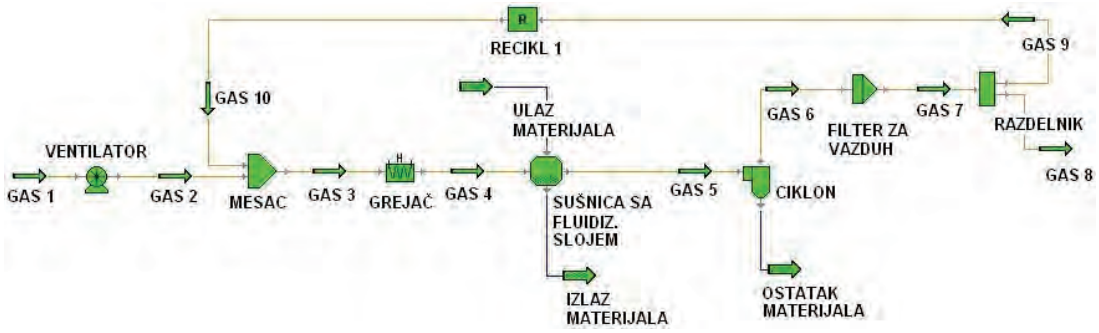

Slika 12. Šema procesa sušenja vlažnog materijala uz recirkulaciju agensa za sušenje iz programskog paketa Simprosys.
Figure 12. Scheme of the drying process with a recirculation of the drying agent from the Simprosys software package.

ZAKLJUČAK

U ovom radu ispitan je proces sušenja bakar(II)-sulfat-pentahidrata do bakar(II)-sulfat-monohidrata. Rezultati TGA-analize ukazali su da je za proces sušenja optimalna temperatura od 180 °C i da sušenje kraće traje ukoliko je uzorak krupnije granulacije. Za uzorak pentahidrata čije su čestice srednjeg prečnika 0,5 mm, monohidrat se dobija za 35 min. U laboratorijskoj koloni sa fluidizovanim slojem ispitane su fluidizacione karakteristike materijala i određena je kriva sušenja. Eksperimentima je potvrđeno da čestice iz uzorka $CuSO_4 \cdot 5H_2O$ sitnije granulacije ne fluidizuju, tako da su u daljim proračunima posmatrane samo krupnije čestice. Nakon laboratorijskih eksperimenata izvršeno je materijalno i energetsko bilansiranje realnog postrojenja sa kapacitetom proizvodnje od 300 t mesečno tj. 500 kg h^{-1} bakar(II)-sulfat-monohidrata. Proračuni neophodne količine agensa za sušenje i dimenzija postrojenja izvršeni su korišćenjem programskih paketa SuperPro Designer i Simprosys. Takođe, analizirana je i mogućnost recirkulacije agensa za sušenje. Na osnovu postavljenih bilansnih jednačina doobijene su približno jednake vrednost masenog protoka agensa za sušenje kao i primenom Super Pro Designer softvera, ali se dimenzije kolone značajno razlikuju. Sa druge strane Symprosis daje za oko 20% veće masene protoke vazduha i zahtevane količine toplote za njegovo zagrevanje u odnosu na računski proračun i Super Pro Designer. Potvrdilo se očekivano da se sa povećanjem količine povratnog vazduha potreba za toplotom koja se dovodi u grejaču za zagrevanje ambijentalnog vazduha smanjuje.

U ovom radu se pokazalo da je jedino eksperimentalnim merenjima moguće proveriti i potvrditi realno ponašanje određenog sistema. Iako je na osnovu Geldartove klasifikacije zaključeno da čestice iz uzorka sitnije granulacije imaju dobre fluidizacione karakteristike, eksperimentalno je potvrđeno da ove čestice ne mogu fluidizovati, čime je potvrđena važnost ispitivanja u laboratorijskim i pilot postrojenjima. Sa druge strane, neslaganje u rezultatima koji su dobijeni primenom tri različita pristupa u bilansiranju i projektovanju sušnice navode na zaključak da je za utvrđivanje pouzdanosti komercijalnih softvera za projektovanja novih postrojenja neophodno prethodno testirati što veći broj različitih realnih industrijskih procesa.

LITERATURA

[1] A.D. Haris, L.H. Kalbus, Decomposition of copper(II) sulfate pentahydrate: A sequential gravimetric analysis, J. Chem. Edu. **56** (1979) 417.

[2] R.L. White, Variable temperature infrared study of copper sulfate pentahydrate dehydration, Thermochim. Acta **528** (2012) 58–62.

[3] G.B. Frost, R.A. Campbell, The rate of dehydration of copper sulphate pentahydrate at low pressures of water vapor, Chin. J. Chem. **31** (1953) 107–119.

[4] J.J.M Órfão, F.G Martins, Kinetic analysis of thermogravimetric data obtained under linear temperature programming – A method based on calculations of the temperature integral by interpolation, Thermochim. Acta **390** (2002) 195–211.

[5] V. Valent, Sušenje u procesnoj industriji, TMF, Beograd, 2001.

[6] A. S. Mujumdar, (Ed.), Handbook of Industrial Drying, 3rd ed., Taylor & Francis, New York, 2006.

[7] D.Kunii, O. Levenspiel, Fluidization Engineering, 2nd ed., John Wiley & Sons, New York, 1969.

[8] D. Geldart, Types of Gas Fluidization, Powder Technol. **7** (1973) 285-292.

[9] Simprosys 3.0, Simprotec corporation, USA, 2013.

[10] Super Pro Designer 5.1, Intelligen, USA, 1991.

[11] T.I. Taylor, H.P. Klug, Thermal transitions in copper sulphate pentahydrate molecular rotation and the dehydration of hydrates, J. Chem. Phys. (1936) 601–607.

[12] B. Djordjević, V. Valent, S. Šerbanović, M. Kijevčanin Termodinamika, Tehnološko–metalurški fakultet, Beograd, 2012.

[13] B. Djordjević, S. Šerbanović, A. Tasić, E. Živković, M. Kijevčanin, V. Valent, Toplotne operacije, Tehnološko––metalurški fakultet, Beograd, 2013.

SUMMARY

CALCULATION AND OPTIMIZATION OF THE COPPER (II) SULPHATE MONOHYDRATE FROM COPPER (II) SULPHATE PENTAHYDRATE PRODUCTION PROCESS IN A FLUIDIZED BED DRYER

Tatjana Kaluđerović Radoičić, Ivona Radović, Marija Ivanović, Nevenka Rajić, Željko Grbavčić

University of Belgrade, Faculty of Technology and Metallurgy, Belgrade, Serbia

(Professional paper)

In this paper the process of the copper (II) sulphate monohydrate from copper (II) sulphate pentahydrate (also known as a Blue vitriol or Bluestone) production was analyzed. Copper (II) sulphate pentahydrate is one of the most important copper salts which has been known since the ancient Egyptians. In the nineteenth century its application as a fungicide was discovered which provoked wide industrial production. Molecule of the copper (II) sulphate pentahydrate is a crystalohydrate with five water molecules linked by chemical bonds to a molecule of the copper (II) sulphate. Copper (II) sulphate exists as a series of compounds that differ in their degree of hydratation. The anhydrous form is a pale green or gray––white powder, whereas the pentahydrate ($CuSO_4 \cdot 5H_2O$), the most commonly encountered salt, is bright blue. In order to obtain copper (II) sulphate monohydrate from copper (II) sulphate pentahydrate, it is necessary to remove four water molecules. To determine the optimum temperature and time required for the removal of four water molecules from a molecule of pentahydrate in this work thermogravimetric (TGA) analysis was performed. Thermogravimetric (TGA) analysis – dehydration of copper (II) sulphate pentahydrate is done using simultaneous TG–DSC thermal analyzer DTG-Q600 SDT from TA Instruments. Analysis was carried out for two types of samples, the samples containing particles of the average diameter equal to 0.17 mm and the particles of the average diameter 0.5 mm. In addition, fluidization and drying curve were determined using a semi-industrial fluidization column. On the top, the industrial fluidization column, aimed to produce 300 tonnes per month of copper (II) sulphate monohydrate, was designed. Material and energy calculations were performed using software packages Simprosys 3.0 and SuperPro Designer 5.1. Simprosys 3.0 is a software package designed for the modeling and simulation of a drying process, as well as for 20 different unit operations. SuperPro Designer 5.1 facilitates modeling, evaluation and optimization of different industrial processes including drying. These software packages were applied for the calculation of the air flow rate, heat exchange and for the scoping of a dryer.

Keywords: Fluidized bed drying • Copper(II) sulphate pentahydrate • Copper(II) sulphate monohydrate • TGA analysis

Optimization of the arsenic removal process from enargite based complex copper concentrate

Aleksandra M. Mitovski[1], Ivan N. Mihajlović[1], Nada D. Štrbac[1], Miroslav D. Sokić[2], Dragana T. Živković[1], Živan D. Živković[1]

[1]*University of Belgrade, Technical Faculty in Bor, Bor, Serbia*
[2]*Institute for Technology of Nuclear and Other Mineral Raw Materials, Belgrade, Serbia*

Abstract
Selective arsenic extraction from enargite based complex concentrate from Copper Mine in Bor (Serbia), using sodium hypochlorite as a leaching agent, was investigated in this paper. The aim was to assess the optimal conditions for the most efficient arsenic removal from the investigated concentrate, based on factorial design applied to experimentally obtained data. Five important factors with three factor levels were used as the input variables and experimentally obtained arsenic extraction yield was taken as the output variable. The first and the second final order model equations were obtained. It was found that the leaching temperature had the strongest effect on the arsenic extraction. The strongest positive interaction was between the sodium hypochlorite molar concentration and the stirring speed during extraction.

Keywords: enargite, extraction, experiment, modeling, variable.

Available online at the Journal website: http://www.ache.org.rs/HI/

SCIENTIFIC PAPER

UDC 622.343(497.11Bor):66.061:54

Hem. Ind. **69** (3) 287–296 (2015)

doi: 10.2298/HEMIND140203042M

Most of the world's refined copper production is based on pyrometallurgical processing of copper concentrates, which includes roasting, smelting and refining in order to obtain high-quality copper cathodes. In Europe, ore deposits that contain metals in viable concentrations have been progressively depleted and few indigenous sources remain. Most concentrates are therefore imported from a variety of sources worldwide.

Some metals are essential as trace elements but at higher concentrations are characterised by the toxicity of the metal, ion or compounds and many are included under various lists of toxic materials [1]. Enargite (Cu_3AsS_4) is one of the most common contaminants in copper concentrates, as it leads to formation of volatile arsenic compounds during roasting and smelting, and it is accompanied by various environmental problems [2]. In order to have sufficiently low levels of arsenic prior to entering the acid plant, gases have to be cooled then submitted to a process step eliminating the bulk of arsenic as As_2O_3. Subsequent to this step, the residual arsenic is eliminated from the gas by a wet process, usually in a electrostatic precipitator. Different dry and wet methods for removal of arsenic from SO_2-bearing gases were described by Dalewski [3]. As a result, most smelters do not practice smelting of copper concentrates containing arsenic in excess of 0.5 %, due to high penalties and state legislative. Various techniques for arsenic removal from contaminated copper concentrate were proposed [4]. The World Health Organization (WHO) published 2nd Edition of Air Quality Guidelines for Europe in 2001, where it was explained that the value of arsenic in the air above 1.5×10^{-3} μg m^{-3} presented a high risk for human lives [5,6].

Typical arsenic contents in the air surrounding industrial zones should be up to 50 ng m^{-3} [7], including the zone in the vicinity of the copper smelter plant in Bor (Serbia). On the other hand, practically it is difficult to obtain the proposed level of arsenic in the air, after smelting copper concentrates produced by a selective flotation procedure applied to the sulfide ore deposits [8]. Having in mind the tendency of copper prices that increased strongly from 2003, due to global copper demands and economic expansion of the BRIC* countries (world refined usage has more than tripled in the last 50 years thanks to expanding sectors such as electrical and electronic products, building construction, industrial machinery and equipment, transportation equipment, consumer and general products) [9], it is necessary to find the most optimal technological process for the removal of excess arsenic and other toxic elements before further pyrometallurgical processing of complex copper concentrate.

Arsenic in complex copper concentrates

Minerals which contain arsenic can be found in copper concentrates produced from Bor (Serbia) ore deposits – enargite (Cu_3AsS_4) and luzonite (Cu_3AsS_4),

Correspondence: A.M. Mitovski, University of Belgrade, Technical Faculty in Bor, Vojske Jugoslavije 12, 19210 Bor, Serbia.
E-mail: amitovski@tf.bor.ac.rs
Paper received: 3 February, 2014
Paper accepted: 7 May, 2014

*Brasil, Russia, India and China

while realgar (As_4S_4) and arsenopyrite (*FeAsS*) are present in smaller quantities. The presence of enargite in copper based minerals leads to relatively high arsenic quantities in copper concentrates which considerably reduces their economic value due to hazardous emissions generated from the pyrometallurgical processing [10]. During the melting process, arsenic, present in the concentrate, forms dangerous oxide dusts and fumes difficult to stabilize for safe disposal [11]. Therefore, this problem becomes more challenging for all subjects that are directly or indirectly involved in the pyrometallurgical copper production from complex copper – sulphide concentrates.

The basic technological problem, which needs to be solved, is the question how to minimize the arsenic concentration emitted from the copper smelter plant, if the raw materials that are going to be used, besides high copper content, have high arsenic values. During pyrometallurgical processes of arsenic-containing copper ores or concentrates some of the arsenic inevitably reports to the final effluents, which have to be stabilized prior to disposal. The disposal of arsenic has been accomplished in practice by the formation of metal arsenates and metal arsenites, *e.g*., Ca^{2+}, Cu^{2+} and Fe^{2+} due to their low solubility. Arsenic has been precipitated by adding lime to the solution, obtaining a calcium arsenate compound, $Ca_3(AsO_4)_2$ [12]. Twidwell *et al*. [13] investigated the stability and solubility of $Ca_3(As0_4)_3$. They noted that the solubility decreased one to two orders of magnitude over the range of pH 9.0–12.6, in the presence of phosphate ions.

To find the possible solution to the problem of arsenic in complex copper concentrates, authors have explored the possibilities of using hydrometallurgical treatment applied to the complex copper concentrate in order to dissolve arsenic, before further pyrometallurgical processing.

The available literature in this area is mainly based on the study of the chalcopyrite behavior [14–16], while the enargite characteristics have not been widely investigated. Recently, research aims have been directed to determining the influence of different leaching media on the arsenic utilization from copper ores and concentrates [2,4,17–32].

Basically, all techniques for the arsenic removal from enargite, applied in practice or still in the experimental phase, described in the literature, can be divided in two groups:

1. enargite leaching in acidic solutions and
2. enargite leaching in alkaline solutions.

The application of alkaline solutions of sodium sulfide gives priority to arsenic leaching, while copper, which remains as part of the solid residue, is suitable for further pyrometallurgical treatment.

Authors decided to evaluate the possibility of enargite leaching with sodium hypochlorite, because the process is technically attractive in terms of its potential use in a commercial scale based on the previous investigations of this matter. Selective oxidative alkaline leaching solution of enargite with hypochlorite may be used to remove arsenic from copper concentrates. Experimental investigations, presented in this paper, have shown that more than 90% of arsenic can be separated by extraction from alkaline enargite leaching at temperatures above 60ºC in atmospheric conditions.

Enargite leaching with hypochlorite can be described by the following chemical reaction:

$$Cu_3AsS_4 + 11NaOH + \frac{35}{2}NaClO = 3CuO +$$
$$+Na_3AsO_4 + 4Na_2SO_4 + \frac{11}{2}H_2O + \frac{35}{2}NaCl$$

These results are in agreement with literature data [8,10,11,17] in terms of the tenorite formation (CuO) as a product of enargite oxidation in the described conditions.

After successful transport of arsenic into solution, arsenic can be stabilized by means of sedimentation with $Ca(OH)_2$ [33]. The mechanism of leaching with sodium hypochlorite was described in details in references [10,33,34].

The technique, used to obtain the optimal conditions for the future technical approach to research the problem, was a mathematical modeling, based on the factorial experimental design.

Environmental issue

Some ore bodies in the Bor copper mine, besides the copper bearing minerals, contain the minerals: Se, Bi, Cr, Sb, Cd, As, Zn, Pb, S, Ni, Fe and Hg, which partially remain in the final copper concentrate, even after the flotation separation process. The largest problem is with the sulfide copper minerals containing arsenic, which are converted into the copper concentrates entirely, being unable to separate them from the other sulfidic copper bearing minerals. At the increased temperatures of copper extraction in the pyrometallurgical processes, heavy metal sulfidic minerals are oxidized or sublimated, leaving the smelting unit in the form of fumes or in the PM form [35]. Modern copper smelters are equipped with contemporary facilities for PM removal from the off gases, as well as for high SO_2 utilization. However, even such facilities present the largest environmental polluters in the regions where they operate [36]. Copper smelters, using the outdated technologies, or smelting the low quality concentrates, are emitting the PM_{10} and the SO_2 high above the prescribed limits, which presents a serious hazard for peoples' health [5,37].

This is why the investigation, presented in this paper, was based on the complex copper based concentrate obtained from the Bor copper mine (ore body H), containing 9.52% Cu and 11.0% S, accompanied by the 3.44% As. With such a high arsenic content, this material shouldn't be treated for copper extraction pyrometallurgicaly in its initial form, under any circumstances.

Theoretical fundamentals

Mathematical modeling aims to describe the different aspects of the real world, their interaction and their dynamics through mathematics. Nowadays modeling has a key role in fields such as the environment and industry [38]. The aim of the modeling in this study was to obtain the mathematical model equation through which it will be possible to carry out the optimization of arsenic removal from enargite based complex copper concentrates.

To obtain a reliable statistical model, previous knowledge of the investigated procedure is surely required. The three steps used in the experimental design include the statistical design of experiments, the estimation of coefficients through a mathematical model with response prediction, and the statistical analysis [39].

The experimental design methodology, widely used to estimate main effects and interaction effects, is also the 2^n factorial design, where each variable (X_i; i = 1–n) is investigated at two levels minimum [40,41]. In a factorial design, all levels of each independent variable are combined with all levels of the other independent variables to produce all possible conditions.

When the factor number (n) increases, the number of runs for a design complete replicate also increases rapidly. The first order model can be used to perform the process modeling, defined by the following equation:

$$y = b_o + \sum_{i=1}^{n} b_i x_i + \sum_{i=1}^{n}\sum_{j>1}^{n} b_{i_j} x_i x_j \quad (1)$$

Or the second order model, which is:

$$y = b_o + \sum_{i=1}^{n} b_i x_i + \sum_{i=1}^{n} b_{ii}(x_{i^2} - \overline{x_{i^2}}) + \sum_{i=1}^{n}\sum_{j>1}^{n} b_{i_j} x_i x_j \quad (2)$$

Where:

$$\overline{X_{i^2}} = \frac{1}{N}\sum_{i=1}^{N} x_{i^2} \quad (3)$$

Where N is the total number of experiments, including the holdout cases.

This way, with the following approximation:

$$b_o' = b_o - \sum_{i=1}^{n} b_{ii}\overline{x_i^2} \quad (4)$$

the second order model can be presented as:

$$y = b_o' + \sum_{i=1}^{n} b_i x_i + \sum_{i=1}^{n} b_{ii} x_{i^2} + \sum_{i=1}^{n}\sum_{j>1}^{n} b_{i_j} x_i x_j \quad (5)$$

The estimation of the developed model accuracy (for both the first or the second order) can be done using the root means squared error (*RMSE*) calculation between the model predicted and experimentally obtained value of the output variable, applied to the holdout cases, which are added to the experimental plan to estimate pure experimental errors:

$$RMSE = \sqrt{\frac{1}{m_o}\sum_{i=1}^{m_o}\left(y_i - y_i^{'}\right)^2} \quad (6)$$

Where y_i is the model predicted and $y_i^{'}$ is the actual value of the output variable, m_0 is the number of holdout cases.

EXPERIMENTAL

One of the possible solutions for the environmental problems caused by pyrometallurgical treatment of complex copper concentrates may be leaching of natural enargite with sodium hypochlorite under alkaline oxidizing conditions with enargite converted into crystalline CuO and the arsenic solubility forming AsO_4^{3-}.

The XRD analysis results of the initial concentrate sample, are given in Figure 1.

Based on the results shown in Figure 1, it can be seen that the crystalline form of the given sample consists of enargite, chalcopyrite, tennantite, olivine and quartz.

Chemical composition of the enargite based complex copper concentrate is shown in Table 1.

The experimental procedure included the concentrate sample preparation – grinding to coarseness of 80% – 0.074 mm, as it the most dominant fraction in conventional copper concentrates), followed by the hydrometallurgical treatment. Leaching of samples was done in a 1 dm^3 three-neck tank with a condenser, a mechanical stirrer and an ultra-thermometer (Fig. 2). The leaching process kinetic experiments were performed at different hypochlorite concentrations (X_1), with different solid to liquid ratios (X_2). The leaching solution was mechanically stirred at different rates (X_3). Leaching temperatures were in the range: 25–60 °C (X_4), and time intervals up to 120 min (X_5).

The reaction progress was determined by analyzing arsenic from the obtained leaching solution using the

ICP-AES method (Inductively Coupled Plasma Atomic Emission Spectroscopy). Based on the arsenic content in the initial sample, the amount of extracted arsenic (Y) was determined.

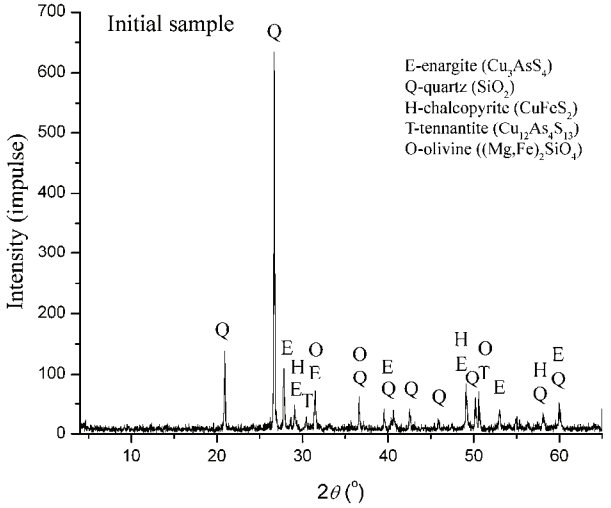

Figure 1. The XRD analysis results of the initial ore feed.

Table 1. Chemical composition of the initial sample

Element	Cu	Zn	Fe	Pb	Ni	Cd	Sb	S	As
mass %	9.52	0.18	10.07	0.006	0.0005	0.0009	0.15	11,0	3.44

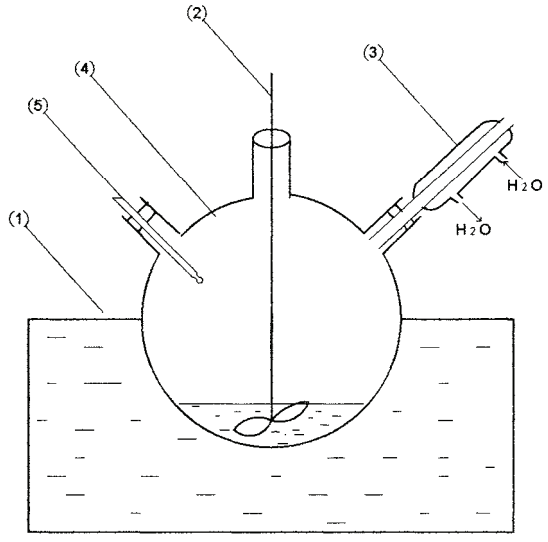

Figure 2. Schematic view of the apparatus used for the experiments; (1) – ultrathermostat; (2) – mechanical stirrer, (3) – condenser,(4) – three-neck tank; (5) – ultrathermometer.

RESULTS AND DISCUSSION

As indicated in previous sections, there are five factors important for the investigated process, namely, the sodium hypochlorite solution concentration (variable X_1); the solid sample mass (variable X_2); stirring rates (variable X_3); leaching temperatures (variable X_4) and leaching time intervals (variable X_5). The low, medium and high levels of all factors, are shown in Table 2.

Both, the first (Eq. (1)) and the second (Eq. (5)) order models were used to fit the obtained experimental data. When five factors (X_1 to X_5), and three factor levels are taken into consideration, the SPSS software [42] resulted in the factorial experimental design that required 16 runs. Six holdout cases were added to the experimental plan to estimate only experimental errors (Table 3). The experiments were run at random order to avoid systematic errors.

After conducting all 22 experiments, the results of arsenic extraction were included in the database as the output variable – Y (Table 2). Experiments 20, 21 and 22, were repeated to asses the replicability of the obtained experimental results. Results of repeated experiments were in accordance with results presented in Table 2, with an error of ±0,5%.

Using the multiple linear regression analysis (MLRA) on the results of the first 16 experiments, presented in Table 3, a first order model (Eq. (1)) was obtained. Based on these results, the final first order model equation resulted from the regression analysis (Eq. (7)):

$$Y = 2.749 + 106.465X_1 - 210.109X_2 - 0.045X_3 + 2.352X_4 + + 0.828X_5 + 279.439X_1X_2 + 0.172X_1X_3 - 6.615X_1X_4 + + 0.075X_1X_5 + 0.135X_2X_3 + 3.187X_2X_4 - 0.277X_2X_5 - - 0001X_3X_5 - 0.010X_4X_5 \quad (7)$$

Table 2. Factor levels

Factor	Low level (–)	Medium level (0)	High level (+)
Sodium hypochlorite molar concentration (X_1)	0.18	0.30	0.42
Mass of the solid sample, g (X_2)	0.30	0.50	0.70
Stirring speed, rpm (X_3)	100	300	600
Leaching temperature, °C (X_4)	25	40	60
Leaching time, min (X_5)	20	60	120

The internal validity of the obtained model was than tested using control tests made on six holdout cases presented in Table 3. After calculating the Root Means Squared Error (Eq. (6)) between the model predicted and experimentally obtained copper extraction, for holdout cases, it was concluded that the data obtained experimentally and the model estimations are in good agreement.

Table 3. Experimental design and arsenic leaching yield; [a] – holdout cases

Exp. No.	X_1, M_{NaClO} / mol dm^{-3}	X_2 Solid phase, g	X_3 Stirring speed, min^{-1}	X_4 Temperature, °C	X_5 Time, min	Y Arsenic yield, %
1	–	–	–	–	–	30.05
2	+	–	+	–	0	63.95
3	–	–	–	0	+	87.21
4	0	–	0	+	–	87.21
5	0	–	+	0	–	93.02
6	–	–	–	–	–	29.07
7	+	0	–	+	–	81.39
8	–	0	0	0	0	87.21
9	+	+	–	0	–	69.77
10	+	–	0	–	+	69.77
11	–	0	+	–	–	34.88
12	–	+	0	–	–	23.67
13	–	+	+	+	+	93.02
14	0	0	–	–	+	57.56
15	0	–	–	0	+	98.84
16	–	–	–	+	0	93,02
17[a]	0	0	–	0	0	75.58
18[a]	0	+	–	–	0	35.71
19[a]	+	0	–	0	0	75.58
20[a]	–	–	–	0	–	81.39
21[a]	+	+	+	–	+	75.58
22[a]	+	+	+	+	+	95.51

The coefficient of determination of the final first order model is R^2 = 0.85 as indicated in Figure 3. This coefficient is the squared value of the multiple correlation coefficients, which presents the linear correlation between the observed and model predicted values of the dependent variable. Its large value indicates a strong relationship.

Since the coefficient of determination of the first order model was not satisfactorily high, it was decided to apply the second order model (Eq. (5)) in the sub-

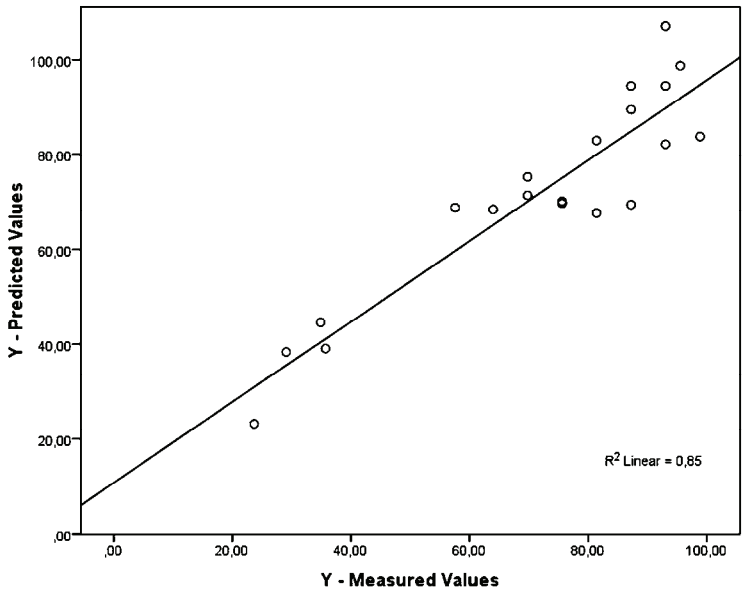

Figure 3. Correlation between experimentally determined and first order model predicted values of the arsenic extraction from the enargite sample; (— = regression lines; o = values calculated using the first order MLRA model).

sequent analysis.

The values of obtained model coefficients, which have statistical significance ($p < 0.01$), are indicated in Table 4.

Based on these results (Table 4), the final second order model equation obtained by using the stepwise method in six iterations, is presented in Eq. (8):

$$Y = -130.414 + 8.105X_4 + 0.444X_5 - 0.073X_4^2 + \\ + 0.093X_1X_3 - 0.599X_2X_4 - 0.006X_4X_5 \quad (8)$$

Only the variables with the significant level ($p < 0.05$) remained in the final model equation.

According to the coefficients in the Eq. (8), it is possible to analyze the regression equation and to determine the effect of each factor. Accordingly, the regression equation shows the principal effects of the five selected factors on the arsenic yield. If observing only the unstandardized coefficients (b unstandardized in Table 4), the leaching temperature (X_4) has the strongest effect on the response since the corresponding coefficient (b = 8.105) is larger than the coefficients of other investigated factors. The positive sign of this coefficient indicates that an increase in the leaching temperature improves the arsenic removal from the enargite sample.

Another important factor is the leaching time (X_5 with b = 0.444). This coefficient also has a positive sign indicating that leaching time increase leads to more efficient arsenic removal. On the other hand, other input variables ($X_1 - X_3$), do not have any statistical significance in the independent form. The design of experiments for arsenic removal, after leaching from enargite sample, also exhibits interactions between the various factors studied.

The strongest positive interaction is among the sodium hypochlorite molar concentration (X_1) and the stirring speed during leaching (X_3), with the coefficient b = 0.093. However, if analyzing the coefficient obtained after standardization of the input variables (beta standardized in Table 4), which removes the effect of magnitude of the value of different variables, the situation is to some extend different. It can be concluded that the strongest positive interaction is between the mass of the solid sample (X_2) and the leaching temperature (X_4), with the coefficient b = = 0.176. Anyhow, as expected, the principal influence on arsenic removal comes from the leaching temperature (X_4) and the leaching time (X_5).

The internal validity of the obtained model was than tested using control tests made on six holdout cases, presented in Table 3. After calculating the root means squared error (Eq. (6)) between the model predicted and experimentally obtained arsenic removal values, for holdout cases, it was concluded that the data obtained experimentally and the model estimations are in a good agreement.

The reliability of the final model was further tested using the ANOVA test. The results of ANOVA tests of developed model are presented in Table 5.

Table 5. Results of ANOVA test of the finally obtained second order model; dependent variable: Y

Source	Sum of squares	df	Mean squares	*F*	Sig.
Regression	10356.189	6	1726.031	78.529	0.000
Residual	307.712	14	21.979	–	–
Uncorrected total	10663.901	20	–	–	–

Significant *F* statistics (Table 5) indicate that using the model is better than guessing the mean [43,44].

Also, the significance value of F statistics is less than 0.05 which means that the variations explained by the model are not caused by chance. The regression ratio to residual is 97 pct:13 pct, advocating that 97 pct of the dependent variable (Y) values are explained by the model. The determination coefficient of the final model is R^2 = 0.971, as indicated in Figure 4. Its large value indicates a strong relationship between observed and the model predicted values of the dependant variable. Also, standard error estimate (SEE) for the model was calculated and it equaled to 4.68823. Accordingly, it was decided that the obtained second order model could be used to predict the arsenic removal from the enargite sample accurately enough.

Using the final model equation (Eq. (5)), which predicts the amount of arsenic removal accurately enough (R^2 = 0.971), it is possible to determine optimal con-

Table 4. The second order model of the arsenic removal process from the initial sample

Model	*b* Unstandardized	Standard error	Beta standardized	*t*	Significance (*p*)
Constant	–130.414	14.248	/	–9.153	0.000
X_4	8.105	0.653	4.826	12.404	0.000
X_5	0.444	0.078	0.833	5.686	0.000
X_4X_4	–0.073	0.008	–3.688	–9.634	0.000
X_1X_3	0.093	0.014	0.330	6.530	0.000
X_2X_4	–0.599	0.176	–0.256	–3.400	0.004
X_4X_5	–0.006	0.002	–0.552	–3.209	0.006

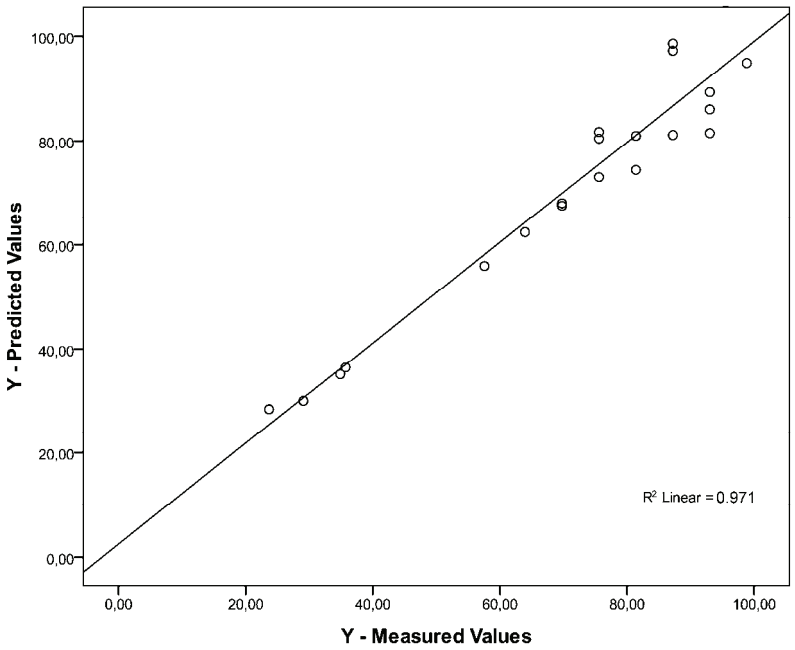

Figure 4. The correlation between experimentally determined and second order model predicted values of the arsenic removal from the enargite sample.

ditions for the operation management of the process, since the model fits the experimental results well enough. The optimization consists of finding such a set of operational variable values which would result in the optimal arsenic extraction yield. The localization of the optimum set of operational variable values can be obtained in various ways [39]. However, the layout of the surface contours plot is the easiest method to interpret, if having a model equation. Surface contour plots were analyzed, using Matlab 7.0 software [45] to determine the optimal solution. The surface response and contour plots, given in Figures 5 and 6, are drawn in the plane leaching temperature – leaching time when the remaining variables are kept at their optimal values responding to the experiment No. 15 (Table 3). These curves allow us to determine the region of the work domain where the arsenic removal from the samples is optimal. Accordingly, if the sodium hypochlorite molar concentration (X_1) is 0.3 M; mass of the initial enargite sample (X_2) is 0.3 g; stirring speed (X_3) is 100 rpm then the arsenic removal (Y) can reach the value of 97.93% if leaching the enargite ore during 120 min at temperatures above 40 °C. This value closely agrees with the experimental arsenic removal of 98.84% in the experimental run 15.

CONCLUSIONS

The recovery of copper from complex concentrates with increased level of impurities has both economical

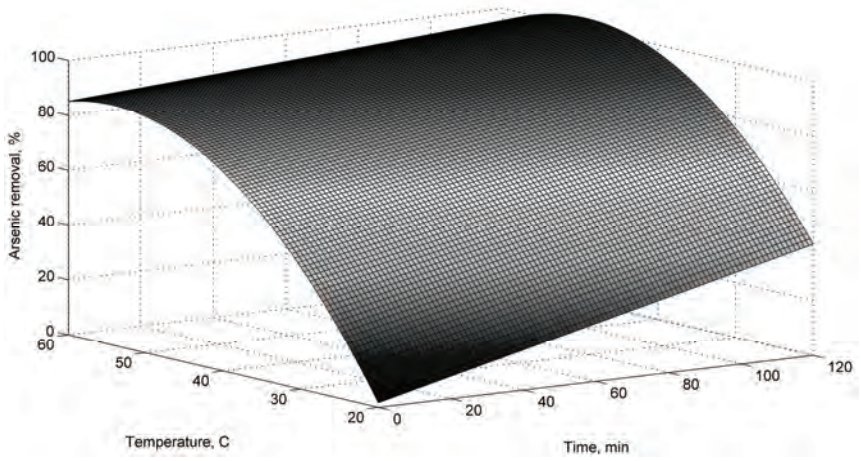

Figure 5. The surface response plot for the arsenic removal in the plane leaching temperature or leaching time at optimal values of the remaining variable (Exp. No. 15).

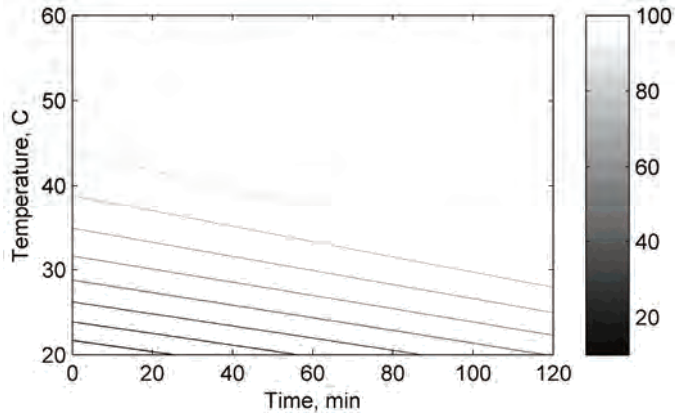

Figure 6. The response contour plot for the arsenic removal in the plane leaching temperature or leaching time at optimal values of the remaining variable (Exp. No. 15).

and ecological aspects – high copper price on the world's market is making this project sustainable. Experimental work in this paper showed that arsenic from enargite can be dissolved by sodium hypochlorite in the form of AsO_4^{3-}, while copper remains in the solid phase in the form of CuO.

Mathematical modeling applied to experimental results, showed that the range of arsenic removal from natural enargite samples was a function of: the sodium hypochlorite molar concentration, the mass of the initial sample, the stirring speed, the leaching temperature and the leaching time. The principal influence on arsenic removal comes from the leaching temperature and leaching time. The positive sign of the coefficients in the final model equation indicate that increase of leaching temperature and leaching time leads to higher arsenic removal efficiency.

The obtained linear correlation dependence with R^2 = 0.971 was calculated using the experimental data acquisition, with experiments prepared according to the factorial experimental design methodology.

The region of the work domain where the arsenic removal from the samples is optimal was determined. The optimal arsenic removal of 97.93% can be achieved under following conditions: the sodium hypochlorite molar concentration (X_1) – 0.3 M; mass of the initial enargite sample (X_2) – 0.3 g; stirring speed (X_3) – 100 rpm; leaching time – 120 min and temperature above 40 °C.

The proposed model can be used to determine the experimental conditions that can generate the optimal arsenic removal after leaching the enargite sample. Using the model equation could support further analyze the effect of each process variable value change on the arsenic removal. Also, it can allow the calculation of kinetic parameters of the process. This would be the subject of authors' further investigations.

Acknowledgement

Research presented in this paper is financially supported by Serbian Ministry of Education, Science and Technological Development, as part of the project No. TR 34023, which is greatly acknowledged.

REFERENCES

[1] European Comission, BAT Reference Document for the Non-Ferrous Metal Industries (Working Draft), 2013.

[2] R. Padilla, C.A. Rivas, M.C. Ruiz, Kinetics of pressure dissolution of enargite in sulfateoxygen media, Metal. Mater. Trans., B. **39** (2008) 399–407.

[3] F. Dalewski, Removing Arsenic fiom Copper Smelter Gases, JOM, **51** (1999) 24–26.

[4] O. Herreros, R. Quiroz, M.C. Hernandez, J. Vinals, Dissolution kinetics of enargite dilute Cl_2/Cl- media, Hydrometallurgy **64** (2002) 153–160.

[5] WHO (World Health Organization), Air Quality Guidelines for Europe, 2nd edition WHO Regional Publications, Regional Office for Europe, Copenhagen, Denmark, 2001.

[6] EU, 2004/107/CE Council Directive relating to arsenic, cadmium, mercury, nickel and polycyclic aromatic hydrocarbons in ambient air, The Council of the European Union, 2004.

[7] A.M. Sanchez de la Campa, J.D. De la Rosa, D. Sanchez-Rodas, et al, Arsenic speciation study of PM2.5 in an urban area near a copper smelter. Atmospheric Environment **26** (2008) 6487–6495.

[8] J. Vinals, A. Roca, M.C. Hernandez, O. Benavente, Topochemical transformation of copper oxide by hypochlorite leaching, Hydrometallurgy **68** (2003) 183–193.

[9] International Copper Study Group, The World Copper Factbook 2013, Portugal (http://www.icsg.org/index.php/press-releases/finish/170-publications-press-releases/1188-2013-world-copper-factbook).

[10] I. Mihajlovic, N. Strbac, Z. Zivkovic, R. Kovacevic, M. Stehernik, A potential method for arsenic removal from copper concentrates, Min. Eng. **20** (2007) 26–33.

[11] D. Dreisinger, The Hydrometallurgical Treatment of Arsenical Copper Concentrates: New Process Options to Unlock Metal Values and Fix Arsenic in Waste. Dept. of Materials Engineering, University of British Columbia, 2005.

[12] V.G. Chuklantsev, J. Inorg. Chem. USSR **1** (1956) 1975.

[13] L.G. Twidwell, K.O. Plessas, P.G. Comba, D.R. Dahnke, 1995, Removal of Arsenic fkom Wastewaters and Stabilization of Arsenic Bearing Waste Solids: Summary of Experimental Studies, Min. Process. Extractive Metall. Rev. **15** (1995) 237–246.

[14] T. Hirato, H. Majima, Y. Awakura, The leaching of chalcopyrite with ferric sulfate, Metall. Trans., B **18** (1987) 489–496.

[15] M. Sokić, B. Marković, D. Živković, Kinetics of chalcopyrite leaching by sodium nitrate in sulphuric acid, Hydrometallurgy **95** (2009) 273–279.

[16] L. Jianming, D. Dreisinger, Copper leaching from chalcopyrite concentrate in Cu(II)/Fe(III) chloride system, Miner. Eng. **45** (2013) 185–190.

[17] W. Tongamp, Y. Takasaki, A. Shibayama, Arsenic removal from copper ores and concentrates through alkaline leaching in NaHS media, Hydrometallurgy **98** (2009) 213–218.

[18] L. Curreli, C. Garbarino, M. Ghiani, G. Orru, Arsenic leaching from a gold bearing enargite flotation concentrate, Hydrometallurgy **96** (2009) 258–263.

[19] P. Balaz, M. Achimovicova, M. Sanchez, R. Kammel, Attrition grinding and leaching of enargite concentrate, Metall. **53** (1999) 53–56.

[20] E. Diamadopoulos, S. Ioannidis, G.P. Sakellaropulos, As(V) removal from aqueous solutions by fly ash, Water Res. **27** (1993) 1773–1777.

[21] W.J. Bruckard, K.J. Davey, F.R.A. Jorgensen, S. Wright, D.R.M. Brew, N. Haque, E.R. Vance, Development and evaluation of an early removal process for the beneficiation of arsenic-bearing copper ores, Miner. Eng. **23** (2010) 1167–1173.

[22] J.E. Dutrizac, R.J.C. MacDonald, The kinetics of dissolution of enargite in acidified ferric sulphate solutions, Can. Metall. Quart. **11** (1972) 469–476.

[23] P. Lattanzi, S. Da Pelo, E. Musu, et al, Enargite oxidation: A review, Earth-Sci. Rev. **86** (2008) 62–88.

[24] P.J. Gabb, A.L. Davies, The industrial separation of copper and arsenic as sulfides, JOM **51** (1999) 18–19.

[25] R. Padilla, D. Giron, M.C. Ruiz, Leaching of enargite in H_2SO_4-NaCl-O_2 media, Hydrometallurgy **80** (2005) 272–279.

[26] K.V. Trivunac, S.M. Stevanović, Effects of operating parameters on efficiency of lead removal by complexation-microfiltration process, Hem. Ind. **66** (2012) 461–467.

[27] M. Al-Harahsheh, S. Kingman, A. Al-Harahsheh, Ferric chloride leaching of chalcopyrite: synergetic effect of $CuCl_2$, Hydrometallurgy **91** (2008) 89–97.

[28] J. Vilcáez, R. Yamada, C. Inoue, Effect of pH reduction and ferric ion addition on the leaching of chalcopyrite at thermophilic temperatures, Hydrometallurgy **96** (2009) 62–71.

[29] M.M. Hourn, D.W. Turner, I.R. Holzberger, Atmospheric mineral leaching process, U.S Patent 5,993,635, 1999.

[30] E.L. Muller, P. Basson, M.J. Nicol, Chloride tank leaching, International Patent WO 2007/134344 A1, 2007.

[31] P.O.L. Littlejohn, D.G. Dixon, The enhancing effect of pyrite on ferrous oxidation by dissolved oxygen, Hydrometallurgy, in Proceedings of the Sixth International Symposium, C.A. Young, P.R. Taylor, C.G. Anderson and Y. Choi, (Eds.), 2008, pp. 955–966.

[32] P.R. Holmes, F.K. Crundwell, The kinetics of the oxidation of pyrite by ferric ions and dissolved oxygen: an electrochemical study, Geochim. Cosmochim. Ac. **64** (2000) 263–274.

[33] M. Kucharski, B. Szafirska, in: P. Palfy, E. Vircikova (Eds.), An investigation on stabilisation of arsenic removed from blister copper, in Proceedings of the V International Conference Metallurgy, Refractories and Environment, Kosice, Stara Lesna, Slovakia, 2002, pp. 153–158.

[34] I. Mihajlovic, N. Strbac, Dj. Nikolic, Potential Metallurgical Treatment Of Copper Concentrates With High Arsenic Contents, J. S. Afr. I. Min. Metall. **111** (2011) 409–416.

[35] F. Habachi, Copper Metallurgy at the Crossroads, J. Min. Metall., B **43** (2007) 1–19.

[36] M. Dimitrijevic, A. Kostov, V. Tasic, N. Milosevic, Influence of pyrometallurgical copper production on the environment, J. Hazard. Mater. **164** (2008) 892–899.

[37] EU, 2004/107/CE Council Directive relating to arsenic, cadmium, mercury, nickel and polycyclic aromatic hydrocarbons in ambient air, The Council of the European Union, 2004.

[38] A. Quarteroni, Mathematical Models in Science and Engineering, Notices of the AMS **56** (2009) 10–19.

[39] F. Oughlis-Hammache, N. Hamaidi-Maouche, F. Aissani-Benissad, S. Bourouina-Bacha, Central Composite Design for the Modeling of the Phenol Adsorption Process in a Fixed – Bed Reactor, J. Chem. Eng. Data **55** (2010) 2489–2494.

[40] D.C. Montgomery, Design and Analysis of Experiments, John Wiley and Sons, New York, 1976.

[41] E. Sayen, M. Bayramogly, Statistical modelling of sulphuric acid leaching of TiO_2, Fe_2O_3 and Al_2O_3 from red mud, Trans IchemE. **79**(B) (2001) 291–296.

[42] SPSS inc. PASW Statistics 18, Predictive Analysis Software Portfolio, available at: www.spss.com.

[43] I. Djuric, P. Djordjevic, I. Mihajlovic, Dj. Nikolic, Z. Zivkovic, Prediction of Al_2O_3 leaching recovery in the Bayer process using statistical multilinear regresion analysis, J. Min. Metall., B **46** (2010) 161–169.

[44] P. Djordjevic, I. Mihajlovic, Z. Zivkovic, Comparison of linear and non-linear statistics for modeling of industrial processes, Serb. J. Manage. **5** (2010) 189–198 (in Serbian).

[45] Matlab 7.0, The MathWorks, 3 Apple Hill Drive Natick, MA 01760-2098, USA, available at: http://www.mathworks.com.

IZVOD

OPTIMIZACIJA PROCESA UKLANJANJA ARSENA IZ KOMPLEKSNOG KONCENTRATA bakra NA BAZI ENARGITA

Aleksandra M. Mitovski[1], Ivan N. Mihajlović[1], Nada D. Štrbac[1], Miroslav D. Sokić[2], Dragana T. Živković[1], Živan D. Živković[1]

[1]*Univerzitet u Beogradu, Tehnički fakultet u Boru, Bor, Srbija*
[2]*Institut za tehnologiju nuklearnih i drugih mineralnih sirovina, Beograd, Srbija*

(Naučni rad)

U prikazanom radu ispitivana je selektivna ekstrakcija arsena iz kompleksnog koncentrata na bazi enargita iz rudnika bakra u Boru, korišćenjem Na-hipohlorita kao agensa za luženje. Osnovni cilj istraživanja sastojao se u utvrđivanju uticajnih parametara i njihovog međusobnog odnosa kako bi se ostvarilo maksimalno uklanjanje arsena iz ispitivanog koncentrata. Enargit (Cu_3AsS_4) spada u rasprostranjene kontaminante koncentrata bakra. Tokom procesa prženja i topljenja arsen obrazuje lako isparljiva jedinjenja koja vrlo negativno utiču na zagađenje ljudi, radne i životne sredine. Zakonska regulativa ne dozvoljava topionicama bakra da tope koncentrate sa više od 0,5% arsena. Za dobijanje optimalnih uslova procesa uklanjanja arsena iz kompleksnog koncentrata bakra na bazi enargita, korišćena je tehnika matematičkog modelovanja. Modelovanje je izvršeno primenom faktorskog dizajna na eksperimentalno dobijene podatke. Odabrano je pet karakterističnih parametara procesa – ulaznih varijabli, za koje se pretpostavlja da imaju uticaja na stepen ekstrakcije arsena: koncentracija rastvora hipohlorita, masa uzorka (koncentrata), brzina mešanja, temperatura luženja i vreme luženja. Faktorski (2^n) dizajn zahtevao je izvođenje 16 eksperimenata sa šest replikanata. Nakon izvođenja 22 eksperimenta, rezultati ekstrakcije arsena uzeti su kao izlazna varijabla. Proračunom su dobijene jednačine modela prvog i drugog reda. Koeficijenti u modelu drugog reda ukazuju da temperatura luženja ima najveći uticaj na ekstrakciju arsena. Drugi faktor po značaju je vreme luženja. Pozitivni predznaci ispred ova dva najuticajnija parametra ukazuju da povećanje temperature luženja, odnosno vremena luženja, utiču na povećanje stepena uklanjanja arsena iz ispitivanog koncentrata. Najveća pozitivna interakcija zapažena je između koncentracije hipohlorita i brzine mešanja tokom procesa ekstrakcije. Proračun RMSE (*root mean square error*) pokazao je dobro slaganje između vrednosti dobijenih eksperimentalnim istraživanjem i vrednosti dobijene modelovanjem. Pouzdanost finalnog modela testirana je primenom ANOVA testa.

Ključne reči: Enargit • Ekstrakcija • Eksperiment • Modelovanje • Varijabla

Effects of temperature and immersion time on diffusion of moisture and minerals during rehydration of osmotically treated pork meat cubes

Danijela Z. Šuput[1], Vera L. Lazić[1], Lato L. Pezo[2], Biljana Lj. Lončar[1], Vladimir S. Filipović[1], Milica R. Nićetin[1], Violeta Knežević[1]

[1]*Faculty of Technology, University of Novi Sad, 21000 Novi Sad, Serbia*
[2]*Institute of General and Physical Chemistry, University of Beograd, 11000 Beograd, Serbia*

Abstract

The aim of this work was to study the changes in osmotically treated pork meat during rehydration. Meat samples were osmotically treated in sugar beet molasses solution, at temperature of 23±2 °C for 5 h. After being osmotically treated, meat samples were rehydrated at constant temperature (20–40 °C) during different times (15–60 min) in distilled water. The effective diffusivity ($m^2 \cdot s^{-1}$) were between 8.35×10^{-10} and 9.11×10^{-10} for moisture, 6.30×10^{-10}–6.94×10^{-10} for Na, 5.73×10^{-10}–7.46×10^{-10} for K, 4.43×10^{-10}–6.25×10^{-10} for Ca, 5.35×10^{-10}–6.25×10^{-10} for Mg, 4.67×10^{-10}–6.78×10^{-10} for Cu, 4.68×10^{-10}–5.33×10^{-10} for Fe, 4.21×10^{-10}–5.04×10^{-10} for Zn and 5.44×10^{-10}–7.16×10^{-10} for Mn. Zugarramurdi and Lupin's model was used to predict the equilibrium condition, which was shown to be appropriate for moisture uptake and solute loss during rehydration.

Keywords: osmotic treatment, rehydration, sugar beet molasses, pork meat, diffusion coefficient, minerals.

Available online at the Journal website: http://www.ache.org.rs/HI/

SCIENTIFIC PAPER

UDC 637.5'64:664.151.2:66

Hem. Ind. **69** (3) 297–304 (2015)

doi: 10.2298/HEMIND131003041S

The knowledge of the kinetics of moisture and solute transfer during the processing is of great technological importance because it allows estimating the immersion time of samples in an osmotic solution to obtain products with determined moisture and solute contents [1–5].

Dehydrated products are usually rehydrated before further processing [6], or prior use to restore the properties of the raw products [7]. Rehydration of food materials also has an important impact on their nutritional and sensorial properties [8].

During rehydration, absorption of water into the tissue results in an increase in the mass [9]. A study of rehydration kinetics can be used to ascertain the net extent of injuries sustained by any material during rehydration and any other processing step prior to it [10]. Rehydration is influenced by several factors, grouped as intrinsic factors such as product chemical composition, predrying treatment, product formulation, drying techniques and conditions and post drying procedure and extrinsic factors such as composition of immersion media, temperature and hydrodynamic conditions [6,11–14].

Two main approaches can be identified. One approach uses the empirical and semi-empirical models like for instance the Peleg and the Weibull equation [15,16]. Azuara proposed a model avoiding the limitations of Fick's diffusion model to estimate moisture loss and solute uptake during OT [17]. Application of the Zugarramurdi and Lupin's model for osmotic treatment has been performed by Corzo *et al*. [18,19]. The other approach employs diffusive models based on Fick's second law of diffusion [20,21]. Some studies using capillary flow approach to model hydration and/or drying of foodstuffs have been reported recently [22,23]. However, the capillary flow approach is still not widely used [8].

Sugar beet molasses is an excellent medium for osmotic dehydration, primarily due to the high dry matter (80%) and specific nutrient content. According to Sauvant *et al*. [24], mineral concentrations in sugar beet molasses are as follows: 3920 mg K/100 g, 680––1300 mg Na/100 g, 100 mg Ca/100 g, 50-320 mg Mg/100 g and 11.7 mg Fe/100 g. The specific chemical composition (approximately 51% sucrose, 1% raffinose, 0,25% glucose and fructose, 5% proteins, 6% betaine, 1,5% nucleosides, purine and pyramidine bases, organic acids and bases) and high content of solids (around 80%) provide high osmotic pressure in the solution, there for molasses appears to be an excellent osmotic medium [25]. In this article, rehydrated pork meat cubes, previously dehydrated in sugar beet molasses solution, are investigated. The final product, being enriched with minerals is intended to be consumed in bakeries. No work has been found dealing with the rehydration of pork meat previously dehydrated in sugar beet molasses solution in the literature.

The aim of this work was to study the influence of the temperature on the effective diffusivities of mois-

Correspondence: L. Pezo, University of Beograd, Institute of General and Physical Chemistry, Studentski trg 12/V, 11000 Beograd, Serbia.
E-mail: latopezo@yahoo.co.uk
Paper received: 3 October, 2013
Paper accepted: 13 March, 2014

ture and solutes during the rehydration of previously osmotic dehydrated pork meat cubes. Simple regression models were proposed for calculation of the effective diffusivities of moisture and solutes (Na, K, Ca, Mg, Cu, Fe, Zn and Mn), as function of the independent variables, and optimum processing conditions were determined through the use of response surface methodology (RSM).

MATERIAL AND METHODS

Fresh pork meat (M. *triceps brachii*) (24 h *post mortem*) was bought in local butcher store and transported to the laboratory where it was held for 1–2 h at approximately 4 °C. The muscles were trimmed of external fat and connective tissues and manually cut into approximately 1×1×1 cm^3 cubes with sharp sterile knives.

Meat samples were osmotically treated in solutions of sugar beet molasses (soluble solid content = 80 $kg \cdot L^{-1}$) at 23±2 °C for 5 h. The solution to sample mass ratio was 10:1 to avoid significant dilution of the medium by water removal, which would lead to local reduction of the osmotic driving force during the process [26]. Every 5 min meat samples in osmotic solutions were mixed with hand-held agitator in order to induce sample – solution contact and provide better homogenization of the osmotic solution. After treatment, samples were removed from the osmotic solution and gently blotted.

OT meat samples were rehydrated by immersing the meat cubes in distilled water. The process was performed under atmospheric pressure, in laboratory jars at processing temperature of (20, 30 and 40 °C), with manual agitation on every 5 min. The jars were kept in water bath, in order to retain samples at constant temperature. The samples were removed after different immersion periods (15, 30, 45 and 60 min), blotted with tissue paper in order to remove the excess water and examined for mass change.

Dry matter content of the fresh and treated samples was determined by drying the material at 105 °C for 24 h in a oven to achieve the constant weight (Instrumentaria Sutjeska, Croatia). All weight measurements were carried out in accordance to AOAC (1990) [27]. Soluble solids content of the molasses solutions was measured using Abbe refractometer, Carl Zeis Jenna, Switzerland, at 20 °C.

Minerals composition of the raw pork meat and osmotic dehydrated pork meat in the solution of sugar beet molasses were investigated. A combination of thermal treatment at 350 °C and wet acidic treatment at 160 °C was used for preparation of samples. The dry samples were then processed for minerals determination by wet digestion, where ca. 5 g of dried sample, were weighed exactly to four decimal places, and transferred to vessels, into which 4.5 ml 65% HNO_3 and 10.5 ml 35% HCl were added. The procedure was repeated to obtain the white sediments that were dissolved in 0.07 M HNO_3. The content of minerals present in the corresponding solutions was determined by inductively coupled plasma optic emission spectrometry (ICP-OES). ICP-OES measurement was performed using Thermo Scientific ICAP 6500 Duo ICP (Thermo Fisher Scientific, Cambridge, United Kingdom) spectrometer equipped with RACID86 Charge Injector Device (CID) detector, standard glass concentric nebulizer, quartz torch, and alumina injector. Multi-elemental plasma standard solutions (Multi-Element Plasma Standard Solution 4, Specpure®, 1000 µg/ml) certified by Alfa Aesar GmbH & Co KG, Germany was used to prepare calibration solutions for ICP-OES measurement. Investigation of moisture content and all chemical analyses were conducted in triplicate.

The developed models, based on Fick's unsteady-state law of diffusion, determine the amount of moisture entering the sample and the solutes diffusing out of the sample as a function of time. According to Crank [28], Fick's second law solution for diffusion, for perfect cubes, assuming the diffusion to be perpendicular to the surface of the cube is given by Eq. (1):

$$X_r = \frac{x_t - x_0}{x_{eq} - x_0} = \frac{8}{\pi^2} \sum_{i=0}^{\infty} \exp\left(-i^2 \pi^2 D_{ew} \frac{t}{L^2} \right) \quad (1)$$

where X_r denotes the dimensionless values of moisture uptake, or solute loss; x_t, x_0 and x_{eq} are the moisture or the solute contents of a sample at rehydration time t, at the outset and at equilibrium, respectively; D_{eff} ($m^2 s^{-1}$) is the effective diffusivity, L(m) is the dimension of the sample and t(s) is the immersion time.

For long drying periods, Eq. (1) can be simplified to first two terms of the series, and moisture ratio can be expressed in the logarithmic form:

$$\ln X_r = \ln \frac{8}{\pi^2} - \left(\pi^2 \frac{D_{eff} t}{L^2} \right) \quad (2)$$

$$D_{eff} = D_0 \exp\left(-\frac{E_a}{TR} \right) \quad (3)$$

where the effect of temperature on effective diffusivity is expressed using Arrhenius type relationship. E_a is the activation energy (kJ mol^{-1}), D_0 is the diffusivity value for infinite moisture or solute content, and R represent universal gas constant (kJ mol^{-1}). T is absolute processing temperature (K).

Values of the effective diffusion coefficient (D_{eff}) were obtained by non-linear regression analysis from Eqs. (2) and (3) [29].

The following mathematical model, with an exponential approach to the equilibrium value of moisture

and solutes contents, was proposed by Zugarramurdi and Lupin [30]:

$$\frac{\mathrm{d}X_i(t)}{\mathrm{d}t} = k_i\left(X_i^*(t) - X_i(t)\right) \quad (4)$$

$$X_i(t) = \frac{m_i(t)}{m - \sum_{j=1, j\neq i}^{n} m_j},\ X_i^*(t) = \frac{m_i^*(t)}{m - \sum_{j=1, j\neq i}^{n} m_j} \quad (5)$$

where, i – index of moisture, or mineral content, m_i is mass of i-th component at time t, m_i^* is mass of i-th component at equilibrium, m total mass, k_i is specific rate constant for variation of i-th component.

Eqation (4) can be integrated with the following initial condition (t = 0):

$$X_i(0) = X_i^0 \quad (6)$$

The solution is

$$X_i(t) = X_i^* + e^{-k_i t}\left(X_i^0 - X_i^*\right) \quad (7)$$

It is assumed that the Zugarramurdi and Lupin's model (Eq. (7)) would predict the moisture and solutes content in the kinetics of pork meat cubes including equilibrium solute content during the process.

The considered dependent variables were the concentrations of moisture and minerals (Na, K, Ca, Mg, Cu, Fe, Zn and Mn). The results have been written in Table 1.

The following second order polynomial (SOP) model was fitted to the data. Nine models of the following form were developed to relate nine responses (Y) and two process variables (X):

$$Y_k = \beta_{k0} + \sum_{i=1}^{2}\beta_{ki}X_i + \sum_{i=1}^{2}\beta_{kii}X_i^2 + \beta_{k12}X_1X_2,\ k = 1\text{–}9 \quad (8)$$

where: β_{k0}, β_{ki}, β_{kii}, β_{k12}, are constant regression coefficients; Y_k moisture and observed minerals content (Na, K, Ca, Mg, Cu, Fe, Zn and Mn); X_1 – processing time; X_2 – temperature.

All obtained results were expressed as the mean ± standard deviation (*SD*), analysis of variance (ANOVA) of obtained results was performed for comparison of means, using StatSoft Statistica 10 software (Statsoft Inc., Tulsa, OK, USA).

RESULTS AND DISCUSSION

The study was conducted to determine the rehydration conditions for pork meat cubes. The experimental data used for the analysis were obtained from the experimental design, with 3 temperature and 4 duration time levels, and with 2 parameters (temperature and immersion time).

During rehydration of osmotically dehydrated pork meat cubes in sugar beet molasses, the moisture content (X_w; g water per g of dry solids) and minerals content (X_{Na} – mg Na/g sample; X_{Ca} – mg Ca/g sample; X_K – mg K/g sample; X_{Mg} – mg Mg/g sample; X_{Cu} – mg Cu/g sample; X_{Fe} – mg Fe/g sample; X_{Zn} – mg Zn/g sample; X_{Mn} – mg Mn/g sample) were experimentally determined in samples at different immersion times for all of the experiments. Table 1 shows the response variables as a function of independent variables for the analysis.

Maximum moisture content observed has been obtained after 60 min of rehydration process (regardless the temperature), while higher moisture content has been noticed at increased temperatures. Quite the opposite, decreasing trend, with the increase of processing time and temperature, has been observed with minerals content. According to developed models, water content gain rate and also minerals content loss

Table 1. Experimental design and data for the response surface analysis

Time, min	Temp., °C	X_w / %	X_{Na}	X_K	X_{Ca}	X_{Mg}	X_{Cu}	X_{Fe}	X_{Zn}	X_{Mn}
			mg/g							
0	-	41.99	375.52	938.91	118.19	33.41	0.23	1.37	1.99	0.37
15	20	50.69	295.06	711.84	93.50	28.63	0.21	1.24	1.88	0.33
30	20	54.36	255.50	673.58	80.59	25.87	0.20	1.22	1.78	0.30
45	20	57.96	235.34	543.14	75.31	24.03	0.19	1.19	1.64	0.26
60	20	58.37	218.61	480.09	71.03	21.96	0.15	1.17	1.58	0.23
15	30	52.45	279.05	659.98	85.46	27.67	0.14	1.22	1.80	0.30
30	30	57.23	246.33	578.20	78.20	24.73	0.13	1.19	1.72	0.27
45	30	60.10	225.02	514.73	73.25	23.65	0.11	1.15	1.58	0.24
60	30	60.43	212.58	461.53	69.05	21.55	0.10	1.10	1.51	0.21
15	40	55.71	253.53	546.15	83.32	25.37	0.13	1.14	1.75	0.25
30	40	58.44	224.16	500.84	76.72	23.74	0.11	1.09	1.61	0.23
45	40	60.12	207.69	455.34	71.41	21.99	0.10	1.07	1.52	0.21
60	40	61.97	193.62	413.67	66.86	20.90	0.09	1.03	1.45	0.18

rate were increased at higher temperatures. As previously stated sugar beet molasses is rich in mineral content, and special care should be concerned to gain optimal mineral content in the final product. Na and K contents have been exceptionally high after osmotic treatment (375.52, for Na and 938.91, for K content). Decreasing of these values can be observed even at mildest temperature treatment, at 20 °C, shortly after rehydration process starts.

Numerous articles discuss various topics concerning the Dietary Reference Intakes [31–33], for the choice of the best process conditions depending on the final product application. Previous research [34–36] has shown that OT positively influenced on improving microbiological profile and food safety of product, and preliminary sensory analysis has shown that pork meat processed in this manner has satisfactory sensory characteristics. Also, the use of sugar beet molasses during OT improves the nutritional profile of meat, which chemical composition after the process of OT is in optimal range for human health.

According to ANOVA, Table 2, X_w as most influenced by duration of rehydration process (statistically significant at $p < 0.05$ level), but the influence of temperature was also observed and statistically significant. Na and K concentration were mostly influenced by linear terms of immersion time and temperature (both statistically significant at $p < 0.05$), while quadratic terms of duration of process in X_{Na} SOP model were found statistically significant. Ca and Mg losses have been most influenced by linear term of process duration, while linear term of temperature was also significant at $p < 0.05$ level. Cu loss was mostly affected by linear terms of temperature and immersion time, while Fe content was mostly influenced by process duration. Zn content was affected by linear terms in SOP model, and Mn content was mostly influenced by linear terms.

The average error between the predicted values and experimental values (calculated by Eq. (1)) was below 10%. Values of average error below 10% indicate an adequate fit for practical purposes. To verify the significance of the models, analysis of variance (ANOVA) was conducted and the results indicate that all models were significant with minor lack of fit, suggesting they adequately represented the relationship between responses and factors.

The two-dimensional graphics have been plotted for experiment data visualization (white colored points) and for the purpose of observation the fitting of regression models (moisture content and Na, K, Ca, Mg, Cu, Fe, Zn and Mn losses) to experimental data, Fig. 1. All plots showed the "rising ridge" configuration, with mineral content decreased due to both temperature and immersion time increasing, while moisture content has been enhanced with temperature and duration of the rehydration process.

Moisture and solute contents at equilibrium conditions were determined using Zugarramurdi and Lupin's Equation, Eq. (7), and are given in Table 3. Zugarramurdi and Lupin's equation proved to be suitable for modeling water uptake and minerals loss, as the coefficient of determination was above 0.975 for all treatments. At the beginning of the process there is an initially high rate of water uptake and a quick removal of solutes, followed by a slower rate of water uptake and solute loss in the later stages of the process. Equilibrium moisture content is reached at higher levels for increased temperatures, but the equilibrium content of minerals decreased with the augment in processing temperature.

The effective diffusivities at any given set of conditions were calculated numerically, from the Eq. (2). It is generally assumed that diffusion occurs at a constant rate under the influence of a uniform moisture gradient. However, this does not appear to be true in biological materials, especially after the initial stages of the process, as the physical structure of the material begins to change as the rehydration continues. A non-uniform moisture gradient is developed over the course of rehydration treatment and the effective diffusivity changes with position and time of rehydration [14]. In meat D_{ew} generally shows a decreasing trend over time. Thus it is assumed that in meat materials D_{ew} does not show a pseudolinear correlation with time as also reported by Rastogi *et al*. [14]. Values of effective diffusivity of water, effective diffusivity of nutrients for different combinations of temperature of the osmotic

*Table 2. ANOVA calculation for mineral composition; * – significant at p < 0.05 level, ** – significant at p < 0.10, level 95% confidence limit, error terms were found statistically insignificant, df – degrees of freedom*

Parameter	df	X_w	X_{Na}	X_K	X_{Ca}	X_{Mg}	X_{Cu}	X_{Fe}	X_{Zn}	X_{Mn}
t	1	91.04*	7402.15*	61917.73*	549.40*	53.11*	0.002*	0.016*	0.154*	0.013*
t^2	1	6.15*	284.31*	4.60	15.73*	0.36**	0.000	0.000**	0.001	0.000
T	1	27.60*	1969.09*	30338.00*	61.16*	9.01*	0.013*	0.030*	0.038*	0.008*
T^2	1	0.33	75.08*	452.66	1.94	0.31	0.001	0.001*	0.000	0.000*
t·T	1	0.95	71.05*	3662.44*	8.10**	1.12*	0.000	0.000	0.000	0.000*
Error	6	2.59	26.07	1653.74	11.63	0.55	0.001	0.001	0.002	0.000*
r^2		0.977	0.968	0.999	0.929	0.931	0.976	0.931	0.976	0.943

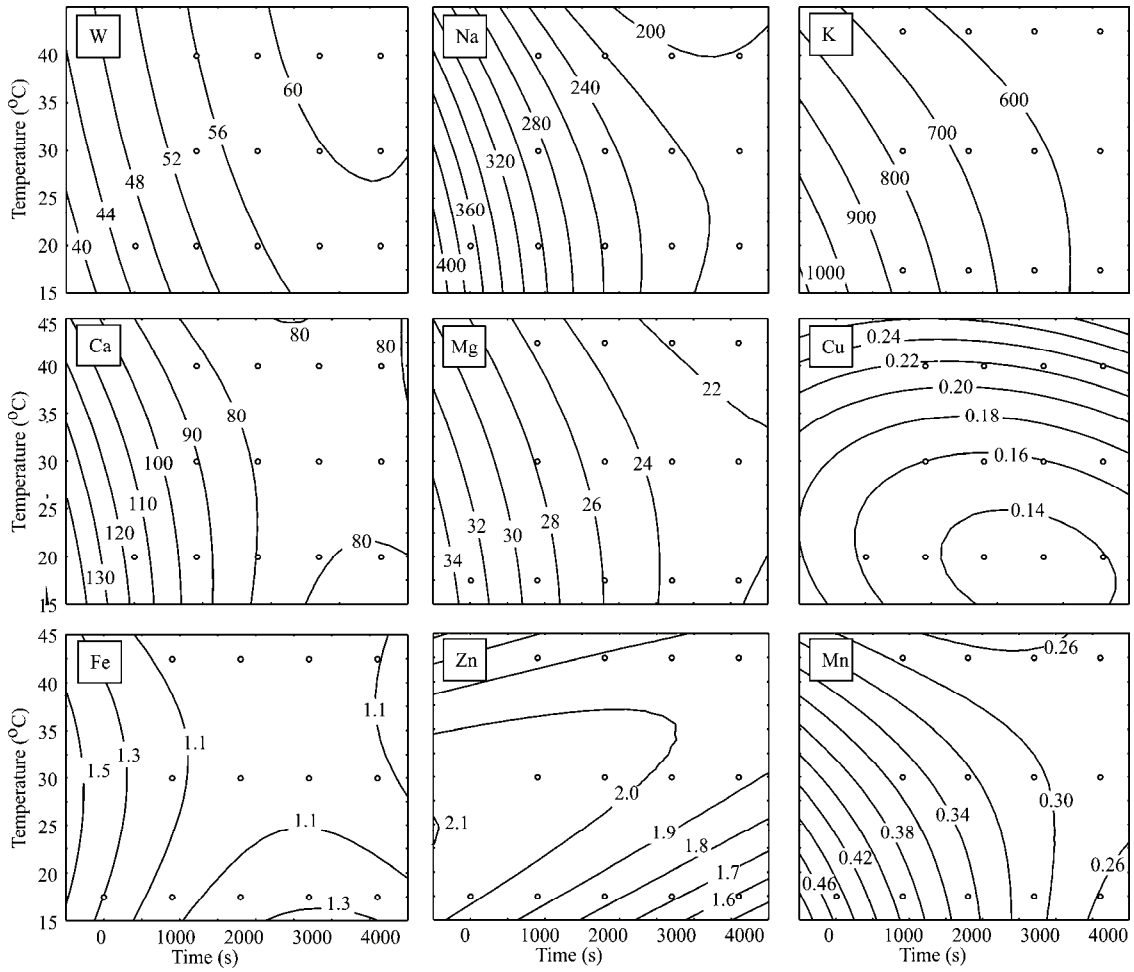

Figure 1. Response surfaces for water content, Na, K, Ca, Mg, Cu, Fe, Zn and Mn contents, as functions of process duration and temperature, during rehydration of meat [mg/100g].

solution, are presented in Table 3. All treatments showed a good fit to the linear equation, giving determination coefficients above 0.98.

The differences between the results of this study and the results found in the literature can be explained by the use of different types of pork meat cubes, and also different degrees of maturation. Another reason for this difference is the use of a sugar beet molasses solution during dehydration process. The presence of the different nutrients in the osmotic solution affects the mechanism involved in the simultaneous flows of water removal and solute penetration and, consequently, affects the diffusivity values. Obtained values for effective diffusivity of moisture, found in this research are in the range of 8.35×10^{-10}–9.11×10^{-10} $m^2\cdot s^{-1}$, which could be compared to the effective diffusivities of moisture in shark filets during brining, found by Mujaffar and Sankat [37], between 0.17×10^{-9} and 0.24×10^{-9} $m^2\cdot s^{-1}$, at temperatures between 20––50 °C, in NaCl solution.

Several authors have made important model studies on the diffusion coefficients of sodium chloride

Table 3. Experimental data fitted to Zugarramurdi and Lupin's Equation

Temp.	X^*_W	r^2	X^*_{Na}	r^2	X^*_K	r^2	X^*_{Ca}	r^2	X^*_{Mg}	r^2
20	60.05	0.998	209.06	0.998	455.69	0.997	70.18	0.993	21.07	0.975
40	61.63	0.997	207.32	0.997	438.88	0.995	68.46	0.993	20.62	0.980
60	63.28	0.994	191.12	0.999	373.47	0.998	65.11	0.995	18.93	0.993
Temp.	X^*_{Cu}	r^2	X^*_{Fe}	r^2	X^*_{Zn}	r^2	X^*_{Mn}	r^2		
20	0.13	0.996	1.17	0.993	1.35	0.998	0.19	0.994		
40	0.09	0.999	1.09	0.997	1.22	0.994	0.18	0.991		
60	0.05	0.992	1.04	0.999	0.12	0.995	0.17	0.996		

and other solutes in meat [38–42]. The diffusion coefficient is suggested to be affected by changes in mineral concentration, swelling and degree of dehydration [40,41,43].

The effective diffusivities of Na in pork meat cubes, found in Table 4, were estimated and values between 6.30×10^{-10} and 6.94×10^{-10} $m^2\cdot s^{-1}$ have been obtained and compared with other studies. The effective diffusivities of Na in chicken breast cuts found by Schmidt *et al.* [5], were between 2.5×10^{-10} and 2.8×10^{-10} $m^2\cdot s^{-1}$, at 5 °C, under stirring conditions, in solutions of NaCl, between 0 and 20%. Gravier *et al*. [41], gained values between 0.6×10^{-10} and 5.0×10^{-10} $m^2\cdot s^{-1}$, in solutions of NaCl, between 30 and 200 g/l.

depends on the temperature, pressure, and on the components involved. Many investigations require that the effective diffusivity is determined at a range of precise temperatures. Frequently, the relationship between effective diffusivity and temperature follows a first order rate process described by an Arrhenius relationship.

High temperatures cause an increase in membrane permeability (which promotes swelling and plasticization of the cell membranes) and a reduction in the solution viscosity, reducing external resistance to mass transfer. Both these phenomena make water and solute transport easier. However, temperatures above 40 °C reduce the final product quality, changing the

Table 4. Effective diffusivities of water and minerals × 10^{10} ($m^2\cdot s^{-1}$) during osmotic rehydration of pork meat

Temp., °C	D_w	D_{Na}	D_K	D_{Ca}	D_{Mg}	D_{Cu}	D_{Fe}	D_{Zn}	D_{Mn}
20	8.35	6.30	5.73	4.43	5.35	4.67	4.68	4.21	5.44
30	8.58	6.52	6.09	6.00	5.61	5.91	5.18	4.76	6.78
40	9.11	6.94	7.46	6.25	6.25	6.78	5.33	5.04	7.16

The effective diffusivities of K in pork meat cubes were estimated in this article, and values between 5.73×10^{-10} and 7.46×10^{-10} $m^2\cdot s^{-1}$ were found. No data for K diffusivities during rehydration of pork meat have been found to be compared with here presented results.

Also, the effective diffusivities of Ca in pork meat cubes were estimated and values between 4.43×10^{-10} and 6.25×10^{-10} $m^2\cdot s^{-1}$ were gained, but due to the lack of data in the literature, presented results could not be compared.

The effective diffusivities of Mg in pork meat cubes were estimated and values between 5.35×10^{-10} and 6.25×10^{-10} $m^2\cdot s^{-1}$ were found. Mg diffusivities data, during rehydration of pork meat were not found elsewhere in the literature to be compared with these results.

The effective diffusivities of Cu in pork meat cubes were estimated and values between 4.67×10^{-10} and 6.78×10^{-10} $m^2\cdot s^{-1}$ and the effective diffusivities of Fe in pork meat cubes were estimated and values between 4.68×10^{-10} and 5.33×10^{-10} $m^2\cdot s^{-1}$ were found. The effective diffusivities of Zn in pork meat cubes were estimated and values between 4.21×10^{-10} and 5.04×10^{-10} $m^2\cdot s^{-1}$. The effective diffusivities of Mn in pork meat cubes were estimated and values between 5.44×10^{-10} and 7.16×10^{-10} $m^2\cdot s^{-1}$ were found.

Cu, Fe, Zn and Mn diffusivities data, during rehydration treatment of pork meat, were not found elsewhere in the literature to be compared with these results.

These results are in agreement with fundamental theories which state that mass diffusivity strongly

structure of cell membranes, resulting in loss of selectivity and leading to greater solute incorporation into the meat. In addition, high temperatures may induce significant changes in texture and nutritional composition of the food as a consequence of the nutrients flow from the product to solution.

CONCLUSIONS

The main objective of this article was to provide an adequate model that allows describing the moisture and solute contents during rehydration (in distilled water) of the previously osmotic treated pork meat cubes in sugar beet molasses solution. Different immersion times (15–60 min) and immersion temperatures were used (20–40 °C). Second order polynomial models fitted the experimental data well. According to developed models, water content gain rate and also minerals content loss rate were increased at higher temperatures. Zugarramurdi and Lupin's model was used for equilibrium content evaluation, and coefficients of determination showed good fitting capabilities. During rehydration, equilibrium moisture content increased with the temperature rise, while equilibrium content of observed minerals decreased with temperature enhancement.

Fick's unsteady-state diffusion equation was shown to be suitable for determining the mass effective diffusivity of water and solutes in pork meat cubes. The temperature and osmotic solution composition showed significant effects on all the responses studied. Increases in temperature, and/or molasses concentration led to higher effective diffusivity of water.

Acknowledgements

This work is part of project „Osmotic dehydration of food - energy and environmental aspects of sustainable production“, project number TR-31055, financed by Ministry of Education, Science and Technological Development, Republic of Serbia.

REFERENCES

[1] J. M. Barat, M. Aliño, A. Fuentes, R. Grau, J. B. Romero, Measurement of swelling pressure in pork meat brining. J. Food Eng. **93** (2009) 108–113.

[2] M. Castro-Giraldez, P.J. Fito, P. Fito, Non-equilibrium thermodynamic approach to analyze the pork meat (*Longissimus dorsi*) salting process. J. Food Eng. **99** (2010) 24–30.

[3] M.Chabbouh, S. Ben Hadj Ahmed, A. Farhat, A. Sahli, S. Bellagha, Studies on the salting step of Tunisian Kaddid meat: Experimental kinetics, modeling and quality, Food Bioprocess Tech. **5** (2012) 1882–1895.

[4] F.C. Schmidt, B.A.M. Carciofi, J.B. Laurindo, Salting operational diagrams for chicken breast cuts: hydration–dehydration, J. Food Eng. **88** (2008) 36–44.

[5] F.C. Schmidt, B.A.M. Carciofi, J.B. Laurindo, Application of diffusive and empirical models to hydration, dehydration, and salt gain during osmotic treatment of chicken breast cuts, J. Food Eng. **91** (2009) 553–559.

[6] A.R.F. Oliveira, L. Ilincanu, Rehydration of dried plant tissue: basic concepts and mathematical modeling, In: A.R.F. Oliveira, J.C. Oliveira (Eds.), Processing Foods, Quality, Optimization and Process Assessment, CRC Press, London, 1999.

[7] S.E. Cunningham, W.A.M. McMinn, T.R.A. Magee, P.S. Richardson, Experimental Study of Rehydration Kinetics of Potato Cylinders, Food Bioprod. Process. **86** (2008) 15.

[8] A.H. Weerts, D.R. Martin, G. Lian, J.R. Melrose, Modelling the hydration of foodstuffs, Simulation Modelling Practice and Theory **13** (2005) 119–128.

[9] M.K. Krokida, D. Marinos-Kouris, Rehydration kinetics of dehydrated products, J. Food Eng. **57** (2003) 1–7.

[10] P.P. Lewicki, A. Lukaszuk, Effect of osmotic dewatering on rheological properties of apple subjected to convective drying, J. Food Eng. **45** (2000) 119–126.

[11] S.K. Jain, R.C. Verma, L.K. Murdia, H.K. Jain, Optimization of process parametars for osmotic dehydration of papaya cubes, J. Food Sci. Techn. **48** (2011) 211–217.

[12] P. Gracia-Segovia, C. Mognetti, A. Andres-Bello, J. Martinez-Monzo, Osmotic dehydration of Aloe vera (Aloe barbadensis Miller). J. Food Eng. **97** (2010) 154–160.

[13] T. Tsironi, I. Salapa, P. Taouki, Shelf life modeling of osmotically treated chilled gilthead soya beam fillets, Innov. Food Sci. Emerg. Technol. **10** (2009) 23–31.

[14] N.K. Rastogi, K.S.M.S. Raghavarao, K. Niranjan, D. Knorr, Recent developments in osmotic dehydration: Methods to enhance mass transfer, Trends Food Sci. Tech. **13** (2002) 48–59.

[15] M. Peleg, An empirical model for the description of moisture sorption curves, J. Food Sci. **53** (1988) 1216––1219.

[16] M.F. Machado, F.A.R. Oliveira, L.M. Cunha, Effect of milk fat and total solids concentration on the kinetics of moisture uptake by ready-to-eat breakfast cereal, Int. J. Food Sci. Technol. **34** (1999) 47–57.

[17] E. Azuara, C.J. Beristain, H.S. Garcia, Development of a mathematical model to predict kinetics of osmotic dehydration, J. Food Sci. Technol. **29**(1992) 239–242.

[18] O. Corzo, N. Bracho, J. Rodriguez, Comparison of Peleg and Azuara et al. models in the modeling mass transfer during pile salting of goat sheets, LWT-Food Sci. Technol. **46** (2012) 448–452.

[19] O. Corzo, N. Bracho, J. Rodriguez, Pile salting kinetics of goat sheets using Zugarramurdi and Lupin's model, J. Food Process. Pres., 2012, doi:10.1111/j.1745--4549.2012.00695.x, 2012.

[20] N. Sanjuan, J.A. Carcel, G. Clemente, A. Mulet, Modelling of the rehydration process of brocolli florets, Eur. Food Res. Technol. **212** (2001) 449–453.

[21] S. Simal, A. Femenia, P. Llull, C. Rossello, Dehydration of aloe vera: simulation of drying curves and evaluation of functional properties, J. Food Eng. **43** (2000) 109–114.

[22] H. Feng, J. Tang, R.P. Cavalieri, O.A. Plumb, Heat and mass transport in microwave drying of porous materials in a spouted bed. AIChE J. **47** (2001) 1499–1512.

[23] H. Ni, A.K. Datta, K.E. Torrance, Moisture transport in intensive microwave heating of biomaterials: a multiphase porous media model, Int.J. Heat Mass Tran. **42** (1999) 1501–1512.

[24] D. Sauvant, J.-M. Perez, G. Tran, Tables de composition et de valeur nutritive des matières premières destinées aux animaux d'élevage: Porcs, volailles, bovins, ovins, caprins, lapins, chevaux, poissons, 2ème édition revue et corrigée. INRA Editions, Versailles, 2004.

[25] N.M. Mišljenović, G.B. Koprivica, L.L. Pezo, LJ.B. Lević, B.LJ. Ćurčić, V. S. Filipović, M. R. Nićetin, Optimization of the osmotic dehydration of carrot cubes in sugar beet molasses, Therm. Sci. **16** (2012) 43–52.

[26] M. Medina-Vivanco, P.J. Sobral, M.D. Hubinger, Osmotic dehydration of tilapia fillets in limited volume of ternary solutions, Chem. Eng. J. **86** (2002) 199–205.

[27] AOAC, Official methods of analysis, 15th ed., Arlington, VA, Association of Official Analytical Chemists, Washington, DC, 1990.

[28] J. Crank, The mathematics of diffusion, 2nd ed., Clarendon, Oxford, 1975.

[29] N.K. Rastogi, K.S.M.S. Raghavarao, Water and solute diffusion coefficients of carrot as a function of temperature and concentration during osmotic dehydration, J. Food Eng. **34** (1997) 429–440.

[30] A. Zugarramurdi, H.M. Lupin, Amodel to explain observed behavior on fish salting, J. Food Sci. **45** (1980) 1305–1311.

[31] S. Barrett, Doing the DRIs: a no-nonsense guide to the nation's new nutritional yardsticks-Dietary Reference Intakes (http://www.findarticles.com/p/articles/ /mi_m0GCU/is_n6_v14/ai_20152543-47k.htm), 1997.

[32] Anon, The Development of the Dietary Reference Intakes. Health Canada. Her Majesty the Queen in Right of Canada Cat. (H44-47/2003E-HTML ISBN 0-662-34956-3) (http://www.hc-sc.gc.ca/fn-an/nutrition/reference/dri_dev-elab_anref-eng.php), 2003.

[33] B. Filipčev, Nutrition profile, antioxidative potential and sensory quality of bread supplemented with sugar beet molasses (in Serbian), , Faculty of Technology, Novi Sad, 2009.

[34] P.P. Lewicki, A. Lenart, Osmotic dehydration of fruits and vegetables, in: A.S. Mujumdar (Ed.), Handbook of industrial drying, 3rd ed., Taylor & Francis Group, LLC, 2006, pp. 665–688.

[35] M.R. Khoyi, J. Hesari, Osmotic dehydration kinetics of apricot using sucrose solution, J. Food Eng. **78** (2007) 1355–1360.

[36] G.B. Koprivica, L.L. Pezo, B.L. Ćurčić, LJ.B. Lević, D.Z. Šuput, Optimization of osmotic dehydration of apples in sugar beet molasses, J. Food Process. Pres., doi: 10.1111/jfpp.12133, 2013.

[37] S. Mujaffar, C. Sankat, The mathematical modeling of the osmotic dehydration of shark fillets at different brine temperatures, Int. J. Food Sci. Techn. **40** (2005) 1––12.

[38] A. Costa-Corredor, I. Muñoz, J. Arnau, P. Gou, Ion uptakes and diffusivities in pork meat brine-salted with NaCl and K-lactate. LWT-Food Sci. Technol. **43** (2010) 1226–1233.

[39] C.L. Hansen, F. Van der Berg, S. Ringgaard, H. Stødkilde-Jørgensen, A.H. Karlsson, Diffusion of NaCl in meat studied by 1H and 23Na magnetic resonance imaging, Meat Sci. **80** (2008) 851–856.

[40] C. Vestergaard, J. Risum, J. Adler-Nissen, Na-MRI quantification of sodium and water mobility in pork during brine curing, Meat Sci. **69** (2005) 663–672.

[41] N. Graiver, A. Pinotti, A. Califano, N. Zaritzky, Diffusion of sodium chloride in pork tissue, J. Food Eng. **77** (2006) 910–918.

[42] T.M. Guiheneuf, S.J. Gibbs, L.D. Hall, Measurement of the inter-diffusion of sodium ions during pork brining by one-dimensional Na-23 magnetic resonance imaging (MRI), J. Food Eng. **31** (1997) 457−471.

[43] A.S. Pajonk, R. Saurel, J. Andrieu, Experimental study and modeling of effective NaCl diffusion coefficients values during Emmental cheese brining, J. Food Eng. **60** (2003) 307–313.

IZVOD

UTICAJI TEMPERATURE I VREMENA NA DIFUZIVNOST VODE I MINERALA TOKOM REHIDRATACIJE OSMOTSKI TRETIRANOG SVINJSKOG MESA

Danijela Z. Šuput[1], Vera L. Lazić[1], Lato L. Pezo[2], Biljana Lj. Lončar[1], Vladimir S. Filipović[1], Milica R. Nićetin[1], Violeta Knežević[1]

[1]*Univerzitet u Novom Sadu, Tehnološki fakultet, 21000 Novi Sad, Srbija*
[2]*Univerzitet u Beogradu, Institut za opštu i fizičku hemiju, 11000 Beograd, Srbija*

(Naučni rad)

Cilj ovog rada bio je da se ispitaju promene u osmotski tretiranom svinjskom mesu koje nastaju tokom procesa rehidratacije. Uzorci mesa su bili podvrgnuti osmotskom tretmanu u rastvoru melase šećerne repe, na temperaturi od 23±2 °C, 5 h. Nakon osmotskog tretmana, uzorci mesa su rehidrirani na konstantnoj temperaturi (20–40 °C) pri različitim vremenima potapanja (15–60 min) u destilovanoj vodi. Metoda odzivnih površina je korišćena za predviđanje efektivnog koeficijenta difuzije vode, i minerala, na određenoj temperature, tokom procesa rehidratacije. Numeričko rešavanje Fikovog zakona (Fick) o prenosu mase, pri nestacionarnim uslovima, za idealnu kocku je korišćeno za izračunavanje efektivnog koeficijenta difuzije vode, saharoze i minerala (Na, K, Ca and Mg). Cuguramendijev (Zugarramurdi) i Lupinov (Lupin) model je korišćen za predviđanje ravnotežnih uslova i pokazalo se da je taj model veoma pogodan za izračunavanje gubitka vlage i priraštaja suve materije tokom rehidratacije. Dobijena efektivna difuzivnost ($m^2 \cdot s^{-1}$)je bila između $8{,}35\times10^{-10}$ i $9{,}11\times10^{-10}$ za vlagu, $6{,}30\times10^{-10}$ i $6{,}94\times10^{-10}$ za Na, $5{,}73\times10^{-10}$ i $7{,}46\times10^{-10}$ za K, $4{,}43\times10^{-10}$ i $6{,}25\times10^{-10}$ za Ca, $5{,}35\times10^{-10}$ i 6.25×10^{-10} za Mg, $4{,}67\times10^{-10}$ i $6{,}78\times10^{-10}$ za Cu, $4{,}68\times10^{-10}$ i 5.33×10^{-10} za Fe, 4.21×10^{-10} i 5.04×10^{-10} za Zn i 5.44×10^{-10} i 7.16×10^{-10} za Mn. Korišćenjem ovde razvijenih matematičkih modela dobijaju se bezdimenzionalne vrednosti priraštaja vlage i gubitaka suve materije, sa tačnošću izraženom preko koeficijenata determinacije (r^2), za x_w, x_{Na}, x_K, x_{Ca}, x_{Mg}, x_{Cu}, x_{Fe}, x_{Zn}, i x_{Mn}: 0,977; 0,968; 0,999; 0,929; 0,931; 0,976; 0,931; 0,976 i 0,943, redom. Širok opseg procesnih promenljivih veličina razmatranih u formiranju ovih modela, kao i njihova laka implementacija u tabelarnim proračunima, čini ove modele veoma praktičnim za projektovanje i kontrolu procesa.

Ključne reči: Osmotski tretman • Rehidratacija • Melasa šećerne repe • Svinjsko meso • Koeficijent difuzije • Minerali

Optimization of β-galactosidase production from lactic acid bacteria

Milica Carević[1], Maja Vukašinović-Sekulić[1], Sanja Grbavčić[2], Marija Stojanović[1], Mladen Mihailović[1], Aleksandra Dimitrijević[3], Dejan Bezbradica[1]

[1]*Department of Biochemical Engineering and Biotechnology, Faculty of Technology and Metallurgy, University of Belgrade, Belgrade, Serbia*
[2]*Innovation center, Faculty of Technology and Metallurgy, University of Belgrade, Belgrade, Serbia*
[3]*Department of Biochemistry, Faculty of Chemistry, University of Belgrade, Belgrade, Serbia*

Abstract

β-galactosidase, commonly known as lactase, represents commercially important enzyme that is prevalently used for lactose hydrolysis in milk and whey. To the date, it has been isolated from various sources. In this study different strains of lactic acid bacteria were assessed for their β-galactosidase productivity, and *Lactobacillus acidophilus* ATCC 4356 resulted with the highest production potential. Thereafter, optimal conditions for accomplishing high yields of β-galactosidase activity were determined. Maximal specific activity (1.01 IU mL^{-1}) was accomplished after 2 days shake flask culture fermentation (150 rpm) at 37 °C, with modified Man Rogosa Sharpe culture broth using lactose (2.5%) as sole carbon source. Finally, in order to intensify release of intracellular β-galactosidase different mechanical and chemical methods were conducted. Nevertheless, vortexing with quartz sand (150 μm) as abrasive was proven to be the most efficient method of cell disruption. The optimum temperature of obtained β-galactosidase was 45 °C and the optimum range pH 6.5–7.5.

Keywords: *Lactobacillus acidophilus*, β-galactosidase, production, disruption, optimization.

Available online at the Journal website: http://www.ache.org.rs/HI/

SCIENTIFIC PAPER

UDC 577.15:579.6:66

Hem. Ind. **69** (3) 305–312 (2015)

doi: 10.2298/HEMIND140303044C

β-Galactosidase (β-D-galactoside galactohydrolases, EC 3.2.1.23) is an enzyme that catalyzes the cleavage of terminal galactosyl groups from the non-reducing ends of different galactosides. The enzyme is ubiquitous in nature, and can be derived from various sources such as plants, animal organs and microorganisms. In the view of easy production of highly active and stable enzymes, microorganisms are the sources of choice. Nowadays, β-galactosidases are extensively being used in food and pharmaceutical industries due to their capability to hydrolyse lactose, the most abundant sugar in milk and its by-products. This enables alleviation of lactose intolerance problem, prevalent in high share of the human population, and thus broadens consumption of these products [1,2]. It also plays an important role in diminishing some technological difficulties associated with lactose application in food industry such as low solubility, easy crystallization and lack of sweetness [2–4]. In addition, sensorial features of dairy products are improved by disabling lactose strong tendency to absorb flavors and odors [2,5]. Another broad field of β-galactosidase utilization includes the treatments of wastewaters from dairy industries. Namely, disposal of whey and whey permeates causes huge problems in the environment, owing to the low lactose biodegradability. Hence, hydrolyzed whey lactose provides solution for the problem of pollution [5–7]. On the other hand, under specific conditions such as high lactose concentration, low water activity, and high temperatures, β-galactosidases can catalyze reaction of galactosyde synthesis [8,9]. Interest in this aspect of β-galactosidase utilization has been growing rapidly, especially in the field of galacto-oligosaccharides (GOS) production due to their high prebiotic activity and potential positive impacts on human health [8–10].

Additionally, amongst numerous available microbial sources (yeasts, molds and bacteria) lactic acid bacteria strains attract great interest [10–12]. They seem to be the preferable option with respect to their GRAS (generally regarded as safe) status, which provides unhampered usage of their enzymes without any profuse and expensive purification [11,12]. β-Galactosidase derived from lactic acid bacteria (LAB) is found to be a neutral enzyme, suitable for sweet whey and milk lactose hydrolysis as well as GOS production. LAB represents a diverse group of widely applicable industrial microorganisms owing to their GRAS status [11,12]. Although they are already used in large scale lactic acid production, their full potential in the enzyme, predominantly β-galactosidase, commercial production is yet to be achieved. So far, most exploited strains are *Bifidobacterium* species and *Streptococcus thermophiles*, and

Correspondence: D. Bezbradica, Faculty of Technology and Metallurgy, University of Belgrade, Karnegijeva 4, 11000 Belgrade, Serbia.
E-mail: dbez@tmf.bg.ac.rs
Paper received: 3 March, 2014
Paper accepted: 8 May, 2014

only a few β-galactosidases from *Lactobacilus* sp. have been characterized [1,2,11,12].

The aim of this study was to assure the production of highly active β-galactosidase from LAB. In the first part of experiments potential highest activity producer among available LAB strains was selected. In the next experimental phase focus was on identifying the optimal culture conditions crucial for maximizing the β-galactosidase production such as fermentation time, carbon source and its concentration. In order to achieve satisfactory β-galactosidase exploitation, different cell disruption methods, chemical or mechanical, were investigated. As pointed above, LAB enzymes do not have to be subjected to extensive purification procedures, and can be straightaway used as a crude cell-free extracts in different reactions, thus their characterization (pH and temperature optimum) in reaction with *o*-nitrophenol-β-D-galactopyranoside was performed.

EXPERIMENTAL

Materials

In this study, several lactic acid bacteria (*Lactobacillus acidophilus* ATCC 4356, *Lb. rhamnosus* ATCC 7469, *Lb. reuteri* ATCC 23271, *Lb. helveticus* ATCC 15009, *Lb. delbrueckii* subsp. *bulgaricus* ATCC 11842 and *Streptococcus termophilus* S3) obtained from the American Type Culture Collection (ATCC, Rockville, USA) were screened for β-galactosidase production. Chemicals used for cultivation and fermentation purposes were purchased from Torlak Institute of Immunology and Virology (Belgrade, Serbia). Other chemicals were of analytical grade and obtained from Sigma Aldrich (St. Louis, USA) unless stated otherwise.

Microorganisms and fermentation

Lactic acid bacteria (LAB) strains used in this experiment were maintained at –20 °C in sterile vials in Man Rogosa Sharpe (MRS) broth medium containing 50% (*V*/*V*) glycerol as a cryoprotective agent. The culture activation and propagation was conducted by three successive transfers every 24 h into MRS broth under microaerophilic conditions at 37 °C.

Fermentations were performed as batch cultures using modified MRS broth (peptone, 10 g L^{-1}; meat extract, 10 g L^{-1}; yeast extract 5 g L^{-1}; lactose, 20 g L^{-1}; di-potassium hydrogen phosphate, 2 g L^{-1}; tri-ammonium citrate, 2 g L^{-1}; sodium acetate, 5 g L^{-1}; magnesium sulfate, 0.2 g L^{-1}; manganese sulfate, 0.04 g L^{-1}; Tween® 80, 1 mL L^{-1}, distilled water, 1 L) under microaerophilic conditions at 37 °C.

First set of experiments was carried out in order to screen for best β-galactosidase producer, and the next ones to optimize fermentation parameters such as incubation period, carbon source and its preferable concentration, as described later.

Optimization of fermentation

Lactobacillus acidophilus ATCC 4356, a homofermentative L-(+)-lactic acid bacteria strain, chosen as highest activity β-galactosidase producer, was used for further optimization. In order to define optimum fermentation time, fermentation was performed under previously defined conditions for four days. Each day, samples for monitoring bacterial cell concentration and enzyme production, were taken and analyzed. For estimation of bacterial cell concentration plate counting of CFU on MRS agar was used.

Afterwards, modifications of culture medium used for fermentation were introduced. Different carbon sources (overall concentration of 2%) such as glucose, galactose, lactose and their mixtures were applied. Finally, the optimal concentration of the best carbon source was determined. The range of the sugar concentration (1–4%) was chosen on the basis of literature survey.

Extraction of intracellular β-galactosidase

In order to obtain β-galactosidase from *Lb. acidophilus*, bearing in mind its intracellular location, microbial cells were firstly harvested by centrifugation at 12000*g* for 10 min. Then, after being washed twice with 0.1 M sodium phosphate buffer (pH 6.8), they were re-suspended in the same buffer. Finally, the cell suspension was subjected to different chemical and mechanical methods of cell disruption.

Cell disruption with mechanical methods

Effectiveness of several mechanical cell disruption methods was tested. One group of methods included usage of abrasives. In the first experiment, the cell suspension was ground with glass beads for 10 min, using mortar and pestle (GGB). Then, in the second, the mixture of obtained cell suspension and glass beads (30 μm) was stirred vigorously on vortex for 10 min with occasional cooling in the ice bath (VGB). Finally, the same method was used with other kind of abrasive – quartz sand (150 μm), under the same conditions (VS). During the further cell disruption optimization, by vortexing mixture of abrasives and cell suspension, three batches of quartz sand (53, 150 and 350 μm) were used. Activity of released β-galactosidase was measured after removing cell debris by centrifugation (3000*g* for 10 min).

A second group of mechanical methods were ultrasonication methods. In the first case, the cell suspension was treated for 5 min in ultrasonication bath (Ei Niš-Ro-VEP, Niš, Serbia) with intermittent cooling in 5 cycles (US), while in second, the cell suspension was frozen, and then thawed in ultrasonication bath

(FT/US), under the same conditions. The disrupted cell suspension was centrifuged (3000*g* for 10 min) and enzyme activity was assayed in obtained cell extract.

Extraction with solvents

The cell suspension was treated with 2 % chloroform (CH) and 80% ethanol (ET). After being incubated at 37 °C for 9 and 20 h, respectively, mixtures were centrifuged (3000*g* for 10 min), and the enzymatic activity of released β-galactosidase in supernatants was determined.

β-Galactosidase assays

β-Galactosidase activity was determined using 10 mM *o*-nitrophenol-β-D-galactopyranoside (*o*-NPG) in 0.1 M sodium phosphate buffer (pH 6.8) as a substrate. The reaction course was monitored for 2 min, by measuring the concentration of released *o*-nitrophenol (*o*-NP) spectrophotometrically at 410 nm. One unit (IU) is defined as the amount of the enzyme that catalyzes the liberation of 1 μmol *o*-NP per min under the specified assay conditions. The molar extinction coefficient for *o*-NP was found to be 1357 $dm^3\ mol^{-1}\ cm^{-1}$.

The amount of proteins in the crude cell-free extracts was determined using Bradford assay with bovine serum albumin as the standard [13].

Effects of temperature and pH on enzymatic activity

The effect of temperature on β-galactosidase activity was examined by incubation of the enzyme and the substrate (10 mM *o*-NPG in 0.1 M sodium phosphate buffer pH 6.8) at temperatures ranging from 30 to 60 °C. Further, the effect of pH was determined on 45 °C by varying buffers used for substrate preparation. Sodium acetate buffer (pH 4.0–5.5) and sodium phosphate buffer (pH 6–8) were used for this purpose. The enzyme activity measurement was conducted in the previously described manner.

RESULTS AND DISCUSSION

Screening for β-galactosidase producing microorganisms

In this paper, several lactic acid bacteria strains (listed in Table 1) were tested for capability of high yield β-galactosidase production. Fermentation was carried out in shake flask on a rotary shaker (150 rpm), using modified MRS broth as a medium for two days. Other fermentation parameters such as temperature (37 °C), initial pH (6.5) and inoculum size (5%) were fixed and chosen on the basis of literature survey.

The results of these experiments have shown that *Lb. acidophilus* (0.671 IU mL^{-1}) is the most efficient β-galactosidase activity producer. In addition, significantly active β-galactosidases were extracted from *Lb. reuteri* (0.420 IU mL^{-1}) and *Lb. helveticus* (0.344 IU mL^{-1}), while *Lb. rhamnosus* and *Lb. bulgaricus* showed insignificant β-galactosidase productivity (Table 1). Consequently, in the later stages of this study, *Lb. acidophilus* was used for further optimization of fermentation conditions with the aim of accomplishing greater yields of β-galactosidase.

Table 1. Production of β-galactosidase using LAB

Lactic acid bacteria strain	Activity, IU mL^{-1}
Lb. acidophilus ATCC 4356	0.671
Lb. rhamnosus ATCC 7469	0
Lb. reuteri ATCC 23271	0.420
Lb. helveticus ATCC 15009	0.344
Lb. delbrueckii subsp. *bulgaricus* ATCC 11842	0.011

Time course of β-galactosidase production

In order to define an optimum fermentation time for maximum β-galactosidase production, the kinetics of β-galactosidase production, as well as cell concentration of *Lb. acidophilus* through time, were studied (Fig. 1). For the purpose of this experiment, fermentation was carried out for 4 days under the previously defined conditions. As shown in Fig. 1, the enzyme activity production exhibited a similar trend as the cell concentration curve, and increased gradually as the fermentation started, reaching the maximum activity (0.718 IU mL^{-1}) after two days. Thereafter, a continuous decrease in the enzyme activity was observed. This is presumably closely related to the fact that the culture has reached the stationary phase after two days. Similar trends, with a maximum production of the enzyme at the beginning of the stationary phase, have previously been reported on production of β-galactosidase from various microorganisms [14,15]. Most probably, such a behavior of *Lb. acidophilus* could be explained by previous findings that during stationary phase, changes in cell wall structure and composition occur, which leads to hampered intracellular enzyme extraction [16]. Besides, reduced lactose concentration and larger amounts of liberated glucose, as a product of lactose hydrolysis, present in the medium during this phase were believed to cause repression of β-galactosidase production. And finally, intracellular enzyme instability is increased by greater amount of produced proteases [15,17].

Simultaneously with intracellular enzyme activity measurements, samples of fermentation medium were screened for implied extracellular activity. It has been previously reported that some LAB, namely *Lb. brevis* and *Lb. plantarum,* excrete β-galactosidase into the fermentation medium by alleged cell autolysis [18]. However, the extracellular activity was not observed in our experiments (results not shown).

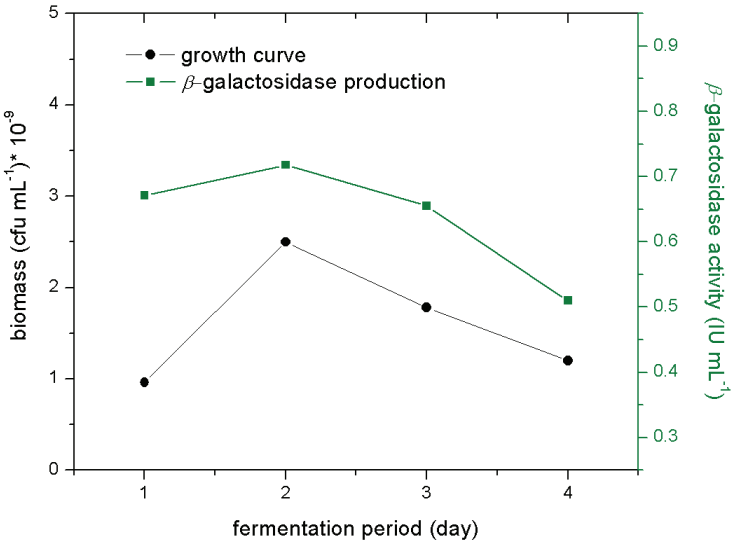

Figure 1. Time course of β-galactosidase production.

Optimization of carbon sources

Several studies reported the major influence of the carbon sources on the β-galactosidase production by various microorganisms. It was concluded that the role of carbon source in this biosynthesis may vary greatly depending upon the used microorganisms [19,20]. Literature data concerning carbon source regulation within *Lb. acidophilus* are rather scarce [20]. Therefore, in this study, different carbohydrates (glucose, galactose, lactose and their mixtures) were tested in order to select the best carbon source. Initial concentrations of above mentioned carbohydrates (2%) corresponded to the one used in previous experiments.

Results presented in Fig. 2 undoubtedly indicate that lactose tends to promote high β-galactosidase activities, since three mediums containing lactose showed considerable enzymatic activity production. Lactose, as sole source, proved to be the inducer of the maximum β-galactosidase production, while lactose mixtures with glucose and galactose displayed moderate levels of β-galactosidase activity induction. Our results were compatible with those reported by Hsu *et al.* claiming that highest β-galactosidase activity was detected in cultures containing lactose as the sole carbon source, followed by galactose and the lowest activity with glucose as the carbon source [19]. These results could be explained on the basis of catabolic repression with intracellular accumulation of glucose by-products, and the fact that bacteria primarily consume simpler sugars, thus does not induce significant β-galactosidase production [17].

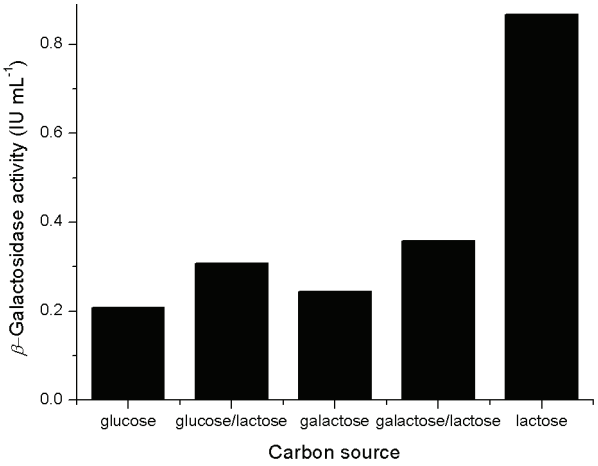

Figure 2. Effect of different carbon sources on β-galactosidase production.

Besides the nature of carbon sources in the culture media, the amount of it proved to be equally important from the aspect of the β-galactosidase production yield [20,17]. Different lactose concentrations (1.0–3.5% *w*/*V*) were used as substrates for β-galactosidase production. The β-galactosidase activity increased progressively with increscent initial lactose concentrations up to 2.5% (Fig. 3). Further growth of the lactose content resulted in the reduction of β-galactosidase activity, which implies that together with the rise of lactose content, there is an increase in degradation products concentrations leading to repression of inducible β-galactosidase production. Similar phenomenon was observed by Murad *et al*. who investigated *Lb. reuteri* and *St. termophilus* [17]. Their results showed that enzyme activity increased with the increase of lactose concentration (up to 6%), reaching 2.54 and 2.59 IU mL^{-1}, respectively. Further increase of lactose concentration up to 10% decreased the *Lb. reuteri* enzyme production dramatically, while it increased the *St. thermophilus* enzyme production (3.01 IU mL^{-1}). These results suggest that there is clear pattern, regardless of microorganism used, in β-galactosidase production.

β-Galactosidase is lactose inducible enzyme, and its activity yield represents a compromise between lactose induction and intracellular glucose repression.

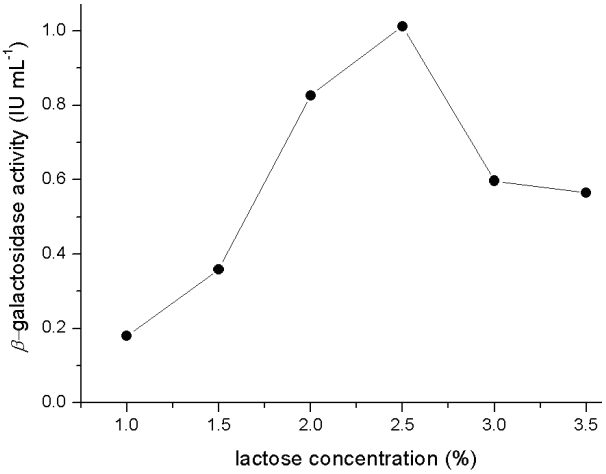

Figure 3. Effect of lactose concentration on β-galactosidase production.

Extraction of intracellular β-galactosidase activity

Since the results of preliminary experiments had shown that significant β-galactosidase activity could be detected only inside the cell, following experimental series was focused on optimization of the cell disruption process. Various methods can be used to release intracellular products depending on their location, stability and purpose [16]. In previous studies, a wide range of mechanical, physical, chemical, enzymatic and combined methods have been applied for β-galactosidase extraction from various microorganisms [21–24]. Nevertheless, systematic study comprising a wide selection of extraction methods and comparing their effects on released activity has not yet been undertaken. Therefore, throughout this study, the effects of different mechanical (vortexing with abrasives, grinding with abrasives, ultrasonication) and chemical (ethanol or chloroform extraction) methods on released β-galactosidase activity were compared. As reagents for chemical permeabilization ethanol and chloroform were used, and in both experiments negligible β-galactosidase activity was observed (Fig. 4A). Use of ethanol and chloroform, as well as several other organic solvents has been widely applied in permeabilization of yeast and some bacterial cells for production of biomass with increased galactosidase activity [22,25]. Nevertheless, reports of LAB cell disruption and release of intracellular β-galactosidase activity are very scarce. Significant yield was achieved only in study by Choonia and Lele when ethanol (10%, *w*/*V*) and chloroform (7.5%, *w*/*V*) were used as plasmolysis solvents, but even in that case mechanical methods proved to be more efficient [24]. Generally, it is plausible that low extracellular yield observed in our study is due to the fact that Gram-positive bacteria, *Lb. acidophilus*, has high portion of peptidoglycan layer, which imparts rigidity to cell wall and obstructs the release of intracellular biomolecules, such as β-galactosidase [16,26].

Mechanical methods, on the other hand, widely investigated and used in bacterial β-galactosidase production, are proved to be more efficient than chemical methods in this study (Fig. 4A). Amongst mechanical methods the most efficient was cell disruption by abrasives. Two abrasive materials were used, and quartz sand was shown to be far more effective (2.1 IU mL^{-1}) comparing to glass beads (0.678 IU mL^{-1}). Also, different types of mechanical force were applied to

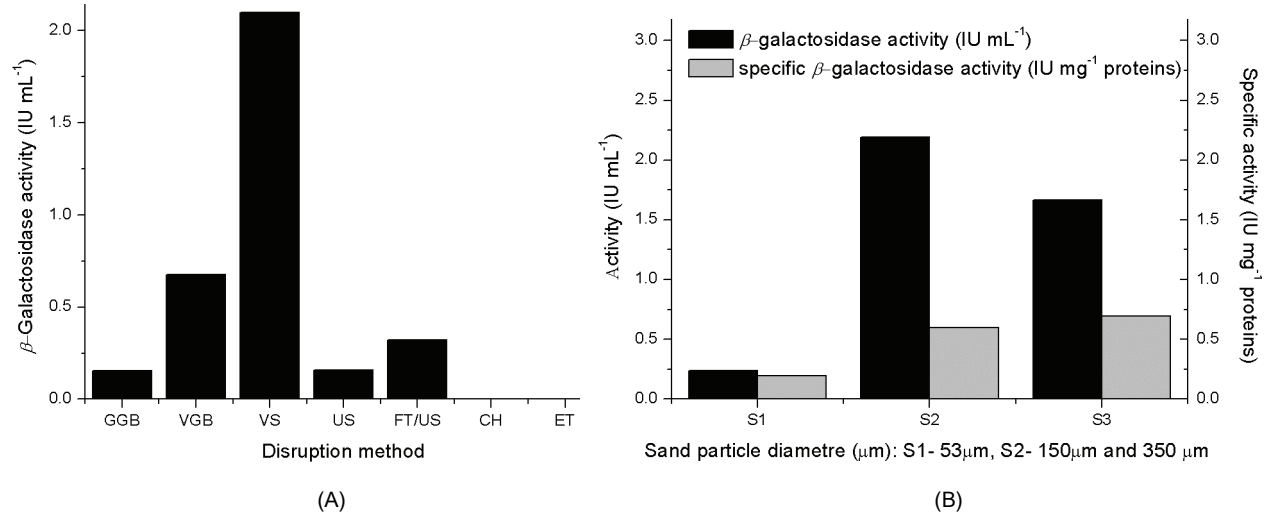

Figure 4. Effect of different cell disruption methods on released β-galactosidase activity (A): VGB – vortexing with glass beads, SO – sonication, GGB – grinding with glass beads, FT/US – freezing-thawing/ultrasonication, VS – vortexing with quartz sand, CH – treatment with chloroform, ET – treatment with ethanol. Effect of different sand particle diameter on β-galactosidase activity (IU mL^{-1}) and specific β-galactosidase activity (IU mg^{-1} proteins) (B): S1 – 53 μm, S2 – 150 μm and S3 – 350 μm.

intensify friction between abrasives and biomass, and around 4 times higher β-galactosidase activity was obtained by means of vortexing cell suspension than by grinding.

Disruption methods which don't include use of abrasives were less effective, hence repeated freeze-thawing in ultrasonication bath released β-galactosidase activity of 0.322 IU mL^{-1}, while sole treatment in ultrasonication bath liberated activity of 0.157 IU mL^{-1}. Higher activity yields obtained using mechanical methods are in accordance with numerous studies indicating superiority of mechanical methods for intracellular enzyme isolation [16,24]. The main requirement for cell disruption methods is that they should be robust enough to disrupt cell envelopes efficiently, but at the same time gentle enough to preserve enzyme activity [15]. Therefore, poor results achieved by ultrasonication methods (Fig. 4A) can be explained by the fact that absorption of energy is intertwined with significant heat release and free radicals production, which can lead to lowering enzyme activity. Similar results were published by Bury *et al*. who investigated the effect of disruption methods on *Lb. delbrueckii* ssp. *bulgaricus* β-galactosidase production, finding that bead milling and high-pressure homogenization were comparable methods, while the sonication was the least effective [21]. Likewise, Dagbagli and Goksungur found sonication significantly less effective than glass beads treatment [15].

Since cell disruption with quartz sand gave the best results, further optimization was made by investigating the effect of abrasive particle size on activity yield. Three batches with different particle diameters (53, 150 and 350 μm) were tested under same conditions with vortexing method. Even though the best choice, regarded the obtained specific β-galactosidase activity (0.695 IU mg^{-1} proteins), would be the usage of 350 μm diameter quartz sand particles, differences in overall produced β-galactosidase activity were by far larger and favor usage of 150 μm diameter particles (Fig. 4B). Therefore, all further experiments were performed with 150 μm quartz sand particles.

Temperature and pH

β-Galactosidases characteristics can greatly vary depending on their source. Generally, they can be divided in two groups on the basis of their pH profiles: acidic β-galactosidases that originate from fungal sources and neutral β-galactosidases from yeasts and bacteria [1,2]. As expected, the optimum pH for obtained β-galactosidase from *Lb. acidophilus* is in the range between pH 6.5 and 7.5 (activity over 90% of maximum), with an optimum at pH 6.8 (Fig. 5). Similar neutral optimum pH ranges have been reported for several LAB species, including *Lb. acidophilus* [20].

These values correspond to ones of milk and sweet whey, making these enzymes highly applicable in the real industrial conditions. Yeast β-galactosidases exhibit rather low optimum operation temperatures and consequently are inappropriate for industrial usage due to the ease of contamination, hence LAB β-galactosidases seem to be more adequate choice. The optimum temperature of our obtained enzyme was found to be 45 °C. Literature data, however, showed no consistency on this matter. Nguyen *et al.* claimed that the optimum temperature for both lactose and *o*-NPG hydrolysis was 55 °C [27]. On the other hand, results published by Ismail *et al.* showed that temperature optimum is around 40 °C [20]. Keeping in mind all presented results in this study, it is clear that our enzyme represents a valuable tool in milk and sweet whey processing and potential GOS production.

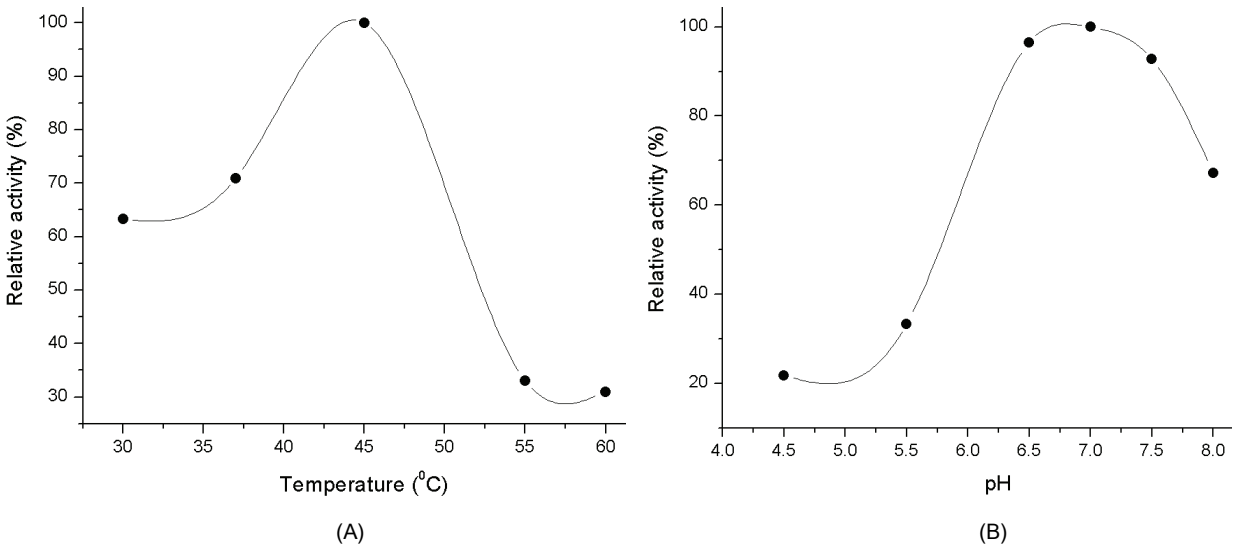

Figure 5. Effect of temperature (A) and pH (B) on relative β-galactosidase activity.

CONCLUSION

It was concluded that the highest biocatalytic potential was achieved by using *Lb. acidophilus*. In view of the greater efficiency of β-galactosidase exploitation, optimization of the relevant cultivation factors (fermentation time, carbon source and later lactose concentration) was conducted. Maximal enzyme activity was achieved by shake flask culture fermentation after 48 h. Culture medium yielding highest β-galactosidase activity comprised of modified MRS culture broth with 2.5% lactose. Accomplished β-galactosidase activities were significantly increased in continuance, by optimizing enzyme extraction method. Mechanical cell disruption, namely, vortexing with quartz sand of 150 μm diameter particles proved to be an optimal choice. Based on the results reported in this paper, obtained crude cell-free extract β-galactosidase from *Lb. acidophilus* has potential application in the food industry especially in the field of milk and sweet whey hydrolysis, as well as in GOS production.

Acknowledgements

This work was supported by Grant number III 46010 from The Ministry of the Education, Science and Technological Development, Republic of Serbia.

REFERENCES

[1] P.S. Panesar, S. Kumari, R. Panesar, Potential Applications of Immobilized β-Galactosidase in Food Processing Industries, Enzyme Res. **2010** (2010), doi: 10.4061/2010/473137.

[2] P.S. Panesar, R. Panesar, R.S. Singh, J.F. Kennedy, H. Kumar, Microbial production, immobilization and applications of β-D-galactosidase, J. Chem. Technol. Biot. **81** (2006) 530–543.

[3] D.C. Vieira, L.N. Lima, A.A. Mendes, W.S. Adriano, R.C. Giordano, R.L.C. Giordano, P.W. Tardioli, Hydrolysis of lactose in whole milk catalyzed by β-galactosidase from *Kluyveromyces fragilis* immobilized on chitosan-based matrix, Biochem. Eng. J. **81** (2013) 54–64.

[4] M. Ghosh, K.K. Pulicherla, V.P.B. Rekha, A. Vijayanand, K.R.S. Sambasiva Rao, Optimisation of process conditions for lactose hydrolysis in paneer whey with cold-active β-galactosidase from psychrophilic *Thalassospira frigidphilosprofundus*, Int. J Dairy Technol. **66** (2013) 256–263.

[5] Q. Husain, β Galactosidases and their potential applications: a review, Crit. Rev. Biotechnol. **30** (2010) 41–62.

[6] M.R. Kosseva, P.S. Panesar, G. Kaur, J.F. Kennedy, Use of immobilised biocatalysts in the processing of cheese whey, Int. J. Biol. Macromol. **45** (2009) 437–447.

[7] S. Sen, L. Ray, P. Chattopadhyay, Production, Purification, Immobilization, and Characterization of a Thermostable β-Galactosidase from *Aspergillus alliaceus*, Appl. Biochem. Biotech. **167** (2012) 1938–1953.

[8] D.P.M. Torres, M.P.F. Goncalves, J.A. Teixeira, L.R. Rodrigues, Galacto-Oligosaccharides: Production, Properties, Applications, and Significance as Prebiotics, Compr. Rev. Food Sci. F. **9** (2010) 438–454.

[9] R. Jovanovic-Malinovska, P. Fernandes, E. Winkelhausen, L. Fonseca, Galacto-oligosaccharides Synthesis from Lactose and Whey by β-Galactosidase Immobilized in PVA, Appl. Biochem. Biotech. **168** (2012) 1197–1211.

[10] B. Splechtna, T.H. Nguyen, M. Steinböck, K.D. Kulbe, W. Lorenz, D. Haltrich, Production of Prebiotic Galacto-Oligosaccharides from Lactose Using β-Galactosidases from *Lactobacillus reuteri*, J. Agric. Food Chem. **54** (2006) 4999−5006.

[11] C. Schwab, V. Lee, K.I. Sřrensen, M.G. Gänzle, Production of galactooligosaccharides and heterooligosaccharides with disrupted cell extracts and whole cells of lactic acid bacteria and bifidobacteria, Int. Dairy J. **21** (2011) 748–754.

[12] T. Vasiljevic, P. Jelen, Oligosaccharide production and proteolysis during lactose hydrolysis using crude cellular extracts from lactic acid bacteria, Lait **8** (2003) 453–467.

[13] M.M. Bradford, A rapid and sensitive method for the quantification of microgram quantities of protein utilizing the principle of protein dye binding, Anal. Biochem. **72** (1976) 248–254.

[14] F. Alves, F. Filho, J. Medeiros Burkert, S. Kalil, Maximization of β-Galactosidase Production: A Simultaneous Investigation of Agitation and Aeration Effects, Appl. Biochem. Biotech. **160** (2010) 1528–1539.

[15] S. Dagbagli, Y. Goksungur, Optimization of β-galactosidase production using *Kluyveromyces lactis* NRRL Y-8279 by response surface methodology, Electron. J. Biotechnol. **11** (2008).

[16] J. Geciova, D. Bury, P. Jelen, Methods for disruption of microbial cells for potential use in the dairy industry-a review, Int. Dairy J. **12** (2002) 541–553.

[17] H.A. Murad, R.I. Refaea, E.M. Aly, Utilization of UF-Permeate for Production of β-galactosidase by Lactic Acid Bacteria, Pol. J. Microbiol. **60** (2011) 139–144.

[18] G. Montanari, C. Zambonelli, L. Grazia, M. Benevelli, C. Chiavari, Release of β-galactosidase from Lactobacilli, Food. Technol. Biotechnol. **38** (2000) 129–133.

[19] C.A. Hsu, R.C. Yu, C.C. Chou, Production of β-galactosidase by Bifidobacteria as influenced by various culture conditions, Int. J. Food Microbiol. **104** (2005) 197–206.

[20] S.A.A. Ismail, Y. El-Mohamady, W.A. Helmy, R. Abou-Romia, A.M. Hashem, Cultural condition affecting the growth and production of a β-galactosidase by *Lactobacillus acidophilus* NRRL 4495, Aust. J. Basic Appl. Sci. **4** (2010) 5051–5058.

[21] D. Bury, P. Jelen, M. Kalab, Disruption of *Lactobacillus delbrueckii* ssp. *bulgaricus* 11842 cells for lactose hydrolysis in dairy products: a comparison of sonication, high-pressure homogenization and bead milling, Innov. Food Sci. Emerg. Technol. **2** (2001) 23–29.

[22] G.A. Somkuti, M.E. Dominiecki, D.H. Steinberg, Permeabilization of *Streptococcus thermophilus* and *Lactobacillus delbrueckii* subsp. *bulgaricus* with ethanol, Curr. Microbiol. **36** (1992) 202–206.

[23] M. Puri, S. Gupta, P. Pahuja, A. Kaur, J.R. Kanwar, J.F. Kennedy, Cell Disruption Optimization and Covalent Immobilization of β-D-Galactosidase from *Kluyveromyces marxianus* YW-1 for Lactose Hydrolysis in Milk, Appl. Biochem. Biotech. **160** (2010) 98–108.

[24] H.S. Choonia, S.S. Lele, Release of β-galactosidase from Indigenous *Lactobacillus acidophilus* by Ultrasonication: Process Optimization, Chem. Eng. Commun. **198** (2011) 668–677.

[25] Y. Numanoglu, S. Sungur, β-Galactosidase from *Kluyveromyces lactis* cell disruption and enzyme immobilization using a cellulose-gelatin carrier system, Process. Biochem. **39** (2004) 705–711.

[26] P. Jafarei, M.T. Ebrahimi, *Lactobacillus acidophilus* cell structure and application, Afr. J. Microbiol. Res. **5** (2011) 4033–4042.

[27] T.H. Nguyen, B. Splechtna, S. Krasteva, W. Kneifel, K.D. Kulbe, C. Divne, D. Haltrich, Characterization and molecular cloning of a heterodimeric β-galactosidase from the probiotic strain *Lactobacillus acidophilus* R22, FEMS Microbiol. Lett. **269** (2007) 136–144.

IZVOD

OPTIMIZACIJA PROIZVODNJE β-GALAKTOZIDAZE POMOĆU BAKTERIJA MLEČNE KISELINE

Milica Carević[1], Maja Vukašinović-Sekulić[1], Sanja Grbavčić[2], Marija Stojanović[1], Mladen Mihailović[1], Aleksandra Dimitrijević[3], Dejan Bezbradica[1]

[1]Katedra za biohemijsko inženjerstvo i biotehnologiju, Tehnološko–metalurški fakultet, Univerzitet u Beogradu, Beograd, Srbija
[2]Inovacioni centar, Tehnološko–metalurški fakultet, Univerzitet u Beogradu, Beograd, Srbija
[3]Katedra za biohemiju, Hemijski fakultet, Univerzitet u Beogradu, Studentski trg 12–16, 11000 Beograd, Srbija

(Naučni rad)

Enzim β-galaktozidaza, poznatija kao laktaza, predstavlja industrijski izuzetno važan enzim, koji ima primarnu ulogu u hidrolizi disaharida laktoze. Upotrebom ovog enzima u industriji mleka i mlečnih proizvoda dolazi do poboljšanja fizičkih i senzornih karakteristika proizvoda, kao i do povećanja svarljivosti proizvoda, a samim tim i prevazilaženja problema netolerancije na laktozu. Takođe, hidrolizom laktoze surutke, rešava se pitanje njenog ekološki prihvatljivog odlaganja. Sa druge strane, enzim pod kontrolisanim reakcionim uslovima može katalizovatii proces transgalaktozilacije, odnosno prenošenja galaktozil jedinica na druge šećere prisutne u sistemu (najčešće laktozu), pri čemu nastaju izuzetno važna funkcionalna jedinjenja galaktooligosaharidi. Enzim β-galaktozidaza može biti različitog porekla – biljnog, životinjskog ili mikrobnog. Međutim, najznačajniji među njima su mikrobni postupci proizvodnje, zbog lake fermentacije, velike brzine rasta i razmnožavanja ćelija, visokih prinosa, visoke aktivnosti, kao i stabilnosti enzima. Kao posledica velikog komercijalnog interesa za ovaj enzim, opisane su različite metode dobijanja i prečišćavanja dobijenih enzima iz različitih mikroorganizama. Poslednjih godina bakterije mlečne kiseline privlače sve više pažnje kao potencijalni izvori β-galaktozidaza najviše zahvaljujući svom statusu bezbednih za upotrebu u prehrambenoj i farmaceutskoj indistriji, čime se omogućava neometano korišćenje enzima bez primene komplikovanih metoda prečišćavanja. U ovom radu ispitana je mogućnost proizvodnje β-galaktozidaza pomoću nekoliko vrsta bakterija mlečne kiseline. Kao najbolji producent među ispitanim bakterijama pokazala se bakterija *Lactobacillus acidophilus*. Najveća aktivnost β-galaktozidaze, dobijena je mikroaerofilnom fermentacijom u modifikovanoj komercijalnoj MRS podlozi, sa 2,5% laktoze kao jedinim izvorom ugljenika. Fermentacija je vršena na tresilici (150 rpm) u trajanju od 48 h i na temperaturi od 37 °C. Kako je enzim intracelularan, u cilju razaranja ćelija i oslobađanja enzima, primenjeno je više različitih fizičkih i hemijskih metoda, a daleko najboljom pokazala se metoda vorteksiranja sa kvarcnim peskom (150 μm) kao abrazivnim sredstvom. Ovako dobijen enzim pokazao je maksimalnu aktivnost pri temperaturi od 45 °C i pH u opsegu 6.5–7.5.

Ključne reči: *Lactobacillus acidophilus* • β-Galaktozidaza • Proizvodnja • Razaranje • Optimizacija

Акумулација метала и толеранција одабраних биљних врста на јаловишту азбеста (Страгари)

Снежана Р. Бранковић[1], Радмила М. Глишић[1], Вера Р. Ђекић[2], Марија А. Марин[3]

[1]*Универзитет у Крагујевцу, Природно–математички факултет, Институт за биологију и екологију, Крагујевац, Србија*
[2]*Истраживачко-развојни Центар, Центар за стрна жита, Крагујевац, Србија*
[3]*Универзитет у Београду, Биолошки факултет, Београд, Србија*

Извод

Циљ овог рада био је да се одреди концентрација 11 метала у земљишту и одабраним врстама биљака на јаловишту азбеста код Страгара, као и да се утврди која врста показује најбољу акумулацију и толеранцију на испитиване метале. Садржај метала у биљкама био је различит, зависио је од биљне врсте и врсте метала. Концентрације Ni и Cr у истраживаном земљишту прелазиле су прописане ремедијационе вредности, као и максимално дозвољене концентрације ових метала у земљишту, а концентрације Cd и Co граничне вредности за дате метале у земљишту сагласно уредби и правилнику Републике Србије. Код врсте *Sanguisorba minor* утврђена је толеранција на више метала. Код врсте *Euphorbia cyparissias* биолошки апсорпциони коефицијенти били су већи од један за Zn и Cu, а код врста *Eryngium serbicum* и *Sanguisorba minor* већи од два за Cu.

Кључне речи: акумулација метала, толеранција, јаловиште азбеста, биљке.

Dostupno na Internetu sa adrese časopisa: http://www.ache.org.rs/HI/

НАУЧНИ РАД

УДК 504.5(497.11):58:54:679.867

Hem. Ind. **69** (3) 313–321 (2015)

doi: 10.2298/HEMIND131017045B

Земљиште представља смешу стена различитог минералног састава и хумуса (органске компоненте земљишта која представља биљне и животињске остатке минерализоване у различитом степену). На образовање земљишта утичу бројни фактори, при чему климатски фактори и матична стена од кога земљиште настаје имају пресудну улогу у педогенетским процесима. Минерални састав земљишта се непосредно наслеђује из материнске стене, или се формира трансформацијом у њему, уз пресудан утицај изворних минерала из супстрата. Геолошка подлога и на њој настала земљишта, као скуп еколошких фактора утичу на дивергенцију биљних облика и вегетацијских јединица. Поред хемијског састава геолошке подлоге, на вегетацију која се на њој развија значајан утицај имају физичка структура и квантитативан однос појединих елемената и њихових соли у земљишту.

Биолошки мониторинг подразумева примену живих организама као биоиндикатора промена у животној средини у простору и времену. Биоиндикатори су биљне заједнице, врсте или поједини делови биљака који могу да пруже информације о квалитету животне средине [1]. Поједина земљишта су природно или антропогено обогаћена тешким металима или другим полутантима, на њима се развијају специјализоване биљне врсте (генетички диференцирани хемоекотипови) које се биохемијско-физиолошким, морфо-анатомским адаптацијама, као и општим хабитусом, прилагођавају измењеним условима средине. Биљке представљају важну карику у кружењу елемената у природи, могу бити поуздан показатељ недостатка и/или сувишка појединих елемената. Захваљујући способности виших биљака да апсорбују метале и друге полутанте из земљишта, да их транспортују кроз свој организам и акумулирају, заснива се њихова примена у фиторемедијацији.

Село Котража код Страгара, у централном делу уже Србије, је локалитет серпентинске жице на коме је процесом метаморфозе настао серпентинисани азбест. У перидотитском масиву у непосредној близини Страгара налази се веће тектонизовано лежиште азбеста које је формирано у контакту са кредним седиментима, а на коме лежи велико јаловиште флотације азбеста (сл. 1) у виду његових свежих наслага [2,3]. Страгарачки азбест (хризотилски тип, „кожасти азбест“) је сребрнастоснежне боје и формуле $8MgO{\cdot}2SiO_2{\cdot}2H_2O$, а среће се у виду сочивастих тела и азбестних влакана која се међусобно густо преплићу, топи се на 1550 °C, није отпоран према киселинама, има велику адсорпциону моћ, и слаб је проводник топлоте, електрицитета и звука.

Експлоатација овог азбеста вршена је површинским копом у току четрдесет година, до обуста-

Преписка: С.Р. Бранковић, Универзитет у Крагујевцу, Природно–математички факултет, Институт за биологију и екологију, Радоја Домановића 12, 34000 Крагујевац, Србија.
Е-пошта: pavsnez@yahoo.co.uk
Рад примљен: 17. октобар, 2013
Рад прихваћен: 20. мај, 2014

Слика 1. Локалитет Котража, јаловиште азбеста.
Figure 1. Kotraža locality, asbestos tailings.

лања производње и затварања фабрике, тако да је надомак копа формирано јаловиште на коме су одлагане велике количине материјала насталог после процеса прераде азбеста.

Циљ овог рада био је да се одреде концентрације 11 метала у земљишту на поменутом јаловишту азбеста, као и у одабраним врстама биљака које на њему расту, и испита која од њих показује најбољу акумулацију испитиваних метала, односно толеранцију.

ЕКСПЕРИМЕНТАЛНИ ДЕО

Узорковање

Теренски рад, прикупљање и узорковање земљишта и биљног материјала за истраживање обављени су током вегетацијских сезона 2009–2011. године. Локалитет Котража је јако стрм и претежно го, избраздан дубоким јаругама и смештен у оквиру координата 74° 74’ 761’’ E, 48° 90’ 490’’ N, N експозиције и на 283–311 m надморске висине (очитано помоћу апарата GPS Garmin-etrex, vista HCx). Земљиште је сакупљано у близини кореновог система биљака на дубини од 1 до 10 cm, што одговара кореновој зони већине зељастих биљака и жбунастих форми [4]. Истраживање је рађено на четири биљне врсте: *Alyssum murale* Waldst. et Kit., *Eryngium serbicum* Pančić, *Euphorbia cyparissias* L. и *Sanguisorba minor* Scop. Аутори су се определили за ове врсте јер су литературни подаци показали да је врста *Alyssum murale* хиперакумулатор Ni [5]; врста *Eryngium serbicum* је ендемична биљка са малим ареалом распрострањења; док су врсте *Euphorbia cyparissias* и *Sanguisorba minor* еколошки широке врсте и постоји индиција да имају способност добре акумулације више метала. Одабране биљне врсте су по узорковању са поменутих локалитета идентификоване у лабораторији Института за биологију и екологију Природно-математичког факултета у Крагујевцу, уз помоћ стандардних кључева за детерминацију биљака: Jávorka и Csapody [6], Флора Републике Србије [7] и Флора Европе [8] и испиране дестилованом водом.

Методе анализе

На местима где су сакупљане проучаване биљке узиман је и узорак земљишта. Земљиште је након узорковања мешано, сушено на ваздуху до ваздушно-сувог стања, при чему су из земљишта одстрањени делови стена и крупне фракције, а затим је са њим спроведена процедура узимања средње пробе. Средња проба земљишта је затим просејавана на ситима промера 2 mm, а мањи узорци масе 10 g су поново просејавани и сушени 24 h на температури од 105 °C (у сушници марке Binder/ /Ed15053). Идентификован биљни материјал припремљен од целе биљке је осушен на собној температури, самлевен до праха, након чега је сушен у сушници (Binder/Ed15053), 24 h на температури од 105 °C до константне масе, чиме је припремљен за

даљу хемијску процедуру. После сушења биљних и узорака земљишта, одређена количина припремљеног материјала за хемијске анализе (3 g земљишта и 2 g биљног материјала) је мерена на аналитичкој ваги са тачношћу ±0,1 mg. Дигестија земљишта и биљног материјала рађена је са HNO_3 и $HClO_4$ [9,10]. Одмерени узорак је пренет у балон по Кјелдалу и преливен са 10–20 ml концентроване HNO_3. Реакциона смеша је загревана пажљиво пламеном, све док раствор није упарен скоро до сува. Поступак је понављан све док раствор није постао бистар, а азотове паре нису престале да се ослобађају. После хлађења, садржај у Кјелдаловом суду је преливен са 6 ml концентроване $HClO_4$ и суд је даље загреван. Загревање је прекидано када је запремина у Кјелдаловом суду била око 3 ml, а раствор био бистар и безбојан. Охлађеним растворима додавана је дестилована вода, а потом су садржаји из Кјелдаловог суда филтрирани у нормални суд од 50 ml и овако припремљени раствори су коришћени за одређивање садржаја метала.

Одређиване су концентрације једанаест метала (Ca, Mg, Fe, Mn, Cu, Zn, Ni, Pb, Cd, Co и Cr) у земљишту и узорцима припремљеним од целих биљака (корен стабло, лист и цваст). Очитавање концентрације испитиваних метала у биљном материјалу и земљишту рађено је у Институту за јавно здравље, сектор Хигијена и медицинска екологија у Крагујевцу, коришћењем Оптичке емисионе спектрометрије са индуковано спрегнутом плазмом (ISP-OES iCAP 6500), директно из раствора. Детекциони лимити при одређивању концентрација метала у биљном материјалу за Ca, Mg, Fe, Mn, Cu, Zn, Ni, Pb, Cd, Co и Cr су: 0,0087; 0,007; 0,0053; 0,0051; 0,0056; 0,0055; 0,006; 0,003; 0,0027; 0,0054 и 0,0053 mg kg^{-1}, по наведеном реду. Детекциони лимити при одређивању концентрација метала у земљишним узорцима за Ca, Mg, Fe, Mn, Cu, Zn, Ni, Pb, Cd, Co и Cr су: 0,009; 0,007; 0,0056; 0,0065; 0,0076; 0,0051; 0,0059; 0,0089; 0,003; 0,0079 и 0,0092 mg kg^{-1}, по наведеном реду. Сваки узорак је очитан у шест понављања, након чега је израчуната средња вредност, стандардна девијација и биолошки апсорпциони коефицијент (однос садржаја метала у биљци и његовог садржаја у земљишту) [11]. Концентрације метала у биљном материјалу и земљишту изражене су у mg kg^{-1} суве материје (mg kg^{-1} d.m.). Сви резултати су приказани табеларно.

РЕЗУЛТАТИ И ДИСКУСИЈА

Средње вредности концентрација испитиваних метала у земљишту и одабраним биљкама на локалитету Котража приказане су у Табели 1. Резултати истраживања показују да су се средње вредности концентрација испитиваних метала у земљишту на локалитету Котража кретале у распону од 1,14 mg Cd kg^{-1} до 70425,19 mg Mg kg^{-1}. Средња вредност концентрација испитиваних елемената у земљишту градирана је у следећем поретку: Mg > Fe > Ca > Ni > > Cr > Mn > Co > Zn > Pb > Cu > Cd. Садржај испитиваних метала у биљкама био је различит, зависио је од биљне врсте и врсте метала, и имао је поредак: Mg > > Ca>Fe>Ni>Mn>Cr>Zn>Co>Pb>Cu>Cd.

Резултати овог истраживања су показали да је средња вредност концентрације Ca у земљишту била 830,53 mg kg^{-1}, Mg 70425,19 mg kg^{-1}, а Fe 31798,03 mg kg^{-1}. Добијене вредности су у сагласности са литературним подацима неких аутора [4,12,13], такође су у сагласности са тврдњом да земљишта настала на серпентинској геолошкој подлози садрже Fe у високим концентрацијама [4,13]. Средње вредности концентрације Ca у биљкама су се кретале од 5790 mg kg^{-1}, забележене у врсти *A. murale,* до 9835,83 mg kg^{-1} у врсти *E. serbicum*. Дефицијенција овог елемента може бити

Табела 1. Средње вредности концентрација испитиваних метала (mg kg^{-1}, средња вредност (n = 6) ±стандардна девијација) у земљишту и одабраним биљним врстама на локалитету Котража
Table 1. The mean concentration of investigated metals (mg kg^{-1}) in soil and selected plant species on locality Kotraža

Метал	Земљиште	*Alyssum murale*	*Eryngium serbicum*	*Euphorbia cyparissias*	*Sanguisorba minor*
Ca	830,53±1,50	5790±54,22	9835,83±28,88	9374,17±49,26	7850,83±89
Mg	70425,19±162,54	9844,58±80,35	4454,58±53,51	6368,33±21,66	39108,33±244,27
Fe	31798,03±199,14	638,21±6,3	243±2,45	320±7,15	3310,42±32,65
Mn	276,06±3	54,1±0,34	52,63±0,70	52,14±0,49	147±0,62
Cu	1,91±0,01	0,69±0,02	6,95±0,23	3,81±0,05	3,87±0,02
Zn	17,81±0,19	5,16±0,04	15,51±0,21	22,34±0,15	11,91±0,05
Ni	740,93±19,96	615,25±11,44	39,98±0,42	40,4±0,3	441,08±2,71
Pb	11,51±0,12	7,26±0,09	0,42±0,01	0,39±0,01	9,38±0,07
Cd	1,14±0,01	0,08±0	0,04±0	0,06±0	0,3±0
Co	36,34±0,2	11,2±0,08	1,01±0,01	4,22±0,04	20,57±0,09
Cr	652,27±1,5	44,91±0,64	6,04±0,15	22,8±0,3	315,21±5,71

условљена сувишком K, Mg, B или NH_4^+ [14,15], као и антагонистичким усвајањем између елемената, пре свега у антагонизму између Ca и Mg, обзиром на малу доступност Ca у односу на Mg на оваквом типу земљишта. Земљишта настала на серпентину се карактеришу ниском вредношћу односа Ca/Mg (због ниске вредности Ca и високе Mg, која по некима представља главни узрок "серпентинског синдрома"), малом доступношћу Ca у односу на Mg, недостатаком есенцијалних макронутријената (P, N, K), као и високим садржајем потенцијално токсичних елемента (Fe, Ni, Cr, Co, и понекад Mn и/или Cu) [16].

Код врсте *S. minor* утврђен је највиши садржај Mg (39108,33 mg kg^{-1}), а најнижи код врсте *E. serbicum* (4454,58 mg kg^{-1}). Биљке које расту на серпентинским земљиштима су највише погођене ниским садржајем Ca, и високим садржајем Mg, који компетитивно инхибира усвајање Ca од стране биљака, али и антагонистички делује на понашање и усвајање других елемената. Серпентинофите које су прилагођене оваквом типу земљишта имају могућност да апсорбују одређене количине Ca, без усвајања сувишне количине Mg [17].

Концентрације Fe су се кретала у распону од 243 (у врсти *E. serbicum*) до 3310,42 mg kg^{-1} (у врсти *S. minor*). Према Маркету (Market) [18], концентрације Fe у биљкама се крећу у распону 5–200 mg kg^{-1}. Показано је, такође, да вегетација која расте на земљиштима насталим на серпентинима, као и представници фамилије Poaceae, садрже Fe од 2127 до 3580 mg kg^{-1} [11].

У испитиваном земљишту забележено је 276,06 mg Mn kg^{-1}, а његов садржај у земљиштима широм света варира 411–550 mg kg^{-1} [11]. Према Адриану (Adriano) [19], нормалне вредности Mn за већину типова земљишта су у границама 500–1000 mg kg^{-1}. Код врсте *S. minor* утврђен је највиши садржај овог елемента (147 mg kg^{-1}), а код врсте *A. murale* најнижи (54,1 mg kg^{-1}). Према неким ауторима, за потпуну метаболичку функцију биљака Mn је потребан у ниским концентрацијама (20 mg kg^{-1}), и у већини биљака он је присутан у концентрацијама 20–300 mg kg^{-1}, док је токсична вредност Mn процењена на 300–500 mg kg^{-1} суве материје [20,21].

Према Kabata-Pendias [11], у земљиштима широм света концентрације Cu се крећу у распону 14–109 mg kg^{-1}. Према неким ауторима, садржај Cu у земљишту Србије је променљив, тако да се његов укупни садржај налази у опсегу од 20 до 120 mg kg^{-1}, а лакоприступачни од 2 до 7 mg kg^{-1} [20]. Добијени резултати ове студије показују да је садржај Cu у земљишту (1,91 mg kg^{-1}) испод граница горе наведених вредности, што указује да матични супстрат и педогенетски процеси одређују његов земљишни статус. Садржај Cu у биљкама варирао је од 0,69 mg kg^{-1} у врсти *A. murale* до 6,95 mg kg^{-1} у врсти *E. serbicum*. Према неким ауторима, концентрација Cu у биљкама се креће у просеку 5–30 mg kg^{-1}, док је токсична вредност Cu процењена на 20–100 mg kg^{-1} суве материје [20]. На усвајање Cu утиче његова концентрација и присуство других јона у земљишту (посебно тешких метала Zn, Mn и Fe) [20]. Неке биљне врсте и генотипови су толерантни на присуство Cu у ткивима, тако да га могу акумулирити нарочито у кореновима и ткивима за складиштење. Такође, протени малих молекулских маса који могу да везују Cu, имају велику улогу у његовој хомеостази омогућавајући многим биљама и бактеријама да развију резистентност на повећане концентрације Cu [22].

Средња концентрација Zn у земљиштима широм света варира од 60 до 80 mg kg^{-1} [11]. Укупни садржај Zn у земљиштима широм Србије се креће у опсегу 5–1070 mg kg^{-1}, док лакоприступачни варира 1–3 mg kg^{-1} [20]. Резултати овог истраживања показују да је садржај Zn (17,81 mg kg^{-1}) у проучаваном земљишту нешто нижи од литературних података неких аутора [13,14,23], што може бити условљено природом матичне стене, процесима педогенезе и садржајем органске материје у земљишту. Добијени резултати указују да је врста *E. cyparissias* садржала највише Zn (22,34 mg kg^{-1}), а врста *A. murale* најмање (5,16 mg Zn kg^{-1}). Према неким ауторима концентрација Zn у биљкама је 27–150 mg kg^{-1}, док је токсична вредност процењена на 200–400 mg Zn kg^{-1} суве материје [20]. Према Brunetti [24], нормалан садржај Zn у биљкама је 15–150 mg kg^{-1}, а максимална вредност достиже 300 mg Zn kg^{-1}.

Земљиште на локалитету Котража садржало је 740,93 mg Ni kg^{-1}. Садржај Ni у земљишту зависи од његовог садржаја у матичној стени, али и од педогенетских процеса и антропогене активности. Земљишта широм света садрже Ni у широким опсезима, међутим његова концентрација је процењена на 13–37 mg kg^{-1} [11]. Његов укупни садржај у земљишту Србије варира 4–500 mg kg^{-1} [20]. Према неким ауторима, у земљиштима формираним на серпентинима садржај Ni се креће 500–600 mg kg^{-1} (због адсорпције двовалентног катјона (Ni^{2+}) на колоиде глине) [25]. Ghaderian и други аутори [26] наводе да је укупна концентрација Ni у серпентинским земљиштима у границама 500–8000 mg kg^{-1}. Највиши садржај Ni забележен је у врсти *A. murale* (615,25 mg kg^{-1}), а најнижи у *E. serbicum* (39,98 mg kg^{-1}) и *E. cyparissias* (40,4 mg kg^{-1}). Садржај Ni у биљкама које расту на незагађеним земљштима Србије значајно варира (што је узроковано биолошким и факторима спољашње средине), тако да је његов просечан садржај у биљкама износио 0,1–5,0 mg kg^{-1}, док је токсична вредност Ni процењена на 10–100 mg kg^{-1} суве мате-

рије [20]. Неки аутори наводе да већина биљака садржи 1–5 mg Ni kg^{-1}, док се појава токсичности за биљке везује за концентрације више од 100 mg Ni kg^{-1} [15,27]. Такође, природна вегетација на серпентинским земљиштима садржи Ni и до 19000 mg kg^{-1} [11].

У истраживаном земљишту забележено је 11,51 mg Pb kg^{-1}, а његов садржај у земљиштима широм света варира од 18–32 mg kg^{-1} [11]. Према неким истраживањима садржај Pb у земљишту Србије је варијабилан (што проистиче од варијабилности матичног супстрата) и варира у широком опсегу, 0––44 mg kg^{-1} [20]. Садржај Pb у биљкама се кретао од 0,39 mg kg^{-1} у врсти *E. cyparissias*, до 9,38 mg kg^{-1} у врсти *S. minor*. Kabata-Pendias [11], наводи да се садржај Pb у биљкама које расту на незагађеним земљиштима налази у опсегу 0,05–3,0 mg kg^{-1}, док су Carranza-Ălvarez и други аутори [28] утврдили концентрације Pb у биљкама у границама 10–25 mg kg^{-1}. Порекло Pb у земљишту је углавном из матичног супстрата, али због све присутнијег антропогеног загађења (рударство, индустријска активност, саобраћај), земљишта постају богатија овим металом. Олово се нарочито акумулира у површинским хоризонтима земљишта. Оно је јако везано за готово све типове земљишта, и само 0,005–0,13% Pb у земљишном раствору је доступно биљкама [29]. Упркос чињеници да је Pb слабо доступно биљкама, постоје неке биљке које могу да га акумулирају у великим количинама, нарочито у корену. Различит садржај Pb у проучаваним биљкама се може приписати различитом афинитету саме биљке за његову акумулацију, својству земљишта, као и количини приступачног облика овог елемента.

У истраживаном земљишту утврђено је 1,14 mg Cd kg^{-1}. У земљиштима широм света процењује се да је садржај Cd око 0,41 mg kg^{-1} (0,2–1,1 mg kg^{-1}) [11]. У незагађеним земљиштима садржај Cd је у вези са земљишном текстуром, тако да према неким истраживањима садржај Cd у земљиштима Србије варира 0,01–2,0 mg kg^{-1} [20]. Одабране врсте на локалитету Котража су садржале најмање Cd од свих испитиваних метала. Садржај овог метала се кретао од 0,04 mg kg^{-1} у врсти *E. serbicum* до 0,3 mg kg^{-1} врсти *S. minor*. Према наводима Кастори [20] садржај Cd у биљкама које расту на незагађеним земљштима Србије је значајно варирао, тако да је његов просечан садржај у биљкама износио 0,05––0,2 mg kg^{-1}, док је токсична вредност Cd процењена на 3–30 mg kg^{-1} суве материје. Усвајање овог елемента зависи од pH вредности земљишта, концентрације Cd^{2+} у земљишном раствору, концентрације приступачног фосфора, присуства Ca^{2+} и Zn^{2+} (они инхибирају његово усвајање) и др. [11]. Низак садржај Cd у истраживаним биљкама је последица ниске концентрације овог елемента у земљишту, као и у могућности да се Cd везује за чврсту фазу земљишта, што смањује његову концентрацију у земљишном раствору и његову биодоступност.

Порекло Co у земљишту је већином од матичног супстрата. Измерени садржај Co у проучаваном земљишту био је 36,34 mg kg^{-1}. Средња вредност концентрације Co у површинским хоризонтима земљишта широм света је 11,3 mg kg^{-1}. Повишене концентрације Co забележене су у иловачастим и органским земљиштима, а у земљиштима око рудних наслага концентрације достижу и до 85 mg kg^{-1} [11]. Такође, серпентинска земљишта имају повишене концентрације појединих елемената (попут Ni, Cr и Co), што потврђују и добијени резултати. У врсти *S. minor* забележена је највиша концентрација Co (20,57 mg Co kg^{-1}), а у врсти *E. serbicum* најнижа (1,01 mg Co kg^{-1}). Према неким ауторима, концентрација Co у биљкама се креће у просеку 0,02–1 mg kg^{-1}, док је токсична вредност Co процењена на 15––50 mg kg^{-1} суве материје [20]. Садржај Co у биљкама зависи од својстава земљишта, као и од апсорбционе способности биљака, која је генетски предиспонирана. Такође, акумулација Co и његово усвајање од стране биљака зависи од мобилних фракција Co, његове концентрације у земљишном раствору, као и од интеракције Co са другим елементима (најчешће са елементима који су геохемијски и биохемијски повезани са Fe).

Просечан садржај Cr у земљишима широм света је процењен на 60 mg kg^{-1}. Према Brunetti и другим ауторима [24], истраживана загађена земљишта су садржала 36,18–115,15 mg Cr kg^{-1}. Већи садржај овог метала је пронађен у земљиштима насталим на базним стенама, тако да земљишта настала на серпентинима садрже понекад и више од 100 000 mg kg^{-1} [11]. Садржај Cr у земљишту Србије креће су у широком опсегу од 5 до 100 mg kg^{-1}, ретко од 500 до 1000 mg kg^{-1}, док је његов садржај код земљишта образованих на серпентину 0,1–6,2% [20]. Хром је углавном пореклом из стена, и његове високе концентрације утврђене су у габроидним и ултрабазичним стена које су генерално богате Fe, Ni и Cr [13], на шта указују и резултати овог истраживања (652,27 mg Cr kg^{-1}). Највећи садржај Cr констатован је код врсте *S. minor* (315,21 mg Cr kg^{-1}), а најмањи код врсте *E. serbicum* (6,04 mg Cr kg^{-1}). Reeves и Baker [30] наводе да су нормалне вредности Cr у биљкама 2–5 mg kg^{-1}. Према неким ауторима биљке га просечно садрже 0,2–4 mg kg^{-1}, док су код биљака које расту на серпентину утврђени садржаји и до 100 mg Cr kg^{-1} [11]. Према Кастори [20], просечан садржај Cr у биљкама је износио 0,01–0,5 mg kg^{-1}, док је токсична вредност Cr процењена на 5–30 mg kg^{-1} суве материје. Показано је да биодоступност неког

елемента зависи и од минералног састава земљишта. Већина земљишта садржи значајну количину Cr, али његова доступност биљкама је лимитирана, што зависи од типа земљишта и биљних фактора. Хром је полутант са великим укупним садржајем у земљишту, али само око 0,008% хрома биљке могу да усвоје, обзиром да се готово целокупан његов садржај у земљишту налази у резистентној (мало доступној) фази [31]. Велики садржај Cr у серпентинским земљиштима је често у форми хромита, специфичног непроменљивог минерала, и самим тим недоступног за биљке. Међутим, неке биљке које расту на серпентинским подручјима и онима са наслагама Cr, могу да акумулирају 0,3––3,4% Cr. Такође, Cr је неесенцијалан елемент за биљке, и оне не поседују специфичан механизам којим га усвајају, тако да могући начин његове апсорпције укључује транспортере везане за усвајање неког од есенцијалних елемената за биљке. Велика разлика у садржају хрома у проучаваним врстама може се приписати и различитој апсорпционој способност биљака која је генетски предиспонирана.

Резултати овог истраживања указују да су концентрације Ni и Cr у испитиваном земљишту више од прописаних ремедијационих вредности [32], као и од њихових максимално дозвољених концентрација у земљишту [33], док концентрације Cd и Co прелазе прописане граничне вредности [32] за дате метале у земљиштима Републике Србије.

Код врсте *S. minor* је утврђен највећи садржај више метала (Mg, Fe, Mn, Pb, Cd, Co и Cr). У врсти *E. serbicum* констатоване су највише концентрације Ca и Cu; Ni је највише нађено у *A. murale*, а Zn у врсти *E. cyparissias*.

Биолошки апсорпциони коефицијент (биоконцентрациони фактор) метала се користи да би се одредила количина метала усвојена од стране биљака из земљишта, и представља однос концентрације једног метала у биљкама (цела биљка/ /орган) и његове концентрације у земљишту. Он је широко коришћен и за поређење различитих биљних врста и њихових генотипова [34]. Код свих истраживаних врста биљака показано је да је однос концентрације Ca у биљкама у односу на земљиште већи од један (табела 2). Код врсте *E. cyparissias* утврђени су биолошки апсорпциони коефицијенти већи од 1 за Zn и Cu, а за Cu већи од 2 код врста: *E. serbicum* и *S. minor*. Велика вредност биолошког апсорпционог коефицијента појединих биљака указује на могућност њихове примене у фитоекстракцији, а његова вредност већа од 2 сматра се значајно великом [35].

Биљна толеранција се односи, како на присуство популација у областима са високом контаминацијом, тако и на присуство појединачних биљака или врста које подносе виши ниво токсичности него друге врсте. Толеранција биљака на метале је фенотипски и генотипски стечена. Утврђено је око 450 врста биљка и/или генотипова имају способност толеранције и акумулације метала и других полутанта много више од њихових уобичајних концентрације [36,37]. Резултати ове студије наглашавају висок садржај више метала у врсти *S. minor*, показују способност врсте *E. cyparissias* у акумулацији Zn и Cu, као и врста *E. serbicum* и *S. minor* у акумулацији Cu. Добијени разултати дају тренутну слику проучаваног локалитета, отварају бројна питања везана за однос земљиште-биљка, садржаја елемената у оба система, њихове узајамне везе и утицаје, и представљају основу за даља истраживања.

ЗАКЉУЧАК

Концентрације испитиваних елемената у земљишту локалитета Котража имале су поредак: Mg >

Табела 2. Биолошки апсорпциони коефицијенти за одабране биљке локалитета Котража
Table 2. The biological absorption coefficient for selected plants on locality Kotraža

Елемент	Биљка			
	Alyssum murale	*Eryngium serbicum*	*Euphorbia cyparissias*	*Sanguisorba minor*
Ca	6,97	11,84	11,29	9,45
Mg	0,14	0,06	0,09	0,56
Fe	0,02	0,01	0,01	0,10
Mn	0,20	0,19	0,19	0,53
Cu	0,36	3,63	1,99	2,02
Zn	0,29	0,87	1,25	0,67
Ni	0,83	0,05	0,06	0,60
Pb	0,63	0,04	0,03	0,82
Cd	0,07	0,03	0,05	0,24
Co	0,31	0,03	0,12	0,57
Cr	0,07	0,01	0,04	0,48

> Fe > Ca > Ni > Cr > Mn > Co > Zn > Pb > Cu > Cd. У испитиваном земљишту концентрације Ni и Cr су биле више од њихових максималних концентрација у земљишту, које не смеју да буду прекорачене у циљу спречавања озбиљних неповратних последица по екосистем. Концентрације ових метала у испитиваном земљишту су биле и изнад концентрација за које постоји ризик по екосистем, здравље људи и животиња. Такође, забележене концентрације Cd и Co у овом земљишту су биле више од граничне вредности за дате метале у земљишту. Све ово указује да испитивано земљиште припада категорији контаминираног земљишта.

Садржај испитиваних метала у биљкама био је различит, зависио је од биљне врсте и врсте метала, и градиран је у поретку: Mg > Ca > Fe > Ni > Mn > Cr > > Zn > Co > Pb > Cu > Cd. Код врсте *S. minor* је утврђен највећи садржај више метала (Mg, Fe, Mn, Pb, Cd, Co и Cr); док је врста *E. serbicum* садржала највише Ca и Cu; Ni је највише нађено у *A. murale*, а Zn у врсти *E. cyparissias*.

Врста *E. cyparissias* је садржала Zn и Cu у својим ткивима више од њиховог садржаја у земљишту, док су врсте *E. serbicum* и *S.minor* садржале два пута више Cu од његовог садржаја у земљишту. Такође, код свих истраживаних врста биљака утврђен је већи садржај Ca од његовог садржаја у испитиваном земљишту.

Резултати ове студије наглашавају толеранцију на више метала врсте *S. minor*, показују способност врсте *E. cyparissias* у акумулацији Zn и Cu, као и врста *E. serbicum* и *S. minor* у акумулацији Cu. Добијени разултати дају тренутну слику проучаваног локалитета, отварају бројна питања везана за однос земљиште–биљка, садржаја елемената у оба система, њихове узајамне везе и утицаје, и представљају основу за даља истраживања.

ЛИТЕРАТУРА

[1] B. Markert, From biomonitoring to integrated observation of the environment - the multi-markered bioindication concept, Ecol. Chem. Eng. S. **15**(3) (2008) 315––333.

[2] Ј. Ђурић, Флора брда Чукаре у Котражи код Страгара, Дипломски рад, Природно-математички факултет, Универзитет у Крагујевцу, 1979.

[3] Б. Татић, В. Вељовић, А. Марковић, Б. Петковић, Прилог проучавању серпентинске флоре Југославије, Биосистематика **7** (1981) 123–135.

[4] R.D. Reeves, A.J. M. Baker, T. Becquer, G. Echevarria, Z. J.G. Miranda, The flora and biogeochemistry of the ultramafic soils of Goiás state, Brazil, Plant. Soil **293** (2007) 107–119.

[5] C.L. Broadhurst, R.L. Chaney, J.A. Angle, E.F. Erbe, T.K. Maugel, Nickel localization and response to increasing Ni soil levels in leaves of the Ni hyperaccumulator *Alyssum murale*, Plant. Soil **265** (2004) 225–242.

[6] S. Javorka, V. Csapody, Iconographia Florae parties Austro-Orientalis Europae Centralis, Academiai kido, Budampest, 1979.

[7] M. Josifović, Flora of Serbia I, SAAS, Beograd, 1970––1980, str. 286–311.

[8] T.G. Tutin, Flora Europaea, u: T.G. Tutin, V.H. Heywood, N.A. Burges, D.H. Valentine, S.M. Walters, D.A. Webb (Eds.), Flora Europaea, Cambridge University Press, Cambridge, United Kingdom, 1964–1980.

[9] N.J. Ince, Assessment of toxic interaction of heavy metals in binary mixtures: a statistical approach, Arch. Environ. Con. Tox. **36** (1999) 365–372.

[10] Sh. Wei, Q. Zhou, X. Wang, Identification of weed plants excluding the uptake of heavy metals, Environ. Int. **31** (2005) 829–834.

[11] A. Kabata-Pendias, Trace Elements in Soil and Plants, 4th ed., CRC press, Boca Raton, FL, 2011.

[12] B.H. Robinson, A. Chiarucci, R.R. Brooks, D. Petit, J.H. Kirkman, P.E.H. Gregg, V. De Dominicis, The nickel hyperaccumulator plant *Alyssum bertolonii* as a potential agent for phytoremediation and phytomining of nickel, J. Geochem. Explor. **59** (1997) 75–86.

[13] S. Shallari, C. Schwartz, A. Hasko, J.L. Morel, Heavy metals in soils and plants of serpentine and industrial sites of Albania, The Sci. Total. Environ. **209** (1998) 133––142.

[14] J. Bech, P. Tume, L. Longan, F. Reverter, J. Bech, L. Tume, M. Tempio, Concentration of Cd, Cu, Pb, Zn, Al, and Fe in soils of Manresa, NE Spain, Environ. Monit. Assess. **145** (2008) 257–266.

[15] R.L. Chaney, K.Y. Chen, Y. M. Li, J.S. Angle, A.J.M. Baker, Effects of calcium on nickel tolerance and accumulation in Alyssum species and cabbage grown in nutrient solution, Plant. Soil **311** (2008) 131–140.

[16] K.U. Brady, A.R. Kruckeberg, H.D. Bradshaw, Evolutionary ecology of plant adaptation to serpentine soils, Annu. Rev. Ecol. Evol. S. **36** (2005) 243–266.

[17] R.B. Walker, The ecology of serpentine soils: A symposium, II. Factors affecting plant growth on serpentine soils, Ecology **35** (1954) 259–266.

[18] B. Markert, Presence and significance of naturally occurring chemical elements of the periodic system in the plant organism and consequences for future investigations on inorganic environmental chemistry in ecosystems, Vegetatio **103** (1992) 1–30.

[19] D.C. Adriano, Trace element in terrestrial environments: biogeochemistry, bioavailability and risks of metals, Springer, New York, 2001.

[20] Р. Кастори, Тешки метали и пестициди у земљишту - Тешки метали и пестициди у земљишту Војводине, Пољопривредни факултет, Институт за ратарство и повртарство, Нови Сад, 1993.

[21] I. Pais, J.B. Jones, The Handbook of Trace Elements, St. Luice Press, Boca Raton, FL, 2000.

[22] S. Puig, H. Mira, E. Dorcey, Higher plants possess two different types of ATX1-like copper cheperones, Biochem. Bioph. Res. Co. **365** (2007) 385–390.

[23] D. Obratov-Petković, I. Popović, S. Belanović, R. Kadović, Ecobiological study of medicinal plants in some regions of Serbia, Plant Soil Environ. **52**(10) (2006) 459–467.

[24] G. Brunetti, P. Soler-Rovira, K. Farrag, N. Senesi, Tolerance and accumulation of heavy metals by wild plant species grown in contaminated soils in Apulia region, Southern Italy, Plant. Soil **318** (2009) 285–298.

[25] Р. Кастори, Неопходни микроелементи – физиолошка улога и значај у биљној производњи, Научна књига, Београд, 1990.

[26] A.M. Ghaderian, A. Mohtadi, R. Rahiminejad, R.D. Reeves, A.J.M. Baker, Hyperaccumulation of nickel by two Alyssum species from the serpentine soils of Iran, Plant. Soil **293** (2007) 91–97.

[27] R.D. Reeves, The hyperaccumulation of nickel by serpentine plants, in: A.J.M. Baker, J. Proctor, R.D. Reeves (Eds.), The vegetation of ultramafic (serpentine) soils, Intercept Ltd. Andover, Hampshire, 1992, pp. 253–277.

[28] C. Carranza-Ălvarez, A. J. Alonso-Castro, M. C. Alfaro-De La Torre, R. F. Garciá De La Cruz, Accumulation and Distribution of Heavy Metals in *Scirpus americanus* and *Typha latifolia* from an Artificial Lagoon in San Luis Potosĭ, Mexico, Water Air Soil Poll. **188** (2008) 297–309.

[29] B.E. Davies, Lead, in: Heavy metals in soils, B.J. Alloway, (Ed.), Blackie Acad., London, 1995, pp. 206–223.

[30] R.D. Reeves, A.J.M. Baker, Phytoremediation of toxic metals, in: I. Raskin, B.D. Ensley (Eds.), Using plants to clean up the environment, Wiley and Sons Inc., New York, 2000.

[31] A. Zayed, N. Terry, Chromium in the environment: factors affecting biological remediation, Plant. Soil **249** (2003) 139–156.

[32] Уредба о програму системског праћена квалитета земљишта, индикаторима за оцену ризика од деградације земљишта и методологији за израду ремедијационих програма, Службени гласник РС, бр. 88/ /2010, прилог 3.

[33] Правилник о дозвољеним количинама опасних и штетних материја у земљишту и води за наводњавање и методама њиховог испитивања, Службени гласник РС, бр. 23/94, 1994.

[34] S.P. McGrath, F.J. Zhao, Phytoextraction of metals and metalloids from contaminated soils. Curr. Opin. Biotech. **14** (2003) 277–282.

[35] P. Pandy, K. Tripathi, Bioaccumulation of heavy metal in soil and different plant parts of *Albizia procera* (Roxb.) seedling, Bioscan **5** (2010) 263–266.

[36] M.N.V. Prasad, H.M.O. Freitas, Metal hyperaccumulation in plants – Biodiversity prospecting for phytoremediation technology, Electron. J. Biotechnol. **6** (2003) 285–321.

[37] H. Freitas, M.N.V. Prasad, J. Pratas, Analysis of serpentinophytes from north-east of Portugal for trace metal accumulation-relevance to the management of mine environment, Chemosphere **54** (2004) 1625–1642.

SUMMARY

METAL ACCUMULATION AND TOLERANCE OF SELECTED PLANTS OF ASBESTOS TAILINGS (STRAGARI)

Snežana R. Branković[1], Radmila M. Glišić[1], Vera R. Đekić[2], Marija A. Marin[3]

[1]*University of Kragujevac, Faculty of Science, Institute of Biology and Ecology, Kragujevac, Serbia*
[2]*Research and Development Centre, Small Grains Research Center, Kragujevac, Serbia*
[3]*University of Belgrade, Faculty of Biology, Belgrade, Serbia*

(Scientific paper)

The aim of this study was to determine the concentrations of 11 metals in the soil of asbestos tailings in Stragari, Serbia, and in the selected plant species that grow on it, to determine the ability of the plant species in accumulation and tolerance of researched metals. Concentrations of elements researched in the soil had this order: Mg > Fe > Ca > Ni > Cr > Mn > Co > Zn > Pb > Cu > Cd. Concentrations of the metals in plants was variable, dependent on the plant species and types of metals, and graded in the order: Mg > Ca > Fe > Ni > Mn > Cr > Zn > Co > > Pb > Cu > Cd. The concentrations of Ni and Cr in the investigated soil were above remediation values, as well as the maximum allowable concentration of substances in the soil according to regulation of Republic of Serbia, and the concentration of Cd and Co were above limit values for a given metals in the soil. The metal uptake does not necessarily correlate with metal content in the soil. Metal uptake by plants depends on the bioavailability of the metal in soils, which in turn depends on the retention time of the metal, as well as the interaction with other elements and substances. However, the most Mg, Fe, Mn, Pb, Cd, Co and Cr were found in species *Sanguisorba minor*, Ca and Cu in *Eryngium serbicum*, Ni in *Alyssum murale*, and Zn in *Euphorbia cyparissias*. In the *Euphorbia cyparissias*, it were determined the biological absorption coefficients greater than 1 for Zn and Cu, and in the species *Eryngium serbicum* and *Sanguisorba minor* greater than 2 for Cu. The results of this study emphasize the tolerance of several metal by species *Sanguisorba minor*, present the ability of *Euphorbia cyparissias* in accumulation of Zn and Cu, as well as of *Eryngium serbicum* and *Sanguisorba minor* in accumulation of Cu. Obtained results present the momentary picture of investigated locality, open a lot of questions connected with relationships soil/plant, contents of elements in both systems, their interactions and influences and represented the base for further research.

Keywords: Accumulation of metals • Tolerance • Asbestos tailings • Plants

Influence of pin geometry on mechanical and structural properties of butt friction stir welded 2024-T351 aluminum alloy

Igor Z. Radisavljevic[1], Aleksandar B. Zivkovic[2], Vencislav K. Grabulov[3], Nenad A. Radovic[4]

[1]*Military Technical Institute, Belgrade, Serbia*
[2]*GOSA FOM, Smederevska Palanka, Serbia*
[3]*Institute for Materials Testing, Belgrade, Serbia*
[4]*Faculty of Technology and Metallurgy, Belgrade, Serbia*

Abstract

The aim of this work was to investigate the combined effect of small difference in pin geometry, together with rotation and welding speed on the weldability, mechanical and structural properties of FSW 2024-T351 Al plates. The only difference in tool pin design was the shape of thread: regular and rounded. Specimens were welded using rotation rate of 750 rev/min and welding speeds of 73 and 93 mm/min. Specimens were defect free, with good or acceptable weld surface, in all four cases. Modification in pin design showed strong influence on macro structure and hardness distribution. Weak places are identified as low hardness zone, close to the nugget zone and are in good agreement with fracture location in tensile testing. Weld efficiency, as a measure of weld quality, is better in case of 310 tool, while UTS values can differ up to 13% for the equal welding parameters. Therefore, it can be assumed that small modification in tool design, particularly in pin geometry, can have great influence on weld formation and mechanical properties.

Keywords: friction stir welding, pin geometry, weld quality, Al alloy 2024, heat input.

Available online at the Journal website: http://www.ache.org.rs/HI/

SCIENTIFIC PAPER

UDC 621.791.1:669.715

Hem. Ind. **69** (3) 323–330 (2015)

doi: 10.2298/HEMIND131206020R

Friction stir welding (FSW), a solid-state joining technique invented by TWI in 1991 is new welding technique that offers several advantages over conventional fusion welding process due to its low heat input and absence of melting and solidification [1–3]. FSW run in the solid phase below the melting point of joining materials, approximately at 0.8 of Tm [4]. Therefore, due to absence of melting, weld metal is not present, while new region are introduced: nugget zone (NZ) and thermo-mechanically affected zone (TMAZ), Figure 1a. The most important benefit of FSW is its ability to weld materials that are extremely difficult to weld by conventional fusion welding processes, such as 2xxx and 7xxx series aluminum alloys. The benefits therefore include low distortion and residual stresses, no loss of alloying elements, no arc, no fume and no

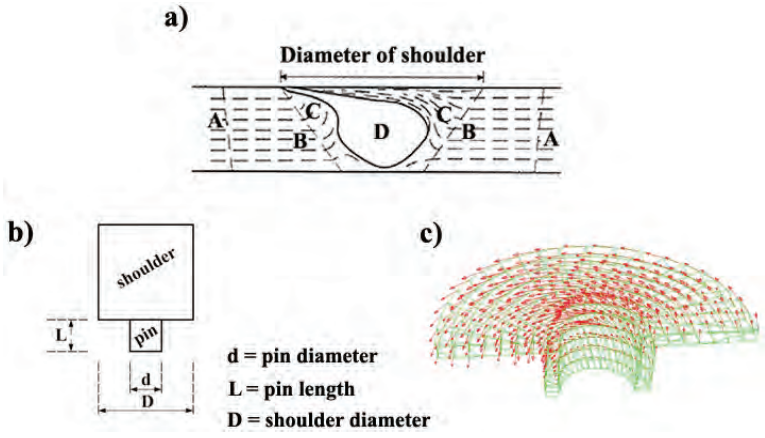

Figure 1. Schematic illustration a) regions of FSW joint: A-base metal (BM), B-Heat Affected Zone (HAZ), C-Thermo-Mechanically Affected Zone (TMAZ), D-Nugget zone (NZ); b) FSW tool; c) material flow during FSW process [5].

Correspondence: I.Z. Radisavljevic, Military Technical Institute, Ratka Resanovica 1, 11030 Belgrade, Serbia.
E-mail: igor.radisavljevic@vti.vs.rs
Paper received:
Paper accepted:

filler wire. Moreover, due to low heat input and the absence of a melting and solidification, high quality welds with minimal microstructural changes and better mechanical properties than conventional welding, with-

out presence of porosity and hot cracking can be created [4,6–8]. Thus, FSW is a very suitable, and increasingly used, for joining high strength aluminum alloys (2xxx, 6xxx, 7xxx and 8xxx series), currently applied to the aerospace, automotive, marine and military industries.

Friction stir welding tool, Figure 1b, is the key art of FSW process [2–4,9–14]. Typical flow of material during FSW is illustrated on Figure 1c. Significant research is done in order to obtain sound welds (in terms of UTS, elongation, weld microstructure, hardness, fatigue resistance etc.) and to establish the influence of welding parameters (rotation and welding speed), tool geometry and position of the pin axes [15–20]. On the other hand, heat generation and material flow (together with final structure and weld mechanical properties) are directly related to the tool shoulder and pin geometry.

Shoulder is the main source of heat generated during the process, the primary constraint to material expulsion and the primary driver for material flow around the tool, the pin is the primary source for material deformation and the secondary source for heat generation in the nugget. Nugget integrity is therefore primarily dependent on a well-designed pin. Furthermore, pin geometry also can affect the weld shape. Consequently, the geometry of both the shoulder and pin are important to the FSW process, since they determine the heat generation and material flow [4,5,9,21––25].

Main aim of this work is to establish the effect of pin thread geometry on the weldability, mechanical and structural properties of friction stir welded 2024-T351 Al plates for constant set of welding parameters (rotation speed and welding speed).

EXPERIMENTAL

Commercial 8.0 mm thick Alclad 2024-T351 aluminum alloy rolled plates were used in this work as the base metal. Plates were machined on both sides to remove the Alclads. Chemical compositions and mechanical properties of the machined plate are given in Table 1. Single welded plates were dimension of 260 mm×65 mm×6 mm. Sides of plates were machined and had stiff contact with supporting plate, and butt-welded along the rolling direction using adopted conventional milling machine. Welding length was approx. 210 mm on each pair of plates. Two different friction stir tools were designed; the only difference was pin design, *i.e*., use of regular (tool 310) or rounded (tool 310-O) threads, Figure 2. Used tools are made of tool steel, with spiral thread on the 5.5 mm length conical pin and concave profiled head on the 25 mm diameter cylindrical shoulder. Taper screw thread pins are designed, with thread slope of 5 degrees and diameter on root and head of 10 and 4 mm, respectively. Pins have angle of 20 degrees. Pitch of thread is 1.5 mm. The tools are heat treated to 51 HRC. Tool tilt angle was 1° and was kept constant. An equal axial (welding) force is obtained by controlling the plunge depth of welding tool, since all the specimens have the same thickness. Plunge depth of tool shoulder was 0.2 mm. All welded joints are in "hot" condition; according to R/V ratio criterion suggested by P. Vilaça *et al*. [2,26]. R represents tool rotation speed per minute (rpm) and V is welding speed in mm/min. Welding parameters used in this study are summarized in Table 2, where ratio R^2/V represents pseudo heat index suggested by Arbegast and Hartley [27].

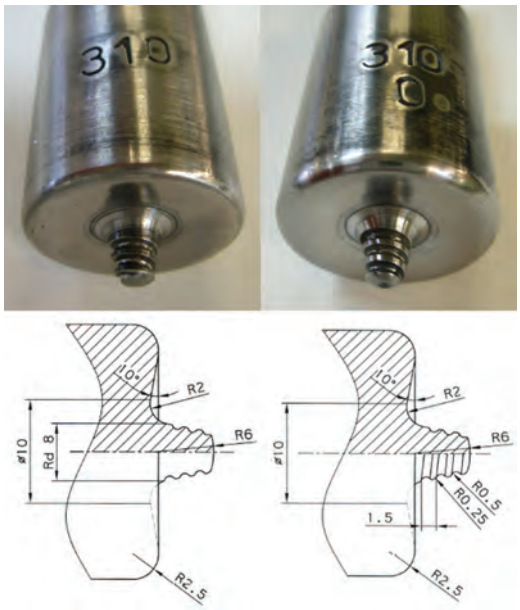

Figure 2. Fabricated FSW tools.

Complete testing methodology is given in Table 3. In order to reveal presence of surface and/or volume defects, welded joints were subjected to visual, penetrants, X-ray and ultrasonic examination. These steps are eliminating, *i.e*., if the joint does not fulfill requirements, it was eliminated from further examination. All welded samples were naturally aged at room temperature for more than 20 days and specimens were cross-

Table 1. Chemical composition and mechanical properties of Al 2024-T351 plate; BA – banding angle

Chemical composition, wt.%										Mechanical properties				
Cu	Mg	Mn	Fe	Zn	Si	Ti	Zr	Ni	Cr	*YS* / MPa	*UTS* / MPa	A_5 / %	*HV*	*BA*
4.70	1.56	0.65	0.17	0.11	0.046	0.032	0.011	0.006	0.004	370	481	18	145	180

Table 2. Welding parameters

Sample	Tool designation	Rotation rate (*R*) rpm	Welding speed (*V*) mm/min	Ratio *R*/*V* rev/mm	Ratio R^2/V	Ratio *V*/*R* mm/rev
A	310	750	73	10.27	7700	0.0973
B			93	8.06	6050	0.1240
C	310-O		73	10.27	7700	0.0973
D			93	8.06	6050	0.1240

-sectioned perpendicular to the welding direction (Figure 3). Metallographic observation was carried out by optical microscopy (OM) using Leica M205A optical microscope. The specimen for OM was ground, polished and etched using Tucker's (45 ml HCl, 15 ml HNO_3, 5 ml HF and 25 ml H_2O) reagent. Much care was taken to ensure location-to-location correspondence between the structural observations and hardness measurements. The nugget zone average size measurements were processed using Leica DFC295 camera and LAS software [28]. In order to obtain fracture locations of the FSW joints, the surfaces of tensile specimens were swab etched using Tucker's solution before testing. Room-temperature tensile tests were carried out at a strain rate of 3.3×10^{-3} s^{-1} on ASTM E8M transverse tensile specimens (Figure 4). In order to asses the reproducibility, at least four specimens were tested and average value was reported. Bend testing was carried out according to EN 910 with joint centered over the mandrel. The bending specimens were tested using face and root side of the joint in tension. Vickers hardness measurement was conducted perpendicular to the welding direction, at cross section of weld joint, using digitally controlled hardness test machine (HVS-1000) applying 9.807 N force for 15 s. The hardness profiles were obtained along 3 horizontal and 17 vertical directions (Figure 5). In order to obtain the hardness distribution maps a total of 183 and 187 indentations in horizontal and vertical directions, respectively, were measured.

Table 3. Testing methodology of welded joints

ActionAction	Step	Investigation
Non-destructive	1	Visual examination
	2	Penetrant examination
	3	X-Ray examination
	4	Ultrasonic examination
Destructive	5	Evaluation of macrostructure
	6	Hardness testing
	7	Tension testing
	8	Bending testing

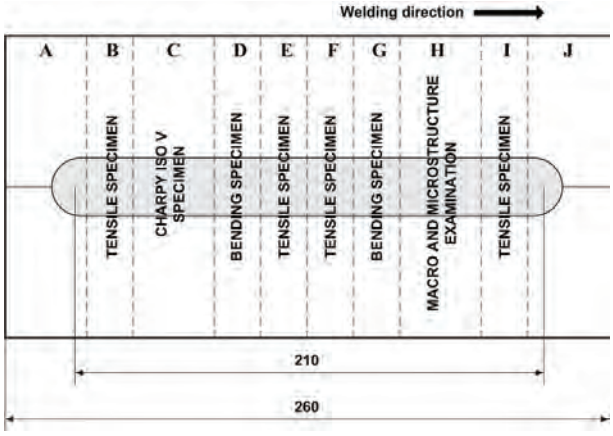

Figure 3. Schematic of specimens' locations in weld.

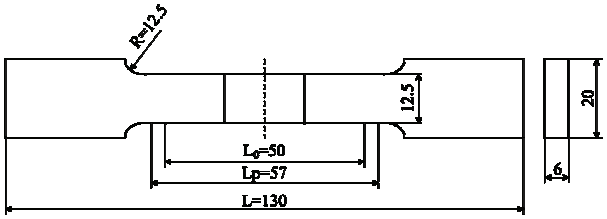

Figure 4. Shape and dimension of tensile specimens in mm.

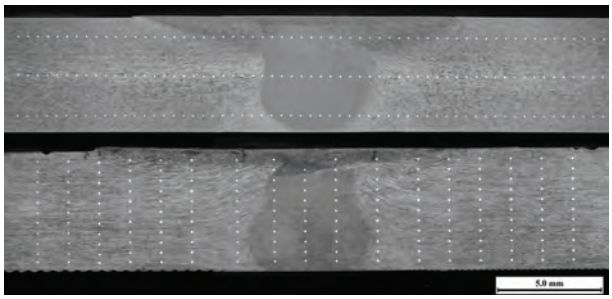

Figure 5. Horizontal (up) *and vertical* (down) *hardness test lines.*

RESULTS AND DISCUSSION

NDT examination did not detect any volume defects, proving that all were defect-free joints. Upper weld surface appearances are shown in Figure 6. It can be seen that in three cases smooth and clean surface appearance is obtained while sample C, in comparison with other three samples, exhibits relatively smooth, but acceptable surface.

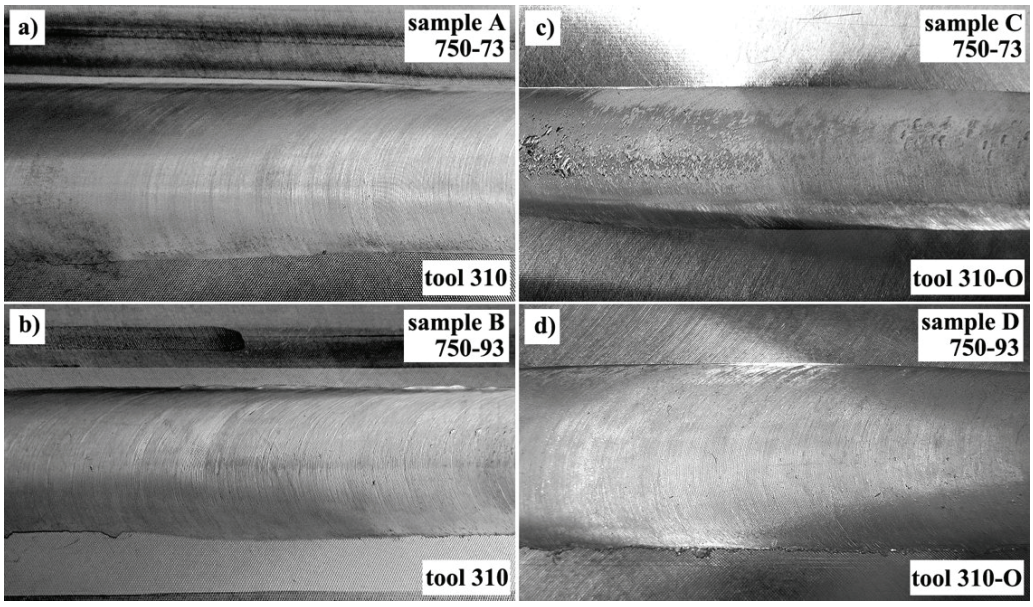

Figure 6. Joints surface appearance.

Figure 7 shows macrostructures of transverse cross section for all four joints. Macro-structural examinations confirmed NDT results; no voids, cracks or other weld defects were observed. Under the drive of tool shoulder and pin, transverse cross section structure of the weld exhibits three distinct zones: nugget zone (NZ), thermo-mechanical affected zone (TMAZ) and heat affected zone (HAZ). According to the role of shoulder and pin in NZ formation, the NZ can be subdivided into three sub-zones; the shoulder-driven zone (SDZ), the pin-driven zone (PDZ), and the swirl zone (SWZ) as shown in Figure 8c [29–32]. Pin geometry doesn't show noticeable influence on TMAZ spread out and shape. On the other hand, NZ and particularly PDZ have strong dependence on pin geometry. A comparatively large PDZ, with regular onion ring structures, a narrow SDZ and SWZ were observed. Onion ring shape in PDZ depends on welding parameters and pin design (Figure 7a–d). Furthermore, decreasing the welding speed for same rotation rate produces the finest spacing between rings. Different spacing between rings is related to the pin forward movement per revolution; *i.e.*, at rotation rate of 750 rpm and welding speed of 73 and 93 mm/min, tool moves 0.0973 and 0.1240 mm/rev, respectively (Table 2). Relationship between pin movement per revolution and onion ring width, can be described as "intermittent" behavior which is related to the pin geometry, particularly pin thread design. Similar observations and findings have been reported and suggested by other authors [33–35]. SDZ and SWZ are more or less pronounced, due to different welding parameters. For the same rotation rate PDZ becomes narrow as a welding speed is increased. However, influence of pin design on NZ and PDZ spread out

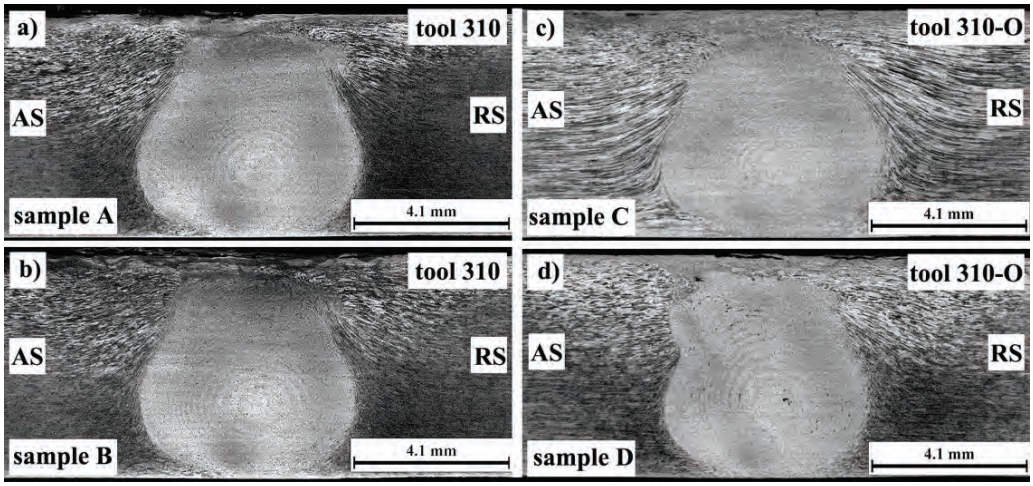

Figure 7. Macrostructure of welded joints.

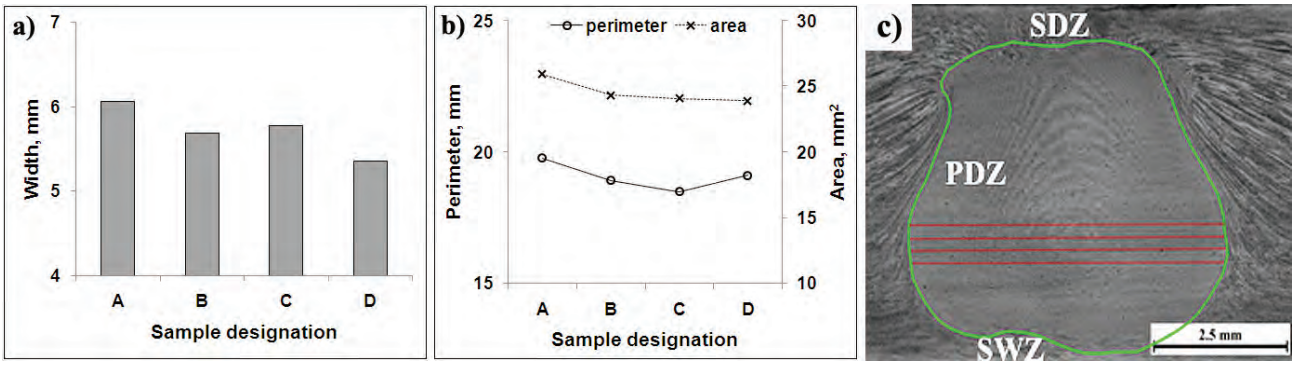

Figure 8. a) PDZ average width; b) PDZ perimeter and area; c) measurement example and general location of PDZ, SDZ and SWZ.

and shape, welded under same rotation rate and welding speed, which means that the same R^2/V pseudo heat index is obtained. Due to small differences in pin design, PDZ width for sample A and C also as B and D are different (Figure 8a). These imply that, during welding process, material flow around the pin is not the same. Mentioned behavior can be attributed to the heat input increasing as the welding speed is decreasing, relative to the rotation rate, leading to an overall increase in width of the plastic zone. On Figure 8b PDZ perimeter and area distribution are presented.

Hardness distribution maps (Figure 9) were used to determine the weakest parts of joints in terms of different process parameters and tools. Also, these maps are plotted in an attempt to predict fracture locations of joints, according to manner that the fracture location is a direct reflection of the weakest part of joint [15,36]. It can be determined that the low hardness zone (LHZ) was generally located at the TMAZ, rather on part of TMAZ near to the contact line between NZ and TMAZ. Low hardness is attributed to grain growth after recrystallization [37].

Average value of joint tensile properties and fracture location under investigated welding parameters are given in Table 4. Ultimate tensile strength, UTS, of each joint is lower than that of base material. Elongation of the joints is far lower than base material elongation, and its maximum is 7.5%. Under the cons-

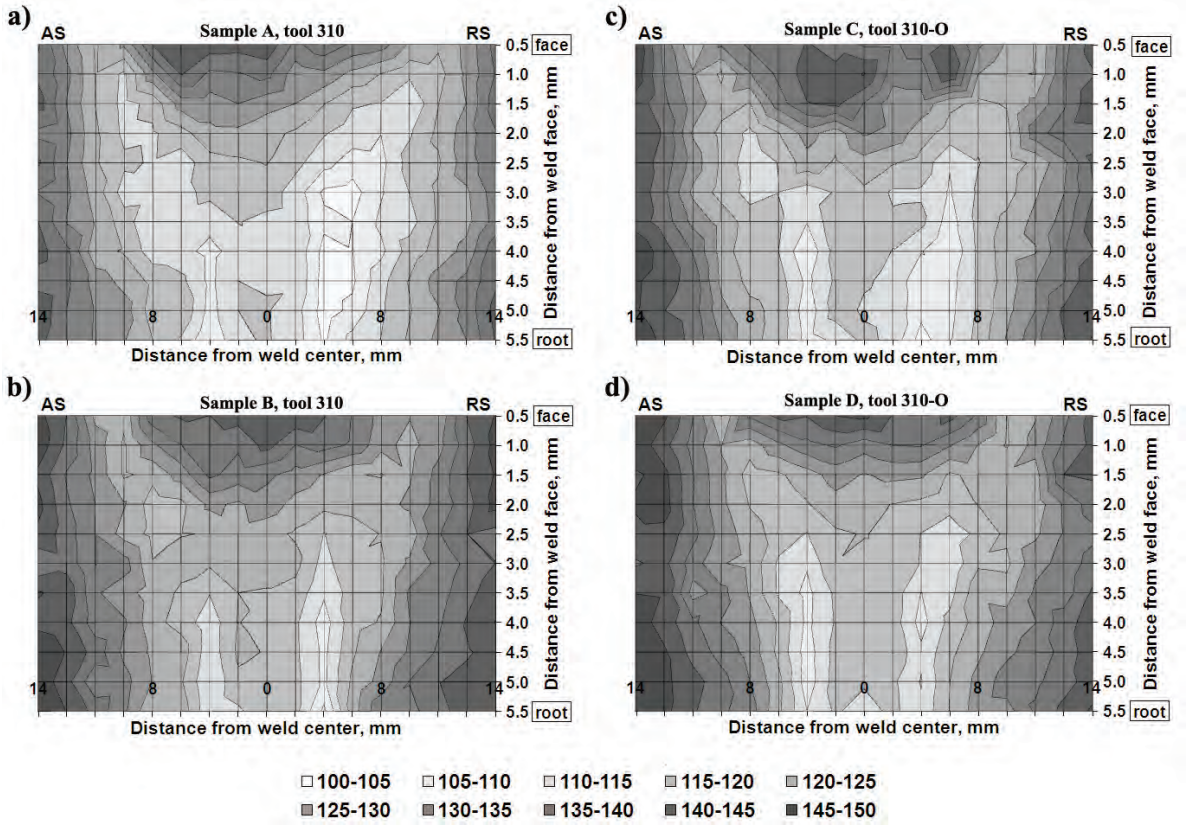

Figure 9. Hardness distribution map.

Table 4. Tensile properties – average value

Sample designation	*UTS* / MPa	A_5 / %	Joint efficiency, UTS_{FSW}/UTS_{BM} (%)	Joint efficiency A_{FSW}/A_{BM} (%)
A	395	7.5	82.2	41.4
B	355	3.9	73.7	21.7
C	365	4.2	75.9	23.2
D	309	2.8	64.2	15.5

tant rotation rate of 750 rpm, for both tools, tensile strength sharply decreased when welding speed is increased. Lower tensile strength for same welding parameters (samples A and C and samples B and D) is a consequence only due to difference in tool pin geometry and resulting microstructures. Maximum UTS was obtained for sample A welded with tool 310 and 10.27 *R*/*V* ratio, while minimum UTS were obtained for sample D welded with tool 310-O and 8.06 *R*/*V* ratio. Furthermore, when compare UTS of samples welded with same welding parameters and *R*/*V* ratio but with different tool (310 and 310-O), it is evident that samples welded with 310-O tool have 7.6 and 12.96% lower UTS. The results are similar in terms of elongation. Samples welded with 310-O tool have 44 and 28.2 % lower elongation then samples welded with 310 tool. If we take into consideration of UTS and elongation in terms of *R*/*V* ratio or pseudo heat index R^2/V, it is clearly that for same ratio actual generated energy is not same and they depend on pin design moreover as on welding parameters. Therefore, it can be assumed that small modification in tool design, particularly in pin geometry, can have great influence on weld formation and mechanical properties. Thus, this implies that overall joint quality show strong dependence on combined effect of heat input and material flow states due to different welding parameters.

The fracture location is very important for understanding and improving joint mechanical properties. According to the observed findings, specimen fracture is dominantly located on NZ/TMAZ interface at AS. In order to accurately determine tensile fracture location, the cross-sections of specimen were etched, as shown in Figure 10. These results are in good agreement with hardness distribution, confirming that fracture will occur at the weakest parts of joints.

Three point bending test was carried out to examine the angle when first crack occurs. Forces when first crack occurs are also noted. The bending test includes bending around face (joint root are exposed to stretching) and around root (joint face are exposed to stretching). The results are shown in Figure 11. It can be seen that bending properties of joints are much lower than BM (Table 1). Most balanced results are obtain for sample A, welded with 310 tool.

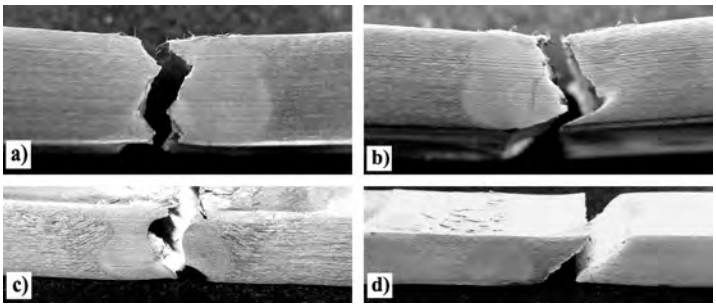

Figure 10. Typical fracture location on tensile specimen: a) NZ/TMAZ interface on AS; b) NZ/TMAZ interface on RS; c) NZ – central area; d) TMAZ/HAZ interface on RS.

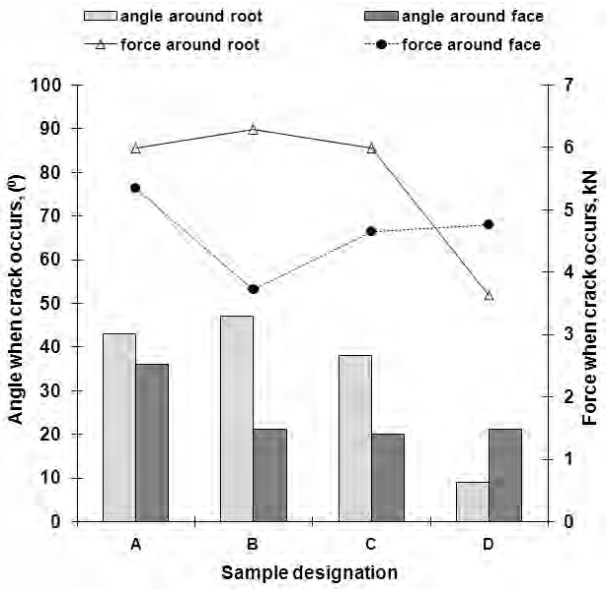

Figure 11. Bending tests results.

CONCLUSUION

In this study combined effect of small modification of pin geometry, together with rotation and welding speed on the weldability, mechanical and structural properties of FSW 2024-T351 Al plates was investigated. In all cases, specimens were defect free, with good or acceptable fracture surface. Modification of pin geometry showed strong influence on macro structure and hardness distribution. Weak places are identified as low hardness positions close to nugget zone and are in good agreement with fracture position in tensile testing. Weld efficiency, as a measure of quality are better in case of 310 tool, while UTS values can differ up to 13% for the equal welding parameters. Therefore, it can be assumed that small modification in tool design, particularly in pin geometry, can have great influence on weld formation and mechanical properties. Sample A has shown the best properties.

Acknowledgements

The authors are indebted to Ministry of Education, Science and Technological Development of the Republic of Serbia for financial support through Project TR34018. The authors also wish to express their sincere thanks to Military Technical Institute of Serbian Army for technical support during performing friction stir welding experiments.

REFERENCES

[1] W.M. Thomas, E.D. Nicholas, J.C. Needham, M.G. Murch, P. Templesmith, C.J. Dawes, GB Patent Application No. 9125978.8, 1991.

[2] P. Vilaça, W. Thomas, Friction Stir Welding Technology in: P.M.G.P Moreira, L.F.M da Silva, P.M.S.T. de Castro (Eds.), Structural connections for lightweight metallic structures, Adv. Struct. Mater. **8** (2012) 85-124.

[3] J.N. Pires, A. Loureiro, G. Bolmsjo, Welding robots: Technology, system issues and applications, Springer, London, 2006, pp. 27–71.

[4] R.S. Mishra, Z.Y. Ma, Friction stir welding and processing, Mater. Sci. Eng. R **50** (2005) 1–78.

[5] D. Veljic, Experimental and numerical thermo-mechanical analysis of friction stir welding of high strength aluminum alloys, PhD thesis, Faculty of Mechanical Engineering, Belgrade, 2012.

[6] M. Ellis, M. Strangwood, Welding of rapidly solidified alloy 8009 (Al-8.5Fe-1.7Si-1.3V) – Preliminary study, Mater. Sci. Tech. **12** (1996) 970–977.

[7] R.S. Mishra, M.W. Mahoney, Friction stir welding and processing, ASM International, Materials Park, OH, 2007.

[8] M. Ericsson, R. Sandstrom, Influence of welding speed on the fatigue of friction stir welds, and comparison with MIG and TIG, Int. J. Fatigue **25** (2003) 1379–1387.

[9] K. Elangovan, V. Balasubramanian, Influences of tool pin profile and welding speed on the formation of friction stir processing zone in AA2219 aluminum alloy, J. Mater. Process. Tech. **200** (2008) 163–175.

[10] R. Rail, A. De, H.K. Bhadeshia, T. DebRoy, Review: friction stir welding tools, Sci. Tech. Weld. Join. **16** (2011) 325–342.

[11] C.J. Dawes, W.M. Thomas, Development of improved tool design for FSW of aluminum, in Proceedings of 1st International conference on friction stir welding, Thousand Oaks, TWI, USA, 1999.

[12] T. Nishihara, Development of simplified FSW tool, in Proceedings of 6th International symposium on friction stir welding, Saint-Sauveur, Quebec, Canada, 2006.

[13] L. Dubourg, P. Dacheux, Design and properties of FSW tools: a literature review, in Proceedings of 6th International symposium on friction stir welding, Saint-Sauveur, Quebec, Canada, 2006.

[14] S.R. Sharma, Z.Y. Ma, R.S. Mishra, Effect of friction stir processing on fatigue behavior of A356 alloy, Scr. Mater. **51** (2004) 237–241.

[15] H.J. Liu, H. Fujii, M. Maeda, K. Nogi, Tensile properties and fracture locations of friction-stir-welded joints of 2017-T351 aluminum alloy, J. Mater. Process. Tech. **142** (2003) 692–696.

[16] G. D'Urso, E. Ceretti, C. Giardini, G. Maccarini, The effect of process parameters and tool geometry on mechanical properties of FSW aluminum butt joints, Int. J. Mater. Form. **2**(1) (2009) 303–306.

[17] Y. Zhao, S. Lin, L. Wu, F. Qu, The influence of pin geometry on bonding and mechanical properties in friction stir weld 2014 Al alloy, Mater. Lett. **59** (2005) 2948––2952.

[18] K.S. Arora, S. Pandey, M. Schaper, R. Kumar, Effect of process parameters on FSW of aluminum alloy 2219--T87, Int. J. Adv. Manuf. Tech. **50** (2010) 941–952.

[19] H. Abd El-Hafez, Mechanical properties and welding power of friction stirred AA2024-T35 joints, J. Mater. Eng. Perform. **20** (2011) 839–845.

[20] A.P. Reynolds, W. Tang, Z. Khandkar, J.A. Khan, K. Lindner, Relationships between weld parameters, hardness distribution and temperature history in 7050 FSW, Sci. Tech. Weld. Join. **10** (2005) 190–199.

[21] G. Buffa, J. Hua, R. Shivpuri, L. Fratini, Design of the friction stir welding tool using the continuum based FEM model, Mater. Sci. Eng., A **419** (2006) 389–396.

[22] M. Boz, A. Kurt, The influence of stirrer geometry on bonding and mechanical properties in friction stir welding process, Mater. Des. **25** (2004) 343–347.

[23] P.A. Colegrove, H.R. Shercliff, Two dimensional CFD modeling of flow round profiled FSW tooling, Sci. Tech. Weld. Join. **9** (2004) 483–492.

[24] S. Lin, Y. Zhao, Z. He, L. Wu, Modeling of friction stir welding process for tools design, Front. Mater. Sci. **5** (2011) 236–245.

[25] M. Guerra, C. Schmidt, J.C. McClure, L.E. Murr, A.C. Nunes, Flow patterns during friction stir welding, Mater. Charact. **49** (2003) 95–101.

[26] P. Vilaça, L. Quintino, J.F. dos Santos, iSTIR - Analytical thermal model for friction stir welding, J. Mater. Process. Tech. **169** (2005) 452–465.

[27] W.J. Arbegast, P.J. Hartley, Friction stir welding technology development at Lockheed Martin Michoud space systems: an overview, in Proceedings of 5th International conference of trends in welding research, Pine Mountain, GA, USA, 1998, p. 541.

[28] Leica Application Suite, ver. 3.8.0, Leica Microsystems Ltd., Switzerland

[29] Z. Zhang, B.L. Xiao, Z.Y. Ma, Effect of welding parameters on microstructure and mechanical properties of friction stir welded Al 2219-T6 joints, J. Mater. Sci. **47** (2012) 4075–4086.

[30] K. Kumar, S.V. Kailas, The role of friction stir welding tool on material flow and weld formation, Mater. Sci. Eng., A **485** (2008) 367–374.

[31] W.J. Arbegast, A flow partitioned deformation zone model for defect formation during friction stir welding, Scr. Mater. **58** (2008) 372–376.

[32] Z. Zhang, B.L. Xiao, Z.Y. Ma, Effect of Alclad Layer on Material Flow and Defect Formation in Friction-Stir-Welded 2024 Aluminum Alloy, Metall. Mater. Trans. A **42** (2011) 1717–1726.

[33] Kh.A.A. Hassan, P.B. Prangnell, A.F. Norman, D.A. Price, S.W. Williams, Effect of welding parameters on nugget zone microstructure and properties in high strength aluminum alloy friction stir welds, Sci. Tech. Weld. Join. **8** (2003) 257–268.

[34] K.N. Krishnan, On the formation of onion rings in friction stir welds, Mater. Sci. Eng., A **327** (2002) 246–251.

[35] M.A. Sutton, B. Yang, A.P. Reynolds, R. Taylor, Microstructural studies of friction stir welds in 2024-T3 aluminum, Mater. Sci. Eng., A **323** (2002) 160–166.

[36] M.J. Jones, P. Heurtier, C. Desrayaud, F. Montheillet, D. Allehaux, J.H. Driver, Correlation between microstructure and microhardness in a friction stir welded 2024 aluminium alloy, Scr. Mater. **52** (2005) 693–697.

[37] K.V. Jata, S.L. Semiatin, Continuous dynamic recrystallization during friction stir welding of high strength aluminum alloys, Scr. Mater. **43** (2000) 743–749.

IZVOD

UTICAJ GEOMETRIJE TRNA ALATA NA MEHANIČKE I STRUKTURNE KARAKTERISTIKE SUČEONOG SPOJA ALUMINIJUMSKE LEGURE 2024-T351 ZAVARENOG POSTUPKOM FSW

Igor Z. Radisavljević[1], Aleksandar B. Živković[2], Vencislav K. Grabulov[3], Nenad A. Radović[4]

[1]*Vojnotehnički institut, Beograd, Srbija*
[2]*GOŠA FOM, Smederevska Palanka, Srbija*
[3]*Institut za ispitivanje materijala, Beograd, Srbija*
[4]*Tehnološko-metalurški fakultet, Beograd, Srbija*

(Naučni rad)

U radu je ispitavano kakav zajednički, kombinovani uticaj brzina rotacije alata, brzina zavarivanja i mala promena u geometriji trna alata imaju na zavarljivost, mehaničke i strukturne karakteristike sučeonog spoja Al legure 2024-T351 zavarene primenom FSW (zavarivanje trenjem alatom) postupka zavarivanja. Zavarivane su ploče dimenzija 260 mm×65 mm×6 mm. Ploče su pre zavarivanja mašinski obrađene i kruto stegnute za potpornu ploču. Zavarivanje je izvedeno u pravcu valjanja ploča, na alatnoj glodalici prilagođenoj postupku FSW. Dužina svakog zavarenog spoja iznosila je oko 210 mm. Korišćena su dva alata sa veoma slično profilisanim trnovima. Razlika u dizajnu trna alata je u obliku zavojnice, normalna (klasična) kod alata oznake 310 odnosno zaobljena za alat 310-O. Zavarivanje je izvedeno pri brzini rotacije alata od 750 o/min i brzinama zavarivanja 73 i 93 mm/min. Ukupno su zavarene četiri kombinacije spojeva. U svim slučajevima dobijen je zavareni spoj bez prisustva grešaka, sa glatkom odnosno delimično hrapavom površinom zavara. Prisutne su tri različite oblasti u spoju – grumen, zona termomehaničkog uticaja i zona uticaja toplote. Promene u dizajnu trna alata imaju znatnog uticaja na makrostrukturu spoja i raspodelu tvrdoće kroz spoj. Mapiranjem spoja, na osnovu raspodele tvrdoće, određene su oblasti sa najnižim vrednostima tvrdoće a nalaze se u neposrednoj blizini grumena, tačnije na liniji dodira grumena i zone termomehaničkog uticaja. Položaj oblasti najmanje tvrdoće je u saglasnosti sa mestom preloma zateznih epruveta. Efikasnost spoja, kao ocena kvaliteta spoja, je veća kod spojeva zavarenih alatom 310. U zavisnosti od alata, pri istim parametrima zavarivanja dobijene su različite vrednosti zateznih čvrstoća a razlika iznosi do 13%. Pokazano je da mala modifikacija u dizajnu trna alata ima velikog uticaja na formiranje spoja i njegove mehaničke karakteristike.

Ključne reči: Zavarivanje trenjem alatom • Geometrija trna alata • Kvalitet spoja • Al legura 2024 • Uneta toplota